FLAGELLAR MOTORS AND FORCE SENSING IN BACTERIA

EDITED BY: Matt Arthur Baker, Jonathan David Partridge, Seiji Kojima and Ashley L. Nord

PUBLISHED IN: Frontiers in Microbiology

frontiers Research Topics

frontiers

ISSN 1664-8714
ISBN 978-2-88974-588-3
DOI 10.3389/978-2-88974-588-3

About Frontiers

Frontiers is more than just an open-access publisher of scholarly articles: it is a pioneering approach to the world of academia, radically improving the way scholarly research is managed. The grand vision of Frontiers is a world where all people have an equal opportunity to seek, share and generate knowledge. Frontiers provides immediate and permanent online open access to all its publications, but this alone is not enough to realize our grand goals.

Frontiers Journal Series

The Frontiers Journal Series is a multi-tier and interdisciplinary set of open-access, online journals, promising a paradigm shift from the current review, selection and dissemination processes in academic publishing. All Frontiers journals are driven by researchers for researchers; therefore, they constitute a service to the scholarly community. At the same time, the Frontiers Journal Series operates on a revolutionary invention, the tiered publishing system, initially addressing specific communities of scholars, and gradually climbing up to broader public understanding, thus serving the interests of the lay society, too.

Dedication to Quality

Each Frontiers article is a landmark of the highest quality, thanks to genuinely collaborative interactions between authors and review editors, who include some of the world's best academicians. Research must be certified by peers before entering a stream of knowledge that may eventually reach the public - and shape society; therefore, Frontiers only applies the most rigorous and unbiased reviews.
Frontiers revolutionizes research publishing by freely delivering the most outstanding research, evaluated with no bias from both the academic and social point of view. By applying the most advanced information technologies, Frontiers is catapulting scholarly publishing into a new generation.

What are Frontiers Research Topics?

Frontiers Research Topics are very popular trademarks of the Frontiers Journals Series: they are collections of at least ten articles, all centered on a particular subject. With their unique mix of varied contributions from Original Research to Review Articles, Frontiers Research Topics unify the most influential researchers, the latest key findings and historical advances in a hot research area! Find out more on how to host your own Frontiers Research Topic or contribute to one as an author by contacting the Frontiers Editorial Office: frontiersin.org/about/contact

FLAGELLAR MOTORS AND FORCE SENSING IN BACTERIA

Topic Editors:
Matt Arthur Baker, University of New South Wales, Australia
Jonathan David Partridge, University of Texas at Austin, United States
Seiji Kojima, Nagoya University, Japan
Ashley L. Nord, INSERM U1054 Centre de Biochimie Structurale de Montpellier, France

Citation: Baker, M. A., Partridge, J. D., Kojima, S., Nord, A. L., eds. (2022). Flagellar Motors and Force Sensing in Bacteria. Lausanne: Frontiers Media SA.
doi: 10.3389/978-2-88974-588-3

Table of Contents

frontiers in Microbiology

EDITORIAL
published: 04 February 2022
doi: 10.3389/fmicb.2022.833011

Editorial: Flagellar Motors and Force Sensing in Bacteria

Matthew A. B. Baker[1]*, *Seiji Kojima*[2]*, *Ashley L. Nord*[3]* and *Jonathan D. Partridge*[4]*

[1] School of Biotechnology and Biomolecular Sciences (BABS), University of New South Wales, Sydney, NSW, Australia, [2] Division of Biological Science, Graduate School of Science, Nagoya University, Nagoya, Japan, [3] Centre de Biochimie Structurale de Montpellier, Montpellier, France, [4] University of Texas at Austin, Austin, TX, United States

Keywords: flagellar, motility, bacteria, force sensing, archaea

Editorial on the Research Topic

Flagellar Motors and Force Sensing in Bacteria

The machinery behind bacterial flagellar motility is an astounding example of natural nanotechnology. The bacterial flagellar motor (BFM) is the end point of chemotaxis, a sensory pathway that helps bacteria to navigate their surroundings in search of an optimally hospitable niche. The BFM, which coordinates the rotation of an extracellular filament to drive motility is sensitive to the electrochemical and mechanical nature of its environment, dynamically tuning its structural composition and power output on the fly. For example, the BFM recruits torque-producing stator units to increase its power output in response to increased mechanical loads. Thus, the motor not only generates force and torque, but is also involved in surface sensing and mechanosensing. Bacterial motility underlies the virulence of pathogens, especially those which infect areas under high flow, as well as the linkage between force sensing, quorum sensing, and biofilm formation. Bacterial motility and surface interactions are a key area of study in the face of rising antimicrobial resistance, which is one of the dominant public health issues of this century. This Research Topic sought to highlight the similarities and diversities of the BFM and chemotaxis systems across species, to understand their evolutionary origins, and to reveal how the BFM's dynamic structure and activity can be modulated by, and in response to changes in its environment.

Many of the articles in this special issue highlight the diversity in both structure and assembly through investigations of traditionally less well-characterized flagellar motors. Zhou and Roujeinikova review the structure and composition of the proteinaceous periplasmic stator scaffolds found in many polar flagellar motors, imaged via electron cryotomography, which are instrumental for sustaining the abnormally high speeds and torques of monotrichous bacteria (as compared to peritrichous bacteria). Arroyo-Pérez and Ringgaard asked how *Vibrio parahaemolyticus* ensures proper positioning of its single flagellum at the old cell pole after cell division. They investigated the subcellular spatiotemporal localization of the polar flagellar determinants FlhF and FlhG, revealing their cell cycle-dependent intracellular coordination, which depends upon the cell pole determinant protein HubP and another still unidentified factor. Xu et al. investigated the mechanism by which the hook penetrates the peptidoglycan (PG) sacculus in spirochetes, providing evidence that FlgJ and BB0259, a previously uncharacterized cell wall-degrading enzyme, coordinate PG penetration in the Lyme disease spirochete *Borrelia burgdorferi*. Ferriera et al. shed light upon how different flagella evolved in closely related lineages. By contrasting data from protein phylogenetics and structural data from electron cryo-tomography and subtomogram averaging, they posit that Enterobacteriaceae flagella were horizontally acquired from an ancestral β-proteobacterium, giving them a "general-purpose" BFM which is able to adjust to a wide range of conditions.

OPEN ACCESS

Edited and reviewed by:
Biswarup Mukhopadhyay, Virginia Tech, United States

Correspondence:
Matthew A. B. Baker
matthew.baker@unsw.edu.au
Seiji Kojima
z47616a@cc.nagoya-u.ac.jp
Ashley L. Nord
ashley.nord@cbs.cnrs.fr
Jonathan D. Partridge
j.partridge@utexas.edu

Specialty section:
This article was submitted to Microbial Physiology and Metabolism, a section of the journal Frontiers in Microbiology

Received: *10 December 2021*
Accepted: *13 January 2022*
Published: *04 February 2022*

Citation:
Baker MAB, Kojima S, Nord AL and Partridge JD (2022) Editorial: Flagellar Motors and Force Sensing in Bacteria. Front. Microbiol. 13:833011. doi: 10.3389/fmicb.2022.833011

Other articles in this series spotlight the diverse ways in which bacteria adapt their behavior in response to external cues. Bacteria sense and adapt to physical forces in their environment, such as shear-induced or surface-induced forces on the membrane. Kenney reviews the ways in which histidine kinases funnel diverse environmental stimuli, including mechanical stress and changes in membrane tension, into changes in gene expression, underscoring that many of the molecular mechanisms underlying mechanical force sensing in bacteria remain to be unraveled. The activity of the BFM is also modulated by external cues, *via* a growing list of proteins and regulators, including the chemotaxis response regulator CheY and c-di-GMP-binding proteins that act as molecular brakes or clutches. In *Shewanella putrefaciens,* Pecina et al. identify MotL as a novel stand-alone PilZ-domain protein which regulates the lateral flagellar system in response to intracellular levels of the secondary messenger c-di-GMP. Exceptionally, MotL does not act upon the polar motor, thus demonstrating differential regulation of two flagellar systems in a single species. The soil motile *Azospirillum brasilense* has a complex chemotaxis system, with two distinct chemotaxis pathways and four CheY homolog response regulators. Ganusova et al. show that, in addition to fine-tuning the rotational bias of the polar flagellum, each of the four CheY homologs plays a distinct role in swimming (planktonic movement), swarming (collective movement across a surface), attachment to abiotic and biotic surfaces, and biofilm formation.

Finally, the emergence of the stator unit as a crucial component in sensing and motor modulation is underlined by three articles here. Islam et al. turn to the longstanding open question of the mechanism of stator ion selectivity and which ion holds energetic primacy for the BFM. They reconstructed and engineered ancestral sequences of the MotB stator sub-unit, and by assessing motor functionality as a function of the ionic power source, they add to our understanding of the contributions of specific residues within the ion channel. Biquet-Bisquert et al. sprovide a comprehensive review of the complex relationship between the ion motive force across the cell membrane, motor activity, and the dynamic assembly of stator units. Lin et al. use a fast perfusion microfluidic system to reveal that stator assembly dynamics in sodium-driven chimeric BFMs show a complex dependence upon the extracellular sodium concentration. Their results call into question current models of stator unit assembly and underline the extent to which the mechanisms of stator unit exchange remain unclear. These works reinforce the versatility of the BFM, as both a functional motor and as a bellwether of the bacterial environment, coordinating signals and response, to drive survival and spread.

AUTHOR CONTRIBUTIONS

All authors listed have made a substantial, direct, and intellectual contribution to the work and approved it for publication.

Conflict of Interest: The authors declare that the research was conducted in the absence of any commercial or financial relationships that could be construed as a potential conflict of interest.

Publisher's Note: All claims expressed in this article are solely those of the authors and do not necessarily represent those of their affiliated organizations, or those of the publisher, the editors and the reviewers. Any product that may be evaluated in this article, or claim that may be made by its manufacturer, is not guaranteed or endorsed by the publisher.

frontiers in Microbiology

ORIGINAL RESEARCH
published: 23 December 2020
doi: 10.3389/fmicb.2020.625837

Ancestral Sequence Reconstructions of MotB Are Proton-Motile and Require MotA for Motility

*Md Imtiazul Islam[1], Angela Lin[1], Yu-Wen Lai[1], Nicholas J. Matzke[2] and Matthew A. B. Baker[1,3]**

[1] School of Biotechnology and Biomolecular Sciences (BABS), University of New South Wales, Sydney, NSW, Australia, [2] School of Biological Sciences, University of Auckland, Auckland, New Zealand, [3] CSIRO Synthetic Biology Future Science Platform, Brisbane, QLD, Australia

The bacterial flagellar motor (BFM) is a nanomachine that rotates the flagellum to propel many known bacteria. The BFM is powered by ion transit across the cell membrane through the stator complex, a membrane protein. Different bacteria use various ions to run their BFM, but the majority of BFMs are powered by either proton (H^+) or sodium (Na^+) ions. The transmembrane (TM) domain of the B-subunit of the stator complex is crucial for ion selectivity, as it forms the ion channel in complex with TM3 and TM4 of the A-subunit. In this study, we reconstructed and engineered thirteen ancestral sequences of the stator B-subunit to evaluate the functional properties and ionic power source of the stator proteins at reconstruction nodes to evaluate the potential of ancestral sequence reconstruction (ASR) methods for stator engineering and to test specific motifs previously hypothesized to be involved in ion-selectivity. We found that all thirteen of our reconstructed ancient B-subunit proteins could assemble into functional stator complexes in combination with the contemporary *Escherichia coli* MotA-subunit to restore motility in stator deleted *E. coli* strains. The flagellar rotation of the thirteen ancestral MotBs was found to be Na^+ independent which suggested that the F30/Y30 residue was not significantly correlated with sodium/proton phenotype, in contrast to what we had reported previously. Additionally, four among the thirteen reconstructed B-subunits were compatible with the A-subunit of *Aquifex aeolicus* and able to function in a sodium-independent manner. Overall, this work demonstrates the use of ancestral reconstruction to generate novel stators and quantify which residues are correlated with which ionic power source.

Keywords: motility, flagellar and chemotaxis, stator, ancestral sequence reconstruction, ion-selectivity

OPEN ACCESS

Edited by:
Masahiro Ito,
Toyo University, Japan

Reviewed by:
Shuichi Nakamura,
Tohoku University, Japan
Katsumi Imada,
Osaka University, Japan

***Correspondence:**
Matthew A. B. Baker
matthew.baker@unsw.edu.au

Specialty section:
This article was submitted to Microbial Physiology and Metabolism, a section of the journal Frontiers in Microbiology

Received: *04 November 2020*
Accepted: *27 November 2020*
Published: *23 December 2020*

Citation:
Islam MI, Lin A, Lai Y-W, Matzke NJ and Baker MAB (2020) Ancestral Sequence Reconstructions of MotB Are Proton-Motile and Require MotA for Motility. Front. Microbiol. 11:625837. doi: 10.3389/fmicb.2020.625837

INTRODUCTION

Bacterial cells can move through liquids or over moist surfaces using rotating flagella to propel themselves in response to chemical stimulus, temperature and pH (Armitage, 2007; Jarrell and McBride, 2008; Gurung et al., 2020). The bacterial flagellar motor (BFM) drives the rotation of the flagellum (Sowa and Berry, 2008). One of the largest molecular machines in bacteria, with a molecular mass of ∼11 MDa (Sowa and Berry, 2008), the BFM is present in a great variety of bacterial taxa from various habitats (Pion et al., 2013). It shares structural and amino acid sequence homology across a diverse range of taxa which suggests early ancestry and makes it a case study for investigating the origins of microbial motility (Mitchell and Kogure, 2006; Thormann and Paulick, 2010; Son et al., 2015).

The stator complexes are motor-associated protein complexes which form a selective ion channel that converts chemical energy into mechanical torque to rotate the rotor (Minamino et al., 2018). The stator proteins are divided into A- and B-subunits and named according to the transferred ion, for example, MotA and MotB in H^+ powered motors in *Escherichia coli,* and PomA and PomB in Na^+ powered motors in *Vibrio alginolyticus* (Yorimitsu and Homma, 2001; Berg, 2003). According to the complete structure of stator complex, the A-subunit (MotA/PomA) consists of four transmembrane (TM) domains and a large cytoplasmic domain that is proposed to interact with the rotor through the rotor component FliG and generate torque (Dean et al., 1984; Blair and Berg, 1991; Zhou et al., 1995; Braun et al., 2004; Onoue et al., 2019). The B-subunit (MotB/PomB) contains a single TM domain followed by a large periplasmic domain which consists of a plug segment to control ion flow and a peptidoglycan-binding domain (PGD) to interact with peptidoglycan layer (Roujeinikova, 2008; Kojima et al., 2018). The stoichiometry of the stator units was until recently believed to be 4(A):2(B) according to the available previous crosslinking, biochemical, and genetic data of MotAB and PomAB (Sato and Homma, 2000; Kojima and Blair, 2001; Kojima et al., 2009). However, in 2020 the full structure of the stator complex was solved and it was reported that the stoichiometry of the stator unit is 5:2 instead of 4:2 for both MotAB/PomAB families (Deme et al., 2020; Santiveri et al., 2020). The new reports suggested that five copies of MotA enclosed the two TM domains from of the two copies of MotB (Deme et al., 2020; Santiveri et al., 2020). The four TM domains of MotA are arranged in two layers, TM3 and TM4 line the central pore, while TM1 and TM2 form a surrounding outer layer of helices (Deme et al., 2020; Santiveri et al., 2020). TM1 and TM2 stabilize the assembly of MotA whereas TM3 and TM4 make direct interactions with MotB, and both of them together span the complete height of MotA and extend to the cytoplasmic domain (Deme et al., 2020; Santiveri et al., 2020). The functional mechanism of MotAB starts with the dimerization and binding of PGDs to the peptidoglycan layer which leads the unplugging of the ion channel to allow ion exchange. Finally, the binding and release of proton or hydronium ions by the universally conserved MotB aspartate residue allow the MotA to bind the neighboring FliG, which trigger the conformational change in the stator complex and generate torque (Deme et al., 2020; Santiveri et al., 2020).

Ion selectivity provides flexibility to bacteria for using suitable ions according to their environmental conditions (Terahara et al., 2008). Generally, most of the bacterial species use a single stator complex to couple with specific ions such as protons (H^+), sodium (Na^+), potassium (K^+), rubidium (Rb^+), magnesium (Mg^{2+}), calcium (Ca^{2+}), or strontium (Sr^{2+}) to drive their motor (Li et al., 2011; Terahara et al., 2012; Minamino and Imada, 2015; Imazawa et al., 2016; Ito and Takahashi, 2017). However, some bacterial species can power their flagella by coupling more than one ion using either multiple types of stator complexes or single dual-functional complexes (Terahara et al., 2006, 2008; Paulick et al., 2015). Previous studies suggested that the TM domain of the B-subunit (MotB, MotS, and PomB) of the stator complex is specifically crucial for the selectivity of H^+ and Na^+ ions in the flagellar motor (Asai et al., 2000; Ito et al., 2005). In the MotAB complex, a conserved aspartic acid residue (D32) at the N-terminal side of the TM region is thought to function as a universally conserved site for ion binding (Zhou et al., 1998). Mutational studies suggested that valine (V42) and leucine (L42) located at the ten amino acids downstream from the universal conserved aspartic acid (D32) are critical for the selection of H^+ and Na^+ ions, respectively (Terahara et al., 2008). Another study has exhibited that the methionine residue (M33) at the TM region of MotS is critical for K^+ selectivity (Terahara et al., 2012). It has also been reported that switching of ion selectivity and use of dual ion into a single stator can be introduced with mutations and hybridizations of the ion-binding transmembrane region of the B-subunit (Terahara et al., 2008; Nishino et al., 2015). However, recently it was proposed that the MotP subunit of the MotPS complex was important for the K^+ selectivity of the flagellar stators of *Bacillus alcalophilus* and *Bacillus trypoxylicola* (Naganawa and Ito, 2020).

Although the recent high-resolution cryoelectron microscopy reconstructions of stator units enable us to gain more detailed information of the structural and functional components of BFM that are involved in the conversion of electrochemical energy to mechanical torque (Deme et al., 2020; Santiveri et al., 2020), the exact mechanism and structural determinants of ion selectivity are yet to be discovered. However, with the help of statistical phylogenetic methods, it is possible to infer the sequences of extinct ancestral proteins from the sequences of their extant descendants (Hochberg and Thornton, 2017). It is possible to then resurrect the ancestral proteins corresponding to these inferred sequences and characterize their *in vitro* biological and biochemical properties (Gaucher et al., 2003; Thornton et al., 2003). Furthermore, ancient proteins can be expressed in contemporary hosts to examine the function of ancient proteins *in vivo*, and their integration and subsequent adaptation in ancient-modern hybrids (Kaçar and Gaucher, 2012; Kacar et al., 2017a,b). It is also possible to reconstruct the ancestral protein using the inferred ancestral sequence and express the reconstructed ancestral proteins using genetic engineering techniques to characterize their biological and biochemical properties (Gaucher et al., 2003; Thornton et al., 2003). In this study, we have built a phylogeny of MotB proteins in proteobacteria and computationally reconstructed the ancestral stator units focusing on the TM region of the B-subunit of the stator complex. We engineered selected nodes into a chimeric plasmid to characterize their motility and evaluate their ion selectivity to interrogate ion selectivity in ancient-modern hybrids of the flagellar motor at specific points in our estimate of history.

MATERIALS AND METHODS

Phylogenetic Analysis and Ancestral Sequence Reconstruction

Sequence Gathering

A sequence similarity network (SSN) was generated as previously described (Atkinson et al., 2009). The protein sequences of 2187 bacterial homologs of MotB (UniProt: P0AF06) were selected using the EFI-EST server (Gerlt et al., 2015) with *E*-value = 10

for the all-versus-all BLAST, and using representative nodes to represent clusters with 90% sequence similarity. A subset of 757 sequences was selected as follows: nodes connected by edges >85% sequence identity were kept (1289 nodes, 5870 edges), and then the 405 least connected nodes (duplexes and triplexes) were removed (down to 884 nodes, 5572 edges). Sequences for these 884 nodes were aligned with MUSCLE (Edgar, 2004) and nodes were restricted to sequences that contained either FAD, YAD, or LAD at residues 30–32 (*E. coli* MotB numbering, 757 nodes, 4326 edges), to ensure conserved residue D32 for function. The clustering of characterized proteins were visualized using the gamma-organic layout on Cytoscape 3.1 (Akiva et al., 2017) and presented in **Supplementary Figure 1**.

Phylogenetics

757 MotB sequences from above were aligned using Clustal Omega (Larkin et al., 2007) with five iterative re-alignments. The phylogeny was then estimated with Quicktree using Kimura translation for pairwise distance and calculating bootstraps with 100 iterations (Howe et al., 2002). The phylogeny was midpoint-rooted in FigTree (Rambaut, 2014) for display purposes, and should be treated cautiously as with any single-protein estimate of a deep phylogeny (Pallen and Matzke, 2006; Abby and Rocha, 2012; Shih and Matzke, 2013; Prangishvili et al., 2017; Ishida et al., 2019). For the purpose of surveying sequence diversity across MotBs, the tree is adequate, and arbitrary re-rooting will not affect estimation of ASRs at nodes.

Node Selection

Thirteen nodes were selected at assessed divergent points between clades based on known sodium swimmers and their proximity and distance from the arbitrary root. Sequences (**Supplementary Figure 2A**) and conservation via sequence logo (Crooks et al., 2004) are shown in **Supplementary Figure 2**.

Reconstruction

Ancestral protein sequences were reconstructed using the empirical Bayes method implemented in PAML (Yang, 2007). MotB sequences were truncated to focus on the TM region between residues 23–65 on MotB. The posterior probability distribution at each site for each ancestral node was also calculated using PAML.

Bacterial Strains and Plasmids and Growth Conditions

The bacterial strains and plasmids used in this study are shown in full in **Supplementary Table 1**. The primary strains used in this work are RP6894 (Block et al., 1989) and RP3087 (Blair et al., 1991). All the *E. coli* strains were cultured in LB broth and LB agar [1% (w/v) Bacto tryptone, 0.5% (w/v) Bacto yeast extract, 0.5% (w/v) NaCl, and 2% (w/v) Bacto agar for solid media] at 37°C. According to the selective antibiotic resistance pattern of the plasmids, chloramphenicol (CAM), ampicillin (AMP) or kanamycin (KAN) were added to a final concentration of 25 μg/mL, 50 μg/mL, and 25 μg/mL, respectively.

Cloning of Selected MotB-ASR Sequences

We engineered the ancestral reconstructed sequences (ASR) in a predesigned form of genetic structure that included the first 22 residues of *E. coli* MotB, followed by 42 residues (23–65) of ancestral sequence and a final 243 residues (66–308) of the MotB chassis (ASR = 1–22 MotB; 23–65 ASR; 66–308 MotB). In summary, this used the *E. coli* N-terminal domain, the ASR for the TM and plug domains (TM: residues 28–49, plug: 52–65) and then the *E. coli* PGD and C-terminal domain (PGD: 196–225). MotB-ASRs were constructed by PCR amplification using the chimeric plasmid pSHU1234 (Nishino et al., 2015) containing PomA and PotB (a hybrid of PomB and MotB) as the cloning vector. Thirteen forward ultramer primers were designed with ∼200 nucleotide overhangs that contained a *Nde*I restriction site, the predicted ancestral sequences and an annealing sequence specific to MotB on PotB in pSHU1234. A common reverse primer was designed to amplify from the end of PotB with a *Pst*I restriction site. IDT synthesized all the primers. The list of all primers is provided in **Supplementary Table 2**. Phusion high-fidelity (HF) DNA polymerase (NEB) was used for the PCR amplification of ASR sequences. Each reaction contained 10 μL of 5X Phusion HF buffer, 200 μM dNTPs, 0.1 μM of each primer, 10 ng of plasmid template, 3% of DMSO, 1 U Phusion HF DNA polymerase, sterile Milli-Q water to final volume of 50 μL. The reactions were started by heating to 98°C for 30 s. The PCR reactions were then subjected to 35 cycles of 98°C for 10 s, 58°C for 30 s, and 72°C for 30 s, with a final 5 min extension step at 72°C.

The amplified MotB-ASR sequences were then separated in 1% (w/v) agarose gel and purified using the Qiagen gel purification kit. Purified MotB-ASR sequences and pSHU1234 were digested with *Nde*I and *Pst*I before ligation with T4 ligase (NEB) using a 1:3 vector to insert molar ratio. All the resulting MotB-ASR plasmids contain a PomA from the vector backbone and an ancestral-contemporary MotB hybrid (**Supplementary Table 1**).

Finally, all the MotB-ASR plasmids were transformed into stator deleted (RP6894) and MotB deleted (RP3087) *E. coli* strains following the chemical transformation protocol from NEB. All engineered and cloning of MotB-ASR sequences were confirmed by colony PCR and Sanger sequencing at The Ramaciotti Centre for Genomics (UNSW, Australia) using ASR sequence-specific primers (**Supplementary Table 2**).

Construction of Single Stator Plasmids

We constructed pMotB via deleting MotA from the MotAB plasmid pDB108 (A gift from David F Blair Lab) and constructed pPomA and pPotB by deleting PotB and PomA, respectively, from PomAPotB plasmid pSHU1234 (Nishino et al., 2015). Site-directed, Ligase-Independent Mutagenesis (SLIM) was used (Chiu et al., 2008) with specific primers (**Supplementary Table 2**). We also constructed a A225D point mutant of

A. aeolicus MotA from the wild type *A. aeolicus* MotA plasmid (pNT7) (Takekawa et al., 2015) using QuikChange Lightning Site-Directed Mutagenesis with the recommended protocol from Agilent. The primers used for this point mutation were provided in the **Supplementary Table 2**.

Evaluation of Swimming Properties of MotB-ASRs in Soft Agar Motility Assay

We performed swim plate motility assays according to the previous protocol (Ishida et al., 2019) with slight modifications to check whether ancestral MotB proteins could restore motility. LB swim plates [0.25% (w/v) Bacto agar] were used to screen bacteria with swimming properties. Minimal medium swim plates [10 mM of $KHPO_4$, 0.1% (v/v) of glycerol, 0.1 mM of Thr, 0.1 mM of Leu, 0.1 mM of His, 0.1 mM of Met, 0.1 mM of Ser, 1 mM of $MgSO_4$, 1 mM of $(NH_2)_2SO_4$, 1 μg/mL of thiamine, and 85 mM of NaCl or 85 mM of KCl, respectively, 0.25% (w/v) agar, 0.02% (w/v) of arabinose, pH 7.0] were used to determine the dependency of coupling ions (Na^+ or H^+) as the medium contained only the desired ion and the pure forms of nutrients that did not contain any other ionic contaminants. Antibiotics (25 μg/mL CAM or 50 μg/mL AMP or 25 μg/mL KAN) were added according to the plasmids used. Additionally, minimal

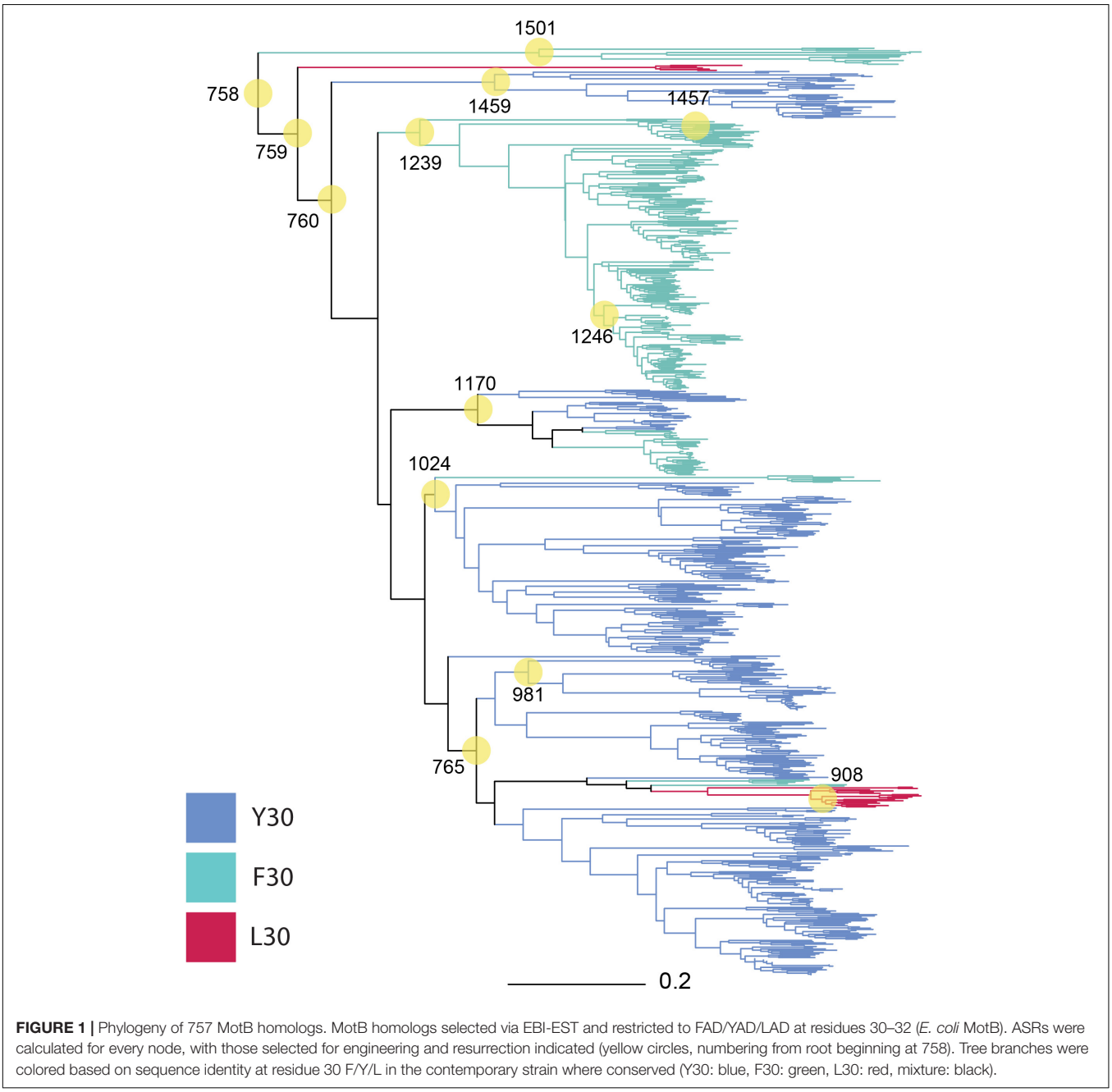

FIGURE 1 | Phylogeny of 757 MotB homologs. MotB homologs selected via EBI-EST and restricted to FAD/YAD/LAD at residues 30–32 (*E. coli* MotB). ASRs were calculated for every node, with those selected for engineering and resurrection indicated (yellow circles, numbering from root beginning at 758). Tree branches were colored based on sequence identity at residue 30 F/Y/L in the contemporary strain where conserved (Y30: blue, F30: green, L30: red, mixture: black).

swim plates with different Na^+ concentrations in combination with 100 μM phenamil (Sigma-Aldrich) were used to assess the of Na^+ dependency on swimming properties.

Swim plates were inoculated with a single 1 day old colony with a sterile toothpick and incubated at 30°C for 14 h (for LB swim plates) or 16 h (minimal swim plates) to allow proper development of a swimming ring. Swimming zones were first visually checked, imaged with the ChemiDoc MP Imaging System (Bio-Rad), and swimming diameters measured using ImageJ software (Version 1.52).

Determination of the Effect of Sodium (Na^+) Concentration on the Rotation Speed of MotB-ASRs

The effect of different Na^+ concentrations on the rotation speed of MotB-ASRs and sodium/proton controls were determined by tethered cell assays in the presence of a range of Na^+ concentrations following a previous protocol (Nishiyama and Kojima, 2012) with some modifications. *E. coli* RP3087 containing MotB-ASR plasmids were inoculated into TB broth [1% (w/v) Bacto tryptone, 0.5% (w/v) NaCl] containing 0.02% (w/v) arabinose and 25 μg/ml chloramphenicol and were grown overnight (17 h) with 180 rpm at 30°C. The overnight cultures were sub-cultured with a 50-fold dilution into fresh TB broth and incubated for 5 h with 180 rpm at 30°C to get more motile cells. At OD_{600} ∼0.80, the flagella of the cells were sheared by passing the culture multiple times (∼35) through a 26G needle syringe. After shearing the flagella, the cells were washed three times with motility buffer [10 mM potassium-phosphate, 10 mM lactic acid, 100 mM NaCl, and 0.1 mM EDTA, pH 7.0]. Cells were then attached on glass slides pre-treated with an anti-*E. coli* flagellin antibody with a 1:10 dilution (Nishiyama and Kojima, 2012) and washed sequentially with a Na^+ concentration gradient containing motility buffer. The rotational speed of the cells was observed using phase-contrast microscopy (Nikon)

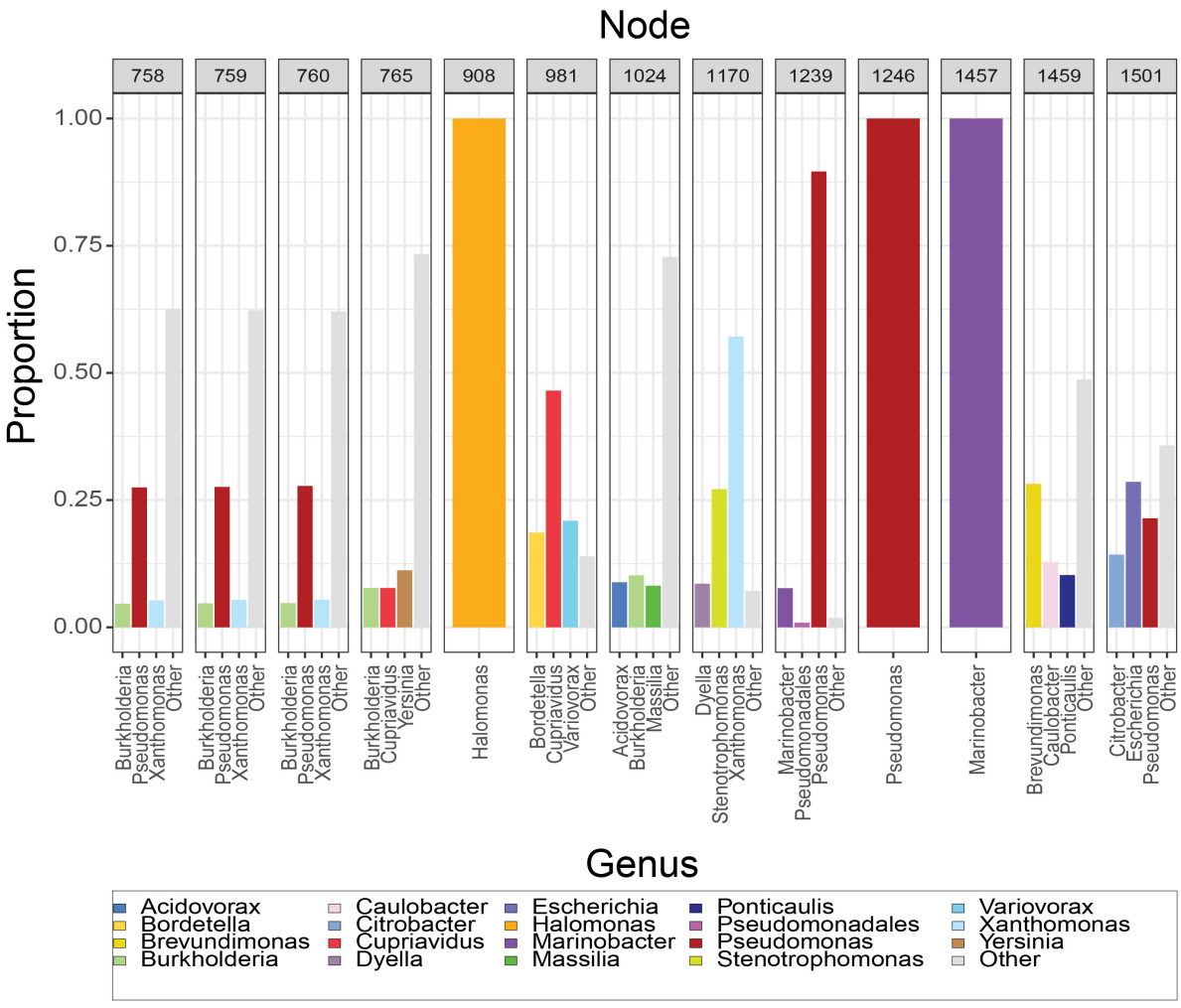

FIGURE 2 | Composition of resurrected MotB-ASRs. For each node, the set of tips descendant from that node was used to calculate the proportion of genera downstream from that node. Majority genera are indicated in legend and the top three contributors to each node noted on axis. Nodes 908, 1246, and 1457 have descendants that are solely *Halomonas*, *Pseudomonas* and *Marinobacter*, respectively, while others are mixtures.

and was recorded at 20 frames per second (FPS) through the 40X objective with a camera (Chameleon3 CM3, Point Grey Research). Rotational motion of the cells was analyzed using Lab view 2019 software (National Instruments) and rotational speeds were calculated from 20 individual cells.

Growth Curve Assays

Growth assays were executed to exclude possible growth impact of MotB-ASRs. Growth of *E. coli* strain RP3087 transformed with all the MotB-ASRs, pSHU1234, and pMotB plasmids were monitored as described (Santiveri et al., 2020) with slight modifications. Briefly, overnight cultures of the test strains with OD_{600} 1.0 were diluted 1:100 in 96-well plates (Corning) with fresh LB broth containing different concentrations of NaCl, 0.02% (w/v) arabinose and 25 μg/ml chloramphenicol and incubated at 37°C. The OD_{600} were measured in a microplate reader (FLUOstar OPTIMA, BMB LABTECH) every hour for 8 h with a brief shaking interval before each measurement. The experiment was performed in a triplicate.

Correlation Analysis of Mutations at Each Respective Site of MotB Ancestral Sequences

To determine the correlation of mutations at each respective site of MotB ancestral sequences, we selected 19 species of bacteria (**Supplementary Table 3**) where the ion selectivity correlation with residue was previously measured (Ishida et al., 2019). Each species in the 19-species subset was classified as Na^+ or H^+ powered, we then added our functional MotB-ASRs as a further 13 H^+ powered units and conducted Fisher's Exact Test analysis (in R) based on a binary response variable. We were interested in whether a binary response might be correlated with a binary amino acid predictor, so we filtered columns in the alignment to exclude columns where the two most common amino acids added up to <85% of the observed residues. We ran Fisher's exact test to correlate each amino acid or the mutational pair with the ionic power source.

RESULTS

Phylogeny of MotB and Node Composition of MotB-ASRs

We selected nodes in our phylogeny (**Figure 1**) for ancestral reconstruction (ASR) by a mixture of early and contemporary nodes to increase the probability of synthesizing a motile gene. Among the selected nodes, ASR981 had descendants that were exclusively betaproteobacteria, ASR1459 had descendants that were exclusively alphaproteobacteria, ASR908, ASR1170, ASR1239, ASR1246, ASR1457, and ASR1501 had descendants that were exclusively gammaproteobacteria, and the remaining, mostly older nodes ASR758, ASR759, ASR760, ASR765, and ASR1024 had descendants that were a mixture of gamma, beta and alphaproteobacterial, with ASR1024 also including all four of the hydrogenophilalias.

The composition of the 13 nodes is shown as the proportion of species represented in the tips downstream from that node (**Figure 2**). All the nodes were distributed to a wide range of bacterial genera among which *Pseudomonas, Xanthomonas, Burkholderia, Yersinia, Paraburkholderia, Cupriavidus, Stenotrophomonas, Marinobacter, Xenorhabdus*, and *Caballeronia* were prevalent. We calculated the top three genera by frequency of occurrence in the tips descendant from the selected nodes. Among all the 13 MotB-ASRs, all the descendants of ASR908 were *Halomonas*, all of ASR1246 were *Pseudomonas*, all of ASR1457 belonged to *Marinobacter,* and

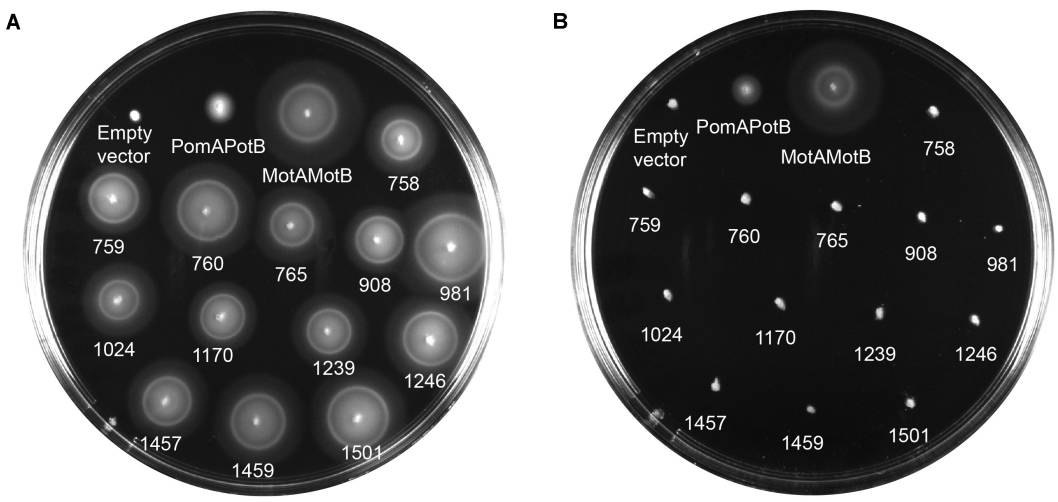

FIGURE 3 | MotB-ASRs are functional. Motility of resurrected MotB-ASRs along with the control Na^+ swimmer (PomAPotB), H^+ swimmer (MotAMotB), and non-swimmer (empty vector: pBAD33) were tested on semi-solid agar swim plates (0.25% w/v agar). **(A)** All MotB-ASRs (presented according to the respective nodes) restore motility in the presence of PomA (from plasmid) and MotA (from genome) in Δ*motB E. coli* strain RP3087. **(B)** None of the resurrected MotB-ASRs restore motility in presence of PomA without MotA in Δ*motAmotB E. coli* strain RP6894. Plates were incubated at 30°C for 14 h.

remaining nodes had descendants from mixed genera (**Figure 2**). With regard to species that could be expected to be sodium swimmers, in our original collection of 2187 MotB homologs we had 72 *Vibrio* species and 13 *Shewanella,* species. Following our network-based selection of refined sequences (**Supplementary Figure 1**), seven *Vibrio* strains remained in our phylogeny, and ASR1459 was the nearest parental-node to these seven strains.

Functional Characteristics of MotB-ASR Proteins

We calculated MotB-ASRs using maximum likelihood methods (Yang, 2007) for each of the nodes above and engineered the TM and plug domains of these ASRs into our existing MotB chassis (**Supplementary Figure 2**). Motility, initially evaluated with swim plates, showed that all MotB-ASR proteins were functional and could restore motility in the presence of contemporary MotA (**Figure 3A** and **Supplementary Figure 3**). However, without MotA, in the presence of existing PomA, none of the MotB-ASRs were functional (**Figure 3B**). This is in contrast with the controls where PotB (chimeric B-unit) was functional together with PomA and non-functional with MotA (**Supplementary Figure 4**).

Ion Dependency of Motile MotB-ASRs

To determine the ion dependency of motile MotB-ASRs, we measured motility both in the presence and absence of Na^+ on minimal swim plates. The minimal swim plate assay results showed that all the ASRs were able to swim in both the presence and absence of Na^+ (**Figures 4A,B**). We further checked the swimming ability of all ASRs and H^+/Na^+ swimming controls (MotAMotB/PomAPotB) in the presence of the Na^+ blocker phenamil. The results showed no inhibition of motility for all MotB-ASRs and the control H^+ swimmer, but showed complete inhibition of motility for the control Na^+ swimmer (PomAPotB) (**Figure 4C**). However, the swimming diameter of

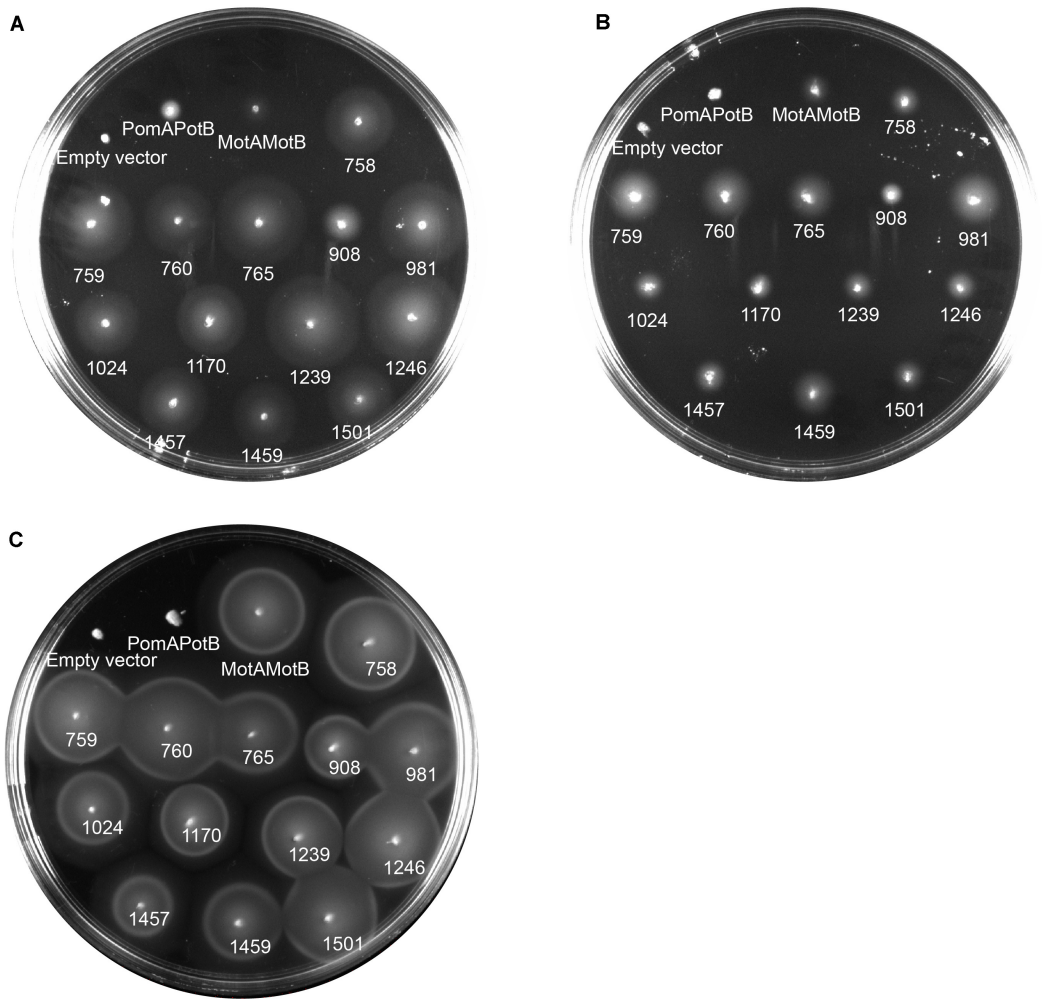

FIGURE 4 | Ion dependency of MotB-ASRs. Characterizing ion dependency of motile MotB-ASRs in the presence of Na^+ control (PomAPotB) and H^+ control (MotAMotB) on minimal swim plates (with/without NaCl). **(A)** All MotB-ASRs (presented according to the respective nodes) restored motility in Δ*motB* strain RP3087 in the presence of Na^+. **(B)** In the absence of Na^+, all the MotB-ASRs restored motility in Δ*motB* strain RP3087. **(C)** All MotB-ASRs restored motility in the presence of Na^+ and 100 μM of the sodium-blocker phenamil. **(A,B)** incubated at 30°C for 16 h, **(C)** at 30°C for 14 h.

all MotB-ASRs and proton and sodium controls (MotAMotB and PomAPotB), was greater at higher Na^+ concentrations (**Supplementary Figure 5**). This occurred despite the observed growth rates for MotB-ASRs and controls being equivalent at all sodium concentrations (**Supplementary Figure 6**). To verify the ionic energy source, we characterized stator energization via tethered cell assays.

Effect of Na^+ on the Rotational Speed of MotB-ASRs

The rotational speed of all 13 MotB-ASRs and the control strains (Na^+ swimmer and H^+ swimmer) were measured in the presence of different Na^+ concentrations (0 mM, 5 mM, 21.25 mM, 42.5 mM, and 85 mM) using the tethered cell assay. Rotation speed of all tested MotB-ASRs showed no dependence on Na^+ concentration similar to the H^+ control swimmer (MotAMotB) (**Figure 5**). However, the Na^+ control swimmer (PomAPotB) showed sodium dependence, with a gradual increase in swimming speed starting from 0 Hz to 2.8 ± 1.25 Hz maximum speed in the presence of 0 mM and 85 mM NaCl, respectively (**Figure 5**).

Among all 13 MotB-ASRs, MotB-ASR981 showed the highest swimming speed of 4.01 ± 0.92 Hz and MotB-ASR908 showed the lowest swimming speed of 2.71 ± 0.51 Hz. The remaining MotB-ASRs showed swimming speeds between 3.07 ± 0.55 Hz and 3.73 ± 0.92 Hz in all tested concentrations of Na^+ (**Supplementary Figure 7**).

Compatibility of MotB-ASRs With Ancient *Aquifex aeolicus* MotA

We co-transformed all the 13 MotB-ASRs with an ancient wild type (WT) *Aquifex aeolicus* (aa) MotA ($MotA^{aaWT}$) into a stator deleted *E. coli* (RP6894) to evaluate compatibility between

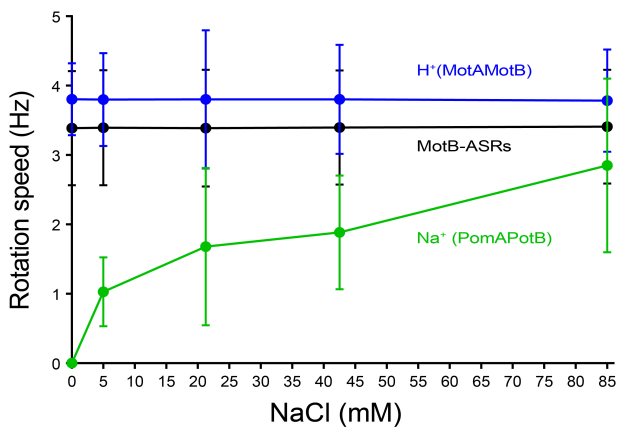

FIGURE 5 | Tethered cell rotational speeds of MotB-ASRs vs. extracellular concentration of Na^+. The averaged tethered cell rotation speed (mean ± SD) of all ASR measurements shows no dependency on external sodium concentration. Full data for each ASR is shown in **Supplementary Figure 7**. Rotation speed of the sodium powered swimming control (PomAPotB, green) and proton powered swimming control (MotAMotB, blue) are indicated for comparison.

A. aeolicus and MotB-ASR stators using the swim plate motility assay. Four (MotB-ASR760, MotB-ASR765, MotB-ASR908, and MotB-ASR981) out of 13 MotB-ASRs were compatible with $MotA^{aaWT}$. All the compatible MotB-ASRs showed Na^+ independent motility and swam both in the presence and absence of Na^+ (presence of K^+) containing plates (**Figures 6A,B**). However, the same $MotA^{aaWT}$ did not show any compatibility with contemporary *E. coli* MotB ($MotB^E$) (**Supplementary Figure 8A**). On the other hand, the point mutant (A225D) of *A. aeolicus* MotA ($MotA^{aa225D}$) was compatible with *A. aeolicus-E. coli* chimeric MotB ($MotB^{AE}$) and produced a much larger swimming zone than $MotA^{aaWT}$ and the identical $MotB^{AE}$ (**Supplementary Figure 8B**). In contrast, no MotB-ASRs were compatible with the point mutant of $MotA^{aa225D}$ and all were non-motile (**Supplementary Figure 8C**).

Confirmation of Na^+ Independence of *A. aeolicus* Compatible Motile MotB-ASRs

Tethered cell assay with various concentration of Na^+ (0 mM, 5 mM, 21.25 mM, 42.5 mM, and 85 mM) was performed to confirm the ionic energy source of the four motile MotB-ASRs (MotB-ASR760, MotB-ASR765, MotB-ASR908, and MotB-ASR981) together with $MotA^{aaWT}$ co-transformed cells. We also measured the rotation speed of $MotA^{aa225D}$ and $MotB^{AE}$ co-transformed cell in the same condition as a Na^+ dependent control (Takekawa et al., 2015). The rotation speeds of all the cells with MotB-ASRs and $MotA^{aaWT}$ were stable and showed no dependence on external sodium concentration, while in contrast the rotation of $MotA^{aa225D}$ and $MotB^{AE}$ showed Na^+ dependence (**Figure 7**). $MotA^{aaWT}$MotB-ASR908 rotated more slowly than $MotA^{aaWT}MotB^{AE}$ with an average swimming speed of 1.59 ± 0.60 Hz but all other MotB-ASRs rotated more quickly, with MotB-ASR765 the fastest swimmer with the average swimming speed of 3.39 ± 0.79 Hz (**Figure 7**).

Pairwise Correlation of Residue With Phenotype

We assembled a sequence alignment including all 13 MotB-ASRs (**Supplementary Figure 2A**) and 19 additional bacterial species (**Supplementary Table 3**) with known sodium or proton motility (Ishida et al., 2019). We examined if the addition of our 13 proton-motile strains affected significance scores for correlation between specific residues and phenotype by Fisher's Exact Test. For the hypothesized correlation between residue 30 F or Y (**Figure 1**) and proton or sodium motility, where the null hypothesis of no correlation was previously strongly rejected based on data from 19 living strains ($p = 0.0034$), the addition of 13 additional proton motile ASR sequences weakened, but did not completely eliminate, statistical significance at the $p < 0.05$ level ($p = 0.014$). However, residue 43 remained strongly significantly correlated with ionic power source ($p = 0.00041$ with living sequences; $p = 0.000028$ with ASRs added, **Supplementary Table 4**).

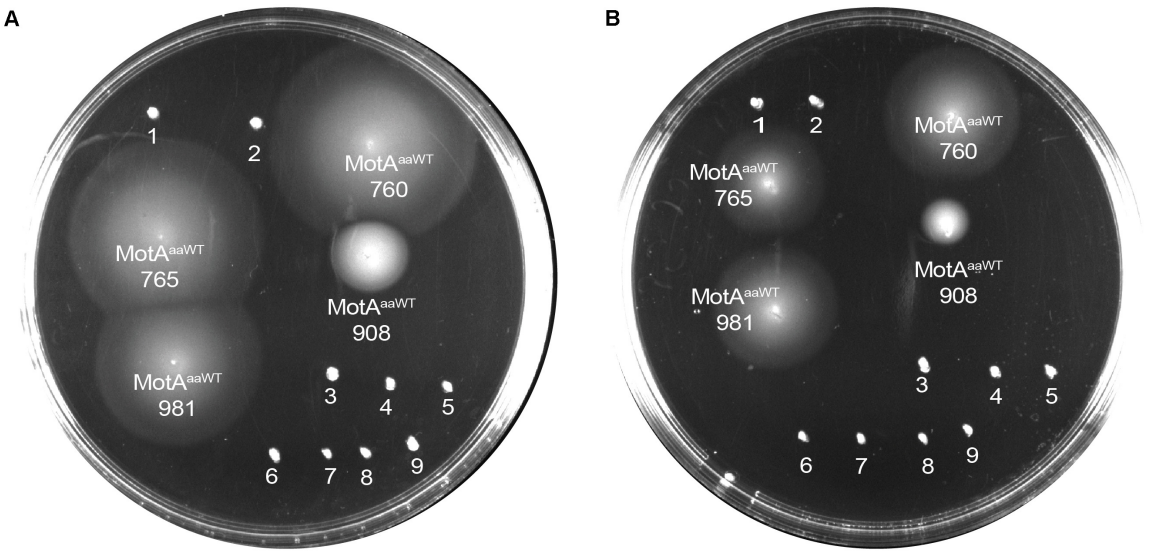

FIGURE 6 | Compatibility of MotB-ASRs with *Aquifex aeolicus* MotA^{aaWT} on minimal swim plates (with/without NaCl). Of the 13 MotB-ASRs, four restored motility in combination with MotA^{aaWT} in both the presence of Na^+ **(A)** and in the absence of Na^+ **(B)**. Legend: 1, MotA^{aaWT}MotB-ASR758; 2, MotA^{aaWT}MotB-ASR759; 3, MotA^{aaWT}MotB-ASR1024; 4, MotA^{aaWT}MotB-ASR1170; 5, MotA^{aaWT}MotB-ASR1239; 6, MotA^{aaWT}MotB-ASR1246; 7, MotA^{aaWT}MotB-ASR1457; 8, MotA^{aaWT}MotB-ASR1459; 9, MotA^{aaWT}MotB-ASR1501.

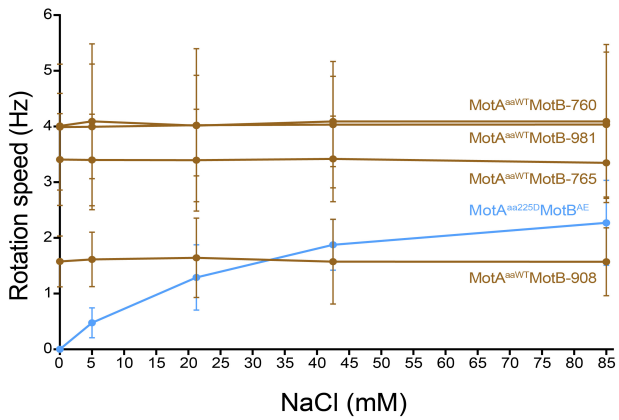

FIGURE 7 | Tethered cell rotational speeds of MotA^{aaWT}MotB-ASRs vs. extracellular concentration of Na^+. Rotational speed measured by tethered cell for varying extracellular concentrations of Na^+ showed that the four *A. aeolicus* compatible MotB-ASRs rotated independently of external concentration of Na^+ (MotB-ASR908, MotB-ASR765, MotB-ASR981, MotB-ASR760, dark brown colored lines). This is in contrast to the control sodium-motile *A. aeolicus* point mutant MotA in combination with *A. aeolicus-E. coli* chimeric MotB (MotA^{aa225D} MotB^{AE}, blue line).

DISCUSSION

The bacterial flagellar motor is a nanomachine powered by the translocation of specific ions across the cell membrane (Sowa and Berry, 2008). Initially, H^+ and Na^+ using bacteria were the primary interests of study but the gradual discovery of bacteria utilizing other ions, such as K^+, Rb^+, Mg^{2+}, Ca^{2+}, or Sr^{2+}, has raised the question about the origin and mechanism of the ion selectivity of bacterial flagellar motors (Li et al., 2011; Terahara et al., 2012; Minamino and Imada, 2015; Imazawa et al., 2016; Ito and Takahashi, 2017). The reliable answer to this question is still not clear as it is not known whether the original swimmer was sodium or proton powered (Schirrmeister et al., 2015). The development of ancestral reconstruction has created the opportunity to recreate historical scenarios using statistical phylogenetics and microbial engineering (Hochberg and Thornton, 2017). In this study, we tried to reconstruct the ancestral MotB protein and engineered them to evaluate their characteristics.

For the reconstruction of ancestral MotB stator protein, we generated a phylogeny of 757 MotB homologs. We focused on engineering the TM and plug region of ancestral MotB as this region controls ion selectivity and has been engineered to make functional chimeras (Asai et al., 2000; Ito et al., 2005; Nishino et al., 2015). Our phylogenies were restricted to include essential D32 to ensure functionality, and we further restricted the phylogenies to include FAD/YAD/LAD in residues 30–32 to have the best chance of generating functional reconstructions, and to examine the effect of residue changes and adaptation at 30F/Y/L to probe correlation with H^+ or Na^+ ion selection and compare with previous work (Ishida et al., 2019; **Supplementary Figure 2B**).

The swim plate assay results of this study showed that all the MotB-ASRs were able to swim both in the presence and absence of Na^+ in the combination with MotA. Also, our MotB-ASRs were not inhibited by the sodium inhibitor phenamil that is a general inhibitor of sodium dependent motors (Atsumi et al., 1990), and amiloride and its derivatives do not inhibit MotAB (Terahara et al., 2008). Na^+ independent motility and resistance to Na^+ blocker together imply that our ancestral

B-subunits function similarly to proton-powered MotB, and our alterations in the TM domain converted a Na^+ dependent swimmer (PomAPotB) into a sodium independent swimmer (MotAPomAMotB-ASR).

Tethered cell assay results confirmed that external Na^+ concentrations did not affect the rotation speed of all MotB-ASRs (**Figure 5**), whereas the rotation speed of the control Na^+ swimmer showed a strong dependence on external sodium concentration (**Figure 5**). The sodium-independence of MotB-ASR swimming speed matches previous measurements for proton-powered MotAB (Imazawa et al., 2016). This result indicates that our resurrected reconstructions are more MotB-like than PomB-like.

Our MotB-ASRs included both YAD and FAD motifs, however, regardless of F/Y at residue 30, all MotB-ASRs displayed proton-based functionality. Previously we quantified the correlation between F/Y and sodium/proton motility in a test set of known sodium and proton swimmers (Ishida et al., 2019). There are known exceptions to the overall trend, such as proton-motile *Pseudomonas aeruginosa* with a FAD motif, but the overall correlation was strong, and both generalized and phylogenetic linear regressions indicated significant correlation ($p < 0.05$) in our previous work. We reexamined our previous data set, and supplemented this with our new ASRs. When we added the new sequences corresponding to our ASRs, which were diverse in F/Y but uniform in phenotype, this resulted in the F/Y locus, in our analysis, having a much weaker correlation with a sodium/proton phenotype. This is further evidence that FAD/YAD in MotB is unlikely to dictate selectivity on its own, alongside ours and others' previous work (Asai et al., 2000, 2003; Sudo et al., 2009).

Additionally, the compatibility of our MotB-ASR with ancient *Aquifex aeolicus* MotA ($MotA^{aaWT}$) and subsequent Na^+ independent swimming properties provided further evidence that the MotB-ASRs generated here are more likely to be proton-powered MotB. In agreement, our ASRs could not restore motility with the mutant *A. aeolicus* MotA ($MotA^{aa225D}$) which had been previously shown to enable sodium-dependent motility (Takekawa et al., 2015).

The primacy of sodium energetics is becoming clear in the case of ATPases (Mulkidjanian et al., 2008), but for flagellar motors this is still an open question. Here, we observed our ASRs to function in a MotB-like sodium-independent manner, and to be functional in the presence of ($MotA^{aaWT}$). Previous work has suggested sodium-energized flagellar rotation predates proton-powered bacterial motion, due to the early diverging *A. aeolicus* being observed to be sodium-dependent (Takekawa et al., 2015). We have not attempted here the difficult task of definitively resolving ancient evolutionary history. To answer which ion holds energetic primacy for the BFM would require more comprehensive phylogenies, across multiple flagellar proteins, to identify and resurrect the best estimate of the historical stator complex at the time of divergence. Here we have demonstrated that such approaches show strong promise: ancestral reconstruction and protein engineering can generate novel stators that are both functional and useful and can be used to probe questions surrounding which residues dictate ion-selectivity.

DATA AVAILABILITY STATEMENT

The datasets presented in this study can be found in online repositories. The names of the repository/repositories and accession number(s) can be found in the article/**Supplementary Material**.

AUTHOR CONTRIBUTIONS

MI and MB designed the experiments and executed molecular biology and microbiology. AL and MB executed bioinformatics surrounding SSNs, correlation, and phylogenetics. NM executed bioinformatics surrounding phylogenetics. MB supervised the design, execution and writing of the project. All authors contributed to writing and revision of the manuscript.

FUNDING

This research was supported by the UNSW Scientia Research Fellowship, the CSIRO Synthetic Biology Future Science Platform 2018 Project Grant, and ARC Discovery Project DP190100497.

ACKNOWLEDGMENTS

We acknowledge the gift of *A. aeolicus* plasmids pNT7 ($MotA^{aaWT}$) and pNT11 ($MotB^{AE}$) from Prof. Seiji Kojima and Prof. Michio Homma and the gift of pDB108 plasmid (*E. coli,* MotA and MotB) and strain RP3087 (ΔMotB) from Prof. David F. Blair.

SUPPLEMENTARY MATERIAL

The Supplementary Material for this article can be found online at: https://www.frontiersin.org/articles/10.3389/fmicb.2020.625837/full#supplementary-material

REFERENCES

Abby, S. S., and Rocha, E. P. C. (2012). The Non-Flagellar Type III Secretion System Evolved from the Bacterial Flagellum and Diversified into Host-Cell Adapted Systems. *PLoS Genet.* 8:e1002983. doi: 10.1371/journal.pgen.1002983

Akiva, E., Copp, J. N., Tokuriki, N., and Babbitt, P. C. (2017). Evolutionary and molecular foundations of multiple contemporary functions of the nitroreductase superfamily. *Proc. Natl. Acad. Sci. U S A.* 114, E9549–E9558. doi: 10.1073/pnas.1706849114

Armitage, J. P. (2007). "Bacterial Taxis," in *Encyclopedia of Life Sciences*, ed. Wiley (New Jersey, NJ: Wiley-Blackwell).

Asai, Y., Kawagishi, I., Sockett, R. E., and Homma, M. (2000). Coupling ion specificity of chimeras between H^+- and Na^+-driven motor proteins, MotB and PomB, in *Vibrio* polar

flagella. *EMBO J.* 19, 3639–3648. doi: 10.1093/emboj/19.14.3639

Asai, Y., Yakushi, T., Kawagishi, I., and Homma, M. (2003). Ion-coupling determinants of Na^+-driven and H^+-driven flagellar motors. *J. Mol. Biol.* 327, 453–463. doi: 10.1016/S0022-2836(03)00096-2

Atkinson, H. J., Morris, J. H., Ferrin, T. E., and Babbitt, P. C. (2009). Using sequence similarity networks for visualization of relationships across diverse protein superfamilies. *PLoS One* 4:e4345. doi: 10.1371/journal.pone.0004345

Atsumi, T., Sugiyama, S., Cragoe, E. J., and Imae, Y. (1990). Specific inhibition of the Na^+-driven flagellar motors of alkalophilic *Bacillus* strains by the amiloride analog phenamil. *J. Bacteriol.* 172, 1634–1639. doi: 10.1128/jb.172.3.1634-1639.1990

Berg, H. C. (2003). The rotary motor of bacterial flagella. *Annu. Rev. Biochem.* 72, 19–54. doi: 10.1146/annurev.biochem.72.121801.161737

Blair, D. F., and Berg, H. C. (1991). Mutations in the MotA protein of *Escherichia coli* reveal domains critical for proton conduction. *J. Mol. Biol.* 221, 1433–1442. doi: 10.1016/0022-2836(91)90943-Z

Blair, D. F., Kim, D. Y., and Berg, H. C. (1991). Mutant MotB proteins in *Escherichia coli*. *J. Bacteriol.* 173, 4049–4055. doi: 10.1128/jb.173.13.4049-4055.1991

Block, S. M., Blair, D. F., and Berg, H. C. (1989). Compliance of bacterial flagella measured with optical tweezers. *Nature* 338, 514–518. doi: 10.1038/338514a0

Braun, T. F., Al-Mawsawi, L. Q., Kojima, S., and Blair, D. F. (2004). Arrangement of Core Membrane Segments in the MotA/MotB Proton-Channel Complex of *Escherichia coli*. *Biochemistry* 43, 35–45. doi: 10.1021/bi035406d

Chiu, J., Tillett, D., Dawes, I. W., and March, P. E. (2008). Site-directed, Ligase-Independent Mutagenesis (SLIM) for highly efficient mutagenesis of plasmids greater than 8kb. *J. Microbiol. Methods* 73, 195–198. doi: 10.1016/j.mimet.2008.02.013

Crooks, G. E., Hon, G., Chandonia, J. M., and Brenner, S. E. (2004). WebLogo: A sequence logo generator. *Genome Res.* 14, 1188–1190. doi: 10.1101/gr.849004

Dean, G. E., Macnab, R. M., Stader, J., Matsumura, P., and Burks, C. (1984). Gene sequence and predicted amino acid sequence of the motA protein, a membrane-associated protein required for flagellar rotation in *Escherichia coli*. *J. Bacteriol.* 159, 991–999. doi: 10.1128/jb.159.3.991-999.1984

Deme, J. C., Johnson, S., Vickery, O., Muellbauer, A., Monkhouse, H., Griffiths, T., et al. (2020). Structures of the stator complex that drives rotation of the bacterial flagellum. *Nat. Microbiol.* 5, 1553–1564. doi: 10.1038/s41564-020-0788-8

Edgar, R. C. (2004). MUSCLE: A multiple sequence alignment method with reduced time and space complexity. *BMC Bioinformatics* 5:113. doi: 10.1186/1471-2105-5-113

Gaucher, E. A., Thomson, J. M., Burgan, M. F., and Benner, S. A. (2003). Inferring the palaeoenvironment of ancient bacteria on the basis of resurrected proteins. *Nature* 425, 285–288. doi: 10.1038/nature01977

Gerlt, J. A., Bouvier, J. T., Davidson, D. B., Imker, H. J., Sadkhin, B., Slater, D. R., et al. (2015). Enzyme function initiative-enzyme similarity tool (EFI-EST): A web tool for generating protein sequence similarity networks. *Biochim. Biophys. Acta Proteins Proteomics* 1854, 1019–1037. doi: 10.1016/j.bbapap.2015.04.015

Gurung, J. P., Gel, M., and Baker, M. A. B. (2020). Microfluidic techniques for separation of bacterial cells via taxis. *Microb. Cell* 7, 66–79. doi: 10.15698/mic2020.03.710

Hochberg, G. K. A., and Thornton, J. W. (2017). Reconstructing Ancient Proteins to Understand the Causes of Structure and Function. *Annu. Rev. Biophys.* 46, 247–269. doi: 10.1146/annurev-biophys-070816-033631

Howe, K., Bateman, A., and Durbin, R. (2002). QuickTree: Building huge neighbour-joining trees of protein sequences. *Bioinformatics* 18, 1546–1547. doi: 10.1093/bioinformatics/18.11.1546

Imazawa, R., Takahashi, Y., Aoki, W., Sano, M., and Ito, M. (2016). A novel type bacterial flagellar motor that can use divalent cations as a coupling ion. *Sci. Rep.* 6:19773. doi: 10.1038/srep19773

Ishida, T., Ito, R., Clark, J., Matzke, N. J., Sowa, Y., and Baker, M. A. B. (2019). Sodium-powered stators of the bacterial flagellar motor can generate torque in the presence of phenamil with mutations near the peptidoglycan-binding region. *Mol. Microbiol.* 111, 1689–1699. doi: 10.1111/mmi.14246

Ito, M., and Takahashi, Y. (2017). Nonconventional cation-coupled flagellar motors derived from the alkaliphilic *Bacillus* and *Paenibacillus* species. *Extremophiles* 21, 3–14. doi: 10.1007/s00792-016-0886-y

Ito, M., Terahara, N., Fujinami, S., and Krulwich, T. A. (2005). Properties of motility in *Bacillus subtilis* powered by the H^+-coupled MotAB flagellar stator. Na^+-coupled MotPS or hybrid stators MotAS or MotPB. *J. Mol. Biol.* 352, 396–408. doi: 10.1016/j.jmb.2005.07.030

Jarrell, K. F., and McBride, M. J. (2008). The surprisingly diverse ways that prokaryotes move. *Nat. Rev. Microbiol.* 6, 466–476. doi: 10.1038/nrmicro1900

Kacar, B., Garmendia, E., Tuncbag, N., Andersson, D. I., and Hughes, D. (2017a). Functional constraints on replacing an essential gene with its ancient and modern homologs. *mBio* 8:e01276-17. doi: 10.1128/mBio.01276-17

Kaçar, B., and Gaucher, E. (2012). "Towards the recapitulation of ancient history in the laboratory: combining synthetic biology with experimental evolution," in *Artificial Life 13: Proceedings of the 13th International Conference on the Simulation and Synthesis of Living Systems, ALIFE 2012* (East Lansing, MI), 11–18.

Kacar, B., Ge, X., Sanyal, S., and Gaucher, E. A. (2017b). Experimental evolution of Escherichia coli harboring an ancient translation protein. *J. Mol. Evol.* 84, 69–84. doi: 10.1007/s00239-017-9781-0

Kojima, S., and Blair, D. F. (2001). Conformational change in the stator of the bacterial flagellar Motor. *Biochemistry* 40, 13041–13050. doi: 10.1021/bi011263o

Kojima, S., Imada, K., Sakuma, M., Sudo, Y., Kojima, C., Minamino, T., et al. (2009). Stator assembly and activation mechanism of the flagellar motor by the periplasms region of MotB. *Mol. Microbiol.* 73, 710–718. doi: 10.1111/j.1365-2958.2009.06802.x

Kojima, S., Takao, M., Almira, G., Kawahara, I., Sakuma, M., Homma, M., et al. (2018). The Helix Rearrangement in the Periplasmic Domain of the Flagellar Stator B Subunit Activates Peptidoglycan Binding and Ion Influx. *Structure* 26, 590.e–598.e. doi: 10.1016/j.str.2018.02.016

Larkin, M. A., Blackshields, G., Brown, N. P., Chenna, R., Mcgettigan, P. A., McWilliam, H., et al. (2007). Clustal W and Clustal X version 2.0. *Bioinformatics* 23, 2947–2948. doi: 10.1093/bioinformatics/btm404

Li, N., Kojima, S., and Homma, M. (2011). Sodium-driven motor of the polar flagellum in marine bacteria *Vibrio*. *Genes Cells* 16, 985–999. doi: 10.1111/j.1365-2443.2011.01545.x

Minamino, T., and Imada, K. (2015). The bacterial flagellar motor and its structural diversity. *Trends Microbiol.* 23, 267–274. doi: 10.1016/j.tim.2014.12.011

Minamino, T., Terahara, N., Kojima, S., and Namba, K. (2018). Autonomous control mechanism of stator assembly in the bacterial flagellar motor in response to changes in the environment. *Mol. Microbiol.* 109, 723–734. doi: 10.1111/mmi.14092

Mitchell, J. G., and Kogure, K. (2006). Bacterial motility: Links to the environment and a driving force for microbial physics. *FEMS Microbiol. Ecol.* 55, 3–16. doi: 10.1111/j.1574-6941.2005.00003.x

Mulkidjanian, A. Y., Dibrov, P., and Galperin, M. Y. (2008). The past and present of sodium energetics: May the sodium-motive force be with you. *Biochim. Biophys. Acta Bioenerg.* 1777, 985–992. doi: 10.1016/j.bbabio.2008.04.028

Naganawa, S., and Ito, M. (2020). MotP subunit is critical for ion selectivity and evolution of a k^+-coupled flagellar motor. *Biomolecules* 10:691. doi: 10.3390/biom10050691

Nishino, Y., Onoue, Y., Kojima, S., and Homma, M. (2015). Functional chimeras of flagellar stator proteins between *E. coli* MotB and *Vibrio* PomB at the periplasmic region in *Vibrio* or *E. coli*. *Microbiologyopen* 4, 323–331. doi: 10.1002/mbo3.240

Nishiyama, M., and Kojima, S. (2012). Bacterial motility measured by a miniature chamber for high-pressure microscopy. *Int. J. Mol. Sci.* 13, 9225–9239. doi: 10.3390/ijms13079225

Onoue, Y., Iwaki, M., Shinobu, A., Nishihara, Y., Iwatsuki, H., Terashima, H., et al. (2019). Essential ion binding residues for Na^+ flow in stator complex of the *Vibrio* flagellar motor. *Sci. Rep.* 9:11216. doi: 10.1038/s41598-019-46038-6

Pallen, M. J., and Matzke, N. J. (2006). From the origin of species to the origin of bacterial flagella. *Nat. Rev. Microbiol.* 4, 784–790. doi: 10.1038/nrmicro1493

Paulick, A., Delalez, N. J., Brenzinger, S., Steel, B. C., Berry, R. M., Armitage, J. P., et al. (2015). Dual stator dynamics in the *Shewanella oneidensis* MR-1 flagellar motor. *Mol. Microbiol.* 96, 993–1001. doi: 10.1111/mmi.12984

Pion, M., Bshary, R., Bindschedler, S., Filippidou, S., Wick, L. Y., Job, D., et al. (2013). Gains of bacterial flagellar motility in a fungal world. *Appl. Environ. Microbiol.* 79, 6862–6867. doi: 10.1128/AEM.01393-13

Prangishvili, D., Bamford, D. H., Forterre, P., Iranzo, J., Koonin, E. V., and Krupovic, M. (2017). The enigmatic archaeal virosphere. *Nat. Rev. Microbiol.* 15, 724–739. doi: 10.1038/nrmicro.2017.125

Rambaut, A. (2014). *FigTree v1.4.2, A Graphical Viewer of Phylogenetic Trees*. Available Online at: http://tree.bio.ed.ac.uk/software/figtree/

Roujeinikova, A. (2008). Crystal structure of the cell wall anchor domain of MotB, a stator component of the bacterial flagellar motor: Implications for peptidoglycan recognition. *Proc. Natl. Acad. Sci. U S A.* 105, 10348–10353. doi: 10.1073/pnas.0803039105

Santiveri, M., Roa-Eguiara, A., Kühne, C., Wadhwa, N., Hu, H., Berg, H. C., et al. (2020). Structure and Function of Stator Units of the Bacterial Flagellar Motor. *Cell* 183, 244.e–257.e. doi: 10.1016/j.cell.2020.08.016

Sato, K., and Homma, M. (2000). Multimeric structure of PomA, a component of the Na^+-driven polar flagellar motor of *Vibrio alginolyticus*. *J. Biol. Chem.* 275, 20223–20228. doi: 10.1074/jbc.m002236200

Schirrmeister, B. E., Gugger, M., and Donoghue, P. C. (2015). Corrigendum to Cyanobacteria and the Great Oxidation Event: Evidence from genes and fossils. *Palaeontology* 58, 935–936. doi: 10.1111/pala.12193

Shih, P. M., and Matzke, N. J. (2013). Primary endosymbiosis events date to the later Proterozoic with cross-calibrated phylogenetic dating of duplicated ATPase proteins. *Proc. Natl. Acad. Sci. U S A.* 110, 12355–12360. doi: 10.1073/pnas.1305813110

Son, K., Brumley, D. R., and Stocker, R. (2015). Live from under the lens: Exploring microbial motility with dynamic imaging and microfluidics. *Nat. Rev. Microbiol.* 13, 761–775. doi: 10.1038/nrmicro3567

Sowa, Y., and Berry, R. M. (2008). Bacterial flagellar motor. *Q. Rev. Biophys.* 41, 103–132. doi: 10.1017/S0033583508004691

Sudo, Y., Terashima, H., Abe-Yoshizumi, R., Kojima, S., and Homma, M. (2009). Comparative study of the ion flux pathway in stator units of proton- and sodium-driven flagellar motors. *Biophysics* 5, 45–52. doi: 10.2142/biophysics.5.45

Takekawa, N., Nishiyama, M., Kaneseki, T., Kanai, T., Atomi, H., Kojima, S., et al. (2015). Sodium-driven energy conversion for flagellar rotation of the earliest divergent hyperthermophilic bacterium. *Sci. Rep.* 5:12711. doi: 10.1038/srep12711

Terahara, N., Fujisawa, M., Powers, B., Henkin, T. M., Krulwich, T. A., and Ito, M. (2006). An intergenic stem-loop mutation in the *Bacillus subtilis* ccpA-motPS operon increases motPS transcription and the MotPS contribution to motility. *J. Bacteriol.* 188, 2701–2705. doi: 10.1128/JB.188.7.2701-2705.2006

Terahara, N., Krulwich, T. A., and Ito, M. (2008). Mutations alter the sodium versus proton use of a *Bacillus clausii* flagellar motor and confer dual ion use on *Bacillus subtilis* motors. *Proc. Natl. Acad. Sci. U S A.* 105, 14359–14364. doi: 10.1073/pnas.0802106105

Terahara, N., Sano, M., and Ito, M. (2012). A *Bacillus* Flagellar Motor That Can Use Both Na^+ and K^+ as a Coupling Ion Is Converted by a Single Mutation to Use Only Na+. *PLoS One* 7:e46248. doi: 10.1371/journal.pone.0046248

Thormann, K. M., and Paulick, A. (2010). Tuning the flagellar motor. *Microbiology* 156(Pt 5), 1275–1283. doi: 10.1099/mic.0.029595-0

Thornton, J. W., Need, E., and Crews, D. (2003). Resurrecting the ancestral steroid receptor: Ancient origin of estrogen signaling. *Science* 301, 1714–1717. doi: 10.1126/science.1086185

Yang, Z. (2007). PAML 4: Phylogenetic analysis by maximum likelihood. *Mol. Biol. Evol.* 24, 1586–1591. doi: 10.1093/molbev/msm088

Yorimitsu, T., and Homma, M. (2001). Na^+-driven flagellar motor of *Vibrio*. *Biochim. Biophys. Acta Bioenerg.* 1505, 82–93. doi: 10.1016/S0005-2728(00)00279-6

Zhou, J., Fazzio, R. T., and Blair, D. F. (1995). Membrane topology of the MotA protein of *Escherichia coil*. *J. Mol. Biol.* 251, 237–242. doi: 10.1006/jmbi.1995.0431

Zhou, J., Sharp, L. L., Tang, H. L., Lloyd, S. A., Billings, S., Braun, T. F., et al. (1998). Function of protonatable residues in the flagellar motor of *Escherichia coli*: A critical role for Asp 32 of MotB. *J. Bacteriol.* 180, 2729–2735. doi: 10.1128/jb.180.10.2729-2735.1998

Conflict of Interest: The authors declare that the research was conducted in the absence of any commercial or financial relationships that could be construed as a potential conflict of interest.

frontiers in Microbiology

CORRECTION
published: 19 March 2021
doi: 10.3389/fmicb.2021.650373

Corrigendum: Ancestral Sequence Reconstructions of MotB Are Proton-Motile and Require MotA for Motility

Md Imtiazul Islam[1], *Angela Lin*[1], *Yu-Wen Lai*[1], *Nicholas J. Matzke*[2] *and Matthew A. B. Baker*[1,3]*

[1] School of Biotechnology and Biomolecular Sciences (BABS), University of New South Wales, Sydney, NSW, Australia, [2] School of Biological Sciences, University of Auckland, Auckland, New Zealand, [3] CSIRO Synthetic Biology Future Science Platform, Brisbane, QLD, Australia

Keywords: motility, flagellar and chemotaxis, stator, ancestral sequence reconstruction, ion-selectivity

OPEN ACCESS

Edited and reviewed by:
Masahiro Ito,
Toyo University, Japan

***Correspondence:**
Matthew A. B. Baker
matthew.baker@unsw.edu.au

Specialty section:
This article was submitted to Microbial Physiology and Metabolism, a section of the journal Frontiers in Microbiology

Received: *07 January 2021*
Accepted: *11 February 2021*
Published: *19 March 2021*

Citation:
Islam MI, Lin A, Lai Y-W, Matzke NJ and Baker MAB (2021) Corrigendum: Ancestral Sequence Reconstructions of MotB Are Proton-Motile and Require MotA for Motility. Front. Microbiol. 12:650373. doi: 10.3389/fmicb.2021.650373

A Corrigendum on

Ancestral Sequence Reconstructions of MotB Are Proton-Motile and Require MotA for Motility

by Islam, M. I., Lin, A., Lai, Y.-W., Matzke, N. J., and Baker, M. A. B. (2020). Front. Microbiol. 11:625837. doi: 10.3389/fmicb.2020.625837

In the original article, in the **Introduction**, **paragraph four**, we referenced previous work on ancestral reconstruction. We would like to add a further sentence and three additional citations for the work that first demonstrated the resurrection of ancient genes into contemporary hosts to form ancient modern hybrids and examine function *in vivo*:

It is possible to then resurrect the ancestral proteins corresponding to these inferred sequences and characterize their *in vitro* biological and biochemical properties (Gaucher et al., 2003; Thornton et al., 2003). Furthermore, ancient proteins can be expressed in contemporary hosts to examine the function of ancient proteins *in vivo*, and their integration and subsequent adaptation in ancient-modern hybrids (Kaçar and Gaucher, 2012; Kacar et al., 2017a,b).

Whilst our work does not explore subsequent adaptation of these ancient-modern hybrids, citation of these references is appropriate to give appropriate credit and to guide the reader to consider the research in ancestral reconstruction that has enabled our work.

The authors apologize for this error and state that this does not change the scientific conclusions of the article in any way. The original article has been updated.

REFERENCES

Gaucher, E. A., Thomson, J. M., Burgan, M. F., and Benner, S. A. (2003). Inferring the palaeoenvironment of ancient bacteria on the basis of resurrected proteins. *Nature* 425, 285–288. doi: 10.1038/nature01977

Kacar, B., Garmendia, E., Tuncbag, N., Andersson, D. I., and Hughes, D. (2017a). Functional constraints on replacing an essential gene with its ancient and modern homologs. *mBio* 8:e01276-17. doi: 10.1128/mBio.01276-17

Kaçar, B., and Gaucher, E. (2012). "Towards the recapitulation of ancient history in the laboratory: combining synthetic biology with experimental evolution," in *Artificial Life 13: Proceedings of the 13th International Conference on the Simulation and Synthesis of Living Systems, ALIFE 2012* (East Lansing, MI), 11–18.

Kacar, B., Ge, X., Sanyal, S., and Gaucher, E. A. (2017b). Experimental evolution of Escherichia coli harboring an ancient translation protein. *J. Mol. Evol.* 84, 69–84. doi: 10.1007/s00239-017-9781-0

Thornton, J. W., Need, E., and Crews, D. (2003). Resurrecting the ancestral steroid receptor: ancient origin of estrogen signaling. *Science* 301, 1714–1717. doi: 10.1126/science.1086185

frontiers in Microbiology

MINI REVIEW
published: 11 March 2021
doi: 10.3389/fmicb.2021.639490

The Structure, Composition, and Role of Periplasmic Stator Scaffolds in Polar Bacterial Flagellar Motors

Xiaotian Zhou[1,2] *and Anna Roujeinikova*[1,2,3]*

[1]*Infection and Immunity Program, Monash Biomedicine Discovery Institute, Monash University, Clayton, VIC, Australia,* [2]*Department of Microbiology, Monash University, Clayton, VIC, Australia,* [3]*Department of Biochemistry and Molecular Biology, Monash University, Clayton, VIC, Australia*

In the bacterial flagellar motor, the cell-wall-anchored stator uses an electrochemical gradient across the cytoplasmic membrane to generate a turning force that is applied to the rotor connected to the flagellar filament. Existing theoretical concepts for the stator function are based on the assumption that it anchors around the rotor perimeter by binding to peptidoglycan (P). The existence of another anchoring region on the motor itself has been speculated upon, but is yet to be supported by binding studies. Due to the recent advances in electron cryotomography, evidence has emerged that polar flagellar motors contain substantial proteinaceous periplasmic structures next to the stator, without which the stator does not assemble and the motor does not function. These structures have a morphology of disks, as is the case with *Vibrio* spp., or a round cage, as is the case with *Helicobacter pylori*. It is now recognized that such additional periplasmic components are a common feature of polar flagellar motors, which sustain higher torque and greater swimming speeds compared to peritrichous bacteria such as *Escherichia coli* and *Salmonella enterica*. This review summarizes the data available on the structure, composition, and role of the periplasmic scaffold in polar bacterial flagellar motors and discusses the new paradigm for how such motors assemble and function.

Keywords: bacterial flagellar motor, structure and function, polar flagellum, torque, electron cryotomography

OPEN ACCESS

Edited by:
Matt Arthur Baker,
University of New South Wales, Australia

Reviewed by:
Morgan Beeby,
Imperial College London, United Kingdom
Dipshikha Chakravortty,
Indian Institute of Science (IISc), India

***Correspondence:**
Anna Roujeinikova
anna.roujeinikova@monash.edu

Specialty section:
This article was submitted to Microbial Physiology and Metabolism, a section of the journal Frontiers in Microbiology

Received: *09 December 2020*
Accepted: *16 February 2021*
Published: *11 March 2021*

Citation:
Zhou X and Roujeinikova A (2021) The Structure, Composition, and Role of Periplasmic Stator Scaffolds in Polar Bacterial Flagellar Motors. Front. Microbiol. 12:639490. doi: 10.3389/fmicb.2021.639490

OVERVIEW OF THE BACTERIAL FLAGELLUM

The flagellum (**Figure 1**) comprises the basal body, hook, and filament. The basal body functions as a rotary motor; the turning force (torque) generated by it is transmitted through the hook to the filament, causing it to spin (Zhao et al., 2014; Carroll and Liu, 2020; Takekawa et al., 2020). Four main types of flagellar arrangement have been observed: monotrichious bacteria (e.g., *Vibrio cholerae*) carry a single polar flagellum; amphitrichous cells (*Campylobacter jejuni*) have one or more flagella at both poles; lophotrichous bacteria (*Helicobacter pylori*) have multiple flagella at one pole; while peritrichous bacteria (*Escherichia coli*) possess multiple flagella distributed over the cell envelope (Schuhmacher et al., 2015).

The flagellar motor is a remarkable nanoscale molecular engine that self-assembles in the cell wall from many protein components. Current knowledge about its structure and function has been largely acquired from studies on peritrichous bacteria. Flagellar assembly begins with

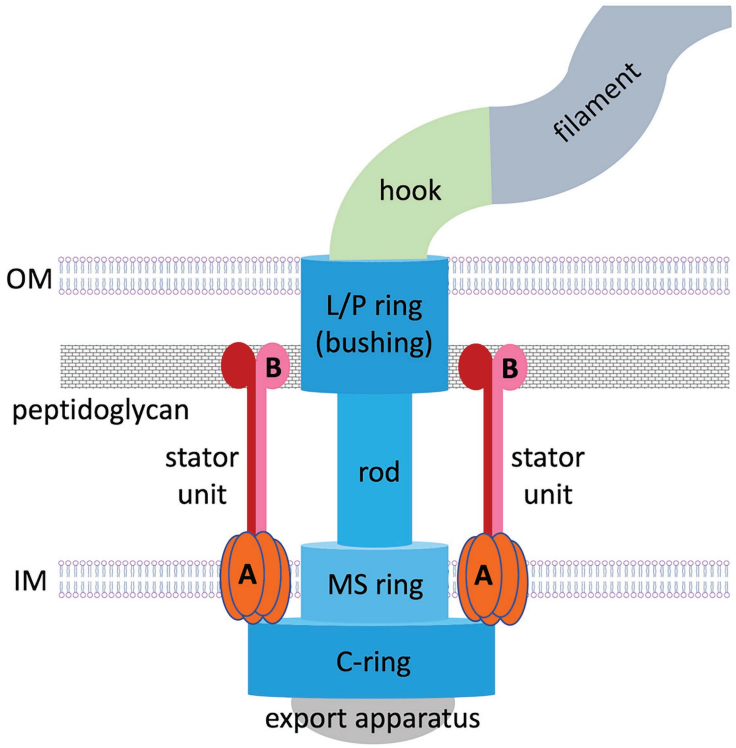

FIGURE 1 | Overall structure of a prototypical flagellar motor in Gram-negative bacteria. Basal body components are colored in shades of blue. Stator components (**A**, MotA; **B**, MotB) are colored in shades of red.

the membrane/supramembrane (MS) ring, export apparatus and switch complex [also known as the cytoplasmic ring (C-ring); Kubori et al., 1992; Li and Sourjik, 2011]. Then the rod and hook are assembled by transporting their components *via* the export apparatus (Minamino et al., 2008), a bushing for the rod [comprising peptidoglycan (P) and outer membrane (OM; lipopolysaccharide, L) rings] is added, and stator units assemble in a ring around the rotor perimeter.

The stator ring generates torque using an electrochemical gradient of protons or sodium ions across the inner membrane (IM). In proton-motive-force-driven motors, a single stator unit is an asymmetric assembly of five MotA subunits enclosing two MotB subunits (Deme et al., 2020; Santiveri et al., 2020). In sodium-motive-force-driven motors, the stator is composed of PomAB or MotPS complexes of the same stoichiometry. Existing theoretical concepts for why the stator itself does not spin are based on the assumption that it is anchored to the cell wall by MotB/PomB/MotS binding to P (Roujeinikova, 2008; O'Neill et al., 2011; Reboul et al., 2011; Andrews et al., 2017; Deme et al., 2020; Santiveri et al., 2020). However, visualization of the intact flagellar motor in whole cells (*in situ*), made possible by recent advances in electron cryotomography, revealed that polar flagellar motors contain a substantial proteinaceous periplasmic structure next to the stator (Murphy et al., 2006; Liu et al., 2009; Chen et al., 2011; Beeby et al., 2016; Qin et al., 2017), which has a morphology of disks, rings, or a round cage. It is now recognized that additional periplasmic components are a common feature of polar motors, which sustain higher torque and greater swimming speeds compared to peritrichous bacteria. Evidence has emerged that this periplasmic scaffold may serve as another anchoring region for the stator units. This review summarizes the data available of the structure, composition, and role of the periplasmic scaffold in polar bacterial flagellar motors and discusses the new paradigm for how these motors assemble and function.

EARLY STUDIES: THE DISCOVERY OF ADDITIONAL PERIPLASMIC DISKS

First evidence that polar flagellar motors possess additional periplasmic components that may be required for their function emerged from electron microscopy (EM) studies of bacterial preparations. Coulton and Murray (1977) observed proteinaceous concentric rings positioned laterally to the basal bodies in *(Aqua)spirillum serpens*. These rings formed 90-nm diameter disks associated with the periplasmic face of the OM. Subsequently, double-layered 90–150-nm diameter disks were observed at the same position in the motors of *C. jejuni* and *Campylobacter* (*Vibrio*) *fetus* subsp. *intestinalis* (Morooka et al., 1983). A similar disk was discovered in the motors of *V. cholerae* (Ferris et al., 1984) and *Wolinella succinogenes* (Engelhardt et al., 1993), but while the diameter

of the former did not exceed 41 nm, the average diameter of the latter was 170 nm, suggesting the architecture of this structure is species-specific.

Work on *W. succinogenes* was important, because it showed that the additional disks (from then on referred to as basal disks) are attached not only to the periplasmic face of the OM, but also to the basal body, and that the L/P disk (bushing) is integrated at the center of the basal disk (Kupper et al., 1989; Engelhardt et al., 1993). By that point, studies converged on the hypothesis that the basal disk may serve to anchor the L/P bushing of the motor to the cell wall and ensure correct positioning of the stator units around the rotor.

Interestingly, early work identified basal disks only in proteobacteria with polar flagella, but the possibility that additional periplasmic structures may exist in other flagellated bacteria could not be discounted. The discovery and characterization of such components was hampered by the fact that many are lost in the process of isolation of flagella for analysis by negative staining. It was not until recently that new techniques, such as electron cryotomography and high-throughput genome sequencing, could provide a detailed picture of the entire flagellar motor.

FIRST ELECTRON CRYOTOMOGRAPHY MOTOR RECONSTRUCTIONS: THE DISCOVERY AND CLASSIFICATION OF PERIPLASMIC SCAFFOLDS

The electron cryotomography technique (Oikonomou and Jensen, 2017) has a distinct advantage over traditional transmission EM methods as it allows visualization of the entire flagellar motor in frozen whole cells, without the need for fixation, dehydration, or staining. In 2006, a pioneering study of the spirochaete *Treponema primitia* provided the first 3D reconstruction of the polar motor that included the stator (Murphy et al., 2006). It also revealed a novel periplasmic structure next to the stator, termed the collar, which appears to be unique to Spirochaetes. Furthermore, the observed size of the stator on its periplasmic side could not be accounted for by MotB only, suggesting the presence of some other proteins. It was hypothesized that these extra structures serve as a periplasmic scaffold that recruits, organizes, and stabilizes the stator units. A subsequent electron cryotomography survey of the motor architectures (Chen et al., 2011) and related studies by other labs (Liu et al., 2009, 2010; Raddi et al., 2012) revealed that periplasmic scaffolds exist in the polar motors of many other species, but are absent in the motors of peritrichous bacteria, and that many polar flagellar motors are significantly more complex than the prototypical motors of *E. coli* and *Salmonella enterica*.

Flagellar motors can be classified according to four scaffold types: non-scaffold motors (**Figures 2A,B**); OM-associated scaffold motors (**Figures 2C,D**); IM-associated scaffold motors (**Figures 2E,F**); and integrated scaffold motors (**Figures 2G,H**).

An example of an OM-associated scaffold is the H/T/O-ring system found in the polar motor in *Vibrio alginolyticus* (Zhu et al., 2017, 2020; **Figure 2D**). The O-ring, associated with the external face of the OM, surrounds the base of the hook. The periplasmic H-ring, associated with the inner face of the OM, surrounds the L/P-ring. The periplasmic T-ring assembles at the outer rim of the H-ring, below the P-ring.

Inner-membrane-associated scaffolds have been found in polar motors driving the periplasmic flagella in Spirochaetes (Murphy et al., 2006; Liu et al., 2009, 2010; Raddi et al., 2012). They are exemplified by the collar-like structures seen in *T. primitia* (**Figure 2E**) and *Borrelia burgdorferi* (Qin et al., 2018; **Figure 2F**). The narrow part of these structures is embedded into the IM between the MS and stator rings, while the wider rim is positioned in the periplasm.

An integrated scaffold, spanning the periplasm and associated with both OM and IM, has been found in the polar motors of the closely related bacteria *H. pylori* and *C. jejuni* (Beeby et al., 2016; Qin et al., 2017; **Figures 2G,H**). The core of the scaffold is a round cage-like structure encircling the rod, the MS, and L/P rings. It is anchored to the IM on one side, and extends to the basal disk associated with the periplasmic face of the OM on the other.

MOLECULAR COMPOSITION OF PERIPLASMIC SCAFFOLDS

The OM-associated scaffold of the *Vibrio* spp. motor has been dissected in detail. The T-ring comprises MotX and MotY (Terashima et al., 2006), while the adjacent H-ring is made up of the OM lipoproteins (OMLPs) FlgO and FlgP and the periplasmic protein FlgT (Terashima et al., 2013; Beeby et al., 2016; Zhu et al., 2018, 2020). The protein make-up of the O-ring is not yet known.

The IM-associated scaffold of the spirochaetal motor has been studied extensively in *B. burgdorferi*. The base of the collar contains FlbB (Chen et al., 2011; Moon et al., 2016), which is anchored to the IM *via* its N-terminal transmembrane helix. Although the full protein composition of the collar is not yet known, the tetratricopeptide repeat (TPR) proteins BB0236 (Moon et al., 2018) and FlcA (Xu et al., 2020) have been identified as putative collar proteins that assemble onto the FlbB base.

The molecular composition of the integrated scaffold of the *H. pylori* motor is yet to be established. However, it is in a similar position to the integrated scaffold seen in *C. jejuni* (**Figures 2G,H**), and it is likely that the two scaffolds share at least some common components. The three main parts of the *C. jejuni* scaffold are: the basal disk associated with the periplasmic face of the OM; a medial disk around the rod; and a disk proximal to the IM (**Figure 2H**). The basal disk is formed by the OMLP FlgP (homologous to *Vibrio* FlgP), likely in complex with FlgQ (Beeby et al., 2016). The medial disk is composed of paralyzed flagellum protein A (PflA), a periplasmic TPR protein. The IM-proximal disk contains the TPR protein PflB, which is anchored to the IM *via* a single transmembrane helix. Proteins homologous to *C. jejuni* FlgP, PflA, and PflB are present in *H. pylori* (Rajagopala et al., 2007;

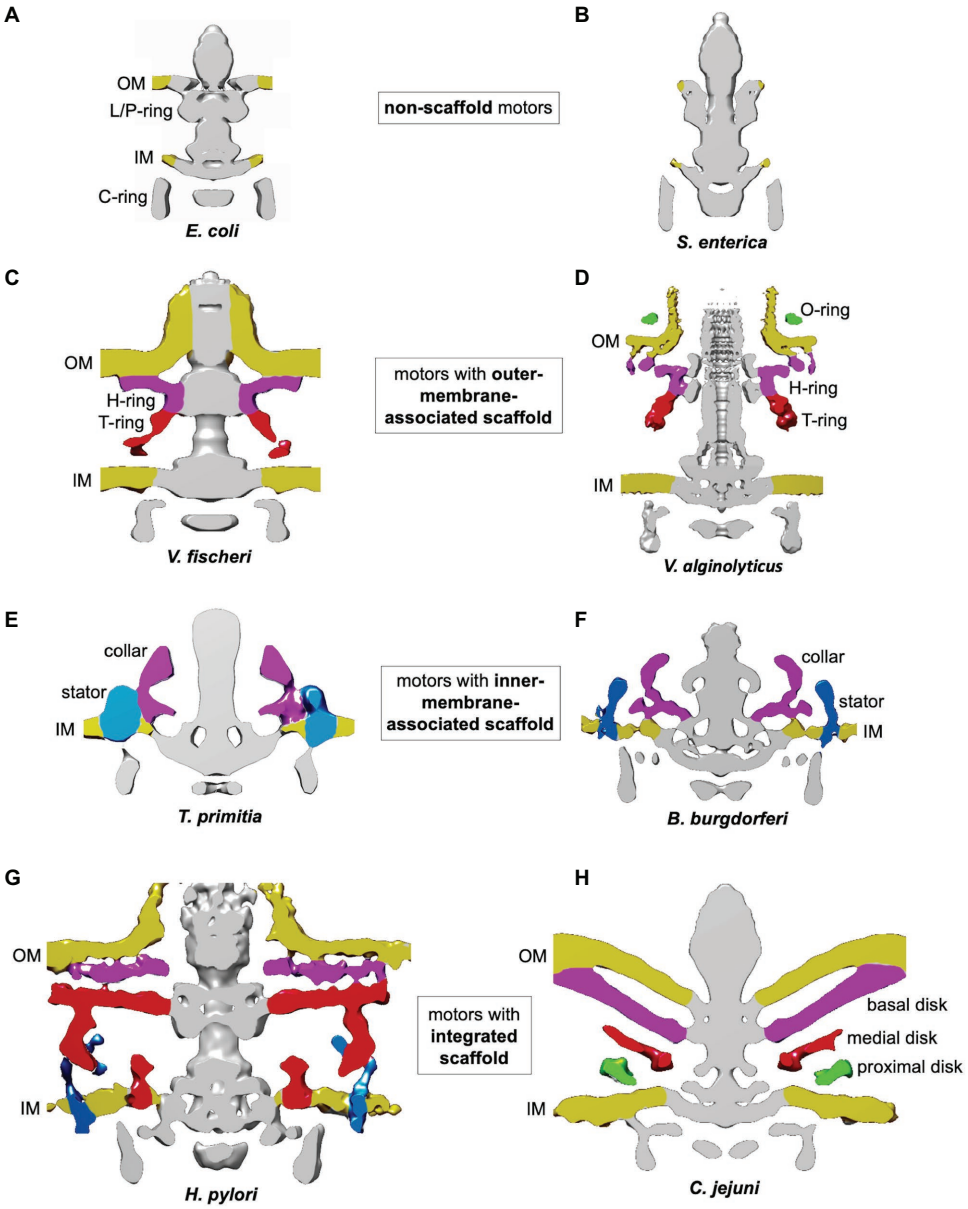

FIGURE 2 | Classification of flagellar motors based on their scaffolds. The figures were prepared using electron cryotomography maps for the flagellar motors from: **(A)** *Escherichia coli* (EMDB-5311; Chen et al., 2011); **(B)** *Salmonella enterica* (EMDB-5310; Chen et al., 2011); **(C)** *Vibrio fischeri* (EMDB 3155; Beeby et al., 2016); **(D)** *Vibrio alginolyticus* (EMDB-21027 and EMDB-21819; Carroll et al., 2020; Zhu et al., 2020); **(E)** *Treponema primitia* (EMDB-1235; Murphy et al., 2006); **(F)** *Borrelia burgdorferi* (EMDB-9122; Qin et al., 2018); **(G)** *Helicobacter pylori* (EMDB-8459; Qin et al., 2017); and **(H)** *Campylobacter jejuni* (EMDB-3150; Beeby et al., 2016).

Sommerlad and Hendrixson, 2007), suggesting *C. jejuni* and *H. pylori* scaffolds assemble in a similar manner.

THE ROLE OF THE INDIVIDUAL SCAFFOLD COMPONENTS

OM-Associated Scaffold of the *Vibrio* Motor

ΔflgT mutant cells lacked the H-ring and mostly produced periplasmic, rather than native, external flagella (Terashima et al., 2010; Zhu et al., 2018). Most of the H-ring was missing in Δ*flgP* mutant cells, which also lacked external hook/filament structures (Beeby et al., 2016). Thus, one apparent function of the H-ring is to mediate the OM penetration during the flagellum biogenesis. This notion is strengthened by reports that mutations in *flgO* also resulted in a reduced number of cells with external flagella (Martinez et al., 2009; Zhu et al., 2018). The other putative function of the H-ring is to anchor the flagellum to the cell wall, by associating with the OM *via* its medial part containing the OMLP FlgP (Morris et al., 2008), and

its outer part, containing the OMLP FlgO (Martinez et al., 2009; Zhu et al., 2018). In addition, the H-ring is required for stator ring assembly (Beeby et al., 2016).

The inner part of the T-ring is formed by MotY (Terashima et al., 2006; Zhu et al., 2017), which is likely anchored to peptidoglycan, as it contains a peptidoglycan-binding motif (Okunishi et al., 1996; Kojima et al., 2008). The stator-proximal edge of the T-ring is formed by MotX (Terashima et al., 2006; Zhu et al., 2017). In the absence of MotX or MotY, bacteria were non-motile (Gosink and Häse, 2000), and the stator units were not recruited to the cell pole (Terashima et al., 2006), indicating that the T-ring is also required for stator assembly.

Inner-Membrane-Associated Scaffold of the Spirochaetal Motor

ΔflbB, Δ*bb0236*, and Δ*flcA* mutant cells had less flagella per cell than the wild type, suggesting that all three putative collar components play an important role in the flagella biogenesis (Moon et al., 2016, 2018; Xu et al., 2020). Furthermore, all three mutants were non-motile, lacked the stator, and produced flagella that were abnormally oriented toward the cell pole rather than to the cell cylinder. This shows that the collar is required for correct orientation of the periplasmic flagella and assembly of the stator in *B. burgdorferi*.

Integrated Scaffold of the Campylobacterotal Motor

The basal disk in the integrated motor scaffold in *C. jejuni* is thought to play a similar role to that of the H-disk in the OM-associated scaffold in the *Vibrio* motor. Both structures contain the OMLP FlgP, although the *C. jejuni* and *Vibrio* proteins share only limited sequence similarity (Beeby et al., 2016). Deletion of *flgP* resulted in the loss of the disk and loss of functionality in both types of the motor, but in contrast to the *Vibrio fischeri* Δ*flgP* mutant, which lacked external hook/filament structures, the Δ*flgP* mutant of *C. jejuni* assembled normal-looking flagella (Sommerlad and Hendrixson, 2007). Another difference is that in the absence of the H-ring, the remainder of the scaffold (the T-ring) still assembled at least in some *Vibrio* species (Zhu et al., 2018), whereas the loss of the basal ring in *C. jejuni* resulted in the loss of the entire scaffold (Beeby et al., 2016). Despite the differences, the loss of function in Δ*flgP* mutants with either type of motor is attributable to the fact that the stator does not assemble in the absence of the basal ring or H-ring (Martinez et al., 2010).

The medial disk containing PflA is required for assembly of the proximal disk containing PflB, and Δ*pflA* mutants are non-motile (Yao et al., 1994) because their motors lack the stators (Beeby et al., 2016). MotB was shown to incorporate into the motor only in the presence of the proximal ring, supporting the hypothesis that upon assembly into the polar motor of *C. jejuni*, the stator units are anchored to the integrated scaffold *via* PflB.

IMPLICATIONS FOR THE MECHANISM OF GENERATION OF HIGHER TORQUE IN POLAR FLAGELLAR MOTORS

Thus, due to recent advances in electron cryotomography, extensive evidence has emerged that in contrast to peritrichous flagella, polar flagellar motors evolved diverse periplasmic scaffolds around the rotor, without which the stator does not assemble and the motor does not function. It is now widely accepted that upon assembly into the polar motors the stator units are anchored not only to peptidoglycan, but also to these scaffolds, and despite unique differences between the architectures of the OM-associated, IM-associated and integrated scaffolds, commonalities start to emerge with regards to their role in the stator function.

It is now recognized that the number of stator units recruited into the motor determines the total torque: the higher the number, the higher the force (Lele et al., 2013). Furthermore, evidence has emerged that, owing to the presence of the stabilizing scaffolds, stator rings in many polar motors are wider than in peritrichous motors (Chen et al., 2011; Beeby et al., 2016; Qin et al., 2017; Chaban et al., 2018; Chang et al., 2019). We now understand that larger-diameter stator rings not only accommodate more stator complexes, but also place them further away from the axis, resulting in a higher momentum of force produced by each complex, and hence higher overall torque. In peritrichous flagella of *S. enterica* and *E. coli*, at least 11 stator complexes can anchor to the peptidoglycan layer and P-ring (Reid et al., 2006; Hizukuri et al., 2010; O'Neill et al., 2011) and apply force on the 40-nm-diameter C-ring, producing ~1,300 pN nm torque (Reid et al., 2006; Thomas et al., 2006). In comparison, the C-ring in the polar motor of *H. pylori*, for example, is significantly larger (57 nM) and surrounded by half as many stator complexes (18; Qin et al., 2017), which is consistent with the observed higher torque (~3,600 pN nm; Celli et al., 2009). The C-ring in the spirochaetal polar motor is similarly large and surrounded by 16 stator complexes (Zhao et al., 2014; Chang et al., 2019), producing a torque of ~4,000 pN nm (Nakamura et al., 2014). Thus, the accumulated structural and functional data on the periplasmic scaffolds in the polar motors are consistent with their role as platforms that recruit a wider power ring to sustain higher torque.

IMPLICATIONS FOR EVOLUTIONARY ADAPTATION

The remarkable structural diversity of scaffolds in polar motors suggests they have evolved from a less complex ancestral motor, composed of the common core components seen today in peritrichous motors, by acquiring accessory proteins (Beeby et al., 2020). The existence of class- and genera-specific scaffold components (such as MotX/MotY in *Vibrio*, FlbB in Spirochaetes and PflA/PflB in Campylobacterota) is indicative of distinct evolutionary pathways resulting in motors with mechanical outputs that,

when combined with other factors, suit specific habitats. At one end of the torque spectrum is the polar motor of *Caulobacter crescentus*. To survive in its low-nutrient freshwater habitat, *C. crescentus* has evolved an efficient motor with no scaffolding structures (Rossmann et al., 2020) that uses a small stator ring comprising only 11 units. The economically low torque (∼350 pN nm; Li and Tang, 2006) is sufficient to propel the cell due to additional thrust created by the helical motion of the cell (Liu et al., 2014). At the other end of the spectrum is the high-torque motor of *H. pylori*. This microorganism resides within the very viscous mucous layer of the stomach (Hooi et al., 2017) and, apparently through natural selection, demonstrates unusually high motility in viscous media (Hazell et al., 1986). Together with the helical cell shape, the high torque, afforded by the wider stator ring supported by a periplasmic scaffold, allows *H. pylori* locomotion in high-viscosity environment.

The mechanism by which the scaffolds recruit and stabilize stator complexes remains enigmatic. TPR domains often serve as protein-protein interaction scaffolds (Blatch and Lässle, 1999), and their presence in FlbB, PflA, and PflB is consistent with their proposed stator scaffolding role. Dissecting the 3D architecture of the periplasmic scaffolds and unraveling the structural basis for their ability to recruit stator units will be a fascinating and worthy task. Achieving this goal will advance our knowledge about the mechanism of the bacterial flagellar motor, and our understanding of the convergent evolutionary pathways to higher-torque polar flagellar motors.

AUTHOR CONTRIBUTIONS

All authors listed have made a substantial, direct and intellectual contribution to the work, and approved it for publication.

REFERENCES

Andrews, D. A., Nesmelov, Y. E., Wilce, M. C., and Roujeinikova, A. (2017). Structural analysis of variant of *Helicobacter pylori* MotB in its activated form, engineered as chimera of MotB and leucine zipper. *Sci. Rep.* 7:13435. doi: 10.1038/s41598-017-13421-0

Beeby, M., Ferreira, J. L., Tripp, P., Albers, S. -V., and Mitchell, D. R. (2020). Propulsive nanomachines: the convergent evolution of archaella, flagella and cilia. *FEMS Microbiol. Rev.* 44, 253–304. doi: 10.1093/femsre/fuaa006

Beeby, M., Ribardo, D. A., Brennan, C. A., Ruby, E. G., Jensen, G. J., and Hendrixson, D. R. (2016). Diverse high-torque bacterial flagellar motors assemble wider stator rings using a conserved protein scaffold. *Proc. Natl. Acad. Sci. U. S. A.* 113, E1917–E1926. doi: 10.1073/pnas.1518952113

Blatch, G. L., and Lässle, M. (1999). The tetratricopeptide repeat: a structural motif mediating protein-protein interactions. *Bioessays* 21, 932–939. doi: 10.1002/(SICI)1521-1878(199911)21:11<932::AID-BIES5>3.0.CO;2-N

Carroll, B. L., and Liu, J. (2020). Structural conservation and adaptation of the bacterial flagella motor. *Biomolecules* 10:1492. doi: 10.3390/biom10111492

Carroll, B. L., Nishikino, T., Guo, W., Zhu, S., Kojima, S., Homma, M., et al. (2020). The flagellar motor of vibrio alginolyticus undergoes major structural remodeling during rotational switching. *Elife* 9:e61446. doi: 10.7554/eLife.61446

Celli, J. P., Turner, B. S., Afdhal, N. H., Keates, S., Ghiran, I., Kelly, C. P., et al. (2009). *Helicobacter pylori* moves through mucus by reducing mucin viscoelasticity. *Proc. Natl. Acad. Sci. U. S. A.* 106, 14321–14326. doi: 10.1073/pnas.0903438106

Chaban, B., Coleman, I., and Beeby, M. (2018). Evolution of higher torque in *Campylobacter*-type bacterial flagellar motors. *Sci. Rep.* 8:97. doi: 10.1038/s41598-017-18115-1

Chang, Y., Moon, K. H., Zhao, X., Norris, S. J., Motaleb, M. A., and Liu, J. (2019). Structural insights into flagellar stator-rotor interactions. *Elife* 8:e48979. doi: 10.7554/eLife.48979

Chen, S., Beeby, M., Murphy, G. E., Leadbetter, J. R., Hendrixson, D. R., Briegel, A., et al. (2011). Structural diversity of bacterial flagellar motors. *EMBO J.* 30, 2972–2981. doi: 10.1038/emboj.2011.186

Coulton, J. W., and Murray, R. G. (1977). Membrane-associated components of the bacterial flagellar apparatus. *Biochim. Biophys. Acta* 465, 290–310. doi: 10.1016/0005-2736(77)90080-3

Deme, J. C., Johnson, S., Vickery, O., Aron, A., Monkhouse, H., Griffiths, T., et al. (2020). Structures of the stator complex that drives rotation of the bacterial flagellum. *Nat. Microbiol.* 5, 1553–1564. doi: 10.1038/s41564-020-0788-8

Engelhardt, H., Schuster, S. C., and Baeuerlein, E. (1993). An archimedian spiral: the basal disk of the wolinella flagellar motor. *Science* 262, 1046–1048. doi: 10.1126/science.8235620

Ferris, F. G., Beveridge, T. J., Marceau-Day, M. L., and Larson, A. D. (1984). Structure and cell envelope associations of flagellar basal complexes of *Vibrio cholerae* and *Campylobacter fetus*. *Can. J. Microbiol.* 30, 322–333. doi: 10.1139/m84-048

Gosink, K. K., and Häse, C. C. (2000). Requirements for conversion of the Na^+-driven flagellar motor of *Vibrio cholerae* to the H^+-driven motor of *Escherichia coli*. *J. Bacteriol.* 182, 4234–4240. doi: 10.1128/JB.182.15.4234-4240.2000

Hazell, S. L., Lee, A., Brady, L., and Hennessy, W. (1986). *Campylobacter pyloridis* and gastritis: association with intercellular spaces and adaptation to an environment of mucus as important factors in colonization of the gastric epithelium. *J. Infect. Dis.* 153, 658–663. doi: 10.1093/infdis/153.4.658

Hizukuri, Y., Kojima, S., and Homma, M. (2010). Disulphide cross-linking between the stator and the bearing components in the bacterial flagellar motor. *J. Biochem.* 148, 309–318. doi: 10.1093/jb/mvq067

Hooi, J. K. Y., Lai, W. Y., Ng, W. K., Suen, M. M. Y., Underwood, F. E., Tanyingoh, D., et al. (2017). Global prevalence of *Helicobacter pylori* infection: systematic review and meta-analysis. *Gastroenterology* 153, 420–429. doi: 10.1053/j.gastro.2017.04.022

Kojima, S., Shinohara, A., Terashima, H., Yakushi, T., Sakuma, M., Homma, M., et al. (2008). Insights into the stator assembly of the *Vibrio* flagellar motor from the crystal structure of MotY. *Proc. Natl. Acad. Sci. U. S. A.* 105, 7696–7701. doi: 10.1073/pnas.0800308105

Kubori, T., Shimamoto, N., Yamaguchi, S., Namba, K., and Aizawa, S. -I. (1992). Morphological pathway of flagellar assembly in *Salmonella typhimurium*. *J. Mol. Biol.* 226, 433–446. doi: 10.1016/0022-2836(92)90958-M

Kupper, J., Wildhaber, I., Gao, Z., and Baeuerlein, E. (1989). Basal-body-associated disks are additional structural elements of the flagellar apparatus isolated from *Wolinella succinogenes*. *J. Bacteriol.* 171, 2803–2810. doi: 10.1128/JB.171.5.2803-2810.1989

Lele, P. P., Hosu, B. G., and Berg, H. C. (2013). Dynamics of mechanosensing in the bacterial flagellar motor. *Proc. Natl. Acad. Sci. U. S. A.* 110, 11839–11844. doi: 10.1073/pnas.1305885110

Li, H., and Sourjik, V. (2011). Assembly and stability of flagellar motor in *Escherichia coli*. *Mol. Microbiol.* 80, 886–899. doi: 10.1111/j.1365-2958.2011.07557.x

Li, G., and Tang, J. X. (2006). Low flagellar motor torque and high swimming efficiency of *Caulobacter crescentus* swarmer cells. *Biophys. J.* 91, 2726–2734. doi: 10.1529/biophysj.106.080697

Liu, B., Gulino, M., Morse, M., Tang, J. X., Powers, T. R., and Breuer, K. S. (2014). Helical motion of the cell body enhances *Caulobacter crescentus* motility. *Proc. Natl. Acad. Sci. U. S. A.* 111, 11252–11256. doi: 10.1073/pnas.1407636111

Liu, J., Howell, J. K., Bradley, S. D., Zheng, Y., Zhou, Z. H., and Norris, S. J. (2010). Cellular architecture of *Treponema pallidum*: novel flagellum, periplasmic

cone, and cell envelope as revealed by cryo electron tomography. *J. Mol. Biol.* 403, 546–561. doi: 10.1016/j.jmb.2010.09.020

Liu, J., Lin, T., Botkin, D. J., McCrum, E., Winkler, H., and Norris, S. J. (2009). Intact flagellar motor of *Borrelia burgdorferi* revealed by cryo-electron tomography: evidence for stator ring curvature and rotor/C-ring assembly flexion. *J. Bacteriol.* 191:5026. doi: 10.1128/JB.00340-09

Martinez, R. M., Dharmasena, M. N., Kirn, T. J., and Taylor, R. K. (2009). Characterization of two outer membrane proteins, FlgO and FlgP, that influence *Vibrio cholerae* motility. *J. Bacteriol.* 191, 5669–5679. doi: 10.1128/JB.00632-09

Martinez, R. M., Jude, B. A., Kirn, T. J., Skorupski, K., and Taylor, R. K. (2010). Role of FlgT in anchoring the flagellum of *Vibrio cholerae*. *J. Bacteriol.* 192, 2085–2092. doi: 10.1128/JB.01562-09

Minamino, T., Imada, K., and Namba, K. (2008). Mechanisms of type III protein export for bacterial flagellar assembly. *Mol. Biosyst.* 4, 1105–1115. doi: 10.1039/b808065h

Moon, K. H., Zhao, X., Manne, A., Wang, J., Yu, Z., Liu, J., et al. (2016). Spirochetes flagellar collar protein FlbB has astounding effects in orientation of periplasmic flagella, bacterial shape, motility, and assembly of motors in Borrelia burgdorferi. *Mol. Microbiol.* 102, 336–348. doi: 10.1111/mmi.13463

Moon, K. H., Zhao, X., Xu, H., Liu, J., and Motaleb, M. A. (2018). A tetratricopeptide repeat domain protein has profound effects on assembly of periplasmic flagella, morphology and motility of the Lyme disease spirochete *Borrelia burgdorferi*. *Mol. Microbiol.* 110, 634–647. doi: 10.1111/mmi.14121

Morooka, T., Umeda, A., and Amako, K. (1983). Morphological differences in flagella in *Campylobacter fetus* subsp. *intestinalis* and *C. fetus* subsp. *jejuni*. *Microbiol. Immunol.* 27, 655–662. doi: 10.1111/j.1348-0421.1983.tb00628.x

Morris, D. C., Peng, F., Barker, J. R., and Klose, K. E. (2008). Lipidation of an FlrC-dependent protein is required for enhanced intestinal colonization by *Vibrio cholerae*. *J. Bacteriol.* 190, 231–239. doi: 10.1128/JB.00924-07

Murphy, G. E., Leadbetter, J. R., and Jensen, G. J. (2006). *In situ* structure of the complete *Treponema primitia* flagellar motor. *Nature* 442, 1062–1064. doi: 10.1038/nature05015

Nakamura, S., Leshansky, A., Magariyama, Y., Namba, K., and Kudo, S. (2014). Direct measurement of helical cell motion of the spirochete *Leptospira*. *Biophys. J.* 106, 47–54. doi: 10.1016/j.bpj.2013.11.1118

Oikonomou, C. M., and Jensen, G. J. (2017). Cellular electron cryotomography: toward structural biology in situ. *Annu. Rev. Biochem.* 86, 873–896. doi: 10.1146/annurev-biochem-061516-044741

Okunishi, I., Kawagishi, I., and Homma, M. (1996). Cloning and characterization of *motY*, a gene coding for a component of the sodium-driven flagellar motor in *Vibrio alginolyticus*. *J. Bacteriol.* 178, 2409–2415. doi: 10.1128/JB.178.8.2409-2415.1996

O'Neill, J., Xie, M., Hijnen, M., and Roujeinikova, A. (2011). Role of the MotB linker in the assembly and activation of the bacterial flagellar motor. *Acta Crystallogr. D Biol. Crystallogr.* 67, 1009–1016. doi: 10.1107/S0907444911041102

Qin, Z., Lin, W. -t., Zhu, S., Franco, A. T., Liu, J., and Zhulin, I. B. (2017). Imaging the motility and chemotaxis machineries in *Helicobacter pylori* by cryo-electron tomography. *J. Bacteriol.* 199:e00695–16. doi: 10.1128/JB.00695-16

Qin, Z., Tu, J., Lin, T., Norris, S. J., Li, C., Motaleb, M. A., et al. (2018). Cryo-electron tomography of periplasmic flagella in *Borrelia burgdorferi* reveals a distinct cytoplasmic ATPase complex. *PLoS Biol.* 16:e3000050. doi: 10.1371/journal.pbio.3000050

Raddi, G., Morado, D. R., Yan, J., Haake, D. A., Yang, X. F., and Liu, J. (2012). Three-dimensional structures of pathogenic and saprophytic *Leptospira* species revealed by cryo-electron tomography. *J. Bacteriol.* 194, 1299–1306. doi: 10.1128/jb.06474-11

Rajagopala, S. V., Titz, B., Goll, J., Parrish, J. R., Wohlbold, K., McKevitt, M. T., et al. (2007). The protein network of bacterial motility. *Mol. Syst. Biol.* 3:128. doi: 10.1038/msb4100166

Reboul, C. F., Andrews, D. A., Nahar, M. F., Buckle, A. M., and Roujeinikova, A. (2011). Crystallographic and molecular dynamics analysis of loop motions unmasking the peptidoglycan-binding site in stator protein MotB of flagellar motor. *PLoS One* 6:e18981. doi: 10.1371/journal.pone.0018981

Reid, S. W., Leake, M. C., Chandler, J. H., Lo, C. J., Armitage, J. P., and Berry, R. M. (2006). The maximum number of torque-generating units in the flagellar motor of *Escherichia coli* is at least 11. *Proc. Natl. Acad. Sci. U. S. A.* 103, 8066–8071. doi: 10.1073/pnas.0509932103

Rossmann, F. M., Hug, I., Sangermani, M., Jenal, U., and Beeby, M. (2020). In situ structure of the *Caulobacter crescentus* flagellar motor and visualization of binding of a CheY-homolog. *Mol. Microbiol.* 114, 443–453. doi: 10.1111/mmi.14525

Roujeinikova, A. (2008). Crystal structure of the cell wall anchor domain of MotB, a stator component of the bacterial flagellar motor: implications for peptidoglycan recognition. *Proc. Natl. Acad. Sci. U. S. A.* 105, 10348–10353. doi: 10.1073/pnas.0803039105

Santiveri, M., Roa-Eguiara, A., Kühne, C., Wadhwa, N., Hu, H., Berg, H. C., et al. (2020). Structure and function of stator units of the bacterial flagellar motor. *Cell* 183, 244.e16–257.e16. doi: 10.1016/j.cell.2020.08.016

Schuhmacher, J. S., Thormann, K. M., and Bange, G. (2015). How bacteria maintain location and number of flagella? *FEMS Microbiol. Rev.* 39, 812–822. doi: 10.1093/femsre/fuv034

Sommerlad, S. M., and Hendrixson, D. R. (2007). Analysis of the roles of FlgP and FlgQ in flagellar motility of *Campylobacter jejuni*. *J. Bacteriol.* 189, 179–186. doi: 10.1128/JB.01199-06

Takekawa, N., Imada, K., and Homma, M. (2020). Structure and energy-conversion mechanism of the bacterial Na^+-driven flagellar motor. *Trends Microbiol.* 28, 719–731. doi: 10.1016/j.tim.2020.03.010

Terashima, H., Fukuoka, H., Yakushi, T., Kojima, S., and Homma, M. (2006). The *Vibrio* motor proteins, MotX and MotY, are associated with the basal body of Na^+-driven flagella and required for stator formation. *Mol. Microbiol.* 62, 1170–1180. doi: 10.1111/j.1365-2958.2006.05435.x

Terashima, H., Koike, M., Kojima, S., and Homma, M. (2010). The flagellar basal body-associated protein FlgT is essential for a novel ring structure in the sodium-driven *Vibrio* motor. *J. Bacteriol.* 192, 5609–5615. doi: 10.1128/JB.00720-10

Terashima, H., Li, N., Sakuma, M., Koike, M., Kojima, S., Homma, M., et al. (2013). Insight into the assembly mechanism in the supramolecular rings of the sodium-driven *Vibrio* flagellar motor from the structure of FlgT. *Proc. Natl. Acad. Sci. U. S. A.* 110, 6133–6138. doi: 10.1073/pnas.1222655110

Thomas, D. R., Francis, N. R., Xu, C., and DeRosier, D. J. (2006). The three-dimensional structure of the flagellar rotor from a clockwise-locked mutant of *Salmonella enterica* serovar Typhimurium. *J. Bacteriol.* 188, 7039–7048. doi: 10.1128/JB.00552-06

Xu, H., He, J., Liu, J., and Motaleb, M. A. (2020). BB0326 is responsible for the formation of periplasmic flagellar collar and assembly of the stator complex in *Borrelia burgdorferi*. *Mol. Microbiol.* 113, 418–429. doi: 10.1111/mmi.14428

Yao, R., Burr, D. H., Doig, P., Trust, T. J., Niu, H., and Guerry, P. (1994). Isolation of motile and non-motile insertional mutants of *Campylobacter jejuni*: the role of motility in adherence and invasion of eukaryotic cells. *Mol. Microbiol.* 14, 883–893. doi: 10.1111/j.1365-2958.1994.tb01324.x

Zhao, X., Norris, S. J., and Liu, J. (2014). Molecular architecture of the bacterial flagellar motor in cells. *Biochemistry* 53, 4323–4333. doi: 10.1021/bi500059y

Zhu, S., Nishikino, T., Hu, B., Kojima, S., Homma, M., and Liu, J. (2017). Molecular architecture of the sheathed polar flagellum in *Vibrio alginolyticus*. *Proc. Natl. Acad. Sci. U. S. A.* 114, 10966–10971. doi: 10.1073/pnas.1712489114

Zhu, S., Nishikino, T., Kojima, S., Homma, M., and Liu, J. (2018). The *Vibrio* H-ring facilitates the outer membrane penetration of the polar sheathed flagellum. *J. Bacteriol.* 200:e00387–18. doi: 10.1128/JB.00387-18

Zhu, S., Nishikino, T., Takekawa, N., Terashima, H., Kojima, S., Imada, K., et al. (2020). In situ structure of the *Vibrio* polar flagellum reveals a distinct outer membrane complex and its specific interaction with the stator. *J. Bacteriol.* 202:e00592–19. doi: 10.1128/jb.00592-19

Conflict of Interest: The authors declare that the research was conducted in the absence of any commercial or financial relationships that could be construed as a potential conflict of interest.

frontiers in Microbiology

ORIGINAL RESEARCH
published: 17 March 2021
doi: 10.3389/fmicb.2021.655239

Interdependent Polar Localization of FlhF and FlhG and Their Importance for Flagellum Formation of *Vibrio parahaemolyticus*

Erick Eligio Arroyo-Pérez[1,2] *and Simon Ringgaard*[2]*

[1] *Max Planck Institute for Terrestrial Microbiology, Marburg, Germany,* [2] *Department of Biology I, Microbiology, Ludwig-Maximilians-Universität München, Munich, Germany*

Failure of the cell to properly regulate the number and intracellular positioning of their flagella, has detrimental effects on the cells' swimming ability. The flagellation pattern of numerous bacteria is regulated by the NTPases FlhF and FlhG. In general, FlhG controls the number of flagella produced, whereas FlhF coordinates the position of the flagella. In the human pathogen *Vibrio parahaemolyticus*, its single flagellum is positioned and formed at the old cell pole. Here, we describe the spatiotemporal localization of FlhF and FlhG in *V. parahaemolyticus* and their effect on swimming motility. Absence of either FlhF or FlhG caused a significant defect in swimming ability, resulting in absence of flagella in a Δ*flhF* mutant and an aberrant flagellated phenotype in Δ*flhG*. Both proteins localized to the cell pole in a cell cycle-dependent manner, but displayed different patterns of localization throughout the cell cycle. FlhF transitioned from a uni- to bi-polar localization, as observed in other polarly flagellated bacteria. Localization of FlhG was strictly dependent on the cell pole-determinant HubP, while polar localization of FlhF was HubP independent. Furthermore, localization of FlhF and FlhG was interdependent and required for each other's proper intracellular localization and recruitment to the cell pole. In the absence of HubP or FlhF, FlhG forms non-polar foci in the cytoplasm of the cell, suggesting the possibility of a secondary localization site within the cell besides its recruitment to the cell poles.

Keywords: FlhG, HubP, intracellular organization, *Vibrio parahaemolyticus*, flagellum, FlhF

OPEN ACCESS

Edited by:
Jonathan David Partridge, University of Texas at Austin, United States

Reviewed by:
Karl Klose, University of Texas at San Antonio, United States
Shiwei Zhu, Yale University, United States

***Correspondence:**
Simon Ringgaard
ringgaard@lmu.de

Specialty section:
This article was submitted to Microbial Physiology and Metabolism, a section of the journal Frontiers in Microbiology

Received: *18 January 2021*
Accepted: *23 February 2021*
Published: *17 March 2021*

Citation:
Arroyo-Pérez EE and Ringgaard S (2021) Interdependent Polar Localization of FlhF and FlhG and Their Importance for Flagellum Formation of Vibrio parahaemolyticus. Front. Microbiol. 12:655239. doi: 10.3389/fmicb.2021.655239

INTRODUCTION

It is essential to understand the mechanisms required for dissemination of bacteria in the environment and for many bacteria, the primary means of motion is flagella-mediated swimming motility. Correct swimming behavior heavily depends on the production of the correct number and proper placement of the flagella within the cell (Schuhmacher et al., 2015b; Blagotinsek et al., 2020; Kojima et al., 2020).

The localization of flagella in several species has been demonstrated to be mediated by landmark proteins. In particular, two proteins have been implicated in regulating the number (the ATPase FlhG) and positioning (the GTPase FlhF) of flagella in several bacterial species (Schuhmacher et al., 2015b). Interestingly, the FlhF/G system is responsible for the positioning of flagella in

peritrichously, lophotrichously, and monotrichously flagellated bacteria. In some γ-proteobacteria, such as *Pseudomonas* sp., *Shewanella* sp., and *Vibrio* sp., the flagella are positioned and formed only at the old cell pole. At cell division, one daughter cell inherits these flagella at its old cell pole, whereas the second daughter is non-flagellated, but begins to produce a flagellum at its old cell pole shortly after division is finalized.

In *Vibrio alginolyticus*, *Shewanella putrefaciens*, and *P. aeruginosa*, the absence of *flhG* results in hyper-flagellated cells (Campos-García et al., 2000; Hulko et al., 2006; Kusumoto et al., 2006, 2008; Schuhmacher et al., 2015a). Hyperflagellation may be a result of increased flagellar protein production, as many flagellar genes have been shown to be upregulated in the absence of FlhG in these organisms (Dasgupta et al., 2000; Dasgupta and Ramphal, 2001; Correa et al., 2005). Deletion of *flhF* has been shown to result in swimming defects due to the absence and/or mislocalization of flagella (Pandza et al., 2000; Correa et al., 2005; Kusumoto et al., 2006; Green et al., 2009). In *Campylobacter jejuni*, *V. alginolyticus*, and *Vibrio cholerae*, the absence of *flhF* results mostly in non-flagellated non-motile cells, however, in the rare cases in which a flagellum is formed nevertheless, it is no longer positioned at the cell pole (Correa et al., 2005; Kusumoto et al., 2008; Balaban et al., 2009). A different phenotype is observed in *Pseudomonas* sp. (Pandza et al., 2000; Murray and Kazmierczak, 2006) and *S. putrefaciens* (Rossmann et al., 2015), where a single mislocalized non-polar flagellum is produced in the absence of FlhF. Importantly, FlhF is thought to establish the site of flagellum assembly by recruiting the earliest flagellar structural component FliF, which constitutes the MS-ring (Green et al., 2009; Kojima et al., 2020; Terashima et al., 2020). Fluorescence microscopy studies have shown that FlhF is localized to the bacterial cell poles in several monotrichous bacterial species, including *P. aeruginosa* (Murray and Kazmierczak, 2006), *S. putrefaciens* (Rossmann et al., 2015), *V. alginolyticus* (Kusumoto et al., 2008), and *V. cholerae* (Green et al., 2009; Yamaichi et al., 2012; Takekawa et al., 2016). In all cases, FlhF shows a specific spatiotemporal localization pattern that is cell cycle-dependent. Particularly, FlhF localizes uni-polarly to the old flagellated cell pole in young short cells and displays a bi-polar localization in older longer cells and as a consequence each daughter cell inherits FlhF localized to its old cell pole when cell division is completed (Murray and Kazmierczak, 2006; Kusumoto et al., 2008; Rossmann et al., 2015; Takekawa et al., 2016).

FlhG has been shown to negatively regulate the intracellular localization of FlhF and positively influences flagellar production by regulating FlhF GTP hydrolysis (Bange et al., 2011). In *V. alginolyticus* and *V. cholerae* species, FlhG too localizes to the cell poles (Kusumoto et al., 2008; Yamaichi et al., 2012), which fits with its function in regulating FlhF localization at this site. However, data suggests that the recruitment of FlhG to the cell pole is independent of FlhF and instead depends on interactions with the polar landmark protein HubP (Yamaichi et al., 2012).

In summary, many different bacteria use FlhF and FlhG to regulate the localization and positioning of their flagella. The system's general function as positive and negative regulators of the flagellum synthesis, respectively, is largely conserved even among different bacterial phyla (Schuhmacher et al., 2015b; Kojima et al., 2020). Nevertheless, differences in the details of the system account for individual differences in the flagellar assembly even between members of the same genus (Schuhmacher et al., 2015b; Kojima et al., 2020). Because of these differences on the effect of the FlhF-FlhG system, also between closely related organisms, it is important to study this flagellum positioning system in different bacterial species in order to understand its importance for flagellum formation in the specific bacterium of interest.

Here, we have analyzed the importance of the FlhF-FlhG system for flagellum formation and swimming motility in the bacterium *Vibrio parahaemolyticus*. *V. parahaemolyticus* is an important human pathogen and the principal course of acute seafood-borne gastroenteritis in the world (Letchumanan et al., 2014). Furthermore, it causes substantial problems in the aquaculture industry with early mortality syndrome (EMS) of shrimps, which is an important shrimp disease particularly in Southeast Asia (Tran et al., 2013). *V. parahaemolyticus* exhibits a dimorphic life-style depending on its environmental conditions – particularly as a swimmer or a swarmer cell. Swimmer cells are monotrichously flagellated and optimized for life in liquid environments. On solid surfaces it lives as a swarmer cell, which is a cell type specialized for colonization of solid environments. Swarmer cells are highly elongated and express a distinct flagellum system in addition to the polar flagellum of swimmer cells, which results in a multiple peritrichous flagella positioned along the length of the swarmer cell (Baumann and Baumann, 1977; McCarter, 2004; Böttcher et al., 2016). In liquid environments *V. parahaemolyticus* exists as a short motile swimmer cell that is propelled by a single polar flagellum, which is positioned at the old cell pole. Swimming motility is essential for the dissemination of *V. parahaemolyticus* in the environment and for its resistance to phage attacks (Zhang et al., 2016; Freitas et al., 2020). Consequently, it is essential to study the mechanisms regulating polar flagellum formation in this specific species in order to fully understand the forces driving its spreading and survival in the environment. Here, we show that FlhF and FlhG are required for proper formation of the polar flagellum and swimming motility in *V. parahaemolyticus*. We further analyze the intracellular localization of FlhF and FlhG during the cell cycle. Both proteins localize to the bacterial cell pole in a dynamic and cell cycle-dependent manner, however, importantly their patterns of localization are distinct from each other and FlhG undergoes a different localization pattern as that of FlhF. Interestingly, their localization patterns depend on each other and in the case of FlhG also on the cell pole determinant HubP.

MATERIALS AND METHODS

Strains and Growth Media

All strains were grown in LB medium at 37°C. When needed, indicated antibiotics were added. Genetic modifications in *V. parahaemolyticus* RIMD 2210633 were performed using

standard allele exchange methods with plasmids derived from pDM4 (Milton et al., 1996). All *V. parahaemolyticus* strains were generated in a Δ*lafA* background to eliminate any cellular movement through the lateral flagella system of *V. parahaemolyticus*. *Escherichia coli* DH5αλpir was used for cloning and SM10λpir for introducing plasmids into *V. parahaemolyticus* by conjugation. All strains and plasmids used are listed in **Supplementary Table 1**. Primers used are listed in **Supplementary Table 2**. A description of each plasmid is also included as **Supplementary Material**.

Swimming Assay

Swimming assays were performed as described in Ringgaard et al. (2013) and Alvarado et al. (2017).

Fluorescence Microscopy

Fluorescence microscopy was carried out essentially as described by Ringgaard et al. (2013), Heering and Ringgaard (2016), Alvarado et al. (2017), and Heering et al. (2017). Bacterial strains for fluorescence microscopy analysis were inoculated in LB medium and cultivated at 37°C and shaking to an OD_{600} = 0.5–0.6. Cells were then spotted on a pad of 1% agarose in 50% PBS + 10% LB on a microscope slide, covered with a coverslip and imaged immediately. All microscopy was performed on a Nikon Eclipse Ti inverted Andor spinning-disk confocal microscope equipped with a 100x lens and an Andor Zyla sCMOS cooled camera and an Andor FRAPPA system. Microscopy images were analyzed using ImageJ imaging software[1] and Metamorph Offline (version 7.10.2.240, Molecular Devices). FlhF-sfGFP fusion was imaged at 400 ms exposure, and sfGFP-FlhG at 1000 ms for all backgrounds. Demographs were constructed by measuring the fluorescence intensity profiles in Fiji and processing the data in R (3.0.1, R Foundation for Statistical Computing), using a script described by Cameron et al. (2014), Alvarado et al. (2017), Heering et al. (2017), and Muraleedharan et al. (2018).

Transmission Electron Microscopy

Cellular cultures were propagated using identical growth conditions as those used for fluorescence microscopy analysis. Cells were grown to an OD600 = 0.5–0.6. Samples were subsequently treated as described by Ringgaard et al. (2007) and spotted on a plasma-discharged carbon-coated copper grid (Plano, Cat#S162-3) and rinsed with 0.002% uranyl acetate, blotted dry with Whatman filter paper, and further dried. TEM images were obtained with a JEOL JEM-1400 Plus 120 KV transmission electron microscope at 80 kV.

Western Blot

Whole-cell extracts from the same cultures as used for microscopy were normalized by cell density, and equal amounts were loaded on a SDS-PAGE, blotted and probed with JL-8 anti-GFP monoclonal antibody (Takara Bio Cat# 632380, RRID:AB_10013427), and detected with horse-radish-peroxidase-conjugated anti-mouse IgG antibodies (Thermo Fisher Scientific Cat# 45-000-680, RRID:AB_2721110).

Sample Size and Statistical Analysis

For microscopy experiments, a minimum of three biological replicates were performed, with >200 cells measured per replicate. Western blots were performed with samples from the same replicates as used for the microscopy analysis. The mean values of the replicates were plotted ± standard deviation. Statistical significance was evaluated with an ANOVA test with *post hoc* Tukey's test. Demographs were plotted using the cellProfiles R package (Cameron et al., 2014). Ten replicates of the swimming assays were performed. The statistical significance was calculated with an ANOVA with different petri dishes as blocks. All calculations were done in R (R Development Core Team, 2008).

RESULTS

In order to understand the importance of the FlhF-FlhG-system and HubP in motility of *V. parahaemolyticus*, we generated strains bearing in-frame deletions of either *flhF, flhG*, and *hubP* (Δ*flhF*, Δ*flhG*, and Δ*hubP*), and their effect on motility was analyzed by measuring swimming motility in soft-agar plates. As a control for no motility, we included a strain lacking the chemotaxis protein CheW (Δ*cheW*). Wild-type *V. parahaemolyticus* spread through the soft-agar, resulting in large swimming colonies, whilst no displacement was observed for the Δ*cheW* strain (**Figures 1A,B**). The absence of FlhF resulted in a complete lack of displacement, similar to the Δ*cheW* strain (**Figures 1A,B**). The absence of FlhG also significantly reduced swimming displacement by ∼50% when compared to wild-type, however, cells were still more proficient swimmers than cells lacking FlhF (**Figures 1A,B**). A strain lacking HubP was also significantly reduced in swimming displacement by ∼65% when compared to wild-type, however, it was significantly more swimming proficient that a strain lacking FlhF (**Figures 1A,B**). Interestingly, the absence of HubP resulted in a significantly stronger reduction in swimming ability than for cells lacking FlhG (**Figures 1A,B**).

Upon analysis of the above strains using transmission electron microscopy (TEM), it became clear that the observed swimming defects in the absence of FlhF, FlhG, or HubP was due to abnormalities in synthesis of the polar flagellum (**Figures 1C,D**). A polar flagellum was observed for ∼50% of wild-type cells whilst the other 50% were non-flagellated. This was in contrast to cells lacking FlhF where 100% were non-flagellated, thus showing that FlhF is required for swimming motility and flagellum production in *V. parahaemolyticus* (**Figures 1C,D**). A different result was obtained for cells lacking FlhG, which on the contrary is a negative regulator of flagellum synthesis, as in its absence there was a significant increase in flagellated cells, with only ∼15% of Δ*flhG* cells being non-flagellated (**Figures 1C,D**). Furthermore, ∼60% of Δ*flhG* cells displayed multiple flagella positioned at the same cell pole, which is virtually never seen for the wild-type.

[1] http://rsbweb.nih.gov/ij

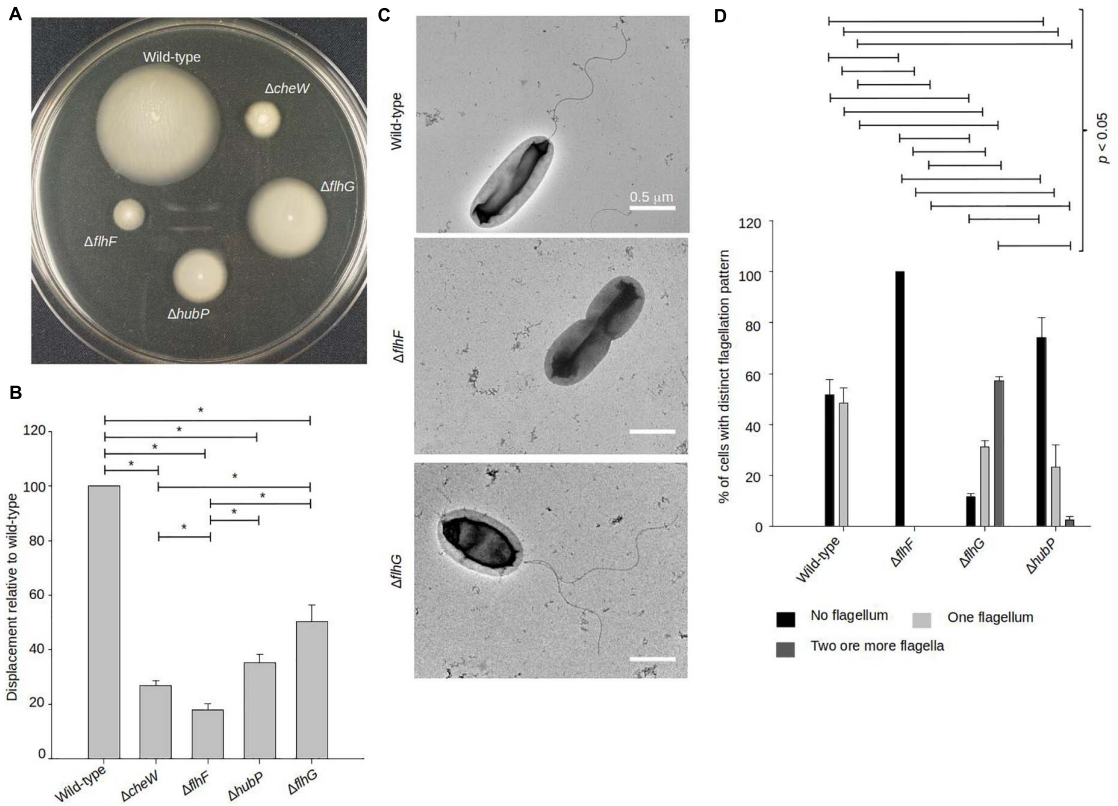

FIGURE 1 | FlhF and FlhG regulate swimming and flagellum production in *V. parahaemolyticus*. **(A)** Representative image of a swimming assay in soft agar of indicated *V. parahaemolyticus* strains. **(B)** Bar graph showing the average diameter of swimming colonies of the indicated *V. parahaemolyticus* strains relative to wild-type cells. **(C)** Representative transmission electron micrographs of the indicated *V. parahaemolyticus* strains stained with uranyl acetate. **(D)** Bar graph depicting the average percentage of cells with distinct flagellation patterns, $n = 200$ cells. **(B,D)** Asterisk, *, indicates $p < 0.05$, Tested with ANOVA in blocks + Tukey HSD. Error bars indicate standard deviation.

Importantly, no mislocalized non-polar flagella were observed in any case. Interestingly, the absence of *hubP* increased both the numbers of non-flagellated cells (∼70%) and multiflagellated cells (**Figures 1C,D**).

FlhF and FlhG Display Distinct Cell-Cycle Dependent Polar Localization Patterns

To further elucidate the role that FlhF and FlhG have in determining the number and position of the polar flagellum, the proteins were tagged with super folder GFP (FlhF-sfGFP and sfGFP-FlhG) and their intracellular localization visualized by fluorescence microscopy. Importantly, both fusion proteins could either completely (FlhF-sfGFP) or partially (sfGFP-FlhG) complement their respective deletion strains when the native locus was replaced by the gene encoding the fusion protein (**Supplementary Figures 1A,B**). This indicates that FlhF-sfGFP is fully functional while sfGFP-FlhG is at least partial functional, and thus are likely to reflect the true localization of the proteins *in vivo*. Both proteins localized in three distinct patterns: diffuse, unipolar, bipolar. Both proteins localized as discreet foci at one of the cell poles (**Figure 2A**, white arrows). In approximately 45% of cells FlhF was diffusely localized, whilst a significantly larger proportion (80%) of cells showed diffuse localization of FlhG (**Figures 2A,B**). About 60% of the cells had at least one focus of FlhF at one of the poles (**Figures 2A,B**), however, interestingly FlhF experienced two types of polar localization – uni-polar (∼40%) (**Figures 2A,B** orange arrow) and bi-polar (∼15%) (**Figures 2A,B** green arrow). Time-lapse microscopy showed that the two types of polar localization, was a result of a cell-cycle dependent transition in the polar localization pattern of FlhF. Particularly, time-lapse microscopy showed that in young new-borne cells FlhF localized uni-polarly at the old flagellated cell pole. Then, later in the cell cycle FlhF was recruited to the new non-flagellated cell pole, resulting in a bi-polar localization pattern. In consequence, each daughter cell inherited an FlhF cluster localized to its old pole upon completion of cell division (**Figure 3A**). Occasionally, we observed that FlhF became diffuse after cell division, resulting in cells with no visible foci.

Similarly, FlhG was localized at the cell poles. However, the proportion of cells with polar FlhG foci was significantly lower than that observed for FlhF. Particularly, over 80% of the population had no visible FlhG foci, which instead was localized diffusely in the cytoplasm (**Figures 2A,B** red arrow). When localized to the cells pole, FlhG was primarily localized in a uni-polar manner (∼18%), while only in a very small

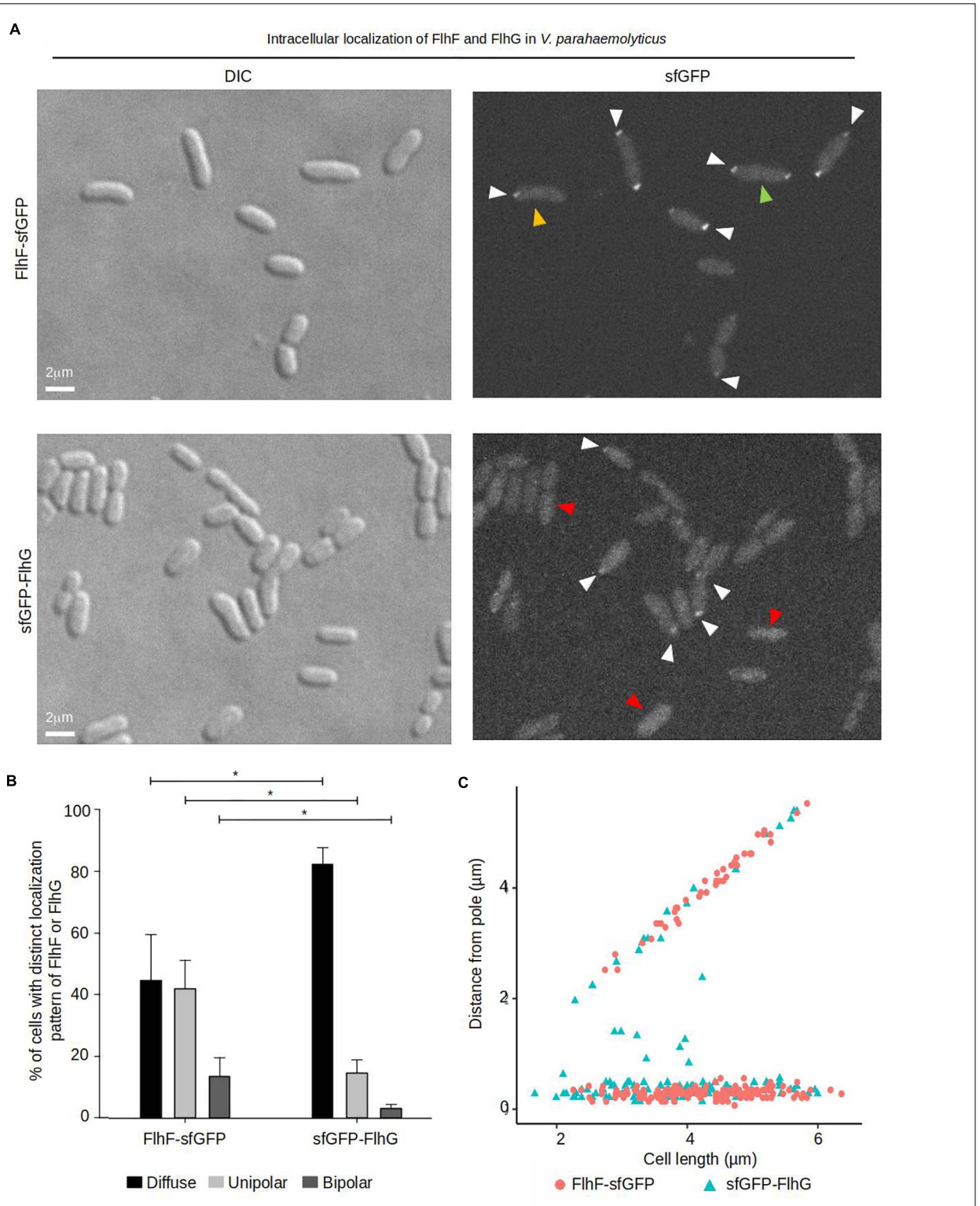

FIGURE 2 | The intracellular localization of FlhF and FlhG in *V. parahaemolyticus*. **(A)** DIC and fluorescence microscopy of *V. parahaemolyticus* strains expressing FlhF-sfGFP or sfGFP-FlhG fusion proteins. White arrows indicate polar foci, orange arrows = unipolar foci, green arrows = bipolar foci, red arrow = diffuse. **(B)** Bar graph showing the percentages of cells with fluorescent foci at one, two, or no poles. Asterisk, *, indicates $p < 0.05$, tested with ANOVA + Tukey HSD. **(C)** Graph depicting the distance of FlhF-sfGFP clusters from the cell poles as a function of cell 2length.

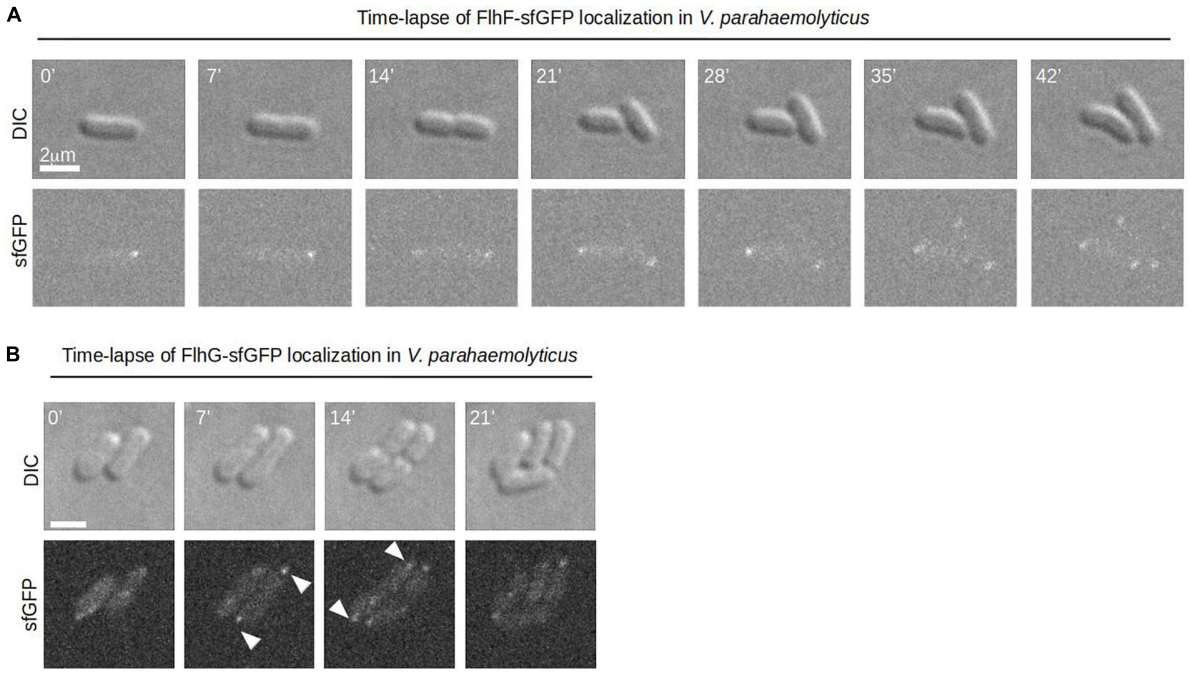

FIGURE 3 | A dynamic spatiotemporal intracellular localization of FlhF and FlhG during the *V. parahaemolyticus* cell cycle. **(A,B)** Time-lapse DIC and fluorescence microscopy of *V. parahaemolyticus* strains expressing **(A)** FlhF-sfGFP or **(B)** sfGFP-FlhG fusion proteins. White numbers indicate minutes elapsed.

percentage (∼2%) of cells was FlhG localized in a bi-polar manner (**Figures 2A–C**) and observed primarily in cells very close to completing cell division. In contrast to FlhF, which was strictly localized in foci at the cell pole, FlhG foci were occassionally localized away from the cell pole within the cytoplasm of the cell (**Figure 2C**). We next analyzed the temporal localization pattern of FlhG during the cell-cycle using time-lapse microscopy. During the majority of the cell cycle, FlhG did not form polar foci but was instead localized diffusely in the cytoplasm (**Figure 3B**). Interestingly, very close to completion of cell division FlhG was recruited to both cell poles resulting in a bi-polar localization pattern and as a consequence each daughter cell inherited FlhG localized to their respective old cell poles. Soon after completion of cell division, FlhG disappeared from the cell pole and was only localized diffusely in the cytoplasm.

FlhG Is Required for Proper Polar Localization of FlhF

We next aimed to analyze how FlhF and FlhG might influence each other's intracellular localization and the importance of HubP on their recruitment to the cell pole. To this effect, the localization of FlhF was analyzed in a Δ*hubP* and a Δ*flhG* background, respectively. FlhF was still capable of forming foci and localizing to the cell pole in the absence of HubP and no significant difference was observed in FlhF localization between wild-type and Δ*hubP* cells (**Figures 4A–C**). Absence of FlhG, on the other hand, had a very clear effect on the intracellular localization of FlhF localization. Particularly, there was a significant increase in the percentage of cells with polarly localized FlhF and a concomitant decrease in cells with diffusely localized FlhF, with ∼90% of cells with polarly localized FlhF in the absence of FlhG compared to ∼55% of wild-type cells (**Figures 4A–C**). Particularly, there was a striking increase in the number of cells with a bi-polar localization of FlhF in the absence of FlhG (∼60%) compared to wild-type (∼12%) (**Figures 4A–C**). Interestingly, demographic analysis showed that FlhF was recruited to the new pole earlier in the cell cycle in the absence of FlhG when compared to wild-type (**Figure 4B**). Furthermore, analysis of the fluorescence intensity polar FlhF clusters, showed that polar FlhF clusters were significantly brighter in a Δ*flhG* background, when compared to wild-type and Δ*hubP*, suggesting an increased level of FlhF localized to the cell pole in the absence of FlhG (**Figure 4D**). Consistently, Western-blot analysis determined that the level of FlhF-sfGFP was ∼8.8 fold higher in the absence of FlhG, compared to wild-type and Δ*hubP* (**Figure 4E**). These results, show that FlhG is required for the proper polar localization of FlhF in *V. parahaemolyticus*. They further indicate that FlhG negatively regulates the intracellular protein level of FlhF and its spatiotemporal localization and cell cycle-dependent transition from a uni-polar to a bi-polar localization pattern. Further, the results suggest that HubP has very little or no influence on the intracellular localization of FlhF.

HubP and FlhF Are Required for Proper Recruitment of FlhG to the Cell Pole

Next, we analyzed the importance of FlhF and HubP on the intracellular localization of FlhG. Both FlhF and HubP were individually required for proper intracellular localization of FlhG

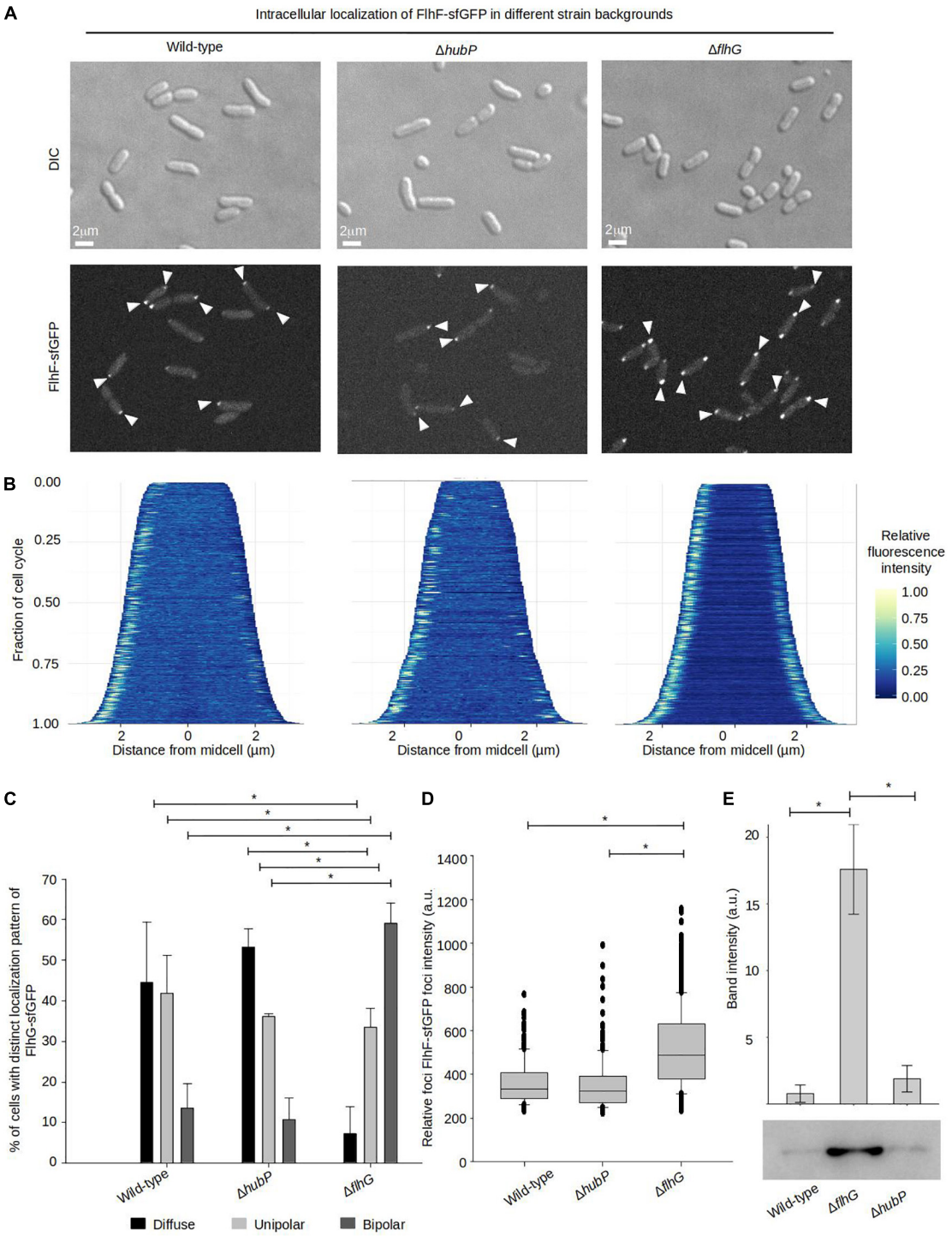

FIGURE 4 | FlhG is required for proper intracellular localization of FlhF. **(A)** DIC and fluorescence microscopy of indicated *V. parahaemolyticus* strains expressing FlhF-sfGFP. White arrows indicate polar FlhF-sfGFP foci. **(B)** Demographs showing the fluorescence intensity of sfGFP along the cell length in a population of *V. parahaemolyticus* cells relative to cell length. Demographs include date from >600 cells pooled from three distinct experiments. **(C)** Bar graph showing the percentage of cells with distinct FlhF-sfGFP localization patterns in the indicated *V. parahaemolyticus* strain backgrounds. Asterisk, *, indicates $p < 0.05$, tested with ANOVA in blocks + Tukey HSD. Error bars indicate standard deviation. **(D)** Box plot showing the fluorescence intensity of polar FlhF-sfGFP foci of the indicated *V. parahaemolyticus* strains. Asterisk, *, indicates $p < 0.05$, tested with ANOVA + Tukey HSD. **(E)** Western blot with anti-GFP monoclonal antibody against whole cell extract of strains expressing FlhF-sfGFP. The bar-graph depicts the quantification of the signal detected from three biological replicates. Error bars indicate standard deviation and asterisk, *, indicates $p < 0.05$, tested with student's *t*-test.

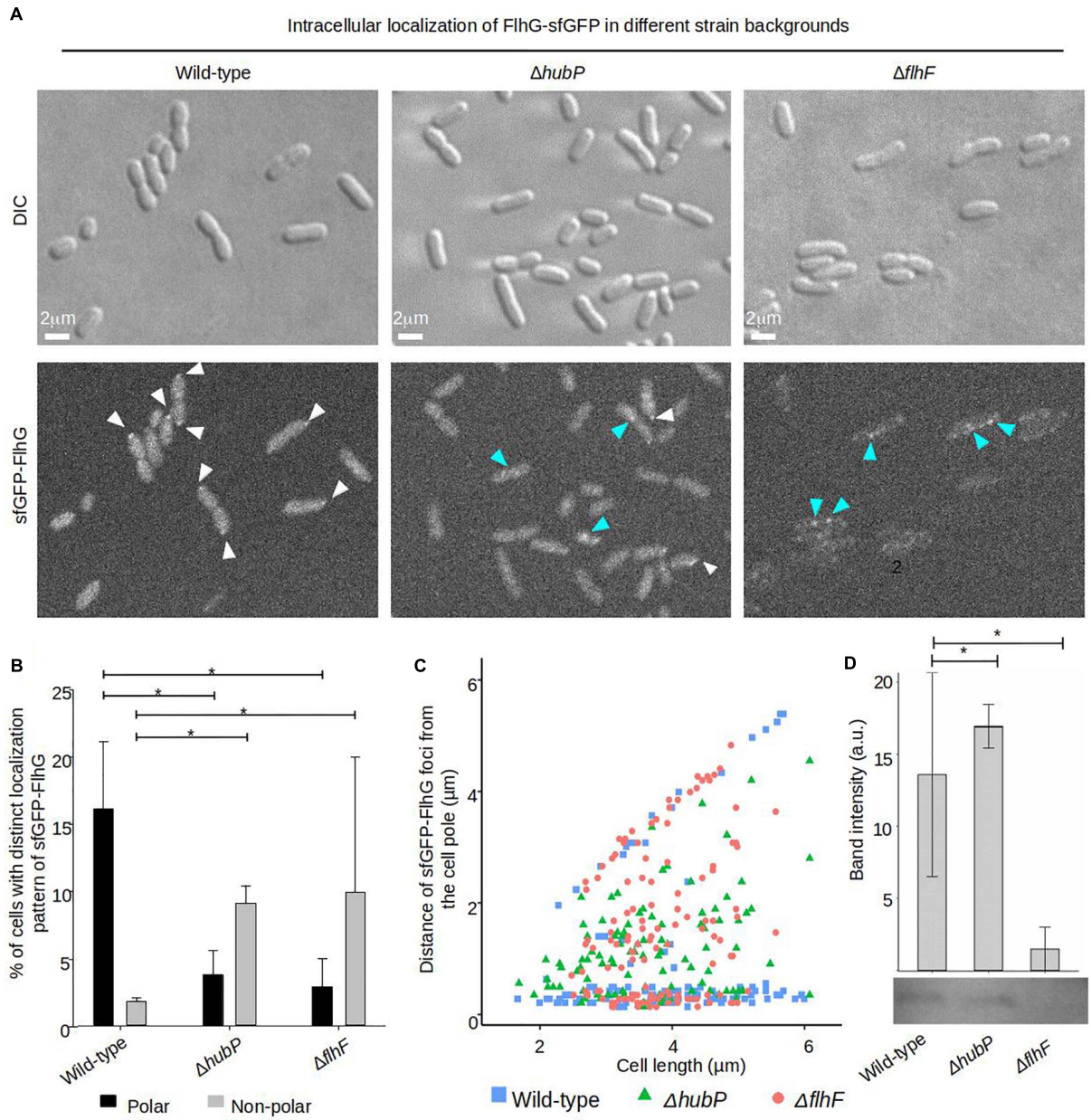

FIGURE 5 | Proper intracellular localization of FlhG is regulated by HubP and FlhF. **(A)** DIC and fluorescence microscopy of sfGFP-FlhG in the indicated *V. parahaemolyticus* strains. White arrows indicate polar foci of sfGFP-FlhG and blue arrows indicate cytoplasmic clusters. **(B)** Bar graphs showing the percentage of cells with distinct localization pattern of sfGFP-FlhG in the indicated strains of *V. parahaemolyticus*. Error bars indicate standard deviation and asterisk, *, indicates $p < 0.05$, tested with ANOVA + Tukey HSD. **(C)** Graph depicting the distance of sfGFP-FlhG clusters from the cell poles as a function of cell length in the indicated *V. parahaemolyticus* strain backgrounds. **(D)** Western blot with anti-GFP monoclonal antibody against whole cell extract of strains expressing sfGFP-FlhG. The bar-graph depicts the quantification of the signal detected from three biological replicates. Error bars indicate standard deviation and asterisk, *, indicates $p < 0.05$, tested with student's *t*-test.

and in the absence of either protein there was a significant reduction in the percentage of cells with polarly localized FlhG (**Figures 5A,B**). Where FlhG was localized as clusters in ∼15% of wild-type cells, only ∼2–3% of cells showed polarly localized FlhG in the absence of HubP or FlhF (**Figures 5A,B**). Interestingly, even though FlhG no longer localized as clusters at the cell pole in the absence of HubP or FlhF, it was observed to localize as distinct foci along the length of the cell in ∼10% of cells (**Figures 5A–C** blue arrows), while such foci only were observed in ∼2% of wild-type cells. However, our results also suggested that sfGFP-FlhG was unstable in the absence of FlhF. Particularly, after culturing of the strain, the fluorescent signal of the sfGFP-FlhG in a Δ*flhF* background, always faded in the population until it was no longer possible to detect. However, a

PCR assay in all cases confirmed the gene encoding *sfGFP-flhG* in its correct locus. Western-blot analysis showed that in the Δ*flhF* background the level of sfGFP-FlhG was significantly lower than in wild-type and Δ*hubP* cells (**Figure 5D**). These results together suggest that both HubP and FlhF are required for the proper polar localization of FlhG and that in their absence FlhG is capable of forming non-polar clusters along the length of the cell.

DISCUSSION

In this study, we have investigated the spatiotemporal localization of the polar flagellum determinants FlhF and FlhG in *V. parahaemolyticus*. We showed that both FlhF and FlhG are required for proper swimming of *V. parahaemolyticus* and that absence of either protein results in a significant defect in swimming ability. Particularly, TEM analysis showed that deleting FlhF resulted in a complete absence of flagella, similar to what has been observed in *V. cholerae* and *V. alginolyticus* (Correa et al., 2005; Kusumoto et al., 2008). This shows that FlhF is essential for flagellum formation in *V. parahaemolyticus* and suggests that the function of FlhF is similar in the three *Vibrio* species (Correa et al., 2005; Kusumoto et al., 2008). Absence of FlhG in *V. parahaemolyticus* resulted in a hyperflagellation phenotype, again similar to what has been observed for other γ-proteobacteria (Correa et al., 2005; Kusumoto et al., 2008; Gao et al., 2015), suggesting that FlhG is a negative regulator of flagellum synthesis and acts to ensure that only one flagellum is formed at the cell pole in *V. parahaemolyticus*. This further supports that the FlhF-FlhG system works in very similar ways, particularly in *Vibrio* species.

We further showed that both FlhF and FlhG undergo a dynamic intracellular localization, where both proteins localized to the cell pole in a cell cycle-dependent manner. FlhF and FlhG displayed very distinct patterns of localization throughout the cell cycle. Particularly, FlhF showed a localization pattern that has been reported for FlhF in other polarly flagellated bacteria and *Vibrio* species as well (Correa et al., 2005; Murray and Kazmierczak, 2006; Rossmann et al., 2015). In young cells, FlhF was uni-polarly localized at the old flagellated cell pole. Then, later in the cell cycle FlhF was recruited to the new non-flagellated cell pole, resulting in a bi-polar localization pattern and as a result, each daughter cell inherited an FlhF cluster localized to its old cell pole. This is further supporting the conclusion that the function of FlhF is identical within *Vibrio* species and similar to that reported in other polar flagellated bacteria.

Despite the wealth of knowledge in regard to the intracellular localization of FlhF, it remains an open question how it is recruited to the cell pole. In other organisms, it has been shown that FlhG relies on the cell pole determinant protein HubP for its recruitment to the cell pole. Here, we show that FlhG in *V. parahaemolyticus* also depends on the protein HubP for its recruitment to the cell pole. But, in contrast to FlhG, the recruitment of FlhF to the pole seemed to be independent of HubP – again consistent with what has been observed for FlhF and FlhG in other *Vibrio* species (Yamaichi et al., 2012; Rossmann et al., 2015; Takekawa et al., 2016). Our data does suggest that, similar to what is observed in *V. alginolyticus* (Kusumoto et al., 2006, 2008), recruitment of FlhF to the cell pole is negatively regulated by FlhG. Particularly, in the absence of FlhG, a much larger proportion of cells showed polarly localized FlhF and there was particularly an increase in the percentage of cells with a bi-polar localization pattern of FlhF in the absence of FlhG. Additionally, FlhF foci at the cell poles were brighter in the absence of FlhG, suggesting an increased recruitment of FlhF to the cell poles in this background. In other *Vibrio* species, deleting *flhG* increases the transcription of flagellar genes, including *flhF* (Correa et al., 2005). It is likely that the increased size and number of FlhF foci observed in our *V. parahaemolyticus* strain was due to an increase in the amount of FlhF molecules present in the cell. Indeed, a Western-blot confirmed that the protein levels of FlhF-sfGFP were much higher in the Δ*flhG* strain compared to the wild-type *V. parahaemolyticus*. Furthermore, we were not able to tell if FlhG directly influences localization of FlhF at the cell poles, however, given data of the system from other organisms, which have shown that FlhG directly interacts with and regulates FlhF's GTP hydrolysis and nucleotide bound state (Balaban et al., 2009; Bange et al., 2011; Kazmierczak and Hendrixson, 2013; Schniederberend et al., 2013), it is likely that this is also the situation in *V. parahaemolyticus*. Thus, the effect of FlhG on FlhF localization is likely a combination of its regulatory function on FlhF's protein level within the cell and FlhG-dependent regulation of FlhF's nucleotide cycle.

FlhG, too, has been reported to localize to the bacterial cell pole in other *Vibrio* species (Kusumoto et al., 2008; Ringgaard et al., 2011; Yamaichi et al., 2012; Rossmann et al., 2015). However, here we show that FlhG, in contrast to FlhF, remained diffusely localized in the cytoplasm for the majority of the cell cycle in *V. parahaemolyticus*, and only when the cell was close to completion of cell division was FlhG recruited to both cell poles, resulting in a bi-polar localization pattern immediately before cell division was finalized. As a result, FlhG localized to the old-cell pole of each daughter cell immediately after cell division, whereafter it was delocalized from the pole and again diffusely localized in the cytoplasm. Thus, not only did FlhF and FlhG show distinct localization patterns, but also relied on different mechanisms for their recruitment to the cell pole. Polar localization of FlhG was strictly dependent on the cell pole-determinant HubP, while polar localization of FlhF was HubP independent. This distinct dependency on HubP for their recruitment to the cell pole has been shown in other related bacterial organisms and *Vibrio* species as well (Kojima et al., 2020). This again supports the notion that FlhF and FlhG work in *V. parahaemolyticus*, in a manner similar to that reported in other *Vibrio* species. The mislocalization of FlhG from the cell pole, could be responsible for the increase in flagellation observed in the Δ*flhG* and Δ*hubP* strains. It remains to be investigated whether this effect is caused by the diminished presence of FlhG at the pole, where in wild-type it interacts with components of the flagellum assembly, or the increased presence of FlhG in the cytoplasm, where it could regulate expression of flagellar genes. A combination of both mechanisms is also possible.

Furthermore, as FlhF still localizes properly to the cell pole in the absence of HubP, where FlhG is mislocalized and found only in the cytoplasm, our data suggest that FlhG does not need to be localized to the cell pole in order to carry out its effect on the localization of FlhF. We further show that the protein levels of FlhF is similar to wild-type levels in the absence of HubP, while there is a significant increase in FlhF levels in the absence of FlhG. Altogether, these results suggest that polar localization of FlhG is not directly to regulate FlhF localization dynamics and protein levels, and thus might serve an additional purpose related to FlhG's function in regulating proper flagellation pattern. Interestingly, we show that in the absence of either HubP or FlhF, FlhG forms non-polar foci in the cytoplasm of the cell, suggesting a secondary localization site for FlhG within the cell, besides its recruitment to the cell poles. In the absence of FlhF, there was an unstable expression of sfGFP-FlhG, which we were unable to explain. Consequently, we are not able to tell for sure if the effect on the localization of sfGFP-FlhG in the absence of FlhF, was a result of this unstable expression of the fusion protein itself or due to the lack of a direct regulatory role of FlhF on FlhG activity via FlhF-FlhG protein-protein interactions. However, as there was no change in sfGFP-FlhG expression level in the absence of HubP and FlhG formed non-polar foci in this background too, we think that these non-polar foci reflect a true secondary localization site of FlhG, which is more prevalent upon its delocalization from the cell pole. Other ParA-like ATPases are known for binding DNA. This ability is essential for their role as spatiotemporal regulators of cell components (Hester and Lutkenhaus, 2007; Ringgaard et al., 2009; Roberts et al., 2012). The FlhG homolog in *P. aeruginosa*, FleN, interacts with the master transcriptional regulator of flagella FleQ. Together they bind specific sites on the chromosome, regulating the transition between biofilm and motile lifestyles (Navarrete et al., 2019). In *V. cholerae*, both FlhF and FlhG are known transcriptional regulators of flagellar genes (Correa et al., 2005). Indeed, very recently it was shown that FlhG plays a very direct role in regulating the expression of flagellum genes in *S. putrefaciens* by connecting the initial phases of flagellum formation with the activity of the transcriptional regulator FlrA (Blagotinsek et al., 2020), which in *V. parahaemolyticus* is referred to as FlaK. It would be interesting to study whether a similar regulatory mechanism exists in *V. parahaemolyticus*. We find it noteworthy that FlhG directly interacts with a transcriptional regulator (Blagotinsek et al., 2020) and we speculate that perhaps its localization in non-polar foci, which we observe in the absence of HubP, could be related to its function in transcriptional regulation and possibly reflect an interaction with transcriptional regulators on the chromosome – hereby giving rise to the distinct focus localization sites that are particularly enhanced in the absence of HubP in *V. parahaemolyticus*. In this way, we would like to hypothesize that the localization of FlhG to the cell pole might not only reflect a function in regulating FlhF activity, but possibly to sequester it spatially to prevent its action on transcriptional regulation in the cytoplasm as a specific cell cycle check point.

Lastly, we would again like to address the polar localization of FlhF. Interestingly, our data show that in the absence of FlhG, FlhF is recruited earlier in the cell cycle to the new cell pole, resulting in an earlier establishment of its bi-polar localization. However, despite FlhF always being bi-polarly localized before cell division, and this occurring even earlier in the cell cycle in the absence of FlhG, *V. parahaemolyticus* is never flagellated at both cell poles at any point during the cell cycle – only ever at its old cell pole. This, indicates that localization of FlhF at the new cell pole is not sufficient to initiate a complete and finalized flagellum formation at this site before cell division has been completed. This further suggests that a so-far unknown factor is required for stimulation of flagellum production at the old cell pole only. Or the presence of an unknown factor prevents or inhibits FlhF function, when FlhF is positioned at the new cell pole. Thus, further studies are required in order to understand how FlhF is recruited to the cell pole and how monotrichously flagellated bacteria inhibit a flagellum to form at their new cell pole during the progression of the cell cycle, despite the flagellum determinant FlhF being bi-polarly localized for a significant part of the cell-cycle. Ultimately, knowledge of these distinct differences between species will help to shed light on the molecular details that allow bacteria to count and position their motility system in many sorts of different arrangements.

DATA AVAILABILITY STATEMENT

The raw data supporting the conclusions of this article will be made available by the authors, without undue reservation.

AUTHOR CONTRIBUTIONS

EEA-P carried out the experimental work. SR conceived the study. EEA-P and SR designed the research and experiments, analyzed the data, and wrote the manuscript. Both authors contributed to the article and approved the submitted version.

FUNDING

This work was supported by the Ludwig-Maximilians-Universität München and the Max Planck Society.

ACKNOWLEDGMENTS

We thank Dr. Kathrin Schirner for helpful comments on the manuscript.

SUPPLEMENTARY MATERIAL

The Supplementary Material for this article can be found online at: https://www.frontiersin.org/articles/10.3389/fmicb.2021.655239/full#supplementary-material

REFERENCES

Alvarado, A., Kjær, A., Yang, W., Mann, P., Briegel, A., Waldor, M. K., et al. (2017). Coupling chemosensory array formation and localization. *Elife* 6:e31058. doi: 10.7554/eLife.31058

Balaban, M., Joslin, S. N., and Hendrixson, D. R. (2009). FlhF and its GTPase activity are required for distinct processes in flagellar gene regulation and biosynthesis in *Campylobacter jejuni*. *J. Bacteriol.* 191, 6602–6611. doi: 10.1128/JB.00884-09

Bange, G., Kümmerer, N., Grudnik, P., Lindner, R., Petzold, G., Kressler, D., et al. (2011). Structural basis for the molecular evolution of SRP-GTpase activation by protein. *Nat. Struct. Mol. Biol.* 18, 1376–1380. doi: 10.1038/nsmb.2141

Baumann, P., and Baumann, L. (1977). Biology of the marine enterobacteria: genera *Beneckea* and *Photobacterium*. *Annu. Rev. Microbiol.* 31, 39–61. doi: 10.1146/annurev.mi.31.100177.000351

Blagotinsek, V., Schwan, M., Steinchen, W., Mrusek, D., Hook, J. C., Rossmann, F., et al. (2020). An ATP-dependent partner switch links flagellar C-ring assembly with gene expression. *Proc. Natl. Acad. Sci. U.S.A.* 117, 20826–20835. doi: 10.1073/pnas.2006470117

Böttcher, T., Elliott, H. L., and Clardy, J. (2016). Dynamics of snake-like swarming behavior of *Vibrio alginolyticus*. *Biophys. J.* 110, 981–992. doi: 10.1016/j.bpj.2015.12.037

Cameron, T. A., Anderson-Furgeson, J., Zupan, J. R., Zik, J. J., and Zambryski, P. C. (2014). Peptidoglycan synthesis machinery in *Agrobacterium tumefaciens* during unipolar growth and cell division. *MBio* 5:e1219–e1214. doi: 10.1128/mBio.01219-14

Campos-García, J., Nájera, R., Camarena, L., and Soberón-Chávez, G. (2000). The *Pseudomonas aeruginosa* motR gene involved in regulation of bacterial motility. *FEMS Microbiol. Lett.* 184, 57–62. doi: 10.1016/s0378-1097(00)00019-7

Correa, N. E., Peng, F., and Klose, K. E. (2005). Roles of the regulatory proteins FlhF and FlhG in the *Vibrio cholerae*. *J. Bacteriol.* 187, 6324–6332. doi: 10.1128/JB.187.18.6324-6332.2005

Dasgupta, N., Arora, S. K., and Ramphal, R. (2000). fleN, a gene that regulates flagellar number in *Pseudomonas aeruginosa*. *J. Bacteriol.* 182, 357–364. doi: 10.1128/jb.182.2.357-364.2000

Dasgupta, N., and Ramphal, R. (2001). Interaction of the antiactivator FleN with the transcriptional activator FleQ regulates flagellar number in *Pseudomonas aeruginosa*. *J. Bacteriol.* 183, 6636–6644. doi: 10.1128/JB.183.22.6636-6644.2001

Freitas, C., Glatter, T., and Ringgaard, S. (2020). The release of a distinct cell type from swarm colonies facilitates dissemination of *Vibrio parahaemolyticus* in the environment. *ISME J.* 14, 230–244. doi: 10.1038/s41396-019-0521-x

Gao, T., Shi, M., Ju, L., and Gao, H. (2015). *Investigation into FlhFG reveals distinct features of FlhF in regulating flagellum polarity in Shewanella oneidensis*. *Mol. Microbiol.* 98, 571–585. doi: 10.1111/mmi.13141

Green, J. C. D., Kahramanoglou, C., Rahman, A., Pender, A. M. C., Charbonnel, N., and Fraser, G. M. (2009). Recruitment of the earliest component of the bacterial flagellum to the old cell division pole by a membrane-associated signal recognition particle family GTP-binding protein. *J. Mol. Biol.* 391, 679–690. doi: 10.1016/j.jmb.2009.05.075

Heering, J., Alvarado, A., and Ringgaard, S. (2017). Induction of cellular differentiation and single cell imaging of *Vibrio parahaemolyticus* swimmer and swarmer cells. *J. Vis. Exp.* 123:e55842. doi: 10.3791/55842

Heering, J., and Ringgaard, S. (2016). Differential localization of chemotactic signaling arrays during the lifecycle of *Vibrio parahaemolyticus*. *Front. Microbiol.* 7:1767. doi: 10.3389/fmicb.2016.01767

Hester, C. M., and Lutkenhaus, J. (2007). Soj (ParA) DNA binding is mediated by conserved arginines and is essential for plasmid segregation. *Proc. Natl. Acad. Sci. U.S.A.* 104, 20326–20331. doi: 10.1073/pnas.0705196105

Hulko, M., Berndt, F., Gruber, M., Linder, J. U., Truffault, V., Schultz, A., et al. (2006). The HAMP domain structure implies helix rotation in transmembrane signaling. *Cell* 126, 929–940. doi: 10.1016/j.cell.2006.06.058

Kazmierczak, B. I., and Hendrixson, D. R. (2013). Spatial and numerical regulation of flagellar biosynthesis in polarly flagellated bacteria. *Mol. Microbiol.* 88, 655–663. doi: 10.1111/mmi.12221

Kojima, S., Terashima, H., and Homma, M. (2020). Regulation of the single polar flagellar biogenesis. *Biomolecules* 10:533. doi: 10.3390/biom10040533

Kusumoto, A., Kamisaka, K., Yakushi, T., Terashima, H., Shinohara, A., and Homma, M. (2006). Regulation of polar flagellar number by the *flhF* and *flhG* genes in *Vibrio alginolyticus*. *J. Biochem.* 139, 113–121. doi: 10.1093/jb/mvj010

Kusumoto, A., Shinohara, A., Terashima, H., Kojima, S., Yakushi, T., and Homma, M. (2008). Collaboration of FlhF and FlhG to regulate polar-flagella number and localization in *Vibrio alginolyticus*. *Microbiology* 154, 1390–1399. doi: 10.1099/mic.0.2007/012641-0

Letchumanan, V., Chan, K. G., and Lee, L. H. (2014). *Vibrio parahaemolyticus*: a review on the pathogenesis, prevalence, and advance molecular identification techniques. *Front. Microbiol.* 5:705. doi: 10.3389/fmicb.2014.00705

McCarter, L. L. (2004). Dual flagellar systems enable motility under different circumstances. *J. Mol. Microbiol. Biotechnol.* 7, 18–29. doi: 10.1159/000077866

Milton, D. L., O'Toole, R., Horstedt, P., and Wolf-Watz, H. (1996). Flagellin a is essential for the virulence of *Vibrio anguillarum*. *J. Bacteriol.* 178, 1310–1319. doi: 10.1128/jb.178.5.1310-1319.1996

Muraleedharan, S., Freitas, C., Mann, P., Glatter, T., and Ringgaard, S. (2018). A cell length-dependent transition in MinD-dynamics promotes a switch in division-site placement and preservation of proliferating elongated *Vibrio parahaemolyticus swarmer* cells. *Mol. Microbiol.* 109, 365–384. doi: 10.1111/mmi.13996

Murray, T. S., and Kazmierczak, B. I. (2006). FlhF is required for swimming and swarming in *Pseudomonas aeruginosa*. *J. Bacteriol.* 188, 6995–7004. doi: 10.1128/JB.00790-06

Navarrete, B., Leal-Morales, A., Serrano-Ron, L., Sarrió, M., Jiménez-Fernández, A., Jiménez-Díaz, L., et al. (2019). Transcriptional organization, regulation and functional analysis of flhF and fleN in *Pseudomonas putida*. *PLoS One* 14:e0214166. doi: 10.1371/journal.pone.0214166

Pandza, S., Baetens, M., Park, C. H., Au, T., Keyhan, M., and Matin, A. (2000). The G-protein FlhF has a role in polar flagellar placement and general stress response induction in *Pseudomonas putida*. *Mol. Microbiol.* 36, 414–423. doi: 10.1046/j.1365-2958.2000.01859.x

R Development Core Team (2008). *R: A Language And Environment For Statistical Computing*, Vol. 1. Vienna: R foundation for statistical computing, 2673. doi: 10.1007/978-3-540-74686-7

Ringgaard, S., Ebersbach, G., Borch, J., and Gerdes, K. (2007). Regulatory cross-talk in the double par locus of plasmid pB171. *J. Biol. Chem.* 282, 3134–3145. doi: 10.1074/jbc.M609092200

Ringgaard, S., Schirner, K., Davis, B. M., and Waldor, M. K. (2011). A family of ParA-like ATPases promotes cell pole maturation by facilitating polar localization of chemotaxis proteins. *Genes Dev.* 25, 1544–1555. doi: 10.1101/gad.2061811

Ringgaard, S., van Zon, J., Howard, M., and Gerdes, K. (2009). Movement and equipositioning of plasmids by ParA filament disassembly. *Proc. Natl. Acad. Sci. U.S.A.* 106, 19369–19374. doi: 10.1073/pnas.0908347106

Ringgaard, S., Zepeda-Rivera, M., Wu, X., Schirner, K., Davis, B. M., and Waldor, M. K. (2013). ParP prevents dissociation of CheA from chemotactic signaling arrays and tethers them to a polar anchor. *Proc. Natl. Acad. Sci. U.S.A.* 111, E255–E264. doi: 10.1073/pnas.1315722111

Roberts, M. A. J., Wadhams, G. H., Hadfield, K. A., Tickner, S., and Armitage, J. P. (2012). ParA-like protein uses nonspecific chromosomal DNA binding to partition protein complexes. *Proc. Natl. Acad. Sci. U.S.A.* 109, 6698–6703. doi: 10.1073/pnas.1114000109

Rossmann, F., Brenzinger, S., Knauer, C., Dörrich, A. K., Bubendorfer, S., Ruppert, U., et al. (2015). The role of FlhF and HubP as polar landmark proteins in *Shewanella putrefaciens* CN-32. *Mol. Microbiol.* 98, 727–742. doi: 10.1111/mmi.13152

Schniederberend, M., Abdurachim, K., Murray, T. S., and Kazmierczaka, B. I. (2013). The GTPase activity of FlhF is dispensable for flagellar localization, but not motility, in *Pseudomonas aeruginosa*. *J. Bacteriol.* 195, 1051–1060. doi: 10.1128/JB.02013-12

Schuhmacher, J. S., Rossmann, F., Dempwolff, F., Knauer, C., Altegoer, F., Steinchen, W., et al. (2015a). MinD-like ATPase FlhG effects location and number of bacterial flagella during C-ring assembly. *Proc. Natl. Acad. Sci.* 112, 3092–3097. doi: 10.1073/pnas.1419388112

Schuhmacher, J. S., Thormann, K. M., and Bange, G. (2015b). How bacteria maintain location and number of flagella? *FEMS Microbiol. Rev.* 39, 812–822. doi: 10.1093/femsre/fuv034

Takekawa, N., Kwon, S., Nishioka, N., Kojima, S., and Homma, M. (2016). HubP, a polar landmark protein, regulates flagellar number by assisting in the proper polar localization of FlhG in *Vibrio alginolyticus*. *J. Bacteriol.* 198, JB.462–JB.416. doi: 10.1128/JB.00462-16

Terashima, H., Hirano, K., Inoue, Y., Tokano, T., Kawamoto, A., Kato, T., et al. (2020). Assembly mechanism of a supramolecular MS-ring complex to initiate bacterial flagellar biogenesis in *Vibrio* species. *J. Bacteriol.* 202. doi: 10.1128/jb.00236-20. [Epub ahead of print].

Tran, L., Nunan, L., Redman, R. M., Mohney, L. L., Pantoja, C. R., Fitzsimmons, K., et al. (2013). Determination of the infectious nature of the agent of acute hepatopancreatic necrosis syndrome affecting penaeid shrimp. *Dis. Aquat. Organ.* 105, 45–55. doi: 10.3354/dao02621

Yamaichi, Y., Bruckner, R., Ringgaard, S., Cameron, D. E., Briegel, A., Jensen, G. J., et al. (2012). A multidomain hub anchors the chromosome segregation and chemotactic machinery to the bacterial pole. *Genes Dev.* 26, 2348–2360. doi: 10.1101/gad.199869.112

Zhang, H., Li, L., Zhao, Z., Peng, D., and Zhou, X. (2016). Polar flagella rotation in *Vibrio parahaemolyticus* confers resistance to bacteriophage infection. *Sci. Rep.* 6:26147. doi: 10.1038/srep26147

Conflict of Interest: The authors declare that the research was conducted in the absence of any commercial or financial relationships that could be construed as a potential conflict of interest.

frontiers in Microbiology

ORIGINAL RESEARCH
published: 30 March 2021
doi: 10.3389/fmicb.2021.643180

OPEN ACCESS

Edited by:
Matt Arthur Baker, University of New South Wales, Australia

Reviewed by:
Nicholas Matzke, The University of Auckland, New Zealand
Aaron White, University of Saskatchewan, Canada

***Correspondence:**
Morgan Beeby
mbeeby@imperial.ac.uk

†ORCID:
Josie L. Ferreira
orcid.org/0000-0002-4411-6131
Izaak Coleman
orcid.org/0000-0003-4697-6079
Tobias Zachs
orcid.org/0000-0002-0836-0989
Bonnie L. Quigley
orcid.org/0000-0003-3787-0993
Morgan Beeby
orcid.org/0000-0001-6413-9835

‡Present address:
Josie L. Ferreira, Centre for Structural Systems Biology, Heinrich-Pette-Institut, Leibniz-Institut für Experimentelle Virologie, Hamburg, Germany
Izaak Coleman, Department of Systems Biology, Columbia University, Irving Cancer Research Center, New York, NY, United States
Max L. Addison, Warwick Medical School, Microbiology and Infection, University of Warwick, Coventry, United Kingdom
Tobias Zachs, Institute of Molecular Biology and Biophysics, Eidgenössische Technische Hochschule Zürich, Zurich, Switzerland
Bonnie L. Quigley, Provectus Algae Pty Ltd., Noosaville, QLD, Australia

Specialty section:
This article was submitted to Microbial Physiology and Metabolism, a section of the journal Frontiers in Microbiology

Received: *17 December 2020*
Accepted: *05 March 2021*
Published: *30 March 2021*

The "Jack-of-all-Trades" Flagellum From *Salmonella* and *E. coli* Was Horizontally Acquired From an Ancestral β-Proteobacterium

Josie L. Ferreira[1†‡], Izaak Coleman[1†‡], Max L. Addison[1‡], Tobias Zachs[1†‡], Bonnie L. Quigley[1†‡], Kristin Wuichet[2] and Morgan Beeby[1*†]

[1] Department of Life Sciences, Imperial College London, London, United Kingdom, [2] Department of Biomedical Informatics, Vanderbilt University Medical Center, Nashville, TN, United States

The γ-proteobacteria are a group of diverse bacteria including pathogenic *Escherichia, Salmonella, Vibrio,* and *Pseudomonas* species. The majority swim in liquids with polar, sodium-driven flagella and swarm on surfaces with lateral, non-chemotactic flagella. Notable exceptions are the enteric Enterobacteriaceae such as *Salmonella* and *E. coli*. Many of the well-studied Enterobacteriaceae are gut bacteria that both swim and swarm with the same proton-driven peritrichous flagella. How different flagella evolved in closely related lineages, however, has remained unclear. Here, we describe our phylogenetic finding that Enterobacteriaceae flagella are not native polar or lateral γ-proteobacterial flagella but were horizontally acquired from an ancestral β-proteobacterium. Using electron cryo-tomography and subtomogram averaging, we confirmed that Enterobacteriaceae flagellar motors resemble contemporary β-proteobacterial motors and are distinct to the polar and lateral motors of other γ-proteobacteria. Structural comparisons support a model in which γ-proteobacterial motors have specialized, suggesting that acquisition of a β-proteobacterial flagellum may have been beneficial as a general-purpose motor suitable for adjusting to diverse conditions. This acquisition may have played a role in the development of the enteric lifestyle.

Keywords: bacterial flagella, electron cryotomography, molecular evolution, subtomogram averaging, horizontal gene transfer

INTRODUCTION

Understanding molecular evolution is fundamental to contemporary biology. Compared to evolutionary processes in large eukaryotes, however, relatively little is known about how molecular machines are acquired, adapted, or change function, and how this relates to the environment. One of the most iconic molecular machines is the bacterial flagellar motor, a self-assembling molecular machine that harnesses ion flux for propulsion.

The best studied flagella are the peritrichous (randomly positioned) motors from the Enterobacteriaceae (henceforth, "enterics") *Salmonella enterica* and *Escherichia coli*, which are used for both aquatic swimming and surface-based swarming. Flagellar rotation is driven by a ring of stator complexes, which incorporate dynamically as a function of load (Reid et al., 2006; Tipping et al., 2013). Ion flux through the stator complexes rotates a cytoplasmic C-ring; torque is

transmitted to the extracellular flagellum via a rigid rod and short universal joint. Enterics swim with a biased random walk: when all flagella rotate counterclockwise, the universal joints facilitate bundling of flagella for propulsion. Binding of the response regulator CheY to the C-ring triggers clockwise rotation, disrupting the flagellar bundle and randomly reorienting the cell (Lee et al., 2001). By phosphorylating CheY when swimming down favorable gradients (or up unfavorable gradients), the bacterium reorients more frequently, leading to a random walk that is biased away from detrimental environments and toward favorable environments (Berg and Brown, 1972; Silverman and Simon, 1974).

Non-enteric γ-proteobacteria such as *Vibrio, Shewanella*, *Pseudomonas,* and *Plesiomonas* swim differently from the enterics. Instead of multifunctional peritrichous flagella, non-enteric γ-proteobacteria have high-torque polar motors, usually Na^+-driven, with high-occupancy stator complexes held in place by large periplasmic disks (Terashima et al., 2006, 2010; Beeby et al., 2016; Zhu et al., 2017); many γ-proteobacteria also have secondary lateral flagella used for surface-based swarming motility, or as "rudders" (Bubendorfer et al., 2014). For chemotaxis, polar motors reorient the cell using a "forward-reverse-flick" motion instead of disrupting the bundle (Xie et al., 2011), while lateral motors are non-chemotactic.

Although previous studies have investigated other incongruencies between flagellar systems and the bacteria they appear in Liu and Ochman (2007); Poggio et al. (2007), the basis of the aforementioned long-known differences between model enteric flagella and flagella in other, closely-related γ-proteobacteria, is unclear. As well as differences in function, the peritrichous, polar, and lateral flagella have distinct wave amplitudes and frequencies (Fujii et al., 2008), suggesting that they come from different families, differences that correlate with habitat: many of the well-studied enterics are gut-dwelling pathogens and commensals. Here, we describe our investigations of the relationship between the different flagellar systems. Phylogenetic and structural results reveal that the enterics acquired a β-proteobacterial flagellar motor by horizontal transfer. This transfer may have provided contemporary enteric bacteria with a general-purpose motor better able to adjust its behavior to a wide range of environmental conditions than the more specialized motors native to the γ-proteobacteria.

RESULTS AND DISCUSSION

To understand the differences between the peritrichous flagella of the enteric γ-proteobacteria and the polar and lateral flagella of other γ-proteobacteria, we determined a flagellar phylogeny across > 90 species manually selected based on relevance and diversity by concatenating the protein sequences of their core flagellar proteins. For this we selected 12 core flagellar proteins, FlgI, FlgC, FliE, FliF, FlhA, FlhB, FliI, FliP, FliQ, FliR, FliG, and FliM (**Figure 1A** and **Supplementary Figure S1**), due to their ubiquity, ease of identification, core structural roles, absence of poorly characterized paralogous duplications, and absence of evidence of horizontal transfers. To assess the validity of our concatenated phylogeny, we examined our individual protein phylogenies. The phylogenies of 10 proteins, FlgI, FlgC, FliE, FliF, FlhA, FlhB, FliI, FliP, FliQ, and FliR, resembled the concatenated phylogeny (**Supplementary Figure S2**), as did the phylogenies of FliG and FliM except those from the γ-proteobacterial lateral motor, which were poorly resolved and with long branch lengths (**Figure 1** and **Supplementary Figure S3**). Because FliG and FliM are components of the chemotaxis-associated C-ring, which has lost chemotactic ability in lateral motors, we speculate that the poorly resolved phylogeny of FliG and FliM in the lateral motor may be due to removal of functional constraints, leading to rapid sequence drift. Phylogenies calculated by omitting these proteins did not affect any of our subsequent conclusions.

We found that the polar and lateral γ-proteobacterial motors clustered together, but the peritrichous enteric motor instead branched from within the β-proteobacterial motors, suggesting horizontal acquisition from a member of the β-proteobacteria (**Figure 1A**), and we focused on a phylogeny of 48 β- and γ-proteobacteria for further inspection (**Figures 1B,D** and **Supplementary Figures S4**, **S5**). Reconstructing the motor phylogeny after removing FliG and FliM did not change this branching of the enteric motor from the β-proteobacterial motors. Our results suggest that the lateral and polar γ-proteobacterial systems diverged at a duplication event: the polar system sub-functionalized via structural elaboration and polar localization, while the non-chemotactic lateral system retained a structure resembling the common ancestral system of β/γ-proteobacteria but lost chemotactic ability.

The enteric motor branches from within a cluster of β-proteobacteria that belong to the *Burkholderiaceae* family (Parks et al., 2018), which includes *Bordetella, Cupriavidus* (ex-*Ralstonia*), and *Burkholderia*. Notably, flagellar genes in *Bordetella* species including *Bordetella bronchiseptica, B. avium,* and *B. parapertussis* are located at a single chromosomal locus (**Figure 1D**), suggesting a mechanism for the wholesale transfer of a single DNA fragment. This transfer would be difficult with other bacteria whose flagellar genes are fragmented across the genome. This putatively transferred chromosomal locus also includes the chemotaxis system that controls flagellar navigation. Furthermore, *cheD* is found outside the *che* locus in *Bordetella*; correspondingly, the enteric *che* systems also lack this component, presumably because only the physical *che* locus was transferred, and genes outside this locus—such as *cheD*—were not (Wuichet and Zhulin, 2010). Simultaneous transfer of the co-evolved, inter-dependent flagellar and sensory systems was likely more immediately useful to the recipient than transfer of individual systems alone. Synteny within operons has previously been shown to be strikingly similar between *Bordetella* and enteric flagella, although the significance of this was not reported (Liu and Ochman, 2007).

The γ-proteobacterial genus *Plesiomonas* phylogenetically branches from the base of the enterics yet retains native γ-proteobacterial and polar and lateral motors. Their presence in *Plesiomonas* suggests that an ancestral enteric γ-proteobacterium lost polar flagella and acquired the β-proteobacterial flagellum, although the order of these events cannot be inferred; some

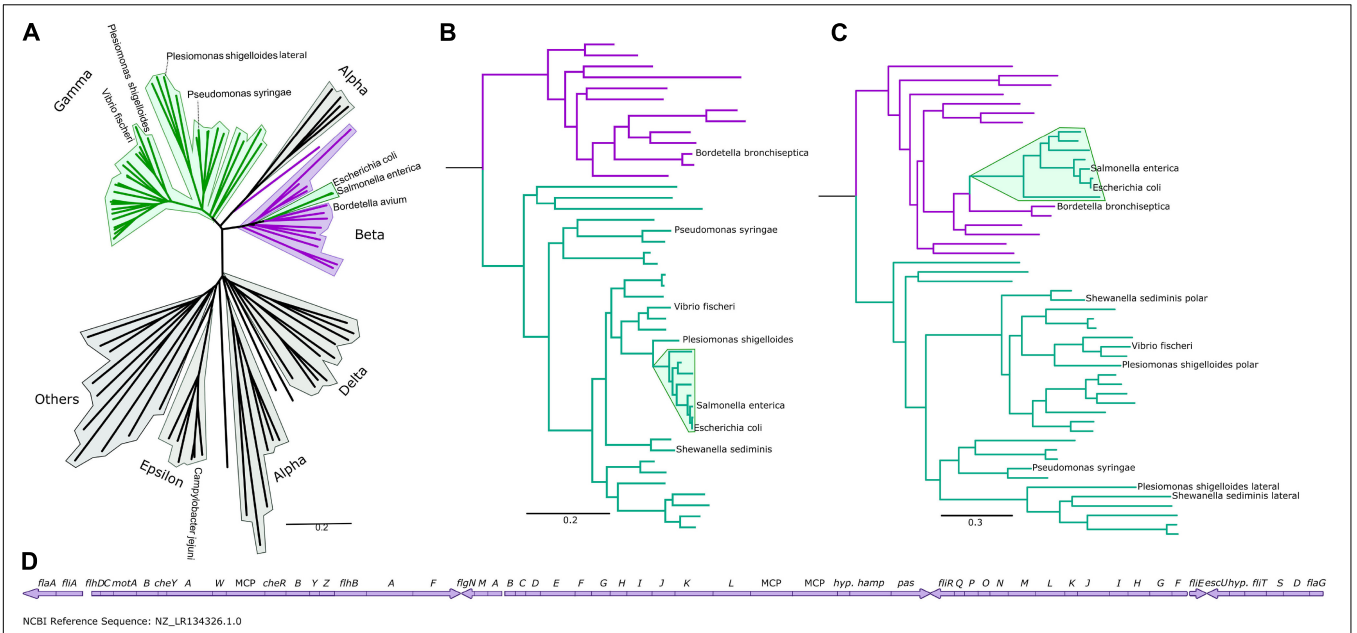

FIGURE 1 | The Enterobacteriaceae have β-like motors. **(A)** An unrooted global flagellar phylogeny. γ -proteobacteria are highlighted in green: the enteric Enterobacteriaceae γ -proteobacteria (*Salmonella enterica* and *Escherichia coli)* are not clustered with the other γ -proteobacteria, but are clustered within the β-proteobacteria (purple). Fully annotated version of this tree is presented in **Supplementary Figure S1**. **(B)** An organismal phylogeny focused on γ - (green) and β-proteobacteria (purple), rooted with an ε-proteobacterium, *Campylobacter jejuni.* The Enterobacteriaceae are highlighted in green. Fully annotated version of this tree is presented in **Supplementary Figure S4**. **(C)** The flagellar phylogeny of the γ - (green) and β-proteobacteria (purple). Note the shift in position of the Enterobacteriaceae (highlighted in green) from the γ -proteobacterial clade to within the β-proteobacterial clade. Rooted with *Campylobacter jejuni.* Fully annotated version of this tree is presented in **Supplementary Figure S5**. **(D)** The *Bordetella bronchiseptica* flagellar gene cluster is arranged in one continuous genetic locus.

enterics retain lateral flagella (Ren et al., 2005), suggesting either selective loss, or reacquisition after species radiation. *Plesiomonas* is primarily aquatic yet also causes gastroenteritis, like many enterics, and whether *Plesiomonas* should be classified as an enteric (Enterobacteriaceae) remains controversial (Janda et al., 2016). The lack of diversity in the *Plesiomonas* genus relative to the other enterics could be explained by rapid diversification of enteric species facilitated by acquisition of the β-proteobacterial flagellum, although there may be other explanations.

To understand the significance of this horizontal transfer, we sought to compare motor structures of *Bordetella*, *Salmonella*, and *Plesiomonas* using electron cryo-tomography and subtomogram averaging. We chose *Bordetella bronchiseptica* as a representative descendant of the ancestral β-proteobacterial donor, and used a Δ*bvgS* deletion to enable flagellation under lab conditions, as wildtype *B. bronchiseptica* uses its BvgAS two-component regulatory system to repress flagellar expression except under specific environmental conditions (Akerley et al., 1992). To reduce sample thickness, we gently deflated *B. bronchiseptica* cells with penicillin, and applied subtomogram averaging to 205 motors from 520 tomograms. Semblance of the *B. bronchiseptica* β-proteobacterial motor with the *Salmonella* and *E. coli* motors was consistent with a horizontal transfer (**Figure 2**), with comparable C-ring radii (20 nm), inter-membrane distances (29 nm), MS-ring and P-ring spacing (15 nm), and distance from the P-ring to the outer membrane (10 nm) (Rossmann and Beeby, 2018). As with the *Salmonella* motor, we could not discern stator complex densities in our subtomogram average structure, indicating that *B. bronchiseptica* stator complexes are dynamic.

We recently determined the structure of the polar motor from *P. shigelloides* (Ferreira et al., 2019) (**Figure 2**). This motor has a ring of 13 stator complexes, similar to the closely related *Vibrio fischeri* (Beeby et al., 2016) and *Vibrio alginolyticus* (Zhu et al., 2017), in contrast to the dynamic stator complexes of *Salmonella* and *B. bronchiseptica*, and likely explained by high stator complex occupancy. These polar motors have large disks required for stator complex assembly associated with their high torque and speed.

We next determined the structure of the lateral motor of *P. shigelloides*. We triggered lateral motor assembly by inhibiting polar motor function using Phenamil (Kawagishi et al., 1996), and thinned cells by penicillin deflation. To ensure identification of lateral motors we also deleted the polar flagellar filament Δ*fliC* and selected only motors with attached flagella; these motors were also distinguished by lateral placement, absence of periplasmic disks, and indistinct or absent C-rings. Subtomogram averaging of 317 motors from 632 tomograms revealed a well-resolved core, but absent stator complexes, and an indistinct C-ring (**Figure 2**). The indistinct C-ring is likely not a dissociation artifact from penicillin deflation, as laterally flagellated cells remained motile after deflation, polar flagella in the deflated cells had clearly resolved C-rings, *B. bronchiseptica* cells and previously imaged *E. coli* and *Salmonella* cells deflated using the same protocol had

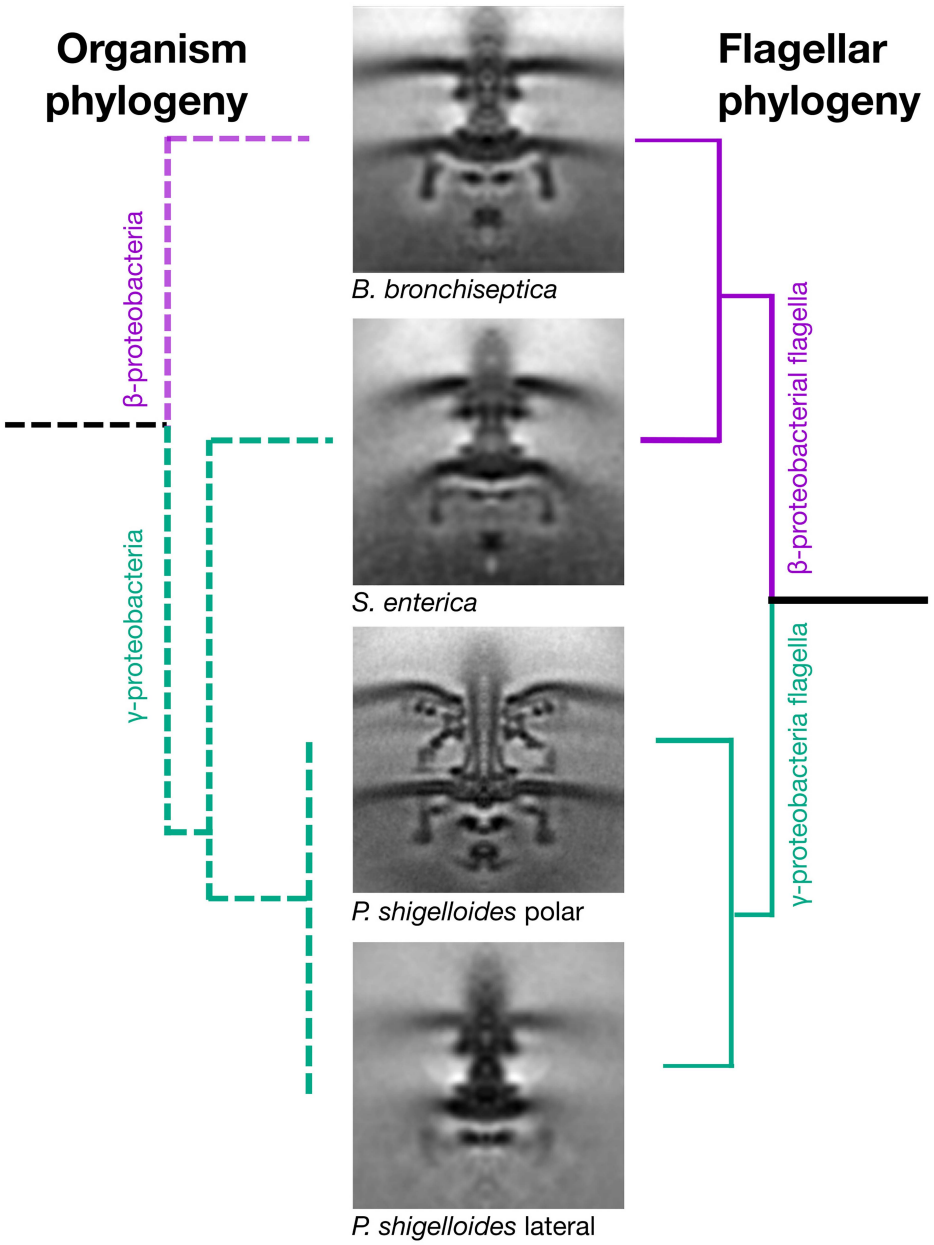

FIGURE 2 | Horizontal transfer of flagellar genes is confirmed by cryo electron tomography and subtomogram averaging. Subtomogram averages of the "donor" (*Bordetella bronchiseptica*) and "acceptor" (*Plesiomonas shigelloides*) strains confirms that the γ-proteobacterium, *Salmonella enterica,* has a flagellar motor that is structurally similar to the β-proteobacterium, *B. bronchiseptica,* and structurally distinct from the two motors of its close relative, the γ-proteobacterium *P. shigelloides.* The organism phylogeny (left) and flagellar phylogeny (right) are inconsistent as the γ-proteobacterium, *Salmonella enterica,* has a β-proteobacterial motor. Middle: Subtomogram averages of *B. bronchiseptica* (EMD-4999), *S. enterica* (EMD-3154), *P. shigelloides* polar motor (EMD-10057) and *P. shigelloides* lateral motor (EMD-10000). Note the faint C-ring density in the lateral motor. Subtomogram average boxes are 100 × 100 nm. Unsymmetrized structures are shown in **Supplementary Figure S7**.

clearly resolved C-rings (Chen et al., 2011), and there was no correlation between lateral C-ring presence in tomograms and the extent of cell lysis. We conclude that lateral motor C-rings are more dynamic, and lower-occupancy, than C-rings from other motors.

The indistinct lateral motor C-ring is likely a result of the loss of chemotactic ability by lateral motors (Bubendorfer et al., 2014), consistent with the divergence of C-ring components found in our phylogenetic studies (**Supplementary Figure S3**). In most flagellar motors the C-ring plays dual roles as a switch complex, responding to phosphorylated CheY from chemoreceptors; and anchor for the FliHIJ complex (Chen et al., 2011; Abrusci et al., 2013). Because the lateral C-ring is only required to anchor FliHIJ, it may have evolved a

more dynamic architecture than chemotactic motors, assembling as needed (Terashima et al., 2018). This is reminiscent of the non-rotating *Salmonella* SPI-1 injectisome "C-ring," which also has the sole function of anchoring corresponding FliHIJ homologs (Hu et al., 2017). Consistent with this we did not resolve FliI in lateral motors, indicating that it, too, is present at lower occupancy.

We suggest that horizontal transfer of the β-proteobacterial flagellar motor to the enterics highlights a principle of evolution: having evolved, complexity is difficult to reverse. Duplication and sub-functionalization of the γ-proteobacterial motors yielded a polar system, which provided high torque and speed in aquatic habitats; and a lateral system, which provided surface swarming motility. This sub-functionalization and niche optimization came at the cost of the flexibility provided by the β-proteobacterial motor, as these specialized motors would be incapable of on-the-fly adjustment to the varied niches occupied by enteric bacteria. The only tractable evolutionary mechanism to provide the benefit of a generalist motor may have been to wholesale replace the specialized motors with a horizontally-transferred motor instead of re-generalization of the existing motors. This transfer was facilitated by co-occurrence of flagellar genes together in one region of DNA in an ancestral β-proteobacterium.

Indeed, we speculate that such a transfer may have accompanied the development of the enteric lifestyle of the enteric γ-proteobacteria. Acquisition of the β-proteobacterial motor provided a single, dynamic flagellum capable of adjusting to diverse environments and viscosities. Indeed, *Bordetella's* role as a mucosal respiratory tract pathogen demonstrates the β-proteobacterial motor's ability to colonize mucosal surfaces (Mattoo and Cherry, 2005; Solans and Locht, 2019). Dynamic stator complexes would facilitate optimal energy consumption, with stator complexes incorporating only as needed (Berg, 2017), at the cost of lower speeds and torques that may have been less important in an gastrointestinal tract than the higher flow rates of an aquatic environment. Because polar motors are usually sodium-driven, the proton-driven β-proteobacterial peritrichous motor could have benefited bacteria moving away from a high-salt aquatic niche.

While horizontal flagellar transfers have previously been described, no studies have recognized that the best-studied flagellar system, that of the enteric γ-proteobacteria, is a horizontal acquisition. An early comprehensive survey by Liu & Ochman noted the superficially similar transfer of a lateral (not to be confused with peritrichous) γ-proteobacteria flagellar system (there termed "secondary," without highlighting that they are lateral systems from enteric γ-proteobacteria) to a β-proteobacterium, and also included a phylogenetic tree that depicted yet did not discuss our finding (Liu and Ochman, 2007). This oversight is also evident in a contemporaneous study describing the transfer of a polar flagellar system from a γ-proteobacterial donor to the α-proteobacterium *Rhodobacter sphaeroides* (Poggio et al., 2007), in which a figure depicting *E. coli* branching from a clade that included *Bordetella bronchiseptica* was not discussed. These and our results highlight the surprising complexity and frequency of wholesale transfers of flagellar systems, with the γ-proteobacteria duplicating their system to form polar (later transferred to an α-proteobacterium) and lateral (later transferred to a β-proteobacterium) systems, while a different β-proteobacterium transferred its (distinct) peritrichous system to the enteric clade of the γ-proteobacteria to supplant their native polar and lateral systems.

Our results show that the model flagellum is not native to its model organism host. Our finding resolves the long-standing paradox that different closely related γ-proteobacteria have different types of flagella. Furthermore, it shows a rare case by which specialization can be reversed by wholesale replacement with more generalized machinery. Our results may also help understand the evolution of the enterics, a family of diverse pathogens, and suggest development of novel, pathogen-specific drugs that target the β-proteobacterial-type motor.

MATERIALS AND METHODS

Strains

Bordetella bronchiseptica Δ*bvgS*	Andrew Preston, University of Bath
Plesiomonas shigelloides Δ*fliC*	Ferreira et al., 2019

Bacterial Growth

Cells from fresh LB plates were grown overnight (36 h for *B. bronchiseptica*) in LB at 37°C, 290 RPM. Cells were diluted 1:100 into fresh LB and grown until $OD_{600} \sim 0.6$. Prior to vitrification, cells were incubated with 466 IU/ml Penicillin G for half of one doubling time.

Phylogenetic Analysis

Complete, annotated genomes (91 for **Figure 1A** or 48 for **Figures 1B,C**, species listed in **Supplementary Table S1**) were exported from GenBank (National Center for Biotechnology Information (NCBI)) and stored in WebApollo (Lee et al., 2013). Proteins were identified or annotations were confirmed by BLASTP (Altschul et al., 1990). Concatenated phylogenies were determined following our previously published protocols (Chaban et al., 2018). In brief, flagella (FlgI, FlgC, FliE, FliF, FlhA, FlhB, FliI, FliP, FliQ, and FliR) and ribosomal protein (RplA, RplB, RplC, RplD, RplE, RplF, RplI, RplJ, RplK, RplM, RplN, RplO, RplP, RplQ, RplR) sequences (see **Supplementary Data Sheet S1**) were aligned using Fast Statistical Alignment (FSA) (Bradley et al., 2009). The T-Coffee Suite was used to determine informative positions using the transitive consistence score (TCS) (Notredame et al., 2000; Di Tommaso et al., 2011). Sequences were concatenated in Seaview (Gouy et al., 2010). The Maximum-likelihood approach was used within Garli (Bazinet et al., 2014) using the Jones, Taylor and Thornton (JTT) amino acid substitution rates (Jones et al., 1994). Trees were created from the best of ten replicates. A topology improvement of 0.0001 in the lnL score and termination criterion of 100,000 were used. For the overall trees: 1,000 bootstraps were calculated with a topology improvement

of 0.01 in the lnL score and termination criterion of 10,000. For the individual flagellar trees: 100 bootstraps were calculated with a topology improvement of 0.01 in the lnL score and termination criterion of 10,000. Bootstraps were added to the tree using SumTrees (SumTrees, 2019) and trees were visualized in FigTree (FigTree, 2017).

Cryo-grid Preparation

Cell pellets were mixed with gold fiducials coated in BSA. 3μl of the cell/fiducial mixture was applied to freshly glow discharged R2/2, 300 mesh copper Quantifoil R2/2 grids (Quantifoil Micro Tools GmbH, Germany). A Vitrobot Mark IV was used to freeze grids in an ethane/propane cryogen at 100% humidity.

Tilt-Series Collection

Tilt-series of *B. bronchiseptica* and *P. shigelloides* lateral motors were collected on an FEI F20 with a Falcon II detector (Thermo Fisher Scientific (formerly FEI), Hillsboro, OR, United States). A total fluence of 120 e-/Å^2 was used and a defocus of between −3 and −4.5 μm. Tilt-series were collected over a tilt range of ± 53° with 3° tilt increments and a pixel size of 8.28 Å.

Tomogram Reconstruction and Subtomogram Averaging

Tomograms of *B. bronchiseptica* and *P. shigelloides* lateral motors were reconstructed automatically using RAPTOR (Amat et al., 2008) and IMOD (Kremer et al., 1996).

Subtomograms were picked manually (205 subtomograms picked from 520 tomograms for *B. bronchiseptica* and 317 subtomograms picked from 632 tomograms for *P. shigelloides*). Template-free alignment was carried out in PEET by superimposing all manually picked subtomograms allowing no shifts or rotations for an initial reference. As no symmetry was observed, and to better visualize the overall motor profile, 100-fold rotational averaging was applied using custom scripts.

DATA AVAILABILITY STATEMENT

The datasets presented in this study can be found in online repositories. The names of the repository/repositories and accession number(s) can be found below: https://www.ebi.ac.uk/pdbe/emdb/, EMD-10000; https://www.ebi.ac.uk/pdbe/emdb/, EMD-4999.

AUTHOR CONTRIBUTIONS

JF, IC, BQ, KW, and MB designed experiments. JF, IC, MA, TZ, and BQ conducted experiments. JF, KW, and MB wrote the manuscript. All authors contributed to the article and approved the submitted version.

FUNDING

This work was supported by a Medical Research Council grant MR/P019374/1 to MB and a Medical Research Council Ph.D. Doctoral Training Partnership award grant no. MR/K501281/1 to JF. TZ was funded by Wellcome Trust Vacation Scholarship award 202596/Z/16/Z. BQ was funded by a BBSRC grant BB/L023091/1.

ACKNOWLEDGMENTS

We thank Andy Preston for the gift of the *Bordetella* Bvg- strain. Paul Simpson for electron microscopy assistance; Teige Matthews-Palmer, Florian Rossmann, Bertus Beaumont, and Marc Erhardt for helpful discussions. Matthias Wolf for providing IC with facilities for preliminary imaging during protocol development. Chaoqun Yao for technical assistance with phylogenetic reconstructions.

SUPPLEMENTARY MATERIAL

The Supplementary Material for this article can be found online at: https://www.frontiersin.org/articles/10.3389/fmicb.2021.643180/full#supplementary-material

Supplementary Figure 1 | Fully annotated wide-scale flagellar phylogeny tree from **Figure 1A**. An unrooted, wide-scale tree of flagellar phylogeny. The Enterobacteriaceae (*Salmonella enterica* and *Escherichia coli)* are not clustered with the other γ-proteobacteria (green), but are clustered within the β-proteobacteria (purple).

Supplementary Figure 2 | Unrooted trees of individual flagellar proteins. Individual flagellar proteins used in the concatenated flagellar tree have similar topologies with each other and with the concatenated tree. β-proteobacteria in purple, γ-proteobacteria in green, lateral flagella highlighted in pink. 1 = polar, 2 = lateral.

Supplementary Figure 3 | Trees made using the flagellar proteins C-ring proteins. Unrooted FliG and FliM trees differ from other flagellar protein trees (depicted in **Supplementary Figure S2**) or the concatenated tree (**Figure 1C**) due to long branches in the lateral flagellar clade (highlighted in pink). 1 = polar, 2 = lateral.

Supplementary Figure 4 | Fully annotated organismal phylogeny tree from **Figure 1B**. β-proteobacteria in purple, γ-proteobacteria in green, Enterobacteriaceae highlighted in green. Rooted with the ε-proteobacterium, *Campylobacter jejuni*. Bootstrap values indicated on nodes.

Supplementary Figure 5 | Fully annotated flagellar phylogeny tree from **Figure 1C**. β-proteobacteria in purple, γ-proteobacteria in green, Enterobacteriaceae highlighted in green. Rooted with the ε-proteobacterium, *Campylobacter jejuni*. Bootstrap values indicated on nodes.

Supplementary Figure 6 | Example tomograms. **(A)** Slice through a representative tomogram of *B. bronchiseptica* with a peritrichous motor pointed out in green. **(B)** Slice through a representative tomogram of *P. shigelloides* with the lateral motor pointed out in purple and the polar motors with only hooks (filament protein, FliC, is deleted) in yellow.

Supplementary Figure 7 | Subtomogram averages prior to C100 rotational averaging. **(A)** Slice through *Bordetella bronchiseptica* motor unsymmetrised subtomogram average, **(B)** Slice through *Plesiomonas shigelloides* lateral motor unsymmetrised subtomogram average. Boxes are 100 nm × 100 nm.

REFERENCES

Reid, S. W., Leake, M. C., Chandler, J. H., Lo, C.-J., Armitage, J. P., and Berry, R. M. (2006). The maximum number of torque-generating units in the flagellar motor of *Escherichia coli* is at least 11. *Proc. Natl. Acad. Sci. U S A.* 103, 8066–8071. doi: 10.1073/pnas.0509932103

Tipping, M. J., Delalez, N. J., Lim, R., Berry, R. M., and Armitage, J. P. (2013). Load-dependent assembly of the bacterial flagellar motor. *mBio* 4, 1–6. doi: 10.1128/mBio.00551-13

Lee, S. Y., Cho, H. S., Pelton, J. G., Yan, D., Henderson, R. K., King, D. S., et al. (2001). Crystal structure of an activated response regulator bound to its target. *Nat. Struct. Biol.* 8, 52–56. doi: 10.1038/83053

Berg, H. C., and Brown, D. A. (1972). Chemotaxis in *Escherichia coli* analysed by Three-dimensional Tracking. *Nature* 239, 500–504. doi: 10.1038/239500a0

Silverman, M., and Simon, M. (1974). Flagellar rotation and the mechanism of bacterial motility. *Nature* 249, 73–74. doi: 10.1038/249073a0

Beeby, M., Ribardo, D. A., Brennan, C. A., Ruby, E. G., Jensen, G. J., and Hendrixson, D. R. (2016). Diverse high-torque bacterial flagellar motors assemble wider stator rings using a conserved protein scaffold. *Proc. Natl. Acad. Sci.* 2016:201518952. doi: 10.1073/pnas.1518952113

Zhu, S., Nishikino, T., Hu, B., Kojima, S., Homma, M., and Liu, J. (2017). Molecular architecture of the sheathed polar flagellum in Vibrio alginolyticus. *Proc. Natl. Acad. Sci. U S A.* 114, 10966–10971. doi: 10.1073/pnas.1712489114

Terashima, H., Koike, M., Kojima, S., and Homma, M. (2010). The Flagellar Basal Body-Associated Protein FlgT Is Essential for a Novel Ring Structure in the Sodium-Driven Vibrio Motor. *J. Bacteriol.* 192, 5609–5615. doi: 10.1128/JB.00720-10

Terashima, H., Fukuoka, H., Yakushi, T., Kojima, S., and Homma, M. (2006). The Vibrio motor proteins, MotX and MotY, are associated with the basal body of Na-driven flagella and required for stator formation. *Mol. Microbiol.* 62, 1170–1180. doi: 10.1111/j.1365-2958.2006.05435.x

Bubendorfer, S., Koltai, M., Rossmann, F., Sourjik, V., and Thormann, K. M. (2014). Secondary bacterial flagellar system improves bacterial spreading by increasing the directional persistence of swimming. *Proc. Natl. Acad. Sci.* 111, 11485–11490. doi: 10.1073/pnas.1405820111

Xie, L., Altindal, T., Chattopadhyay, S., and Wu, X.-L. (2011). Bacterial flagellum as a propeller and as a rudder for efficient chemotaxis. *Proc. Natl. Acad. Sci.* 108, 2246–2251. doi: 10.1073/pnas.1011953108

Fujii, M., Shibata, S., and Aizawa, S.-I. (2008). Polar, Peritrichous, and Lateral Flagella Belong to Three Distinguishable Flagellar Families. *J. Mol. Biol.* 379, 273–283. doi: 10.1016/j.jmb.2008.04.012

Parks, D. H., Chuvochina, M., Waite, D. W., Rinke, C., Skarshewski, A., Chaumeil, P.-A., et al. (2018). A standardized bacterial taxonomy based on genome phylogeny substantially revises the tree of life. *Nat. Biotechnol.* 36, 996–1004. doi: 10.1038/nbt.4229

Wuichet, K., and Zhulin, I. B. (2010). Origins and diversification of a complex signal transduction system in prokaryotes. *Sci. Signal.* 3:ra50. doi: 10.1126/scisignal.2000724

Liu, R., and Ochman, H. (2007). Origins of flagellar gene: Operons and secondary flagellar systems. *J. Bacteriol.* 189, 7098–7104. doi: 10.1128/JB.00643-07

Ren, C.-P., Beatson, S. A., Parkhill, J., and Pallen, M. J. (2005). The Flag-2 locus, an ancestral gene cluster, is potentially associated with a novel flagellar system from *Escherichia coli*. *J. Bacteriol.* 187, 1430–1440. doi: 10.1128/JB.187.4.1430-1440.2005

Janda, J. M., Abbott, S. L., and McIver, C. J. (2016). Plesiomonas shigelloides Revisited. *Clin. Microbiol. Rev.* 29, 349–374. doi: 10.1128/CMR.00103-15

Akerley, B. J., Monack, D. M., Falkow, S., and Miller, J. F. (1992). The bvgAS locus negatively controls motility and synthesis of flagella in Bordetella bronchiseptica. *J. Bacteriol.* 174, 980–990.

Rossmann, F. M., and Beeby, M. (2018). Insights into the evolution of bacterial flagellar motors from high-throughput in situ electron cryotomography and subtomogram averaging. *Acta Crystallogr. Sect. Struct. Biol.* 74, 585–594. doi: 10.1107/S2059798318007945

Ferreira, J. L., Gao, F. Z., Rossmann, F. M., Nans, A., Brenzinger, S., Hosseini, R., et al. (2019). *γ-proteobacteria* eject their polar flagella under nutrient depletion, retaining flagellar motor relic structures. *PLoS Biol.* 17:e3000165. doi: 10.1371/journal.pbio.3000165

Kawagishi, I., Imagawa, M., Imae, Y., McCarter, L., and Homma, M. (1996). The sodium-driven polar flagellar motor of marine Vibrio as the mechanosensor that regulates lateral flagellar expression. *Mol. Microbiol.* 20, 693–699.

Chen, S., Beeby, M., Murphy, G. E., Leadbetter, J. R., Hendrixson, D. R., Briegel, A., et al. (2011). Structural diversity of bacterial flagellar motors. *EMBO J.* 30, 2972–2981. doi: 10.1038/emboj.2011.186

Abrusci, P., Vergara–Irigaray, M., Johnson, S., Beeby, M. D., Hendrixson, D., Roversi, P., et al. (2013). Architecture of the major component of the type III secretion system export apparatus. *Nat. Struct. Mol. Biol.* 20, 99–104. doi: 10.1038/nsmb.2452

Terashima, H., Kawamoto, A., Tatsumi, C., Namba, K., Minamino, T., and Imada, K. (2018). In Vitro Reconstitution of Functional Type III Protein Export and Insights into Flagellar Assembly. *mBio* 9:18. doi: 10.1128/mBio.00988-18

Hu, B., Lara-Tejero, M., Kong, Q., Galán, J. E., and Liu, J. (2017). In Situ Molecular Architecture of the *Salmonella* Type III Secretion Machine. *Cell* 168, 1065.e–1074.e. doi: 10.1016/j.cell.2017.02.022

Mattoo, S., and Cherry, J. D. (2005). Molecular Pathogenesis, Epidemiology, and Clinical Manifestations of Respiratory Infections Due to Bordetella pertussis and Other Bordetella Subspecies. *Clin. Microbiol. Rev.* 18, 326–382. doi: 10.1128/CMR.18.2.326-382.2005

Solans, L., and Locht, C. (2019). The Role of Mucosal Immunity in Pertussis. *Front. Immunol.* 9:03068. doi: 10.3389/fimmu.2018.03068

Berg, H. C. (2017). The flagellar motor adapts, optimizing bacterial behavior. *Protein Sci. Publ. Protein Soc.* 26, 1249–1251. doi: 10.1002/pro.3055

Poggio, S., Abreu-Goodger, C., Fabela, S., Osorio, A., Dreyfus, G., Vinuesa, P., et al. (2007). A Complete Set of Flagellar Genes Acquired by Horizontal Transfer Coexists with the Endogenous Flagellar System in Rhodobacter Sphaeroides. *J. Bacteriol.* 189, 3208–3216. doi: 10.1128/JB.01681-06

Lee, E., Helt, G. A., Reese, J. T., Munoz-Torres, M. C., Childers, C. P., Buels, R. M., et al. (2013). Web Apollo: a web-based genomic annotation editing platform. *Genome Biol.* 14:R93. doi: 10.1186/gb-2013-14-8-r93

Altschul, S. F., Gish, W., Miller, W., Myers, E. W., and Lipman, D. J. (1990). Basic local alignment search tool. *J. Mol. Biol.* 215, 403–410. doi: 10.1016/S0022-2836(05)80360-2

Chaban, B., Coleman, I., and Beeby, M. (2018). Evolution of higher torque in Campylobacter- type bacterial flagellar motors. *Sci. Rep.* 8:97. doi: 10.1038/s41598-017-18115-1

Bradley, R. K., Roberts, A., Smoot, M., Juvekar, S., Do, J., Dewey, C., et al. (2009). Fast Statistical Alignment. *PLoS Comput Biol.* 5:e1000392. doi: 10.1371/journal.pcbi.1000392

Notredame, C., Higgins, D. G., and Heringa, J. T. - (2000). Coffee: A novel method for fast and accurate multiple sequence alignment. *J. Mol. Biol.* 302, 205–217. doi: 10.1006/jmbi.2000.4042

Di Tommaso, P., Moretti, S., Xenarios, I., Orobitg, M., Montanyola, A., Chang, J.-M., et al. (2011). T-Coffee: a web server for the multiple sequence alignment of protein and RNA sequences using structural information and homology extension. *Nucleic Acids Res.* 39, W13–W17. doi: 10.1093/nar/gkr245

Gouy, M., Guindon, S., and Gascuel, O. (2010). SeaView version 4: A multiplatform graphical user interface for sequence alignment and phylogenetic tree building. *Mol. Biol. Evol.* 27, 221–224. doi: 10.1093/molbev/msp259

Bazinet, A. L., Zwickl, D. J., and Cummings, M. P. A. (2014). gateway for phylogenetic analysis powered by grid computing featuring GARLI 2.0. *Syst. Biol.* 63, 812–818. doi: 10.1093/sysbio/syu031

Jones, D. T., Taylor, W. R., and Thornton, J. M. A. (1994). Model Recognition Approach to the Prediction of All-Helical Membrane Protein Structure and Topology. *Biochemistry* 33, 3038–3049. doi: 10.1021/bi00176a037

SumTrees (2019). *Phylogenetic Tree Summarization and Annotation — DendroPy 4.4.0 documentation*. . Available online at: https://dendropy.org/programs/sumtrees.html [accessed date 3, April 2019]

FigTree (2017). . Available online at: http://tree.bio.ed.ac.uk/software/figtree/ (accessed date 2, April 2017).

Amat, F., Moussavi, F., Comolli, L. R., Elidan, G., Downing, K. H., and Horowitz, M. (2008). Markov random field based automatic image alignment for electron tomography. *J. Struct. Biol.* 161, 260–275. doi: 10.1016/j.jsb.2007.07.007

Kremer, J. R., Mastronarde, D. N., and McIntosh, J. R. (1996). Computer visualization of three-dimensional image data using IMOD. *J. Struct. Biol.* 116, 71–76. doi: 10.1006/jsbi.1996.0013

Conflict of Interest: The authors declare that the research was conducted in the absence of any commercial or financial relationships that could be construed as a potential conflict of interest.

Citation: Ferreira JL, Coleman I, Addison ML, Zachs T, Quigley BL, Wuichet K and Beeby M (2021) The "Jack-of-all-Trades" Flagellum From Salmonella and E. coli Was Horizontally Acquired From an Ancestral β-Proteobacterium. Front. Microbiol. 12:643180. doi: 10.3389/fmicb.2021.643180

frontiers in Microbiology

REVIEW
published: 13 April 2021
doi: 10.3389/fmicb.2021.659464

The Dynamic Ion Motive Force Powering the Bacterial Flagellar Motor

*Anaïs Biquet-Bisquert, Gilles Labesse, Francesco Pedaci and Ashley L. Nord**

Centre de Biologie Structurale (CBS), INSERM, CNRS, Université Montpellier, Montpellier, France

The bacterial flagellar motor (BFM) is a rotary molecular motor embedded in the cell membrane of numerous bacteria. It turns a flagellum which acts as a propeller, enabling bacterial motility and chemotaxis. The BFM is rotated by stator units, inner membrane protein complexes that stochastically associate to and dissociate from individual motors at a rate which depends on the mechanical and electrochemical environment. Stator units consume the ion motive force (IMF), the electrochemical gradient across the inner membrane that results from cellular respiration, converting the electrochemical energy of translocated ions into mechanical energy, imparted to the rotor. Here, we review some of the main results that form the base of our current understanding of the relationship between the IMF and the functioning of the flagellar motor. We examine a series of studies that establish a linear proportionality between IMF and motor speed, and we discuss more recent evidence that the stator units sense the IMF, altering their rates of dynamic assembly. This, in turn, raises the question of to what degree the classical dependence of motor speed on IMF is due to stator dynamics vs. the rate of ion flow through the stators. Finally, while long assumed to be static and homogeneous, there is mounting evidence that the IMF is dynamic, and that its fluctuations control important phenomena such as cell-to-cell signaling and mechanotransduction. Within the growing toolbox of single cell bacterial electrophysiology, one of the best tools to probe IMF fluctuations may, ironically, be the motor that consumes it. Perfecting our incomplete understanding of how the BFM employs the energy of ion flow will help decipher the dynamical behavior of the bacterial IMF.

Keywords: ion motive force, bacterial flagellar motor, stator, bacterial electrophysiology, subunit exchange, fluctuations, ion specificity, cell-to-cell signaling

OPEN ACCESS

Edited by:
Masahiro Ito,
Toyo University, Japan

Reviewed by:
Shuichi Nakamura,
Tohoku University, Japan
Yoshiyuki Sowa,
Hosei University, Japan

****Correspondence:***
Ashley L. Nord
ashley.nord@cbs.cnrs.fr

Specialty section:
This article was submitted to Microbial Physiology and Metabolism, a section of the journal Frontiers in Microbiology

Received: *27 January 2021*
Accepted: *02 March 2021*
Published: *13 April 2021*

Citation:
Biquet-Bisquert A, Labesse G, Pedaci F and Nord AL (2021) The Dynamic Ion Motive Force Powering the Bacterial Flagellar Motor. Front. Microbiol. 12:659464. doi: 10.3389/fmicb.2021.659464

INTRODUCTION

Several bacteria propel themselves by rotating their flagella (Berg and Anderson, 1973). The bacterial flagellar motor (BFM) is the powerful molecular nanomachine at the base of each flagellum responsible for such rotation. One of the few known examples of biological rotatory machines, the BFM is unique in its remarkable power and efficiency in converting free energy into mechanical work. Flagellar rotation is driven by the ion-motive force (IMF), the electro-chemical potential difference built across the membrane during cellular respiration. The demonstration that the motor is driven not by the energy of ATP hydrolysis but by the flux of ions across the membrane (Larsen et al., 1974; Manson et al., 1977) came a few years after the realization that flagella rotate (Berg and Anderson, 1973). Given an energy source that is a charged quantized particle, moving along

an electric field, both the experimental and theoretical treatments of the BFM energization are challenging. For example, under physiological conditions, the energy provided by the translocation of a single ion is about three times smaller than that released by ATP hydrolysis. As a consequence, important quantities like the elementary step size and mechanisms like the force generation are difficult to resolve experimentally and model theoretically. Ions move according to both electrical and concentration gradients. The IMF is defined as the sum of these two contributions by

$$\mathrm{IMF} = \Delta\Psi - 2.3\,\frac{RT}{F}\Delta pI \tag{1}$$

where $\Delta\Psi = \Psi_{int} - \Psi_{ext}$ is the difference in membrane potential Ψ, built up by the ensemble of charges separated by the membrane, $\Delta pI = pI_{int} - pI_{ext} = \log\frac{[I]_{ext}}{[I]_{int}}$ is the difference in the specific ion (I) potential, $[I]$ is the ion concentration, R is the gas constant, F is the Faraday constant, and T is the temperature ($2.3\,RT/F \simeq 60\,m\mathrm{V}$ at $T = 300K$). The IMF is maintained out of equilibrium in respiring cells by transmembrane (TM) complexes that actively pump ions outward across the inner membrane. External ions can diffuse and finally fall along the energy potential to be consumed by the BFM and by other TM complexes such as the ATP synthase.

Despite differences in ion selectivity and a rich diversity of evolved structural details (Rossmann and Beeby, 2018), the core structure of the BFM (see **Figure 1**) is well conserved. In *Escherichia coli*, the rotor is about 45 nm in diameter and composed of two main rings, the inner membrane embedded MS-ring and the cytoplasmic C-ring. The rotor couples rotation to the flagellum via the rod and then the extracellular hook. The stator consists of multiple units anchored to the peptidoglycan (PG) at the rotor's periphery. Each stator unit acts as an ion channel through which ions translocate and transfer their energy to generate the force, which rotates the rotor. Ion consumption of the stator unit is specific: MotAB stator units (e.g., in *E. coli* or *Salmonella enterica*) consume the cellular proton motive force (PMF), whereas PomAB stators (e.g., in *Vibrio alginolyticus*) consume the sodium ion motive force (SMF) Sowa and Berry (2008). Importantly, at least in enteric bacteria such as *E. coli* and *S. enterica*, stator units are not always bound to the motor complex, but they are observed to dynamically exchange between an inactive unbound state, diffusing in the inner membrane, and a motor-bound active state (Leake et al., 2006). Moreover, such exchange is mechanosensitive, as the motor can adapt the number of bound stator units depending on the external viscous load, incorporating up to a dozen (Lele et al., 2013; Tipping M. J. et al., 2013; Chawla et al., 2017; Nord et al., 2017; Terahara et al., 2017). Several studies suggest that stators may also be capable of sensing IMF, and that stator assembly is dependent upon the driving ion (Fukuoka et al., 2009; Tipping J. M. et al., 2013).

In this review, we present and discuss some of the major results that shed light on the dynamic bacterial IMF, in particular with respect to the structure and activity of the flagellar motor and its stator units.

BFM SPEED IS PROPORTIONAL TO IMF

Understanding the relations that couple IMF, $\Delta\Psi$, ΔpI, and motor activity (measured via the swimming speed of cells or the angular speed and torque of individual motors) is of great interest, particularly as it provides accurate constraints for physical mechanistic models of the motor. Unfortunately, drawing a conclusive general scheme on how the motor activity depends on the IMF components is complicated by the dependence of membrane and ion potentials on intrinsic cellular homeostasis, large cell-to-cell variability, and differences among strains. Measuring the activity of single motors under controlled conditions helps to obtain the full distribution of behaviors.

A natural parameter to vary when studying the motor behavior as a function of IMF is the concentration of the coupling ion in the external medium, affecting pI_{ext}, as illustrated in **Figure 2** for three published works. For proton-consuming motors (e.g., *E. coli, B. subtilis, Streptococcus*), changing pH_{ext} affects not only motor activity, but also several other cellular mechanisms. This results in a coupling between the components of the PMF. In *B. subtilis* (**Figure 2A**) (Shioi et al., 1980) and *E. coli* (**Figure 2B**) (Minamino et al., 2003), an increase in pH_{ext} is accompanied by an increase in pH_{int} (linear in *E. coli*, with a saturation in *B. subtilis*), with $pH_{int} > pH_{ext}$ up to $pH_{ext} \sim 7.5$. As ΔpH decreases, $\Delta\Psi$ increases in a compensatory manner, resulting in a PMF that does not change dramatically (within $\sim$ 50 mV) in the range of $pH_{ext} = 5 - 8$. The coupling between pI_{ext} and $\Delta\Psi$ has been cleverly avoided by expressing chimeric Na^+-driven stators in *E. coli* (Lo et al., 2007) (**Figure 2C**). In this case, varying pNa_{ext} has very little effect on $\Delta\Psi$. Therefore, the SMF follows ΔpNa, decreasing with increasing pNa_{ext}, given that pNa_{int} increases less rapidly than pNa_{ext}. Moreover, pH_{ext} can also be used to control the SMF, as it linearly affects $\Delta\Psi$ but is almost entirely decoupled from ΔpNa.

In the Na^+-driven chimeric motor of *E. coli*, at high load the speed of the motor is linearly proportional to SMF, with an equivalent dependence upon $\Delta\Psi$ (controlled by pH_{ext}) and ΔpNa (controlled by pNa_{ext}). At lower load (0.35 μm beads), the equivalence between the two components breaks down (**Figure 2C**, right panels). For instance, if $\Delta\Psi$ is decreased and ΔpNa is increased so as to keep the SMF constant, one observes an increase in motor speed. The non-equivalence is graphically shown in the space $(\Delta\psi, \Delta pNa, \omega)$ in **Figure 2C**: : while at high load, the same speed (red dot) can be reached by increasing either $\Delta\psi$ or ΔpNa, at low load, this is no longer true (red dots), as the slope of ω, seen as a function of one component, depends on the other component. The leading hypothesis to explain this non-equivalence is that the rate-limiting step at low load and low $[Na^+]_{ext}$ conditions is the diffusion-limited binding of Na^+ ions to the stator units (Lo et al., 2007).

Despite some descriptions of nonlinearities (threshold, saturation, and the non-equivalence of the IMF components; Khan and Macnab, 1980; Shioi et al., 1980; Lo et al., 2007), reflecting the complexity of the measurements and of their interpretation, numerous results contribute to a general consensus that there exists a linear relationship between the speed of the motor and IMF. **Table 1** summarizes some of the

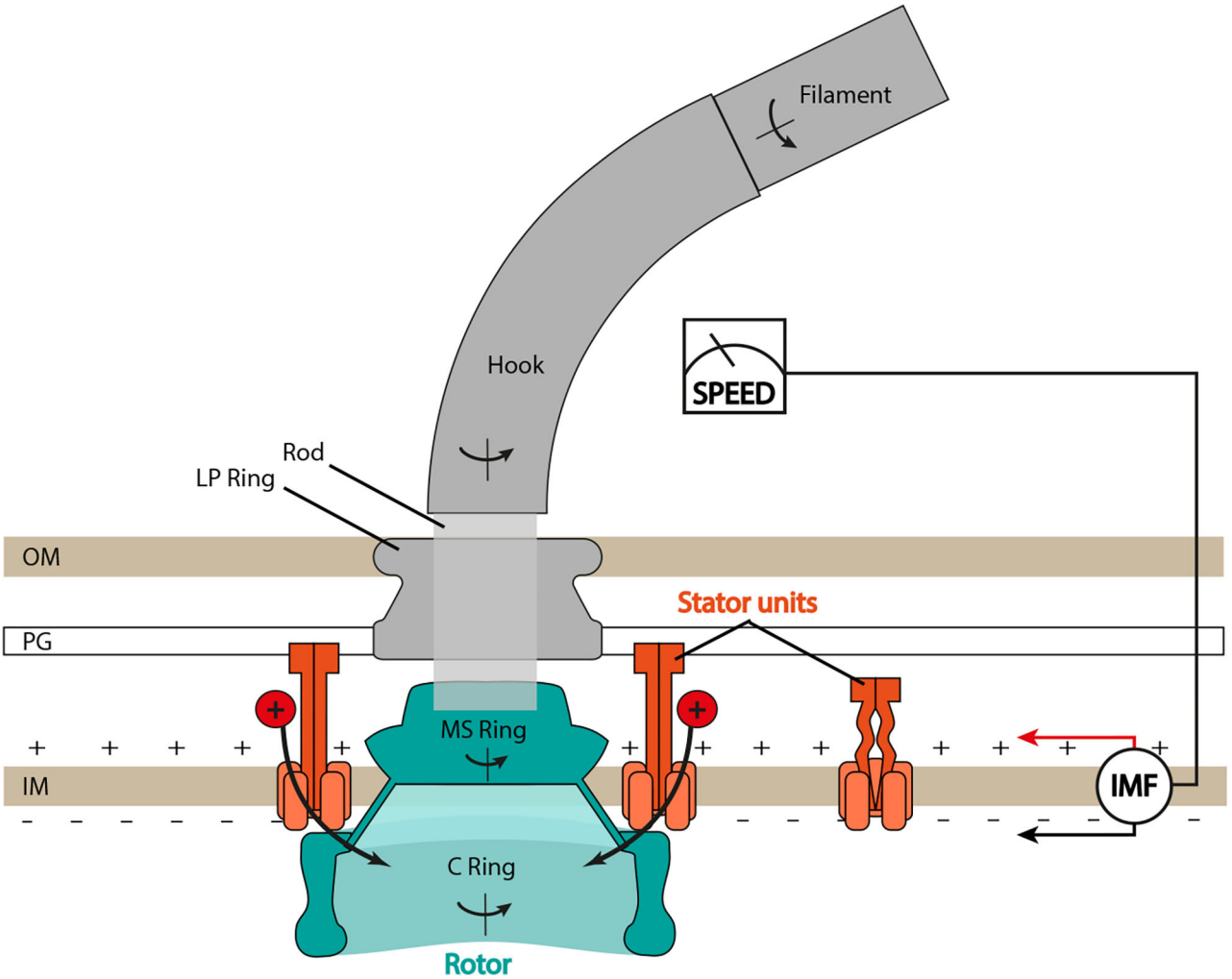

FIGURE 1 | Schematic of the bacterial flagellar motor (BFM) in Gram-negative bacteria. The flagellar filament is connected to the rotor (in blue) through the hook, the universal joint, and the rod, the central driveshaft that connects the hook to the MS ring. The LP ring is assembled around the rod and acts as a bushing. Stator units bind to the peptidoglycan (PG) layer, translocate ions from the periplasm to the cytoplasm, and generate torque by interacting with the C ring. IM, inner membrane; OM, outer membrane. Type III export apparatus not shown.

published works that have described this proportionality and the range of IMF for which it holds, covering the physiological range. In Lo et al. (2007), the authors investigated motor speed per stator unit in Na^+-powered motors, finding that the linear relationship between speed and IMF holds true at the level of an individual stator unit. However, the proportionality breaks down with acidification of the cytoplasm, at least in H^+-powered motors. In the presence of a weak acid (which dissociates upon crossing the cytoplasmic membrane, lowering pH_{int} and partially collapsing ΔpH), a decrease of pH_{ext} from 7 to 5 leads to a total decrease in PMF of only $\sim$ 10 mV, yet causes a strong decline in motor speed. From these results, it was hypothesized that high internal proton concentration hinders proton unbinding from the stators in the cytosol, hampering their function (Minamino et al., 2003). Therefore, the motor seem to respond to the entire IMF, unless pH_{int} is lowered substantially (Gabel and Berg, 2003).

When considering the linearity between IMF and speed, one should also keep in mind the associated time scale. Because of technical limitations, mainly in the dynamical measurement of IMF, the linear relationship has been experimentally demonstrated only at low frequency, i.e., in ensemble averages of ω and IMF acquired over relatively long periods of time. While it is now possible to measure ω with $\sim$ 10 ms resolution in bead assays, the IMF is often measured on a scale of several seconds to minutes, and often averaged over the entire cell population. However, at least two assays have managed to directly and dynamically manipulate the IMF. By applying a varying external voltage directly to a trapped and permeabilized cell within a micropipette, the linearity between ω and IMF was demonstrated with a resolution of a few seconds (Fung and Berg, 1995). By expressing and exciting the proton pump proteorhodopsin to trigger proton efflux (Walter et al., 2007; Tipping J. M. et al.,

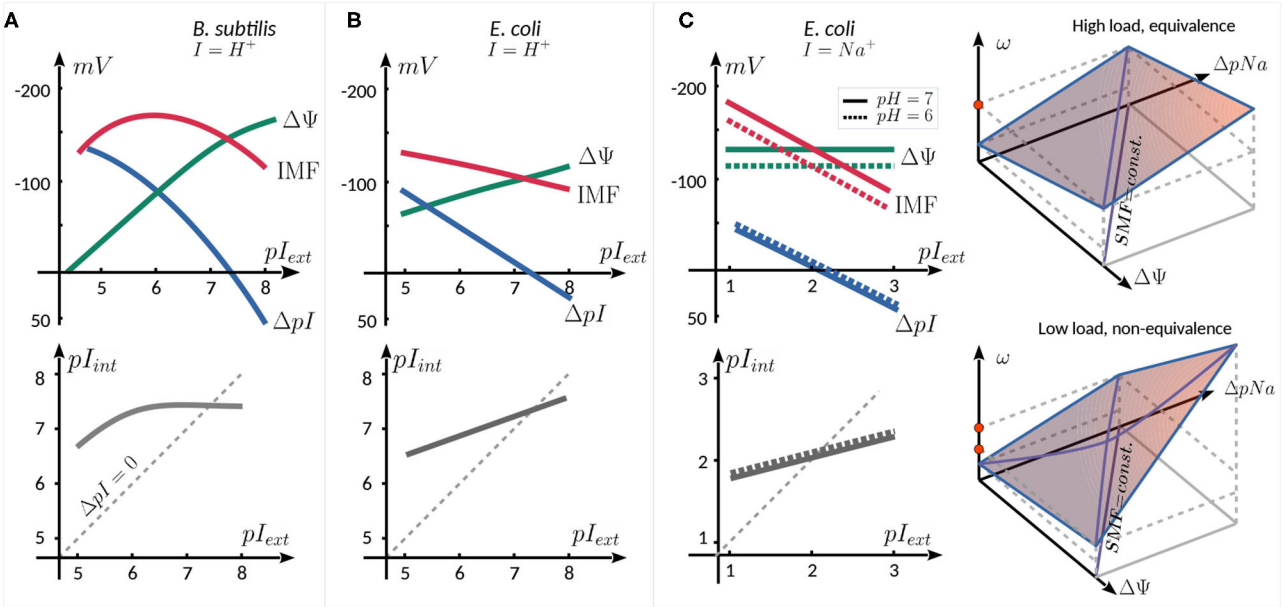

FIGURE 2 | Schematic relation between $\Delta\Psi$, ΔpI, IMF (top panels), and pI_{int} (bottom panels) as a function of external ion concentration. The graphs are reproduced from the data published in **(A)** (Shioi et al., 1980), for the proton consuming motor of *B. subtilis*, **(B)** Minamino et al. (2003), for the proton consuming motor of *E. coli*, and **(C)** Lo et al. (2007) for the sodium consuming chimeric motor of *E. coli* employing chimeric Na^+ stators. The two rightmost panels in **(C)** show schematically the equivalence of the SMF components at high load (top), and their nonequivalence (bottom panel, see text).

TABLE 1 | Published linearity ranges between motor speed ω and ion motive force (IMF) in different strains.

Strain	Ion	IMF (mV)	ω (Hz)	Load	Comment	References
B. subtilis	H^+	−30, −100		H	Threshold, saturation	Shioi et al., 1980
Streptococcus	H^+	−30, −100	0.5, 2	H		Manson et al., 1980
Streptococcus	H^+	0, −50	0, 4	H		Khan et al., 1985
Streptococcus	H^+		20, 70	H	H^+ flux linear with ω	Meister et al., 1987
Streptococcus	H^+	20, −200	0, 10	H		Khan et al., 1990
E. coli	H^+	−50, −150	0.1, 7	H	Voltage via micropipette	Fung and Berg, 1995
E. coli	H^+	0, −150[a]	0, 5	H	Two motors of one cell	Gabel and Berg, 2003
E. coli	H^+	0, −150[a]	10, 250	L	Two motors of one cell	Gabel and Berg, 2003
V. alginolyticus	Na^+	−130, −180[b]	50, 700	H/L	Torque-speed curves	Sowa et al., 2003
E. coli	H^+	−100, −130		H	Const. swimming speed	Minamino et al., 2003
E. coli	Na^+	−54, −187	2.2, 8.7[c]	H	pH_{ext} $[Na^+]_{ext}$ controlled	Lo et al., 2007

The IMF column indicates the range tested. The load column indicates high (H) (tethered cell or ∼ 1μm bead assays) or low (L) load (350–450 nm bead assay) applied to the motor.
[a] *Assumed.*
[b] *Calculated from Lo et al. (2007).*
[c] *Speed of first stator.*

2013), the IMF could be dynamically perturbed (though not measured) while measuring ω with sub-second resolution. Below, we discuss recent techniques for dynamic IMF quantification. When observing motor speed and IMF at higher frequency (i.e., averaging on sub-second time intervals), the analysis is complicated by fluctuations, and resolving the relationship between fast IMF fluctuations and fast speed variations remains challenging. Finally, as discussed further below, dynamic stator assembly and exchange must also be considered (or controlled) when studying the relation between IMF and speed.

The observation that the ion flow through the motor is directly proportional to speed, together with a linear relation between IMF and speed, contributed to a widely used model wherein ion translocation is tightly coupled to rotation, i.e., a fixed number of ions yields a fixed angular displacement (Manson et al., 1980; Meister et al., 1987). The IMF-speed linearity is a necessary condition for the tight-coupling model, and it has been validated

by several measurements, as described above. However, it is not a sufficient condition. Given its importance for BFM mechanistic modeling, as well as other microbiological mechanisms (e.g., mechanosensing and biofilm initiation; Belas, 2013), the tight-coupling hypothesis warrants continued scrutiny, ideally at the single motor level.

STATOR ASSEMBLY IS SENSITIVE TO IMF

Contrary to the long-held assumption that, once assembled, the structure of the BFM was static, it is now well established that multiple motor components dynamically exchange. The most well-studied example of this are the stator units, which exchange between an active motor-bound form and an inactive membrane diffusing form on a timescale of seconds to minutes (Leake et al., 2006). The rate of exchange and the steady-state number of stators is dependent upon the viscous load on the motor (Lele et al., 2013; Tipping M. J. et al., 2013; Chawla et al., 2017; Nord et al., 2017), a property that allows the bacterium to adapt to changes in local viscosity. However, there are multiple clues that suggest that stator exchange and assembly is sensitive not only to the local mechanical environment, but also to the local electrochemical environment. Such a capacity would allow strains that couple multiple ions via separate stators to tune their motor composition to the prevailing conditions (Thormann and Paulick, 2010).

One of the first experiments to suggest that stator assembly was sensitive to IMF was Fung and Berg's micropipette experiment (Fung and Berg, 1995). Once a filamentous cell of *E. coli* was installed in the micropipette, they dissipated the PMF via an ionophore, which halted motor rotation, as expected. But, when the membrane voltage was reinstated, they observed a delay before motors began rotating, after which speed increased in step-wise increments. This suggested that stator units inactivated, in some way, upon PMF collapse, then individually reactivated or reassembled upon reinstatement of the PMF. In an attempt to hold the number of stator units constant while assessing the linearity between speed and IMF, the authors avoided total PMF collapse by maintaining a nonzero DC voltage. However, IMF-dependent stator association was less evident in later experiments of the activity of two motors on the same *E. coli* cell during slow collapse of the IMF. The two motors reached zero speed at the same time, potentially suggesting that the stator units did not dissociate or inactivate at vanishing IMF (Gabel and Berg, 2003), though the low temporal resolution ($\sim$ 5 s) leaves room for uncertainty.

Tipping J. M. et al. (2013) used fluorescent protein (FP)-tagged stators to show that, upon collapse of the PMF in *E. coli*, stators dissociate from the motor on a timescale of minutes. However, these results are in disagreement with two separate studies that, also using FP-tagged stators, observe that the PMF is not necessary for stator assembly in either *S. enterica* or *E. coli* (Morimoto et al., 2010; Suzuki et al., 2019). While it seems well established that the ΔpH component of the PMF is not necessary for assembly in *E. coli* or *S. enterica* (Fung and Berg, 1995; Morimoto et al., 2010; Suzuki et al., 2019), recent work has observed that assembly increases at lower external pH (Suzuki et al., 2019). Thus, the concentration of accessible protons seems to be more important than the gradient across the membrane. Yet, surprisingly, mutation of a conserved protonatable residue in MotB, which renders the stator nonfunctional, has shown that proton translocation is not necessary for stator assembly in *E. coli* or *S. enterica* (Zhou et al., 1998; Kojima and Blair, 2001; Morimoto et al., 2010; Suzuki et al., 2019).

For the Na^+ stator, SMF is required for assembly in *V. alginolyticus* (Fukuoka et al., 2009), and contrary to the H^+ stator, Na^+ conduction is also required for assembly in *V. alginolyticus* and *B. subtilis* (Fukuoka et al., 2009; Terahara et al., 2017). And while the concentration of external Na^+ is crucial for stator assembly in *V. alginolyticus*, *B. subtilis*, and the Na^+-driven hybrid stator in *E. coli* (Fukuoka et al., 2009; Sowa et al., 2014; Terahara et al., 2017), it is not necessary for Na^+-stator assembly in *S. oneidensis* (Paulick et al., 2015).

We summarize the studies to date which probe the ion-related conditions necessary for stator assembly in **Table 2**. There is not yet a coherent universal picture of stator ion sensing; as with other behaviors, it may prove ion and species dependent, though

TABLE 2 | Ion motive force (IMF) and ion related conditions shown to be necessary, ✓, or not, ✗, for stator assembly.

Condition	Necessary for assembly?	Ion	Species	References
PMF	(✓)	H^+	*E. coli*	Fung and Berg, 1995
	✓	H^+	*E. coli*	Tipping J. M. et al., 2013
	✗	H^+	*E. coli*	Suzuki et al., 2019
	✗	H^+	*S. enterica*	Morimoto et al., 2010
	✗	H^+	*S. enterica*	Suzuki et al., 2019
SMF	✓	Na^+	*V. alginolyticus*	Fukuoka et al., 2009
ΔpH	✗	H^+	*E. coli*	Fung and Berg, 1995
	✗	H^+	*E. coli*	Suzuki et al., 2019
	✗	H^+	*S. enterica*	Morimoto et al., 2010
	✗	H^+	*S. enterica*	Suzuki et al., 2019
pH_{ext}	✓	H^+	*E. coli*	Suzuki et al., 2019
	✓	H^+	*S. enterica*	Suzuki et al., 2019
$[Na^+]_{ext}$ or ΔpNa	(✓)	Na^+	*E. coli*	Sowa et al., 2005
	(✓)	Na^+	*E. coli*	Sowa et al., 2014
	✓	Na^+	*V. alginolyticus*	Fukuoka et al., 2009
	✓	Na^+	*B. subtilis*	Terahara et al., 2017
	✗	Na^+	*S. oneidensis*	Paulick et al., 2015
	✗	H^+	*S. oneidensis*	Paulick et al., 2009
	✗	H^+	*B. subtilis*	Terahara et al., 2017
H^+ conduction	(✗)	H^+	*E. coli*	Zhou et al., 1998
	(✗)	H^+	*E. coli*	Kojima and Blair, 2001
	✗	H^+	*E. coli*	Suzuki et al., 2019
	✗	H^+	*S. enterica*	Morimoto et al., 2010
	✗	H^+	*S. enterica*	Suzuki et al., 2019
Na^+ conduction	✓	Na^+	*V. alginolyticus*	Fukuoka et al., 2009
	(✓)	Na^+	*B. subtilis*	Terahara et al., 2017

Marks in parentheses denote indirect evidence for assembly, either via measurements of motor/swimming speed (Fung and Berg, 1995; Zhou et al., 1998; Kojima and Blair, 2001; Sowa et al., 2005, 2014), wherein it cannot be ruled out that the stators are assembled but somehow inactive, or via a structural switch of the stator complex that suggests peptidoglycan (PG) binding (Terahara et al., 2017).

the external concentration of coupling ion seems generally important. It remains to be shown whether this is due to an ion sensing capability of the stator. Alternatively, if stator binding to the PG is stabilized by force (Chawla et al., 2017; Nord et al., 2017), it may be simply the case that increasing ion concentration and rate of ion conduction increases, on average, the stability of the stator-PG bond. The fact that ion conduction in not required for H^+ stator assembly argues against this explanation in the case of the H^+-stator.

Studies that have found both motor speed and single stator speed to be linearly dependent upon IMF seem to make sense only under the assumption that the number of assembled stators is constant. Thus, the fact that stator assembly depends, in some yet-to-be-determined manner, on IMF complicates the interpretation of the linear dependence of speed on IMF. There exists an unresolved contradiction, as a linear relationship between IMF and speed should not be observed if both stator number and speed per stator increase simultaneously. It may prove that the relationship between stator number and IMF is sub-linear, and that stator disassembly mostly occurs only at very low IMF values. Future studies of stator dynamics as a function of IMF will be key to understanding how these pieces fit together.

ION SPECIFICITY

In most bacteria, stators are powered by a single species of cation, mostly commonly protons or sodium ions. Typically, MotAB-type stators are H^+-coupled and PomAB and MotPS-type stators are Na^+-coupled. Yet some bacteria are capable of coupling multiple types of cations. One way in which this is accomplished is via multiple sets of genes that encode multiple types of stator complexes. For example, *B. subtilis*, *V. alginolyticus*, and *S. oneidensis* all encode both an H^+-driven MotAB stator and an Na^+-driven MotPS or PomAB stator (Atsumi et al., 1992; Asai et al., 2000; Ito et al., 2005; Paulick et al., 2009). In *V. alginolyticus*, PomAB stators are constitutively expressed and power the polar flagellar motor, whereas MotAB stators are expressed only under certain environmental conditions and exclusively power lateral flagella motors (Belas et al., 1986; McCarter et al., 1988; Atsumi et al., 1992; Kawagishi et al., 1995). In *B. subtilis* and *S. oneidensis*, both types of stators are constitutive. They incorporate into the same motor, working in unison, though their affinity to the motor depends upon the chemical and physical conditions of the environment (Ito et al., 2005; Paulick et al., 2009). A systematic survey of bacterial genomic data has shown that at least 65 species of bacteria possess two or more putative stators (Thormann and Paulick, 2010). Other species couple multiple cations via a single stator complex. For example, the MotAB stator of *Bacillus clausi* can couple either H^+ or Na^+ (Terahara et al., 2008), and MotPS in *Bacillus alcalophilus* couples Na^+, K^+, or Rb^+ (Terahara et al., 2012). While it was reported that MotAB in *Paenibacilus* sp. was unique in its ability to couple divalent cations Mg^{2+} and Ca^{2+} (Imazawa et al., 2016), recent results suggest that this stator is actually powered by monovalent ions, likely protons (Onoe et al., 2020). Regardless of the coupling ion, a universally conserved aspartate residue at the N-terminal side of the TM region of MotB (D32 in *E. coli*) is believed to serve as the site of ion binding (Zhou et al., 1998).

Many hybrid stators have been created in order to probe the question of what in the stator determines ion specificity. Early work demonstrated that the combination of MotA (*R. Sphaeroidis*) and PomB (*V. alginolyticus*) produced a Na^+-driven stator in *V. alginolyticus*. This hybrid required MotX and MotY proteins in order to function, components which are necessary for PomAB incorporation in *V. alginolyticus* (Terashima et al., 2013). This work ruled out the A subunit as the ion-decisive component (Asai et al., 1999). In *B. subtilis*, hybrid stators MotAS and MotPB were shown to be Na^+ and H^+-coupled, respectively, suggesting that the B/S subunit is the dominant determinant of ion-selectivity (Ito et al., 2005). However, it was observed that MotA and MotP subunits confer an H^+ or Na^+ responsiveness, respectively (Ito et al., 2005). This suggests that either the A/P subunit plays a secondary role in ion-specificity, or, given the evidence presented above for stator sensing of IMF, it may be the case that the A/P subunit is a determining factor of H^+ and Na^+-dependent stator assembly. It was also recently proposed that the P subunit is critical for K^+ ion selectivity in *B. alcalophilus* and *Bacillus trypoxylicola* (Naganawa and Ito, 2020).

To explore which portion of the B subunit determines ion specificity, a chimeric subunit, termed MomB, was constructed from the N-terminus portion of MotB (*R. Sphaeroidis*) and the C-terminus portion of PomB (*V. alginolyticus*). MomB and PomA produced an Na^+ stator in *V. alginolyticus*, and interestingly, the position of the MotB/PomB junction within the conserved TM region affected the Na^+/Li^+ specificity. It was thus hypothesized that the periplasmic region of PomB proximal to the inner membrane plays a role in ion specificity, potentially by changing the size of the TM pore (Asai et al., 2000). Certain MomB constructs also produced a Na^+-driven stator with MotA in *V. alginolyticus*, albeit its function was dependent upon the presence of MotX and MotY (Asai et al., 2000, 2003). The reverse construction, the N terminus of PomB combined with the C terminus of MotB, named PotB, functioned with PomA as a Na^+-powered stator in *V. alginolyticus* or *E. coli*, regardless of presence of MotXY (Asai et al., 2003). Thus, while the periplasmic portion of PomB is not necessary for Na^+ coupling in the PomAB stator, it is sufficient to convert the MotAB stator from H^+- to Na^+-coupling.

Mutations near the surface of the conserved TM segment of the B subunit can cause the dual-ion coupling stator of *B. clausi* to prefer either H^+ or Na^+, and mutations in the same region can confer a dual-ion coupling capacity to *B. subtilis* stators (Terahara et al., 2008). A single mutation in the TM region of MotS of *B. alcalophilus* changed it from multi-ion coupling to single ion coupling (Terahara et al., 2012). Sequence alignment revealed that H^+-coupled MotB stators from many bacteria contain a conserved valine in the middle of the TM segment (residue 43 in *E. coli*), whereas Na^+-coupled PomB and MotS stators contain a conserved leucine at this position, and the $Na^+/K^+/RB^+$-coupled MotS of *B. alcalophilus* contains a methionine (Terahara et al., 2012). Steered molecular dynamic simulations of an atomic model of MotAB constructed based on disulfide cross-linking and tryptophan scanning mutations showed that the size of the

ion channel at its narrowest point was sensitive to mutations at this TM residue, suggesting size exclusion as the mechanism for ion-selectivity (Nishihara and Kitao, 2015).

Recently, the structure of the stator has been determined via cryoelectron microscopy (Deme et al., 2020; Santiveri et al., 2020). In **Figure 3A**, we show portions of a multiple sequence alignment, initially performed with the Clustal Omega alignment program (Madeira et al., 2019), then refined and edited using ViTO (Catherinot and Labesse, 2004), taking into account the published structures (PDB: 6YKP, 3S0Y). These alignments highlight the differentially conserved residues within the transmembrane helix (TMH) of MotB, but they also identify multiple differentially conserved residues in TMH3 and TMH4 of Mot/PomA that map to the A/B interface, which is very compact and largely hydrophobic in its most central part (Deme et al., 2020; Santiveri et al., 2020). The differentially conserved residues generally localize to three rings, as shown in **Figure 3B**, with no tight connections. Near the periplasmic interface, residue $EcMotB_{V43}$ faces residues $EcMotA_{I202}$ and $EcMotA_{A187}$ within TMH4 and TMH3, respectively (**Figure 3C**). While this ring is fully buried and corresponds to hydrophobic substitutions, differences between the H^+ and Na^+ stators here may yield an overall change of size or flexibility of the region, as previously hypothesized (Nishihara and Kitao, 2015). Further into the channel, residues $MotB_{Y30}$ and $MotB_{F33}$ face residues 178–181 of MotA TMH3, and with more accessibility, this presents another region that may control ion specificity (**Figure 3D**). Substitutions at that ring will impact a network of interactions involving hydrogen bonds to the essential aspartate $MotB_{D32}$. Indeed, an imperfect correlation between MotB residue 30 and ion specificity was previously noted (Ishida et al., 2019; Islam et al., 2020), and selection may prove to depend partly upon the facing TMH3 region. Finally, residues 217–219 of MotA TMH4 face the conserved $MotB_{W26}$ residue (**Figure 3**), which forms an H-bond with $MotA_{Y217}$ in H^+ motors. In sodium MotP/PomA stators, a smaller and more flexible asparagine is observed, instead. As a $MotB_{W26A}$ mutation abolishes motility (Deme et al., 2020), this contact is important, though we see no obvious mechanism of ion selection in this open region.

SPATIOTEMPORAL VARIATIONS OF IMF AT THE CELL AND POPULATION LEVEL

The electrochemical gradient across the bacterial cell membrane is central not only for motility, but for other physiological processes from ATP synthesis (Mitchell, 1961; Maloney et al., 1974) to cell division (Strahl and Hamoen, 2010; Chimerel et al., 2012). For this reason, it was traditionally considered to be homeostatic. However, recent work has shown that the IMF can be dynamic, is integrally tied to the cell's physiological state, and plays a role in information signaling. IMF-mediated intra- and intercellular electrical signalings have recently been shown to regulate physiological processes such as mechanosensation and metabolic coordination, sometimes over long distances, either among or between communities (Liu et al., 2015; Bruni et al., 2017). We discuss here a few examples where spatiotemporal variation of the IMF has been observed, both at the single cell and population level.

As a pioneering work in the burgeoning field of bacterial electrophysiology, Kralj et al. (2011) developed a voltage-sensitive fluorescent membrane protein (PROPS) to probe voltage dynamics on the single cell level. They observed that, while cells show great heterogeneity in behavior, many cells displayed quasi-periodic fluctuations in their membrane voltage. Predictably, these transient depolarizations correlated to transient decreases in motor speed. The physiological role of electrical spiking was unclear at the time; as the intensity and frequency were affected by the power of the imaging laser, the authors hypothesized that such fluctuations may be a signature of a bacterial stress response. When PROPS was combined with a genetically encoded calcium sensor, it was observed that transient membrane depolarizations induced transient influxes of calcium, reminiscent of neuronal action potentials (Bruni et al., 2017). Evidence that such a phenomenon is a signature of signaling came from the observation that transient voltage-induced Ca^+ influxes increased upon mechanical stimulation, and that such stimulation led to changes in protein concentrations at the level of individual cells (Bruni et al., 2017).

IMF dynamics have recently been shown to be important for surface-attached communities of bacteria, called biofilms. At the population level, a multi-electrode array system has shown that the intensity of electrical activity correlates with biofilm formation (Masi et al., 2015). With single cell level resolution, it has been shown that biofilms produce spatially propagating waves of oscillating membrane potential, and that these waves correlate with propagating waves of extracellular potassium. There is substantial evidence to support a model in which membrane depolarization is triggered by metabolic stress at the interior of a biofilm, which triggers the release of intracellular K^+, which subsequently depolarizes neighboring cells. Thus, membrane potential is used to conduct long-range electrical signaling to coordinate the metabolic states within a growing biofilm, thereby increasing the fitness of the biofilm as a whole (Prindle et al., 2015). Signals transmitted by these propagating waves of potassium extend beyond the biofilm community. Spatially separated biofilms can capitalize upon this electrochemical signaling to coordinate a time-sharing behavior of resource consumption (Liu et al., 2017), and the swimming behavior of distant planktonic cells can be modified in a manner to recruit cells to join a biofilm. While the majority of this work has been done on *B. subtilis*, the mechanisms may well be generic among bacteria; electrical signaling from a *B. subtilis* biofilm attracts swimming cells from the evolutionary distant *P. aeruginosa* (Humphries et al., 2017).

There appears to be great cell-to-cell heterogeneity in both the steady-state and dynamic behavior of cellular IMF (Kralj et al., 2011). Recent evidence has shown that both the steady-state membrane voltage and the dynamic behavior in response to electrical stimulation is dependent upon a cell's proliferative capacity (Stratford et al., 2019). Additionally, electrical polarization of the cell plays a role in successful spore formation (Sirec et al., 2019). While it may seem that such cell-to-cell heterogeneity may interfere with long-distance electrical

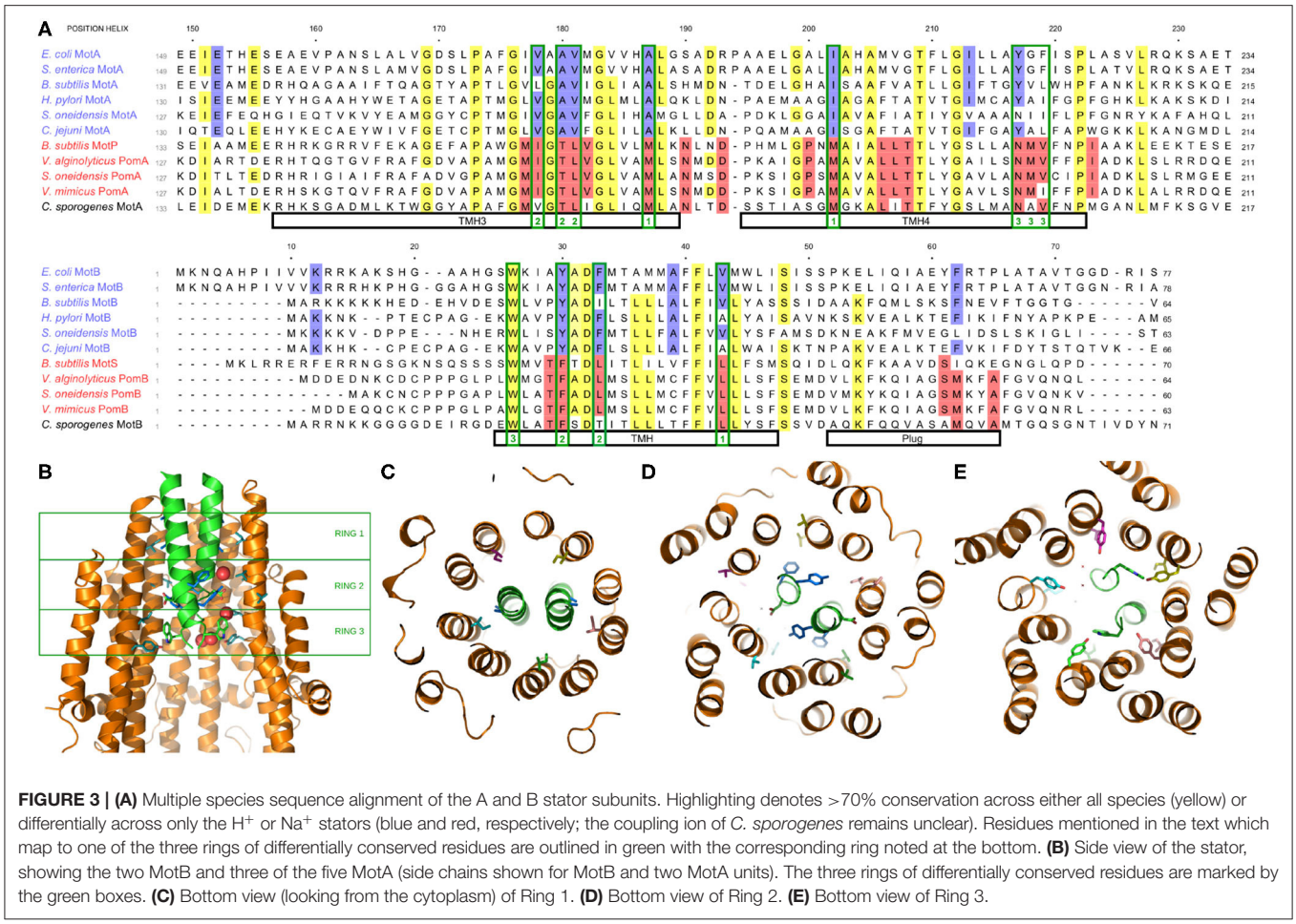

FIGURE 3 | (A) Multiple species sequence alignment of the A and B stator subunits. Highlighting denotes >70% conservation across either all species (yellow) or differentially across only the H^+ or Na^+ stators (blue and red, respectively; the coupling ion of *C. sporogenes* remains unclear). Residues mentioned in the text which map to one of the three rings of differentially conserved residues are outlined in green with the corresponding ring noted at the bottom. **(B)** Side view of the stator, showing the two MotB and three of the five MotA (side chains shown for MotB and two MotA units). The three rings of differentially conserved residues are marked by the green boxes. **(C)** Bottom view (looking from the cytoplasm) of Ring 1. **(D)** Bottom view of Ring 2. **(E)** Bottom view of Ring 3.

signaling, a model based upon percolation theory proposes that the number of cells capable of transmitting the electrical signal is consistent with a predicted phase transition. Thus, a dense biofilm composed of a heterogeneous mixture of signaling and non-signaling cells manages to propagate signals over long distances while minimizing the cost at the single-cell level (Larkin et al., 2018).

SINGLE CELL IMF MEASUREMENTS

While the developing field of bacterial electrophysiology takes its inspiration from the advanced field of eukaryotic electrophysiology, the reduced bacterial cell size and the complexity of the membrane present novel challenges. Techniques employed in the study of eukaryotic cells, such as microelectrode and patch clamp approaches, so far remain impractical, lack single-cell resolution (Masi et al., 2015), or come at the expense of great physical perturbation (Martinac et al., 2008). While bacterial bioenergetics has historically been investigated via bulk population measurements (Kashket, 1985), emerging techniques are enabling measurements of both the electric and chemical components of the IMF at the single bacterial cell level.

Measurements of $\Delta\Psi$ are most commonly made with Nernstian sensors (Lo et al., 2006, 2007; Kralj et al., 2011; Prindle et al., 2015; Sirec et al., 2019; Stratford et al., 2019; Mancini et al., 2020), small fluorescent molecules that diffuse across the membrane in accordance with the Nernst equation. Fluorescent measurements of the ratio of the extracellular to intracellular concentration at equilibrium reports upon $\Delta\Psi$. However, their permeability to Gram-negative bacteria is low, yielding a slow dynamic response ($\sim$ minutes), and so they are not suitable to report upon rapid fluctuations in $\Delta\Psi$. Additionally, while high concentrations are desired for improved signal-to-noise ratio, increasing concentrations of Nernstian dyes actually perturb membrane voltage (Sirec et al., 2019; Mancini et al., 2020). Thus, their application requires careful calibration (Mancini et al., 2020). As mentioned above, an alternative to probe $\Delta\Psi$ is a genetically encoded voltage sensor called PROPS, engineered from green-absorbing proteorhodopsin (Kralj et al., 2011; Bruni et al., 2017). PROPS provides a significantly faster temporal response ($\sim$ 10 ms; Kralj et al., 2011), without the need for a dye-loading step, though at the cost of lower signal-to-noise ratio.

Measurements of the chemical component of the IMF require a reporter for the intracellular concentration of the coupling ion. Intracellular pH was first quantified on the single cell

level using membrane-permeable pH-dependent fluorescent dyes (Siegumfeldt et al., 2000; Rasmussen et al., 2008; Kurre et al., 2013; Chao et al., 2017). A more recent approach, which obviates the need for a dye loading step and its potential invasive effects (Han and Burgess, 2010), uses genetically encoded fluorescent proteins, such as pH-sensitive derivatives of GFP (Miesenböck et al., 1998; Martinez et al., 2012; Kurre et al., 2013; Morimoto et al., 2016; Rupprecht et al., 2017; Arce-Rodríguez et al., 2019). Aside from excellent temporal (< 1 s) and pH (< 0.1) resolution (Kralj et al., 2011), a fusion between pHluorin and FliG of the BFM has shown local pH measurements with sub-cellular spatial resolution (Morimoto et al., 2016). PHluorin can also be combined with PROPS for simultaneous single cell measurements of ΔpH and membrane potential (Kralj et al., 2011; Bruni et al., 2017). Quantitative single cell measurements of intracellular sodium have been demonstrated using membrane-permeable fluorescent Na^+ dyes and applied to studies of the hybrid Na^+-driven motor of *E. coli* (Lo et al., 2006, 2007; Minamino et al., 2016). Relative measurements of cytoplasmic Ca^{2+} have been demonstrated in *E. coli* via a genetically encoded fluorescent Ca^{2+} sensor (Bruni et al., 2017).

The fact that the speed of the BFM is proportional to IMF provides an intriguing opportunity to exploit it as a measuring device for the IMF of the coupling ion. Recently, it has been shown that the BFM of *E. coli* can measure dynamic changes in the PMF during transient exposures to an ionophore as well as dynamic light-induced photodamage to the cell membrane (Krasnopeeva et al., 2019). As the temporal resolution of such measurements are theoretically limited only by the acquisition rate and the relaxation time of the particle attached to the flagellar filament (∼ ms), the BFM presents as an exciting future tool to quantitatively explore rapid electrophysiological dynamics on the single cell level. However, as highlighted above, such measurements will be affected by stochastic stator dynamics, as well as other factors, such as second messenger-mediated binding of cytoplasmic protein YcgR to the rotor, which slows motor speed in *E. coli* (Boehm et al., 2010; Fang and Gomelsky, 2010; Paul et al., 2010).

PERSPECTIVES

In species investigated thus far, the speed of the BFM is linear with IMF. It remains to be fully elucidated when and to what extent stator assembly depends on IMF, as well as the underlying mechanism of this electrical or chemical sensing. Future work will also need to decode how the linearity between speed and IMF arises if both single stator speed and stator assembly are proportional to IMF. Such details will contribute to models of the still elusive mechanism of torque generation, which will be greatly aided by recently solved structures of the stator complex (Deme et al., 2020; Santiveri et al., 2020). These structures will also open the way for future simulations to shed light on ion specificity and ion-dependent assembly.

With recent advances in single-cell electrophysiology techniques, the field is poised to learn a great deal about IMF dynamics and its intrinsic relation to diverse physiological processes, on scales from a single motor complex up to an entire bacterial colony. One of the best tools to investigate IMF dynamics may, ironically, be the motor that consumes it; yet, our understanding of the IMF and its rate of consumption by the BFM remains incomplete.

AUTHOR CONTRIBUTIONS

AB-B, FP, GL, and AN researched and wrote this review. All authors contributed to the article and approved the submitted version.

FUNDING

This work was supported by the ANR FlagMotor project grant ANR-18-CE30-0008 of the French *Agence Nationale de la Recherche* and by the French Infrastructure for Integrated Structural Biology (FRISBI) ANR-10-INBS-0005. The CBS is a member of the France-BioImaging (FBI) and the French Infrastructure for Integrated Structural Biology (FRISBI), 2 national infrastructures supported by the French National Research Agency (ANR-10-INBS-04-01 and ANR-10-INBS-05, respectively).

REFERENCES

Arce-Rodríguez, A., Volke, D. C., Bense, S., Häussler, S., and Nikel, P. I. (2019). Non-invasive, ratiometric determination of intracellular pH in Pseudomonas species using a novel genetically encoded indicator. *Microb. Biotechnol.* 12, 799–813. doi: 10.1111/1751-7915.13439

Asai, Y., Kawagishi, I., Sockett, R. E., and Homma, M. (1999). Hybrid motor with H^+ and Na^+ driven components can rotate Vibrio polar flagella by using sodium ions. *J. Bacteriol.* 181, 6332–6338. doi: 10.1128/JB.181.20.6332-6338.1999

Asai, Y., Kawagishi, I., Sockett, R. E., and Homma, M. (2000). Coupling ion specificity of chimeras between H^+- and Na^+-driven motor proteins, MotB and PomB, in Vibrio polar flagella. *EMBO J.* 19, 3639–3648. doi: 10.1093/emboj/19.14.3639

Asai, Y., Yakushi, T., Kawagishi, I., and Homma, M. (2003). Ion-coupling determinants of Na^+-driven and H^+-driven flagellar motors. *J. Mol. Biol.* 327, 453–463. doi: 10.1016/S0022-2836(03)00096-2

Atsumi, T., McCarter, L., and Imae, Y. (1992). Polar and lateral flagellar motors of marine Vibrio are driven by different ion-motive forces. *Nature* 355, 182–184. doi: 10.1038/355182a0

Belas, R. (2013). When the swimming gets tough, the tough form a biofilm. *Mol. Microbiol.* 90, 1–5. doi: 10.1111/mmi.12354

Belas, R., Simon, M., and Silverman, M. (1986). Regulation of lateral flagella gene transcription in *Vibrio parahaemolyticus*. *J. Bacteriol.* 167, 210–218. doi: 10.1128/JB.167.1.210-218.1986

Berg, H. C., and Anderson, R. A. (1973). Bacteria swim by rotating their flagellar filaments. *Nature* 245, 380–382. doi: 10.1038/245380a0

Boehm, A., Kaiser, M., Li, H., Spangler, C., Kasper, C. A., Ackermann, M., et al. (2010). Second messenger-mediated adjustment of bacterial swimming velocity. *Cell* 141, 107–116. doi: 10.1016/j.cell.2010.01.018

Bruni, G., Weekley, A., Dodd, B., and Kralj, J. (2017). Voltage-gated calcium flux mediates *Escherichia coli* mechanosensation. *Proc. Natl. Acad. Sci. U.S.A.* 114, 9445–9450. doi: 10.1073/pnas.1703084114

Catherinot, V., and Labesse, G. (2004). ViTO: tool for refinement of protein sequence-structure alignments. *Bioinformatics* 20, 3694–3696. doi: 10.1093/bioinformatics/bth429

Chao, J., Song, K., Wang, H., Li, Z., Zhang, Y., Yin, C., et al. (2017). A colorimetric and fluorescent pH probe for imaging in *E. coli* cells. *RSC Adv*. 7, 964–970. doi: 10.1039/C6RA24885C

Chawla, R., Ford, K. M., and Lele, P. P. (2017). Torque, but not FliL, regulates mechanosensitive flagellar motor-function. *Sci. Rep*. 7:5565. doi: 10.1038/s41598-017-05521-8

Chimerel, C., Field, C. M., Pi nero-Fernandez, S., Keyser, U. F., and Summers, D. K. (2012). Indole prevents *Escherichia coli* cell division by modulating membrane potential. *Biochim. Biophys. Acta* 1818, 1590–1594. doi: 10.1016/j.bbamem.2012.02.022

Deme, J. C., Johnson, S., Vickery, O., Muellbauer, A., Monkhouse, A., Griffiths, T., et al. (2020). Structure of the stator complex that drives rotation of the bacterial flagellum. *Nat. Microbiol*. 5, 553–1564. doi: 10.1038/s41564-020-0788-8

Fang, X., and Gomelsky, M. (2010). A post-translational, c-di-GMP-dependent mechanism regulating flagellar motility. *Mol. Microbiol*. 76, 1295–1305. doi: 10.1111/j.1365-2958.2010.07179.x

Fukuoka, H., Wada, T., Kojima, S., Ishijima, A., and Homma, M. (2009). Sodium-dependent dynamic assembly of membrane complexes in sodium-driven flagellar motors. *Mol. Microbiol*. 71, 825–835. doi: 10.1111/j.1365-2958.2008.06569.x

Fung, D. C., and Berg, H. C. (1995). Powering the flagellar motor of *Escherichia coli* with an external voltage source. *Nature* 375, 809–812. doi: 10.1038/375809a0

Gabel, C. V., and Berg, H. C. (2003). Speed of the flagellar rotary motor of *Escherichia coli* varies linearly with protonmotive force. *Proc. Natl. Acad. Sci. U.S.A*. 100, 8748–8751. doi: 10.1073/pnas.1533395100

Han, J., and Burgess, K. (2010). Fluorescent indicators for intracellular pH. *Chem. Rev*. 110, 2709–2728. doi: 10.1021/cr900249z

Humphries, J., Xiong, L., Liu, J., Prindle, A., Yuan, F., Arjes, H. A., et al. (2017). Species-independent attraction to biofilms through electrical signaling. *Cell* 168, 200–209.e12. doi: 10.1016/j.cell.2016.12.014

Imazawa, R., Takahashi, Y., Aoki, W., Sano, M., and Ito, M. (2016). A novel type bacterial flagellar motor that can use divalent cations as a coupling ion. *Sci. Rep*. 6:19773. doi: 10.1038/srep19773

Ishida, T., Clark, J., Matzke, N. J., Sowa, Y., and Baker, M. A. B. (2019). Sodium-powered stators of the bacterial flagellar motor can generate torque in the presence of phenamil with mutations near the peptidoglycan-binding region. *Mol. Microbiol*. 111, 1689–1699. doi: 10.1111/mmi.14246

Islam, M. I., Lin, A., Lai, Y.-W., Matzke, N.-J., and Baker, M. A. B. (2020). Ancestral sequence reconstructions of MotB are proton-motile and require MotA for motility. *Front. Mircrobiol*. 11:3271. doi: 10.3389/fmicb.2020.625837

Ito, M., Terahara, N., Fujinami, S., and Krulwich, T. A. (2005). Properties of motility in *Bacillus subtilis* powered by the H^+-coupled MotAB flagellar stator, Na^+-coupled MotPS or hybrid stators MotAS or MotPB. *J. Mol. Biol*. 352, 396–408. doi: 10.1016/j.jmb.2005.07.030

Kashket, E. (1985). The proton motive force in bacteria: a critical assessment of methods. *Annu. Rev. Micro*. 39, 219–42. doi: 10.1146/annurev.mi.39.100185.001251

Kawagishi, I., Maekawa, Y., Atsumi, T., Homma, M., and Imae, Y. (1995). Isolation of the polar and lateral flagellum-defective mutants in *Vibrio alginolyticus* and identification of their flagellar driving energy sources. *J. Bacteriol*. 177, 5158–5160. doi: 10.1128/JB.177.17.5158-5160.1995

Khan, S., Dapice, M., and Humayun, I. (1990). Energy transduction in the bacterial flagellar motor. Effects of load and pH. *Biophys. J*. 57, 779–796. doi: 10.1016/S0006-3495(90)82598-4

Khan, S., and Macnab, R. M. (1980). Proton chemical potential, proton electrical potential and bacterial motility. *J. Mol. Biol*. 138, 599–614. doi: 10.1016/S0022-2836(80)80019-2

Khan, S., Meister, M., and Berg, H. C. (1985). Constraints on flagellar rotation. *J. Mol. Biol*. 184, 645–656. doi: 10.1016/0022-2836(85)90310-9

Kojima, S., and Blair, D. F. (2001). Conformational change in the stator of the bacterial flagellar motor. *Biochemistry* 40, 13041–13050. doi: 10.1021/bi011263o

Kralj, J. M., Hochbaum, D. R., Douglass, A. D., and Cohen, A. E. (2011). Electrical spiking in *Escherichia coli* probed with a fluorescent voltage-indicating protein. *Science* 333, 345–348. doi: 10.1126/science.1204763

Krasnopeeva, E., Lo, C.-J., and Pilizota, T. (2019). Single-cell bacterial electrophysiology reveals mechanisms of stress-induced damage. *Biophys. J*. 116, 2390–2399. doi: 10.1016/j.bpj.2019.04.039

Kurre, R., Kouzel, N., Ramakrishnan, K., and Oldewurtel, E. R. (2013). Speed switching of gonococcal surface motility correlates with proton motive force. *PLoS ONE* 8:e67718. doi: 10.1371/journal.pone.0067718

Larkin, J. W., Zhai, X., Kikuchi, K., Redford, S. E., Prindle, A., Liu, J., et al. (2018). Signal percolation within a bacterial community. *Cell Syst*. 7, 137–145. doi: 10.1016/j.cels.2018.06.005

Larsen, S. H., Adler, J., Gargus, J. J., and Hogg, R. W. (1974). Chemomechanical coupling without ATP: the source of energy for motility and chemotaxis in bacteria. *Proc. Natl. Acad. Sci. U.S.A*. 71, 1239–1243. doi: 10.1073/pnas.71.4.1239

Leake, M. C., Chandler, J. H., Wadhams, G. H., Bai, F., Berry, R. M., and Armitage, J. P. (2006). Stoichiometry and turnover in single, functioning membrane protein complexes. *Nature* 443, 355–358. doi: 10.1038/nature05135

Lele, P. P., Hosu, B. G., and Berg, H. C. (2013). Dynamics of mechanosensing in the bacterial flagellar motor. *Proc. Natl. Acad. Sci. U.S.A*. 110, 11839–11844. doi: 10.1073/pnas.1305885110

Liu, J., Martinez-Corral, R., Prindle, A., Lee, D.-Y. D., Larkin, J., Gabalda-Sagarra, M., et al. (2017). Coupling between distant biofilms and emergence of nutrient time-sharing. *Science* 356, 638–642. doi: 10.1126/science.aah4204

Liu, J., Prindle, A., Humphries, J., Gabalda-Sagarra, M., Asally, M., Lee, D.-Y. D., et al. (2015). Metabolic co-dependence gives rise to collective oscillations within biofilms. *Nature* 523, 550–554. doi: 10.1038/nature14660

Lo, C. J., Leake, M. C., and Berry, R. M. (2006). Fluorescence measurement of intracellular sodium concentration in single *Escherichia coli* cells. *Biophys. J*. 90, 357–365. doi: 10.1529/biophysj.105.071332

Lo, C. J., Leake, M. C., Pilizota, T., and Berry, R. M. (2007). Nonequivalence of membrane voltage and ion-gradient as driving forces for the bacterial flagellar motor at low load. *Biophys. J*. 93, 294–302. doi: 10.1529/biophysj.106.095265

Madeira, F., Park, Y. M., Lee, J., Buso, N., Gur, T., Madhusoodanan, N., et al. (2019). The EMBL-EBI search and sequence analysis tools APIs in 2019. *Nucleic Acids Res*. 47, W636–W641. doi: 10.1093/nar/gkz268

Maloney, P., Kashket, E., and Hastings Wilson, T. (1974). A proton motive force drives ATP synthesis in bacteria. *Proc. Natl. Acad. Sci. U.S.A*. 71, 3896–3900. doi: 10.1073/pnas.71.10.3896

Mancini, L., Terradot, G., Tian, T., Pu, Y., Li, Y., Lo, C.-J., et al. (2020). A general workflow for characterization of nernstian dyes and their effects on bacterial physiology. *Biophys. J*. 118, 4–14. doi: 10.1016/j.bpj.2019.10.030

Manson, M. D., Tedesco, P., Berg, H. C., Harold, F. M., and Van der Drift, C. (1977). A protonmotive force drives bacterial flagella. *Proc. Natl. Acad. Sci. U.S.A*. 74, 3060–3064. doi: 10.1073/pnas.74.7.3060

Manson, M. D., Tedesco, P. M., and Berg, H. C. (1980). Energetics of flagellar rotation in bacteria. *J. Mol. Biol*. 138, 541–561. doi: 10.1016/S0022-2836(80)80017-9

Martinac, B., Saimi, Y., and Kung, C. (2008). Ion channels in microbes. *Physiol. Rev*. 88, 1449–1490. doi: 10.1152/physrev.00005.2008

Martinez, K. A., Kitko, R. D., Mershon, J. P., Adcox, H. E., Malek, K. A., Berkmen, M. B., et al. (2012). Cytoplasmic pH response to acid stress in individual cells of *Escherichia coli* and *Bacillus subtilis* observed by fluorescence ratio imaging microscopy. *Appl. Environ. Microbiol*. 78, 3706–3714. doi: 10.1128/AEM.00354-12

Masi, E., Ciszak, M., Santopolo, L., Frascella, A., Giovennetti, L., Marchi, E., et al. (2015). Electrical spiking in bacterial biofilms. *J. R. Soc. Interface* 12:20141036. doi: 10.1098/rsif.2014.1036

McCarter, L., Hilmen, M., and Silverman, M. (1988). Flagellar dynamometer controls swarmer cell differentiation of V. parahaemolyticus. *Cell* 54, 345–351. doi: 10.1016/0092-8674(88)90197-3

Meister, M., Lowe, G., and Berg, H. C. (1987). The proton flux through the bacterial flagellar motor. *Cell* 49, 643–650. doi: 10.1016/0092-8674(87)90540-X

Miesenböck, G., De Angelis, D. A., and Rothman, J. E. (1998). Visualizing secretion and synaptic transmission with pH-sensitive green fluorescent proteins. *Nature* 394, 192–195. doi: 10.1038/28190

Minamino, T., Imae, Y., Oosawa, F., Kobayashi, Y., and Oosawa, K. (2003). Effect of intracellular pH on rotational speed of bacterial flagellar motors. *J. Bacteriol*. 185, 1190–1194. doi: 10.1128/JB.185.4.1190-1194.2003

Minamino, T., Morimoto, Y. V., Hara, N., Aldridge, P. D., and Namba, K. (2016). The bacterial flagellar type III export gate complex is a dual fuel engine that can use both H^+ and Na^+ for flagellar protein export. *PLoS Pathog.* 12:e1005495. doi: 10.1371/journal.ppat.1005495

Mitchell, P. (1961). Coupling of phosphorylation to electron and hydrogen transfer by a chemi-osmotic type of mechanism. *Nature* 191, 144–148. doi: 10.1038/191144a0

Morimoto, V. Y., Nakamura, S., Kami-ike, N., Namba, K., and Minamino, T. (2010). Charged residues in the cytoplasmic loop of MotA are required for stator assembly into the bacterial flagellar motor. *Mol. Microbiol.* 78, 1117–1129. doi: 10.1111/j.1365-2958.2010.07391.x

Morimoto, Y. V., Kami-ike, N., Miyata, T., Kawamoto, A., Kato, T., Namba, K., et al. (2016). High-resolution pH imaging of living bacterial cells to detect local pH differences. *mBio* 7, e01911–16. doi: 10.1128/mBio.01911-16

Naganawa, S., and Ito, M. (2020). Motp subunit is critical for ion selectivity and evolution of a k^+-coupled flagellar motor. *Biomolecules* 10:691. doi: 10.3390/biom10050691

Nishihara, Y., and Kitao, A. (2015). Gate-controlled proton diffusion and protonation-induced ratchet motion in the stator of the bacterial flagellar motor. *Proc. Natl. Acad. Sci. U.S.A.* 112, 7737–7742. doi: 10.1073/pnas.1502991112

Nord, A. L., Gachon, E., Perez-Carrasco, R., Nirody, J. A., Barducci, A., Berry, R. M., et al. (2017). Catch bond drives stator mechanosensitivity in the bacterial flagellar motor. *Proc. Natl. Acad. Sci. U.S.A.* 114, 12952–12957. doi: 10.1073/pnas.1716002114

Onoe, S., Yoshida, M., Terahara, N., and Sowa, Y. (2020). Coupling Ion specificity of the flagellar stator proteins MotA1/MotB1 of *Paenibacillus* sp. TCA20. *Biomolecules* 10:1078. doi: 10.3390/biom10071078

Paul, K., Nieto, V., Carlquist, W. C., Blair, D. F., and Harshey, R. M. (2010). The c-di-GMP binding protein YcgR controls flagellar motor direction and speed to affect chemotaxis by a "backstop brake" mechanism. *Mol. Cell* 38, 128–139. doi: 10.1016/j.molcel.2010.03.001

Paulick, A., Delalez, N. J., Brenzinger, S., Steel, B. C., Berry, R. M., Armitage, J. P., et al. (2015). Dual stator dynamics in the *Shewanella oneidensis* MR-1 flagellar motor. *Mol. Microbiol.* 96, 993–1001. doi: 10.1111/mmi.12984

Paulick, A., Koerdt, A., Lassak, J., Huntley, S., Wilms, I., Narberhaus, F., et al. (2009). Two different stator systems drive a single polar flagellum in *Shewanella oneidensis* MR-1. *Mol. Microbiol.* 71, 836–850. doi: 10.1111/j.1365-2958.2008.06570.x

Prindle, A., Liu, J., Asally, M., Ly, S., Garcia-Ojalvo, J., and Süel, G. M. (2015). Ion channels enable electrical communication in bacterial communities. *Nature* 527, 59–63. doi: 10.1038/nature15709

Rasmussen, M. B., Oddershede, L. B., and Siegumfeldt, H. (2008). Optical tweezers cause physiological damage to *Escherichia coli* and listeria bacteria. *Appl. Environ. Microbiol.* 74, 2441–2446. doi: 10.1128/AEM.02265-07

Rossmann, F. M., and Beeby, M. (2018). Insights into the evolution of bacterial flagellar motors from high-throughput *in situ* electron cryotomography and subtomogram averaging. *Acta Crystallogr. Sect. D* 74, 585–594. doi: 10.1107/S2059798318007945

Rupprecht, C., Wingen, M., Potzkei, J., Gensch, T., Jaeger, K.-E., and Drepper, T. (2017). A novel FbFP-based biosensor toolbox for sensitive *in vivo* determination of intracellular pH. *J. Biotechnol.* 258, 25–32. doi: 10.1016/j.jbiotec.2017.05.006

Santiveri, M., Roa-Eguiara, A., Kuhne, C., Wadhwa, N., Hu, H., Berg, H. C., et al. (2020). Structure and function of stator units of the bacterial flagellar motor. *Cell* 183, 1–14. doi: 10.1016/j.cell.2020.08.016

Shioi, J. I., Matsuura, S., and Imae, Y. (1980). Quantitative measurements of proton motive force and motility in *Bacillus subtilis*. *J. Bacteriol.* 144, 891–897. doi: 10.1128/JB.144.3.891-897.1980

Siegumfeldt, H., Rechinger, B., and Jakobsen, M. (2000). Dynamic changes of intracellular pH in individual lactic acid bacterium cells in response to a rapid drop in extracellular pH. *Appl. Environ. Microbiol.* 66, 2330–2335. doi: 10.1128/AEM.66.6.2330-2335.2000

Sirec, T., Benarroch, J. M., Buffard, P., Garcia-Ojalvo, J., and Asally, M. (2019). Electrical polarization enables integrative quality control during bacterial differentiation into spores. *iScience* 16, 378–389. doi: 10.1016/j.isci.2019.05.044

Sowa, Y., and Berry, R. M. (2008). Bacterial flagellar motor. *Q. Rev. Biophys.* 41, 103–132. doi: 10.1017/S0033583508004691

Sowa, Y., Homma, M., Ishijima, A., and Berry, R. M. (2014). Hybrid-fuel bacterial flagellar motors in *Escherichia coli*. *Proc. Natl. Acad. Sci. U.S.A.* 111, 3436–3441. doi: 10.1073/pnas.1317741111

Sowa, Y., Hotta, H., Homma, M., and Ishijima, A. (2003). Torque-speed relationship of the Na^+-driven flagellar motor of *Vibrio alginolyticus*. *J. Mol. Biol.* 327, 1043–1051. doi: 10.1016/S0022-2836(03)00176-1

Sowa, Y., Rowe, A. D., Leake, M. C., Yakushi, T., Homma, M., Ishijima, A., et al. (2005). Direct observation of steps in rotation of the bacterial flagellar motor. *Nature* 437, 916–919. doi: 10.1038/nature04003

Strahl, H., and Hamoen, L. W. (2010). Membrane potential is important for bacterial cell division. *Proc. Natl. Acad. Sci. U.S.A.* 107, 12281–12286. doi: 10.1073/pnas.1005485107

Stratford, J. P., Edwards, C. L. A., Ghanshyam, M. J., Malyshev, D., Delise, M. A., Hayashi, Y., et al. (2019). Electrically induced bacterial membrane-potential dynamics correspond to cellular proliferation capacity. *Proc. Natl. Acad. Sci. U.S.A.* 116, 9552–9557. doi: 10.1073/pnas.1901788116

Suzuki, Y., Morimoto, Y. V., Oono, K., Hayashi, F., Oosawa, K., Kudo, S., et al. (2019). Effect of the MotA(M206I) mutation on torque generation and stator assembly in the Salmonella H^+-driven flagellar motor. *J. Bacteriol.* 201:e00727-18. doi: 10.1128/JB.00727-18

Terahara, N., Kodera, N., Uchihashi, T., Ando, T., Namba, K., and Minamino, T. (2017). Na-induced structural transition of MotPS for stator assembly of the flagellar motor. *Sci. Adv.* 3:4119. doi: 10.1126/sciadv.aao4119

Terahara, N., Krulwich, T. A., and Ito, M. (2008). Mutations alter the sodium versus proton use of a *Bacillus clausii* flagellar motor and confer dual ion use on *Bacillus subtilismotors*. *Proc. Natl. Acad. Sci. U.S.A.* 105, 14359–14364. doi: 10.1073/pnas.0802106105

Terahara, N., Sano, M., and Ito, M. (2012). Bacillus flagellar motor that can use both Na^+ and K^+ as a coupling ion is converted by a single mutation to use only Na^+. *PLoS ONE* 7:e46248. doi: 10.1371/journal.pone.0046248

Terashima, H., Li, N., Sakuma, M., Koike, M., Kojima, S., Homma, M., et al. (2013). Insight into the assembly mechanism in the supramolecular rings of the sodium-driven Vibrio flagellar motor from the structure of FlgT. *Proc. Natl. Acad. Sci. U.S.A.* 110, 6133–6138. doi: 10.1073/pnas.1222655110

Thormann, K. M., and Paulick, A. (2010). Tuning the flagellar motor. *Microbiology* 156(Pt 5), 1275–1283. doi: 10.1099/mic.0.029595-0

Tipping, J. M., Steel, C. B., Delalez, J. N., Berry, M. R., and Armitage, P. J. (2013). Quantification of flagellar motor stator dynamics through *in vivo* proton-motive force control. *Mol. Microbiol.* 87, 338–347. doi: 10.1111/mmi.12098

Tipping, M. J., Delalez, N. J., Lim, R., Berry, R. M., and Armitage, J. P. (2013). Load-dependent assembly of the bacterial flagellar motor. *mBio* 4, e00551–13. doi: 10.1128/mBio.00551-13

Walter, J. M., Greenfield, D., Bustamante, C., and Liphardt, J. (2007). Light-powering *Escherichia coli* with proteorhodopsin. *Proc. Natl. Acad. Sci. U.S.A.* 104, 2408–2412. doi: 10.1073/pnas.0611035104

Zhou, J., Sharp, L. L., Tang, H. L., Lloyd, S. A., Billings, S., Braun, T. F., et al. (1998). Function of protonatable residues in the flagellar motor of *Escherichia coli*: a critical role for ASP 32 of MotB. *J. Bacteriol.* 180, 2729–2735. doi: 10.1128/JB.180.10.2729-2735.1998

Conflict of Interest: The authors declare that the research was conducted in the absence of any commercial or financial relationships that could be construed as a potential conflict of interest.

frontiers in Microbiology

ORIGINAL RESEARCH
published: 22 April 2021
doi: 10.3389/fmicb.2021.664826

Multiple CheY Proteins Control Surface-Associated Lifestyles of *Azospirillum brasilense*

*Elena E. Ganusova, Lam T. Vo, Tanmoy Mukherjee† and Gladys Alexandre**

Department of Biochemistry and Cellular and Molecular Biology, University of Tennessee, Knoxville, TN, United States

Bacterial chemotaxis is the directed movement of motile bacteria in gradients of chemoeffectors. This behavior is mediated by dedicated signal transduction pathways that couple environment sensing with changes in the direction of rotation of flagellar motors to ultimately affect the motility pattern. *Azospirillum brasilense* uses two distinct chemotaxis pathways, named Che1 and Che4, and four different response regulators (CheY1, CheY4, CheY6, and CheY7) to control the swimming pattern during chemotaxis. Each of the CheY homologs was shown to differentially affect the rotational bias of the polar flagellum and chemotaxis. The role, if any, of these CheY homologs in swarming, which depends on a distinct lateral flagella system or in attachment is not known. Here, we characterize CheY homologs' roles in swimming, swarming, and attachment to abiotic and biotic (wheat roots) surfaces and biofilm formation. We show that while strains lacking CheY1 and CheY6 are still able to navigate air gradients, strains lacking CheY4 and CheY7 are chemotaxis null. Expansion of swarming colonies in the presence of gradients requires chemotaxis. The induction of swarming depends on CheY4 and CheY7, but the cells' organization as dense clusters in productive swarms appear to depend on functional CheYs but not chemotaxis *per se*. Similarly, functional CheY homologs but not chemotaxis, contribute to attachment to both abiotic and root surfaces as well as to biofilm formation, although these effects are likely dependent on additional cell surface properties such as adhesiveness. Collectively, our data highlight distinct roles for multiple CheY homologs and for chemotaxis on swarming and attachment to surfaces.

Keywords: *Azospirillum*, CheY, chemotaxis, flagella, swarming, surface attachment

OPEN ACCESS

Edited by:
Seiji Kojima,
Nagoya University, Japan

Reviewed by:
Shuichi Nakamura,
Tohoku University, Japan
Kai Thormann,
University of Giessen, Germany

****Correspondence:***
Gladys Alexandre
galexan2@utk.edu

†Present address:
Tanmoy Mukherjee,
Nationwide Children's Hospital,
Columbus, OH, United States

Specialty section:
This article was submitted to Microbial Physiology and Metabolism, a section of the journal Frontiers in Microbiology

Received: *06 February 2021*
Accepted: *29 March 2021*
Published: *22 April 2021*

Citation:
Ganusova EE, Vo LT, Mukherjee T and Alexandre G (2021) Multiple CheY Proteins Control Surface-Associated Lifestyles of Azospirillum brasilense. Front. Microbiol. 12:664826. doi: 10.3389/fmicb.2021.664826

INTRODUCTION

Navigating chemical gradients requires motile bacteria to sense and bias their direction of movement using chemotaxis. Motile and flagellated bacteria utilize conserved and dedicated chemotaxis signal transduction pathways to modulate swimming bias in chemical gradients. In *Escherichia coli*, the chemotaxis system comprises a single set of membrane-bound chemoreceptors, chemotaxis histidine kinase (CheA), flagellar-motor binding response regulator (CheY), and scaffolding protein (CheW). Adaptation proteins methylesterase CheB and methyltransferase CheR re-set signaling upon excitation by reversibly modifying membrane-bound chemoreceptors (Levit and Stock, 2002). The majority of motile, flagellated bacterial

sequenced genomes indicates the presence of multiple chemotaxis as well as chemosensory (chemotaxis-like) pathways, with the latter displaying non-motility phenotypes such as extracellular matrix formation (Edwards et al., 2011), cyst formation (Berleman and Bauer, 2005; Wu et al., 2011), biofilm formation (Huang et al., 2019), and quorum sensing (Laganenka et al., 2016). In contrast to *E.coli* which possesses a single chemotaxis response regulator CheY to alter the direction of rotation of flagellar motors, the genome of many bacteria encodes for multiple CheY homologs: *Rhodobacter sphaeroides* (Ferré et al., 2004; Porter et al., 2006), *Sinorhizobium meliloti* (Schmitt, 2002), *Rhizobium leguminosarum* (Miller et al., 2007), *Azospirillum brasilense* (Mukherjee et al., 2016, 2019), *Borrelia burgdorferi* (Pitzer et al., 2011), *Vibrio cholerae* (Hyakutake et al., 2005), etc. In some cases, the multiple CheY homologs are encoded within a single chemotaxis pathway (e.g., *S. meliloti*). These CheYs may also be encoded elsewhere on the genome with no apparent genetic link to a particular chemotaxis system (e.g., *B. burgdorferi*; Schmitt, 2002; Pitzer et al., 2011). Why motile bacteria have multiple chemotaxis-related response regulators is not clear. In *R. sphaeroides*, all six CheY homologs are able to bind to the FliM component of the flagellar motor upon phosphorylation, but only one of them is responsible for the flagella motor stopping (Ferré et al., 2004).

The alphaproteobacterium *A. brasilense* are soil motile diazotrophic bacteria able to colonize the roots of diverse plants and promote their growth through phytohormones production and nitrogen fixation (Steenhoudt and Vanderleyden, 2000). *A. brasilense* motility and chemotaxis are important for plant root colonization (Zhulin and Armitage, 1992; Greer-Phillips et al., 2004; O'Neal et al., 2019, 2020). *A. brasilense* cells are motile using a single polar flagellum that allows the cells to swim in liquid media and when the viscosity of the media increases, cells produce multiple lateral flagella, structurally distinct from the polar flagellum, that permit translocation across surfaces by swarming (Moens et al., 1996). The polar flagellum of *A. brasilense* cells rotates in both clockwise and counterclockwise directions, and chemotaxis signaling controls the rotational bias of the polar flagellum in this species (Zhulin and Armitage, 1993; Mukherjee et al., 2019). The *A. brasilense* polar flagellum is comprised of flagellin that is glycosylated (Moens et al., 1995b). The glycosylation on the *A. brasilense* polar flagellin consists of a branched tetrasaccharide with repeated rhamnose, fucose, galactose, and *N*-acetylglucosamine that resemble the LPS *O*-antigen, suggesting that both structures are related (Belyakov et al., 2012). The polar flagellum was suggested to mediate adsorption of *A. brasilense* cells to the roots of wheat plants in a two-step attachment process (Croes et al., 1993): a reversible step that is thought to be mediated by the polar flagellum and an irreversible attachment step that likely involves extracellular polymeric substances. The *A. brasilense* polar flagellum also contributes to biofilm formation *in vitro* and to the stabilization of the biofilm matrix (Viruega-Góngora et al., 2020). The lateral flagella required for swarming are distinct appendages made of proteins unrelated to the polar flagellum, including distinct lateral flagellin, termed Laf1 (Moens et al., 1995a). Lateral flagella are produced when the rotation of the polar flagellum is hindered (Moens et al., 1996), and recent evidence indicates that an extracytoplasmic function (ECF) sigma-factor ultimately regulates lateral flagellar biosynthesis in *A. brasilense* (Dubey et al., 2020).

Chemotaxis in *A. brasilense* controls the polar flagellum and thus swimming through signaling *via* two different chemotaxis systems, named Che1 and Che4, as well as additional CheY response regulators (CheY6 and CheY7) encoded outside of *che1* and *che4* (Bible et al., 2012; Mukherjee et al., 2016, 2019; **Figure 1A**). Histidine kinase CheA1 and the response regulator CheY1, both encoded within the *che1* cluster, regulate transient changes in swimming speed during chemotaxis. CheA4 histidine kinase and the CheY4 response regulator, both encoded within the *che4* operon, control the probability of changes in the swimming direction (herein reversals) during chemotaxis (**Figure 1B**). A *ΔcheY6* mutant has a swimming reversal phenotype similar to that of a *ΔcheY4* mutant, while a strain lacking CheY7 does not display any swimming reversals. All CheY mutants also swim slower than the wild type in the absence of a gradient (**Figure 1C**; Mukherjee et al., 2019). Genetic evidence and behavioral assays indicate that CheY6 activity is controlled by Che1/CheA1 signaling, and CheY7 activity, a mutant of which phenocopies a *ΔcheA4* mutant, is controlled by Che4/CheA4 signaling (Mukherjee et al., 2019; **Figure 1A**). Mutants lacking *cheA4*, *cheY4,* or *cheY7* are unable of chemotaxis in spatial gradients of chemoeffectors, while mutants lacking *cheY1* or *cheY6* still display chemotaxis under these conditions (Bible et al., 2008; Mukherjee et al., 2016, 2019). Another feature of the polar flagellum motor of *A. brasilense* is that it undergoes brief swimming pauses, which are distinct from speed increases or reversals. Swimming pause frequency is reduced in strains lacking CheY1, CheY6, and CheY7 but is increased in a strain lacking CheY4, although the mechanism for these differential effects is not known (**Figure 1B**; Mukherjee et al., 2019). The effects of these CheY homologs on the swimming motility pattern of *A. brasilense* are thought to optimize navigation in the spatially and physically heterogeneous environment of the soil, although this remains to be experimentally demonstrated.

Rotation (or lack thereof) of flagella controlling swimming motility has been implicated in the swim-to-sessile transitions in diverse bacteria, perhaps through the flagellum acting as a "mechanosensor" (Gordon and Wang, 2019; Chawla et al., 2020). Such swim-to-sessile transitions occur during swarming on surfaces, the formation of biofilms, and surface attachment (Guttenplan and Kearns, 2013). Chemotaxis and chemotaxis mutants with different motility biases have been implicated in bacterial social behaviors, promoting cell-to-cell interactions or interaction with eukaryotic hosts (Alexandre, 2015). However, the exact role of the rotational bias of flagella or multiple chemotaxis CheY homologs in these behaviors has been seldom, if at all, addressed. Here, we take advantage of the different effects of *A. brasilense* CheYs (CheY1, CheY4, CheY6, and CheY7) on the rotational bias of the polar flagellum and chemotaxis to examine contributions to behaviors related to swim-to-stick transitions such as swarming, surface (abiotic and wheat) attachment, and biofilm formation. We show that only some of these CheYs (CheY4 and CheY7) but not chemotaxis *per se* induce swarming, and CheYs mediate distinct abiotic

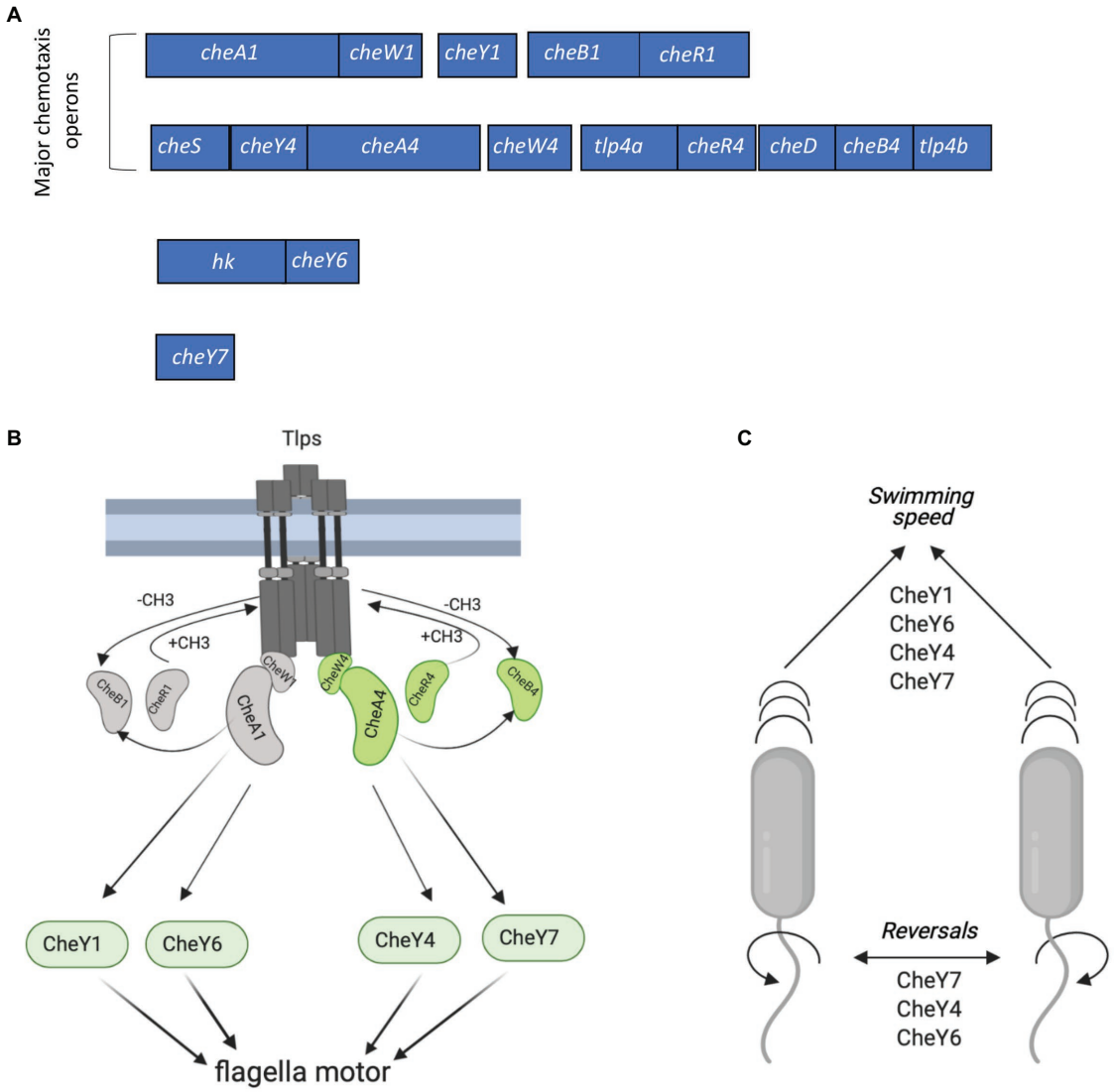

FIGURE 1 | Chemotaxis signaling in *Azospirillum brasilense* and gene clusters encoding CheY response regulators. **(A)** Open reading frames (ORFs) are drawn to scale. The chemotaxis-related genes within each cluster were either previously characterized or identified by homology searches. hk, histidine kinase. Response regulators CheY1 and CheY4 are encoded with each of the two major chemotaxis operons (*che1* and *che4*). CheY6 and CheY7 are encoded elsewhere on the genome. **(B)** Membrane bound chemotaxis receptors (Tlps) are organized in signaling arrays with mixed base plates consisting of CheW1/CheA1 and CheW4/CheA4 proteins. Environmental signals (repellent or chemoattractant) received by Tlps modulate changes in their conformation and autophosphorylation activity of CheA1 and/or CheA4, which ultimately affect the phosphorylation states of flagellar-motor switching response regulators (CheYs). The activity of Tlps is switched off by the addition of the methyl groups chemoreceptor-specific methyltransferase (CheR1 and CheR4) and switched on by the removal of the methyl groups by the chemoreceptor-specific methylesterase, CheB1 and CheB4. Activity of CheB1 and CheB4 depends on autophosphorylation of CheA1 and CheA4. **(C)** Scheme depicting the role of CheYs in the modification of the swimming speed and reversals. Figures in panels **(B,C)** were created using Biorender.com.

surfaces and wheat roots attachment as well as biofilm formation. Together, the findings indicate that CheY homologs contribute to distinct swim-to-stick behaviors.

MATERIALS AND METHODS

Bacterial Strains and Culture Conditions

The bacterial strains used in this study are listed in **Table 1**. *A. brasilense* strains were cultured in the minimal medium (MMAB; Hauwaerts et al., 2002) or TY (tryptone 10 g/L, yeast extract 5 g/L; Bible et al., 2012); and washed in a chemotaxis buffer [10 mM phosphate buffer (pH 7.0), 1 mM EDTA] as described previously (Stephens et al., 2006). Conjugation was performed on D-plates (8 g/L Bacto Nutrient broth, 0.25 g/L $MgSO_4$ $7H_2O$, 1.0 g/L KCl, 0.01 g/L $MnCl_2$, 2% agar) and, after conjugation, MMAB with appropriate antibiotics was used for selection of *A. brasilense* transconjugants. The *A. brasilense* wild type (Sp7), mutant strains, and complemented derivatives were grown at 28°C, with shaking. Unless otherwise stated,

TABLE 1 | The list of strains and plasmid used in this study.

Strain or plasmid	Description	Reference or source
A. brasilense Sp7	Wild type strain	ATCC 29145
ΔcheY1	*ΔcheY1*::Km (Km^r)	Bible et al., 2008
ΔcheY4	*ΔcheY4*::Cm (Cm^r)	Mukherjee et al., 2016
ΔcheY7	*ΔcheY7*::Gm (Gm^r)	Mukherjee et al., 2019
ΔcheY6	*ΔcheY6,* markerless	Mukherjee et al., 2019
rpoN::Km^r	*rpoN::Kmr* in Sp7 (Km^r)	Milcamps et al., 1996
E. coli	General cloning	Invitrogen™
TOP10	F-*mcr*A Δ(*mrr-hsd*RMS-*mcr*BC) φ80*lac*ZΔM15 Δ*lac*X74 *rec*A1 *ara*D139 Δ(*araleu*)7697 *gal*U *gal*K λ$^-$ *rps*L (Str^R) *end*A1 *nup*G	Simon et al., 1983
pRK2013	Helper plasmid for triparental mating (ColE1 replicon, Tra, Km^r)	Figurski and Helinski, 1979
pHRGFP	pBBR1 origin plasmid expressing GFP (Tc^r)	Ramos et al., 2002
pRH005	Gateway-based destination vector expressing proteins fused with YFP at the C-terminus, Km^r, Cm^r	Hallez et al., 2007
pRHCheY4	pRH005 plasmid with CheY4 ORF fused with YFP at the C-terminus (CheY4-YFP)	O'Neal et al., 2019
pRHCheY7	pRH005 plasmid with CheY7 ORF fused with YFP at the C-terminus (CheY7-YFP)	this study
pRK415	Broad host range vector (Tc^r)	Keen et al., 1988
pRKCheY1	pRK415 containing *cheY1* (Tc^r)	Bible et al., 2008
pRKCheY4	pRK415 containing *cheY4* (Tc^r)	Mukherjee et al., 2016
pRKCheY6	pRK415 containing *cheY6* (Tc^r)	Mukherjee et al., 2019
pRKCheY7	pRK415 containing *cheY7* (Tc^r)	Mukherjee et al., 2019

the antibiotics were used at the following concentrations: 200 μg/ml ampicillin, 30 μg/ml kanamycin (Km), 20 μg/ml gentamicin (Gm), 34 μg/ml chloramphenicol (Cm), and tetracycline (Tc) 5 μg/ml. CheY7-YFP complementation construct was obtained using Gateway cloning (Invitrogen) and the pRH005 vector according to the published protocols (Hallez et al., 2007). *cheY7* gene was amplified using Gateway primers (**Table 1**) and Sp7 *A. brasilense* genomic DNA as a template. Five microliters of PCR product were run on a 0.8% gel for verification of the insert, and PCR cleanup (Nucleospin Gel and PCR cleanup, Macherey-Nagel™) was performed on the remainder of the PCR product. The resulting PCR product was used for a BP Clonase (Invitrogen™) reaction with the pDONR2.1 vector (Invitrogen™). This reaction was then transformed into *E. coli* Top10 chemically competent cells and plated on Luria broth (LB, 10 g/l tryptone, 5 g/l yeast extract, 10 g/l NaCl) with 50 mg/ml kanamycin. Colonies from these plates were grown in 5 ml of LB with kanamycin (50 μg/ml) and subjected to plasmid purification (Qiagen™). The resulting plasmids were used for the LR Gateway reaction (in the Gateway cloning LR Reaction stands for a recombination reaction between attL and attR sites; Invitrogen™) with the pRH005 plasmid.

Chemotaxis, Swimming, and Swarming Behavioral Assays

For the aerotaxis spatial gradient assay, free-swimming cells from exponentially grown cultures were washed twice with chemotaxis buffer and placed in a 1 mm flat capillary tube (inner dimensions, 0.1 by 2 by 50 mm; VitroCom, Mountain Lakes, NJ, United States). The formation of a band of motile bacteria near the air-liquid interface was observed at 60 s post-introduction into the capillary tube, and the distance between the meniscus and the band was measured. Aerotaxis band formation was recorded using a Nikon microscope with a Nikon Coolpix mounted camera.

For the swimming and swarming assays in Petri plates, a single colony from each strain was inoculated in 5 ml of MMAB medium and grown until OD_{600} = 0.8. The culture was then washed once with modified chemotaxis buffer [10 mM phosphate buffer (pH 7.0)], and 5 μl of the culture was placed on top of 13 g/l Nutrient broth (Fisher Scientific™) solidified with 0.2, 0.3, 0.4, 0.5 0.6, or 0.7% (w/vol) of noble agar (Fisher Scientific™). A swarming time-course assay was conducted using 0.6% noble agar added to MMAB and supplemented with 0.5% Tween-20 since preliminary data indicated its addition promoted reproducible and robust swarming (Wu et al., 2020). The plates were incubated at 28°C for 24–96 h, and the diameter of the expansion rings was measured.

To observe the development of swarming colonies under the microscope, we used the pHRGFP plasmid with constitutive green fluorescent protein (GFP) expression in *A. brasilense* (Ramos et al., 2002). The pHRGFP plasmid was introduced into the wild type Sp7 strain and its *cheY* mutant derivatives by conjugation. Three hundred microliters of the swarming medium [MMAB with 0.6% (w/v) noble agar and supplemented with 0.5% Tween-20] were placed in the well of an EISCO Concavity Microscope slide (Fischer Scientific™). Two microliters of the cell culture, prepared as for the swarm plates assay above, were diluted to an OD_{600} = 0.8 and placed at the center of the swarming medium. Under these conditions, swarming of the cells was observed using a GFP filter, 4x objective mounted to a Nikon ECLIPSE 80i fluorescence microscope with a Nikon CoolSnap HQ2-cooled charge-coupled device (CCD) camera and photographed in 2, 6, and 24 h. The experiment was conducted in triplicate. Whole colony swarming fluorescence images were obtained using a Leica MZ167A dissecting scope equipped with a GFP fluorescence filter. Leica application suite software was used for the image collection. To observe the formation of cell clusters in swarming colonies of *A. brasilense* Sp7 and a *rpoN::Km^r* harboring a pHRGFP plasmid, slides were prepared the same way as described above except a cover slip was placed on the top of the agar inoculated with cells. Clusters were observed using a GFP filter, 100x objective mounted to a Nikon ECLIPSE 80i fluorescence microscope with a Nikon CoolSnap HQ2-cooled charge-coupled device (CCD) camera and photographed at 2, 6, and 24 h post inoculation.

Flagella Staining

Flagella staining was performed on cells grown in liquid medium (swimming) or collected from swimming/swarming MMAB media made with 0.2–0.7% (w/vol) agar plates after 48 h incubation and stained using Alexa Fluor™ 488 NHS Ester (Succinimidyl Ester; Fisher Scientific™) as described in (Gunsolus et al., 2014) with slight modifications. Briefly, cells were resuspended in 75 µl of in phosphate buffer saline (PBS; 137 mM NaCl, 2.7 mM KCl, 10 mM Na_2HPO_4, 1.8 mM KH_2PO_4) supplemented with 1 mM EDTA and 0.5% Brij^{Tm}-35 detergent (Fisher Scientific™) to avoid cell-to-cell adhesion at OD_{600} = 1 and 25 µl of 1 M sodium bicarbonate bicarbonate buffer was added to the cell suspension to stabilize the pH. A 1 µl of 0.5 mg ml^{-1} Alexa Fluor 488 carboxylic acid succinimidyl ester (Fisher Scientific™) in DMSO (Sigma Aldrich) was added. The resulting suspension was incubated in the dark for 1 h at room temperature with frequent mixing. The suspension was then centrifuged at 4,000 rpm for 3 min, the supernatant was discarded, and the cell pellet was washed with 500 µl of PBS. Cells were mounted on an agar pad (1% low melting point agarose in PBS) and covered with a glass coverslip, and left on the bench for 10 min. Images were taken using a 63x objective with oil immersion mounted to a Leica SP8 with White Light Laser Confocal System; Leica, Wetzlar, Germany). Images were collected using a 488-nm excitation Argon ion laser with an emission maximum at 517 nm.

Measurements of Cell Size

Cells were washed once with PBS buffer and resuspended in TBAC buffer [PBS containing 1 mM EDTA and 0.01% (v/v) Tween 20] to avoid the formation of bacterial aggregates (Alves et al., 2017). Cell sizes were measured using the Prism 8 program for a minimum of 60–100 cells per sample taken from at least four different fields of view. Confocal microscopy (Leica SP8 White Light Laser Confocal System) images were taken at random fields of view. Several images were collected for each experiment. For cell length measurements, all cells within the field of view were measured from one cell pole to the other at the longest axis.

Western Blotting, Coomassie Staining, and Flagella Glycosylation Staining

For isolation of polar flagella, each strain was grown to the mid-log phase (OD_{600} = 0.7–0.8) in liquid MMAB. Cells were pelleted for 3 min at 4,600 rpm using a tabletop Eppendorf centrifuge and washed once with 1 ml of PBS buffer. The resulting pellet was resuspended in 150 µl of 1x Laemmli buffer (4% SDS, 10% beta-mercaptoethanol, 20% glycerol, 0.1 M Tris pH 6.8, and 0.005% of bromophenol blue) in PBS. Cells were vigorously vortexed for 1 min and spun down for 15 min at 4°C and 13,000 rpm using a tabletop Eppendorf centrifuge. The supernatant was collected and heated for 5 min at 65°C to denature proteins. For isolation of lateral flagella, each strain was grown on the top of the swarming medium (MMAB supplemented with 0.6% of noble agar and 0.5% of Tween-20) for 48 h at 28°C. Cells were then scraped from the plate and resuspended in PBS. Flagella isolation was done as described for the isolation of polar flagella. Twenty microliters of isolated flagellins were loaded on SDS-PAGE gels (8% resolving gel for polar flagellin analysis and 12% resolving gel for lateral flagellin detection). Mini-Protean gel system was used for protein separation (Bio-Rad™). The gel ran at 120 V for 90 min. The gel was then transferred to a 0.45 µm hydrophobic polyvinylidene difluoride (PVDF) transfer membrane (Immobilon) using a wet transfer apparatus (Bio-Rad). The transfer ran at 90 V for 1 h and 10 min. The membrane was blotted for 40 min in 5% milk in Tris-buffered saline (TBS; 6.05 g/L Tris, 8.76 g/L NaCl, pH 7.5) supplemented with Tween-20 (0.1%; TBST). After blocking, the membrane was incubated with primary polyclonal anti-polar and anti-lateral flagellin antisera (Alexandre et al., 1999) in TBST at 1:1,000 for 16 h at 4°C with agitation. The membrane was washed twice with 5% milk in TBST, twice in TBST, and twice in TBS. The membrane was then incubated with secondary anti-rabbit antibodies, diluted to 1:10,000 in TBS for 1 h, and washed again with the solutions mentioned above. Lateral protein production was quantitated using Fiji ImageJ (NIH). Coomassie blue dye (2 g/L of water) was used to monitor total proteins loaded. SDS-PAGE gels were de-stained using a mix of H_2O, methanol, and acetic acid detected using the Glycoprotein Staining Kit (Thermo Scientific™ Pierce™) according to the manufacturer's manual. Briefly, *A. brasilense* cells were grown in flasks with 25 ml of MMAB medium with shaking at 175 rpm, at 28°C. Cell cultures were spun down at 3,000 rpm in a 50-ml Falcon tube, cell pellets were washed once with PBS, and flagella were sheared for 1 min using a vortex, resuspended in 20 ml of PBS, kept on ice for 5 min, and spun down at 22,000 rpm using a Beckman ultracentrifuge with a T70i fixed-angle titanium rotor for 90 min. The pellets were resuspended in 200 µl of 1x Laemmli buffer in PBS. Samples were heated for 5 min at 60°C before loading onto an 8% SDS-PAGE gel.

Abiotic Surface Attachment Assay

For the abiotic surface attachment assay, *A. brasilense* Sp7 strain and its *cheY* mutant derivatives carrying the pHRGFP plasmid (Ramos et al., 2002) were cultured overnight in TY medium supplemented with tetracycline for plasmid maintenance. Cells were washed with a chemotaxis buffer and resuspended in the chemotaxis buffer to a final OD_{600} = 0.4. Economy Plain Glass Microscope Slides Glass slides (Fisher Scientific™) were covered with 0.01% poly-lysine (Sigma™) and left to dry for 15 min. Ten microliters of cell cultures were placed on the slide and kept in a humidity chamber (square Petri dishes lined up with Kim Wipes wetted with sterile water) to prevent buffer evaporation. Cells remaining on the slide were washed with chemotaxis buffer 2 h after inoculation and imaged using a GFP filter, 4x objective mounted to a Nikon ECLIPSE 80i fluorescence microscope with a Nikon CoolSnap HQ2-cooled charge-coupled device (CCD) camera.

Biofilm Formation

Biofilm assay was performed in modified MMAB medium modified to achieve a C:N ratio = 2 using fructose at 27.6

and 13.8 mM KNO3 as N source (Arruebarrena Di Palma et al., 2013). Two hundred microliters per well were transferred to sterile, clear flat-bottom polystyrene 96-well plates (Corning™) and incubated without agitation for 96 h at 28°C. Biofilm formation was determined using crystal violet staining (Arruebarrena Di Palma et al., 2013). Briefly, 200 µl of 0.5% crystal violet was added to each well, followed by incubation 30 min at room temperature, and then washed carefully three times with tap water. Crystal violet remaining attached to the wells was extracted with 200 µl of 33% v/v acetic acid. The OD_{590} of supernatants was determined using a microplate Absorbance Reader with Gen5 software (BioTek Instruments, Winooski, Vermont, United States). Data were normalized by total growth estimated by OD_{600} measured on the planktonic culture.

Wheat Root Attachment Assay

Triticum aestivum cv. Jagger (wheat) seeds were utilized throughout this study. *T. aestivum* seeds were surface-sterilized 10 min with 90% ethanol and 20 min with a sterilization buffer containing 1% Triton X-100, 10% bleach and sterile water. After sterilization, seeds were planted into c (0.132 g/l $CaCl_2$, 0.12 g/l $MgSO_4$ $7H_2O$, 0.1 g/l KH_2PO_4, 0.075 g/l Na_2HPO_4 $2H_2O$, 5 mg/l Fe-citrate, and 0.07 mg/l each of $MnCl_2$ $4H_2O$, $CuSO_4$ $5H_2O$, $ZnCl_2$, H_3BO_3, and Na_2MoO_4 $2H_2O$, adjusted to pH 7.5 before autoclaving; Zamudio and Bastarrachea, 1994; de Oliveira Pinheiro et al., 2002; Greer-Phillips et al., 2004) and placed in the dark for 48 h to germinate. Next, seedlings were placed in 250 ml Mason jars containing 50 ml of semi-solid (0.5% w/vol Noble agar) Fahraeus medium and allowed to grow with 8 h day/16 h dark at 22°C in the plant growth chamber at 90,000 lux or 1,670 µmol m^{-2} s^{-1}. All assays were performed on germinated and surface-sterilized seedlings that were 7–10 days old.

For the root attachment assay, *A. brasilense* strains were cultured in MMAB liquid overnight (28°C, 200 rpm). The cultures were normalized to an OD_{600} = 0.6 using sterile chemotaxis buffer and resuspended in 2 ml of Fahraeus medium in a 15 ml Falcon tube. Wheat seedling with cut-off leaves was placed inside the tube, and tubes were incubated either at room temperature for 2 h or with shaking on a Ferris wheel for 2 h. After incubation, roots were washed three times with sterile chemotaxis buffer, resuspended in 2 ml sterile chemotaxis buffer and sonicated for 10 s, using a cell dismembrator (Model 100; Fisher Scientific™, Waltham, MA, United States). CFU recovered from the inoculum or after detachment from roots were counted by plating serial dilutions on TY plates supplemented with ampicillin. The results were expressed as a root attachment index, calculated as CFU detached from roots/CFU in the initial culture normalized to the total fresh weight of roots in milligrams.

Statistical Analysis

We used Student *t*-test using GraphPad Prism (version 8) software (GraphPad Software Inc., San Diego, CA, United States) to compare the wild type and mutant phenotypes (swimming/swarming behavior on the plates, band quantitation, western blotting flocculation, biofilm formation, and plant root attachment).

RESULTS

Azospirillum brasilense CheY6 and CheY7 Response Regulators Have Different Contributions to Aerotaxis

Our previous work has shown that minor (*ΔcheY1* and *ΔcheY6* mutants) and severe (*ΔcheY4* and *ΔcheY7* mutants) defect in chemotaxis of the mutant strains could be functionally rescued by expressing parental genes from broad host range vectors (Bible et al., 2008, 2012; Mukherjee et al., 2016, 2019). Here, we confirm these previous observations by analyzing chemotaxis in swim plate assays (**Figure 2A**). The *ΔcheY1*, *ΔcheY4*, *ΔcheY6*, and *ΔcheY7* mutants had slight or major chemotaxis defects that were partially complemented by expressing *parental genes* expressed from broad host range plasmids (**Figures 2A,B**). Partial functional complementation from this type of plasmids was reported previously (Bible et al., 2008). We also performed the aerotaxis assay with the mutant strains. Aerotaxis is a particular form of chemotaxis in air gradients and is regulated by the same chemotaxis pathways. Aerotaxis depends on near-immediate responses to the air gradient (~1–2 min) instead of the several days for observing a response in chemotaxis spatial gradient assays. Aerotaxis thus provides a more direct evaluation of the ability of cells to navigate gradients. In the aerotaxis gradient assay, an open-ended capillary tube is filled with a suspension of motile *A. brasilense* cells. An air gradient is established through the diffusion of air from the atmosphere into the cell suspension (Zhulin et al., 1996; Alexandre et al., 2000). Under these conditions, motile and chemotaxis-competent *A. brasilense* cells form a tight band of motile cells at a location in the gradient that corresponds to maximal energy generation (Zhulin et al., 1996; **Figures 2C–F**). Chemotaxis defects of the different *cheY* mutant strains were also complemented by expressing parental genes from plasmids (**Figures 2A,B,E,F**).

The Absence of *CheY7* Causes Defects in Polar Flagellin Molecular Weight but Not Swimming Motility

All of the mutants lacking CheY1, CheY4, CheY6, or CheY7 are motile in liquid media and, as expected, possess polar flagella (**Figure 3A**). We used polyclonal antisera raised against the polar flagellin and Western blots to compare levels of production of the polar flagellin in the wild type Sp7 and its *cheY* mutant derivatives (**Figure 3B**). As a negative control, we used a *rpoN::Km*^{r} mutant which lacks both polar and lateral flagella production (Milcamps et al., 1996; **Figures 3A,B**). As expected, the anti-polar flagellin antisera recognized a band at a predicted ~100 kDa in all but the *ΔcheY7* mutant. In this mutant, the band corresponding to the polar flagellin migrated with an apparent molecular weight of ~90 kDa. A second band at about 45–50 kDa was also observed in the *ΔcheY6* mutant. This molecular weight is much lower than

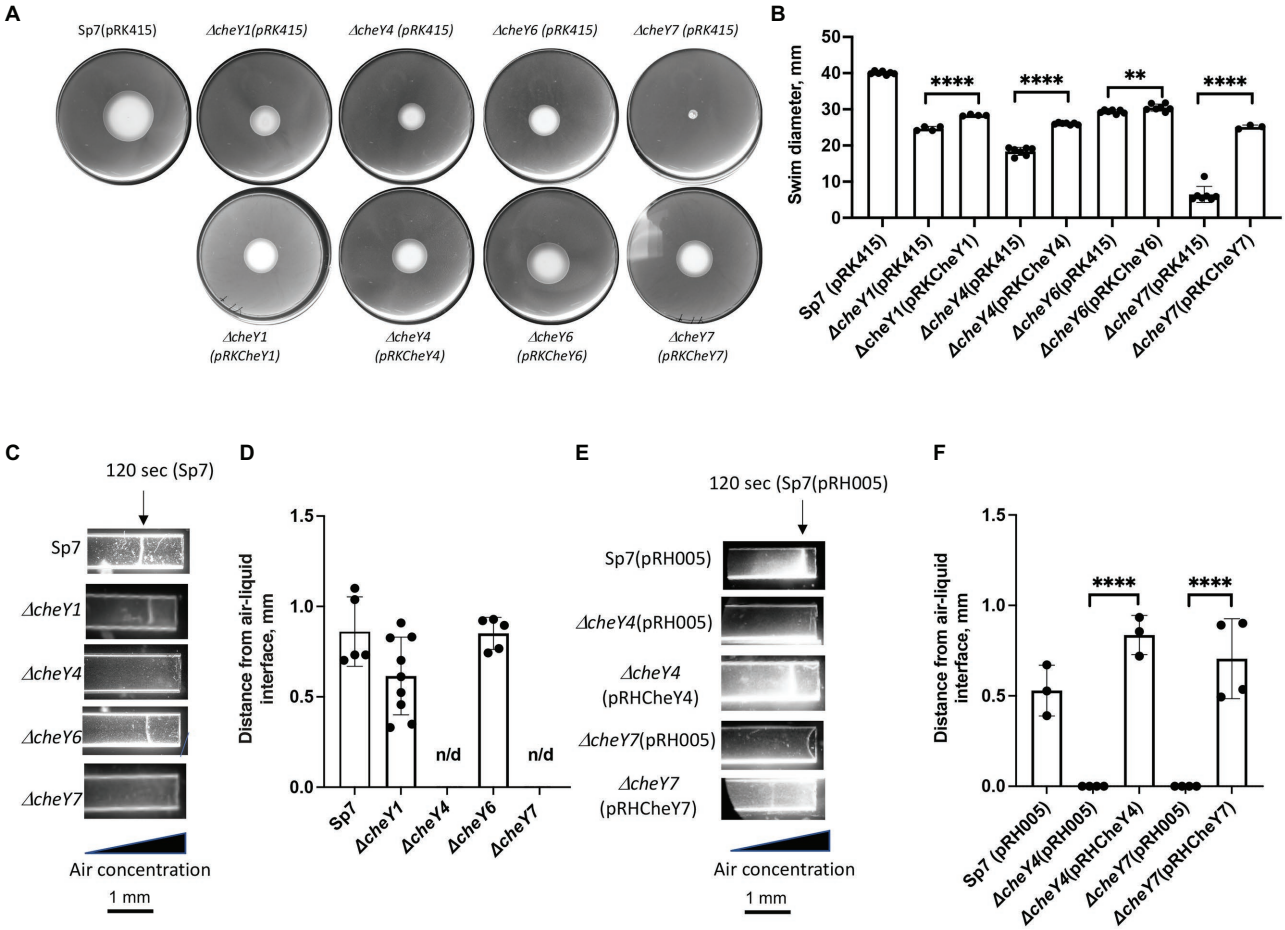

FIGURE 2 | Detection and quantification of chemotaxis **(A,B)** and aerotaxis **(C-F)** responses in the *A. brasilense* and ΔcheY mutant derivatives. **(A)** Chemotaxis in the soft agar plate assay. **(B)** Quantification of chemotaxis in the soft-agar plate assay. **(C)** Aerotaxis in the spatial gradient capillary assay. The air gradient is established by diffusion into capillary tubes filled with a suspension of motile cells. The triangle represents decreasing air concentration as a result of diffusion within the cell suspension. The images were taken 120 s after placement of the cells into the capillary tubes. **(D)** Quantitation of the aerotaxis response represented as the distance from the edge of the air-liquid interface. **(E)** Aerotaxis of Sp7 (pRH005), *ΔcheY4* (pRH005), *ΔcheY7* (pRH005), and mutants complemented with CheY4-YFP, expressed as pRHCheY4 (for *ΔcheY4*) and CheY7-YFP, expressed as pRHCheY7 (for *ΔcheY7*) in the spatial gradient assay for aerotaxis. **(F)** Quantitation of the aerotaxis response in Sp7(pRH005), *ΔcheY4* (pRH005), *ΔcheY7* (pRH005), and mutants complemented with CheY4-YFP, expressed as pRHCheY4 (for *ΔcheY4*) and CheY7-YFP, expressed as pRHCheY7 (for *ΔcheY7*) in the spatial gradient assay represented as the distance from the edge of the air-liquid interface. $^{**}p < 0.01$ and $^{****}p < 0.001$.

the predicted molecular weight for the two polar flagellins encoded in the *A. brasilense* genome (AMK58_10890 and AMK58-18185), which are expected to be about 65 kDa. The nature of this cross-reacting band is not known. The polar flagellin is glycosylated in *A. brasilense* and a fully glycosylated polar flagellin has a molecular weight of about 100 kDa, while complete chemical deglycosylation of the polar flagellin yields a band at ~65–70 kDa (Moens et al., 1995b). Therefore, we hypothesized that changes in the molecular weight of the polar flagellin in the *ΔcheY7* strain could result from reduced glycosylation of the polar flagellin. Analysis of glycosylated proteins from the same samples as those used for the Western blot above, identified a single band for a glycosylated protein at the same molecular weight as the polar flagellin for all strains except for the non-flagellated *rpoN::Km*^{r} strain (**Figure 3C**). Noticeably, a glycosylated band corresponding to the polar flagellin of the *ΔcheY7* mutant was still present at a lower molecular weight (**Figure 3C**). The reduced molecular weight of the polar flagellin of the *ΔcheY7* mutant could suggest reduced glycosylation levels in this species. A *ΔcheY7* mutant is still fully motile, so this different glycosylation level has no apparent effect on polar flagellum function. This observation is intriguing because it suggests a functional link between CheY7 and polar flagellin maturation.

Azospirillum brasilense Chemotaxis CheY Homologs Contribute to Movement in Media of Varying Viscosity

CheY homologs have different effects on the free-swimming motility pattern of *A. brasilense*: CheY1 affects the transient increase in swimming speed and has a minor impact on the probability of swimming reversals. In contrast, CheY4 and

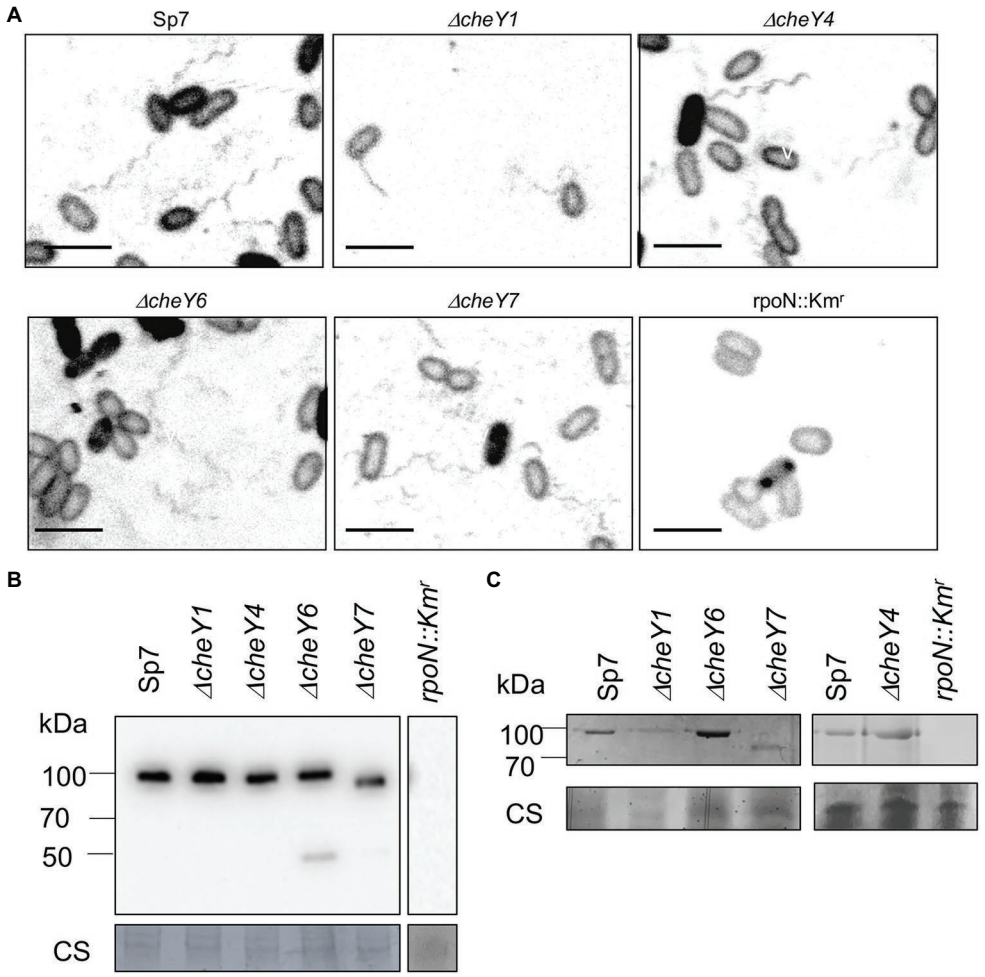

FIGURE 3 | Visualization of the polar flagella in *A. brasilense* strains. **(A)** Representative images of Sp7, *ΔcheY1*, *ΔcheY4*, *ΔcheY6*, and *ΔcheY7* cells with polar flagella stained with Alexa fluor™ 488 NHS Ester. A *rpoN::Km*^{r} mutant which is aflagellate and non-motile was used as a negative control. Images are presented as the negatives of the original images. Scale bar = 5 μm. **(B)** Western blot analysis with anti-polar flagellin (1:1,000) polyclonal antisera of whole-cell preparations of *A. brasilense* Sp7, *ΔcheY1*, *ΔcheY4*, *ΔcheY6*, *ΔcheY7*, and *rpoN::Km*^{r} mutants grown in liquid media. Coomassie staining is shown below for an evaluation of loading control. **(C)** Glycoprotein staining of polar flagellin produced by wild type Sp7 and *ΔcheY1*, *ΔcheY4*, *ΔcheY6*, and *ΔcheY7* cells *ΔcheY1*, *ΔcheY4*, *ΔcheY6*, and *ΔcheY7* mutants. *rpoN::Km* strain was used as the negative control. The black lines indicate junctions separating lanes that were spliced from the original image in order to show samples run on the same gel in a single row.

CheY6 have severe defects in swimming reversals, and CheY7 cannot reverse the swimming direction (Mukherjee et al., 2019). These different effects are hypothesized to provide *A. brasilense* with swimming navigation strategies optimized for the heterogeneous physicochemical conditions found in the soil. Here, we probe the chemotaxis response regulators' role in controlling the swimming bias in modulating navigation in porous media by comparing the movement of cells under conditions of increasing agar concentrations (**Figures 4A,B**). We also included *ΔcheA1* and *ΔcheA4* mutants that are impaired or null for chemotaxis, respectively (**Figures 4A,B**; Bible et al., 2008; Mukherjee et al., 2016), and the *rpoN::Km*^{r} mutant strain that is immotile and lacks flagella (Milcamps et al., 1996). At low agar concentrations (0.2–0.3%), *A. brasilense* cells are swimming through the medium using their polar flagellum, given the abundance of water under these conditions and previous observation by others (Hall and Krieg, 1983; Moens et al., 1995b; **Figure 4**). At higher agar concentrations (0.6–0.7%), wild type cells are preferentially swarming using lateral flagella, given that they are observed to move on top of the medium and that these agar concentrations were previously described as optimum for swarming for *A. brasilense* (Hall and Krieg, 1983; Moens et al., 1995b). Navigation of the wild type cells within or on top of the medium at intermediate agar concentrations (0.4%) was minimal, suggesting that both swimming and swarming are limited under these conditions (**Figures 4A,B**).

Compared to the wild type, the *rpoN::Km*^{r} mutant did not expand beyond the inoculation point, regardless of agar concentrations, a behavior mimicked by the chemotaxis null

mutants *ΔcheA4* and *ΔcheY7*. The *ΔcheY4* mutant had reduced expansion at low agar concentrations (0.2–0.5%) and did not expand beyond the site of inoculation at higher agar concentrations (**Figures 4A,B**). The *ΔcheY4* mutant is non-chemotactic because it seldom reverses swimming direction and this strain also has an elevated frequency of swimming pauses (Mukherjee et al., 2019). We surmise that the limited expansion of the *ΔcheY4* cells in media with low agar concentrations is related to these cells' ability to pause with a high frequency during swimming, which would allow them to escape entrapment into the agar polymers. This swimming bias would not be sufficient to promote movement at higher agar concentrations (0.6–0.7%). The mutants that are impaired but not null for chemotaxis (*ΔcheA1*, *ΔcheY1*, and *ΔcheY6*) displayed either no or only minor defects in navigating within or on top of media of different viscosity. The *ΔcheA1* mutant

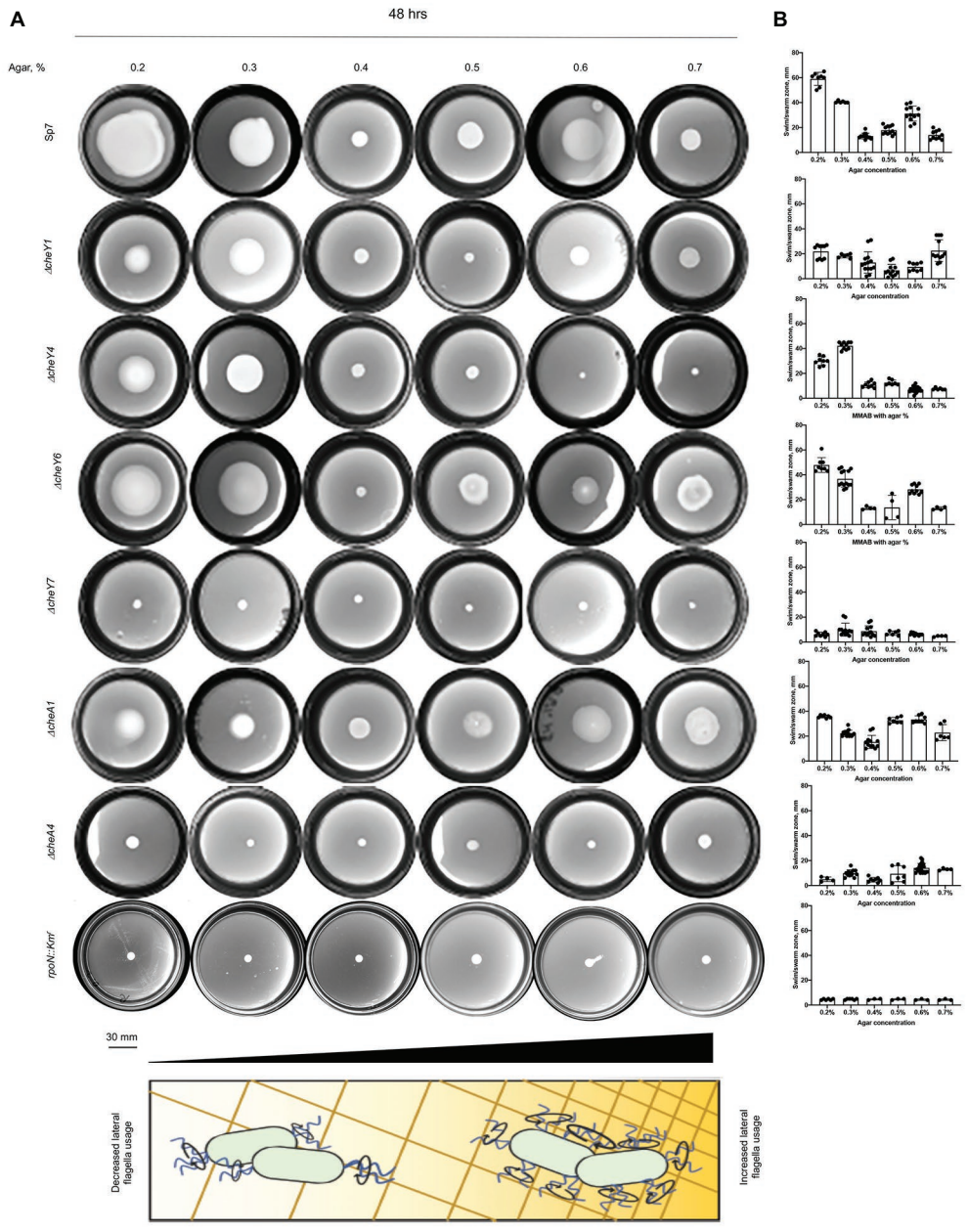

FIGURE 4 | Navigation of *A. brasilense* and its chemotaxis mutant derivatives in soft agar media of varying viscosity. **(A)** Chemotaxis behavior of *A. brasilense* Sp7, *ΔcheY1*, *ΔcheY4*, *ΔcheY6*, *ΔcheY7*, *ΔcheA1*, *ΔcheA4*, and *rpoN::Km^r* strains in the semi-solid medium supplemented with 0.2–0.7% agar. The triangle at the bottom and the scheme represents increasing concentrations of agar. **(B)** Quantitation of the swimming/swarming ring diameters. Arrows indicate a significantly higher swimming/swarming diameter of the colonies in the mutant strains than Sp7. Student *t*-test was used to determine significance between Sp7 and mutants. $^{*}p < 0.05$, $^{**}p < 0.01$, $^{***}p < 0.005$, and $^{****}p < 0.001$. All studies were done in three biological replicates.

had a marginally increased expansion through media at the highest agar concentration tested (**Figures 4A,B**). Together, these data indicate that chemotaxis is essential for the ability of cells to navigate media of varying viscosity, including across surfaces by swarming. Chemical gradients are produced by metabolism as cells move through the agar media and grow indicating that the existence of a gradient is sufficient to trigger an expansion in viscous media by either swimming or swarming. The data presented here confirm the hypothesis that *ΔcheY1* and *ΔcheY6* mutants are functionally linked to *ΔcheA1*, while *ΔcheY4* and *ΔcheY7* cells are related to *ΔcheA4* mediated signaling.

We next confirmed the type of motility employed by the cells under these conditions by visualizing the wild type strain's flagellation when inoculated in semi-soft media at different agar concentrations (**Figure 5A**). At 48 h post-inoculation, both polar and lateral flagella were visible regardless of agar concentration (**Figure 5A**). Lateral flagella are not produced constitutively in contrast to the polar flagellum in *A. brasilense*. However, we observed some wild type cells with lateral flagella, even at low viscosity [0.2% (v/v) of agar]. This suggests that conditions in the soft agar plates are heterogeneous and do not perfectly replicate a single motility type. To confirm these observations, we used polyclonal antisera raised against the polar and lateral flagellins and Western blots (**Figures 5B,C**). As expected, the anti-polar flagellin antisera recognized a single band at ~100 kDa in cells grown at various viscosity. The most significant induction of the lateral flagellin production, relative to the polar flagellin production, was observed starting at 0.4% agar in the medium and remained elevated at higher viscosity conditions (**Figures 5B,C**). Concurrent to these changes, we also observed that cell size distribution varied depending on agar concentrations. The wild type cells were the shortest when incubated in 0.2% agar plates. They tended to increase in size when cells were incubated in media with 0.3–0.6% agar and became shorter at 0.7% agar. However, cells from 0.7% agar were longer than cells at 0.2% agar (**Supplementary Figure 1**). The longer cell sizes roughly match the induction of lateral flagellin production under these conditions, suggesting that cell elongation is concomitant with swarming. These findings are consistent with similar differentiation observed in other species (Kim et al., 2003; Skerker and Laub, 2004; Little et al., 2019).

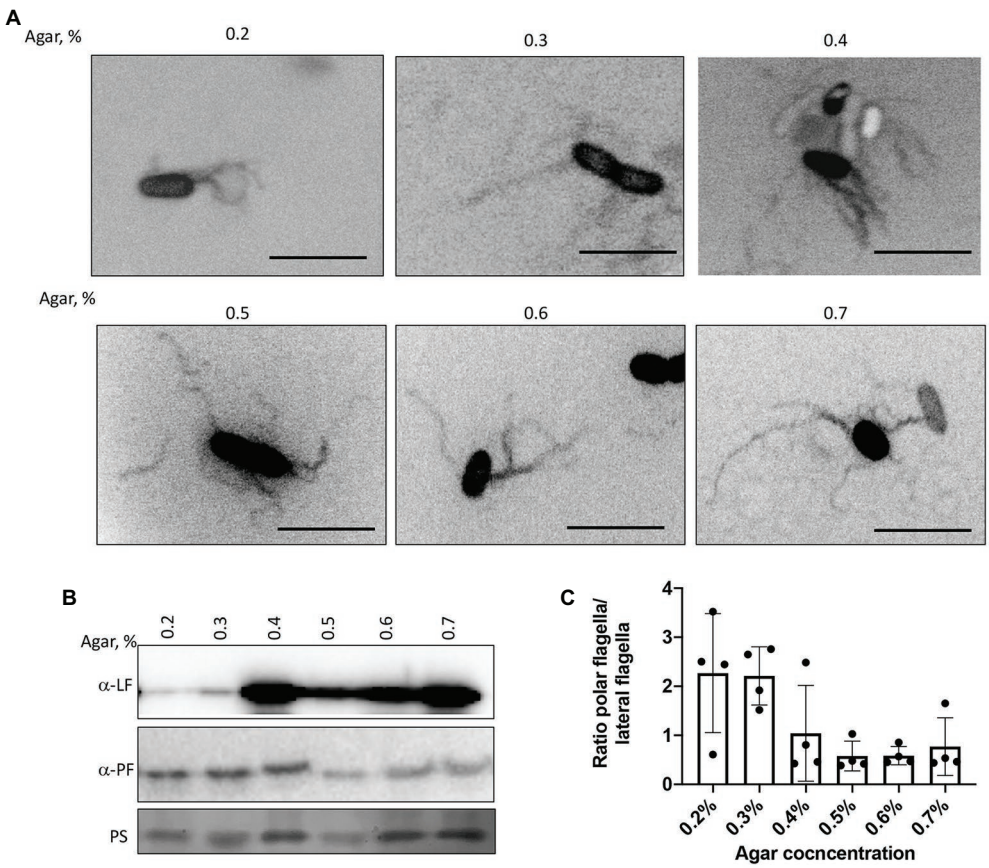

FIGURE 5 | Visualization of the polar and lateral flagella in *A. brasilense* strains. **(A)** Representative images of Sp7 cells collected from the media with 0.2–0.7% agar and stained with Alexa fluor™ 488 NHS Ester. Arrows indicate localization of the polar flagella. Images are presented as the negatives of the original images. Scale bar = 5 μm. **(B)** Western blot analysis with anti-polar (1:1,000) and anti-lateral flagellin (1:1,000) polyclonal antisera of whole-cell preparations of *A. brasilense* Sp7 collected from the media with 0.2–0.7% agar. Ponceau staining (PS) is shown below for evaluation of loading control. **(C)** Ratio between polar and lateral flagellin abundance in wild type cells grown in media solidified with 0.2–0.7% (w/vol) agar. Quantitation was performed based on the Western blotting analysis *p*-values.

To determine whether the defects were due to lack of swarming vs. delayed swarming, we also compared *ΔcheY1*, *ΔcheY4*, *ΔcheY6*, and *ΔcheY7* mutants with the wild type Sp7 strain for swarming over time. We performed the experiments using MMAB medium solidified with 0.6% noble agar and supplemented with Tween-20, corresponding to conditions that permit robust swarming (**Figures 6A,B**). Compared to the wild type strain, all mutants had reduced swarming over the 96 h time-course experiment except for the *ΔcheY4* strain, which increased swarming at 96 h post-inoculation, following a reduced swarming at other time points (**Figures 6A,B**). The *ΔcheY4* strain also appeared to expand into a larger swarm colony than the wild type strain under these conditions. This result indicates that the *ΔcheY4* strain, but not the other strains, is delayed in inducing swarming. Collectively, the data suggest that CheY7 is essential for swarming and that CheY4 is necessary for timely swarming.

The surface of swarming colonies also differ between the strains: the swarming colonies of the wild type, the *ΔcheY6*, and *ΔcheY7* mutants had a homogenous surface appearance while the swarming colonies of the *ΔcheY1* and *ΔcheY4* displayed a thick front edge and a thinner, less dense inner region, suggesting that the reduced swarming of the strains could be caused by different group behaviors within the swarming colony. To further characterize cells' behavior in swarming colonies, we next labeled cells with a constitutively expressed GFP from a plasmid (Ramos et al., 2002) and inoculated these on top of a swarming agar pad. We used fluorescent microscopy to observe cellular behavior at the initiation of swarming (first 24 h). Under these conditions, the wild type cells appeared to organize into a dense edge at the expanding front of the swarming colony, while cells formed clusters that grew in density over time behind this front (**Figure 6C**). A thick edge was seen in the *rpoN::Km*^{r} mutant that is non-motile and non-flagellated, suggesting that it corresponds to non-motile cells. Still, the density of cells under these conditions did not change behind this front in the mutant, suggesting that motility is required for this organization (**Figure 6C**). A major difference was evident between the wild type swarming colony and the *cheY* mutants: no increasing clustering of cells behind the expanding front was observed in any of the mutants (**Figure 6C**). This observation indicates that the organization of cells as high-density clusters is required for the ability of a swarming colony to expand on a surface. Given the differences in the *cheY* and *rpoN::Km*^{r} mutant strains, the lack of cellular clustering suggests that swimming motility, a polar flagellum able to reverse, change swimming speed, and pause is essential for this behavior. A second difference was that the *ΔcheY1* and *ΔcheY4* swarming colony's edge was thicker and diffuse compared to that of the wild type or the other mutants. In contrast,

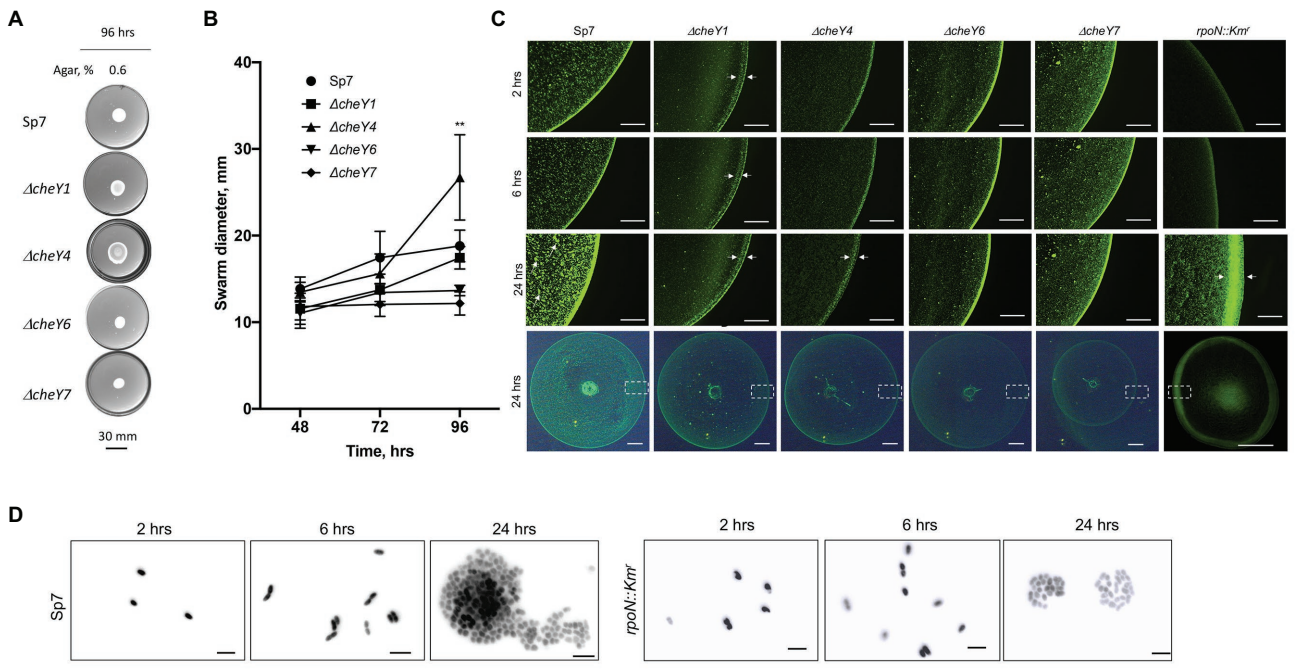

FIGURE 6 | Time course of swarming of *A. brasilense* and its chemotaxis response regulator mutants. The plates were solidified with 0.6% (w/vol) agar and incubated for 96 h post-inoculation at 28°C. **(A)** Representative images of swarming for the strains tested. **(B)** Quantitation of the ring diameters of Sp7 and mutant strains after 24–96 h of incubation on the swarming medium. Student *t*-test was used to determine significance between Sp7 and mutant strains (**$p < 0.01$). All experiments were done in triplicate. **(C)** The appearance of the border of the swarming colony of Sp7, *ΔcheY1*, *ΔcheY4*, *ΔcheY6*, *ΔcheY7*, and *rpoN::Km* strains harboring pHRGFP plasmid. The edge of the colony was photographed at 2, 6, and 24 h. The scheme at the bottom represents the area photographed. Scale bar: colony border images is 0.45 mm, whole colony is 1 mm. Exposure time for the colony border imaging is 9 s, for the whole colony 6.6 s. Arrows indicate inner and outer swarming rings in colonies of the *ΔcheY1* and *ΔcheY4* strains and cell clusters in the Sp7 swarming colony. **(D)** Visualization of the cell cluster formation by Sp7 (left panel) and *rpoN::Km*^{r} cells in time. Scale bar = 5 μm.

the *ΔcheY6* and *ΔcheY7* swarm colonies had a uniform and bright expanding edge that did not thicken over time compared to that of the wild type (**Figure 6C**). When compared to the behavior of the *rpoN::Km*^{r} mutant under these conditions, the *ΔcheY6* and *ΔcheY7* mutant strains may differ in the timing or proportion of cells losing motility that produces the edge of the swarm under these conditions compared to the *ΔcheY1* and *ΔcheY4* or wild type swarming colonies (**Figure 5C**). In all *cheY* and the *rpoN::Km*^{r} mutants, cell density was noticeably reduced behind this expanding edge. Consistent with the results above, the size of the swarming colonies at 24 h was similar in all the mutants, except for the *ΔcheY7* and the *rpoN::Km*^{r} mutants, which produced significantly smaller swarms at 24 h post-inoculation under these conditions (**Figure 6C**). These results suggest that swarming requires that cells be able to form high-density clusters behind a sharp and dense expanding edge that may be composed of non-motile cells. When observed under high magnification (**Figure 6D**), cells behind the expanding edge appeared to organized as growing clusters that adopt a three-dimensional organization in the wild type but not in the immotile *rpoN::Km*^{r} mutant, suggesting a role of motility for these clusters (**Figure 6D**). Given that some of the mutants are still able of chemotaxis (CheY1, CheY6) while others are chemotaxis null (CheY4 and CheY6), these results indicate that chemotaxis *per se* is not required for the formation of these clusters but that functional CheY response regulators are essential for this behavior. Together, our data indicate that chemotaxis underlies the expansion of a swarming colony across media of high viscosity and that motility and functional CheYs, but not chemotaxis *per se*, is required for initial cell-cell interactions and clustering within a swarming colony.

Lateral Flagella Are Produced in All but the *ΔcheY7* Mutant

Swarming depends on the production of lateral flagella, prompting us to analyze lateral flagella and flagellin production in the chemotaxis mutants (**Figures 7A–C**). Flagella staining revealed that lateral flagella were abundant at 24 h post-inoculation in the *ΔcheY1*, *ΔcheY4*, and *ΔcheY6* mutants, less abundant in the *ΔcheY7* mutant and, as expected, absent in the *rpoN::Km*^{r} mutant (**Figures 7A–C**). This suggests that the reduced swarming of the *cheY* mutant strains is not due to the inability to induce lateral flagella production. Next, we used polyclonal antisera raised against the lateral flagellin and Western blots to compare lateral flagellin production in the wild type and the chemotaxis mutant strains with the immotile *rpoN::Km*^{r} strain as a negative control (**Figures 7B,C**). As expected, the anti-lateral flagellin antisera recognized a single band, at ~45 kDa, in all strains, except the *rpoN::Km*^{r} mutant. Relative to the wild type Sp7 strain, the *ΔcheY7* mutant, but not the other strains, had a significantly lower abundance of lateral flagellin, consistent with our observations from flagella staining (**Figure 7A**). Thus, the inability of strain *ΔcheY7* to swarm is likely related to its reduced lateral flagellin production. The other mutants' reduced swarming is not related to defects in the production of lateral flagella or lateral flagellin.

Compared to the wild type, swarming cells of the *ΔcheY1*, *ΔcheY4*, *ΔcheY6*, and *ΔcheY7* and the *rpoN::Km*^{r} mutant strains were shorter in length compared to the wild type, consistent with their defective swarming (**Figure 7D**). Together, these data suggest that productive swarming requires lateral flagellin production and cell elongation in *A. brasilense* and that cells with defective swarming also display defective cell elongation. These observations are consistent with observations by others that productive swarming requires cell elongation and increased lateral flagella production (Little et al., 2019). Together, the data indicate that the chemotaxis mutants studied here can induce lateral flagella and differentiate into swarmer cells, albeit at different levels. The reduced (or lack of) swarming of these mutants is not due to an inability to produce cellular structures required for swarming.

Functional CheY Homologs, but Not Chemotaxis, Contribute to Attachment to Abiotic and Root Surfaces

Given the previously reported role of the polar flagellum in an initial attachment to a surface (about 2 h; Michiels et al., 1991), we next compared CheY homologs for contribution to attachment to abiotic surfaces. We used a wild type Sp7, *ΔcheY1*, *ΔcheY4*, *ΔcheY6*, and *ΔcheY7* strains harboring pHRGFP plasmid (Ramos et al., 2002) to monitor attachment to poly-lysine coated glass slides over a 2-h incubation period. Relative to the wild type, the *ΔcheY1* cells attached better while the Δ*cheY4*, Δ*cheY6*, and to a lesser extent, *ΔcheY7* cells, attached significantly less to abiotic surfaces (**Figures 8A,B**).

A similar pattern of attachment to sterile wheat roots was observed (**Figure 8C**), with the *ΔcheY*1 attaching better to wheat roots within a 2-h incubation compared to the wild type or the other mutant strains.

We also monitored formation of biofilms *in vitro* and detected major differences at 96 h post-inoculation. The *ΔcheY1* strain formed more biofilms relative to the wild type strain, and the *ΔcheY4* and *ΔcheY6* strains formed less biofilm. The *ΔcheY7* mutant did not display any significant defect in biofilm formation relative to the wild type (**Figure 8D**). The data obtained here in abiotic surface and root attachment and biofilm formation are in good agreement and indicate that CheY homologs are required for attachment and biofilm formation. However, the differences between the strains are unrelated to their steady-state swimming bias or their chemotaxis abilities. These results suggest that functional chemotaxis, which is absent in strains lacking CheY4 or CheY7 and present in strains lacking CheY1 and CheY6, is not directly implicated in these behaviors. The results also imply that the control of the polar flagellum rotation by CheY homologs triggers distinct attachment behaviors.

DISCUSSION

Here, we show that the four CheY homologs that regulate the polar flagellum rotational bias in *A. brasilense* and differentially alter chemotaxis and aerotaxis responses have distinct effects on

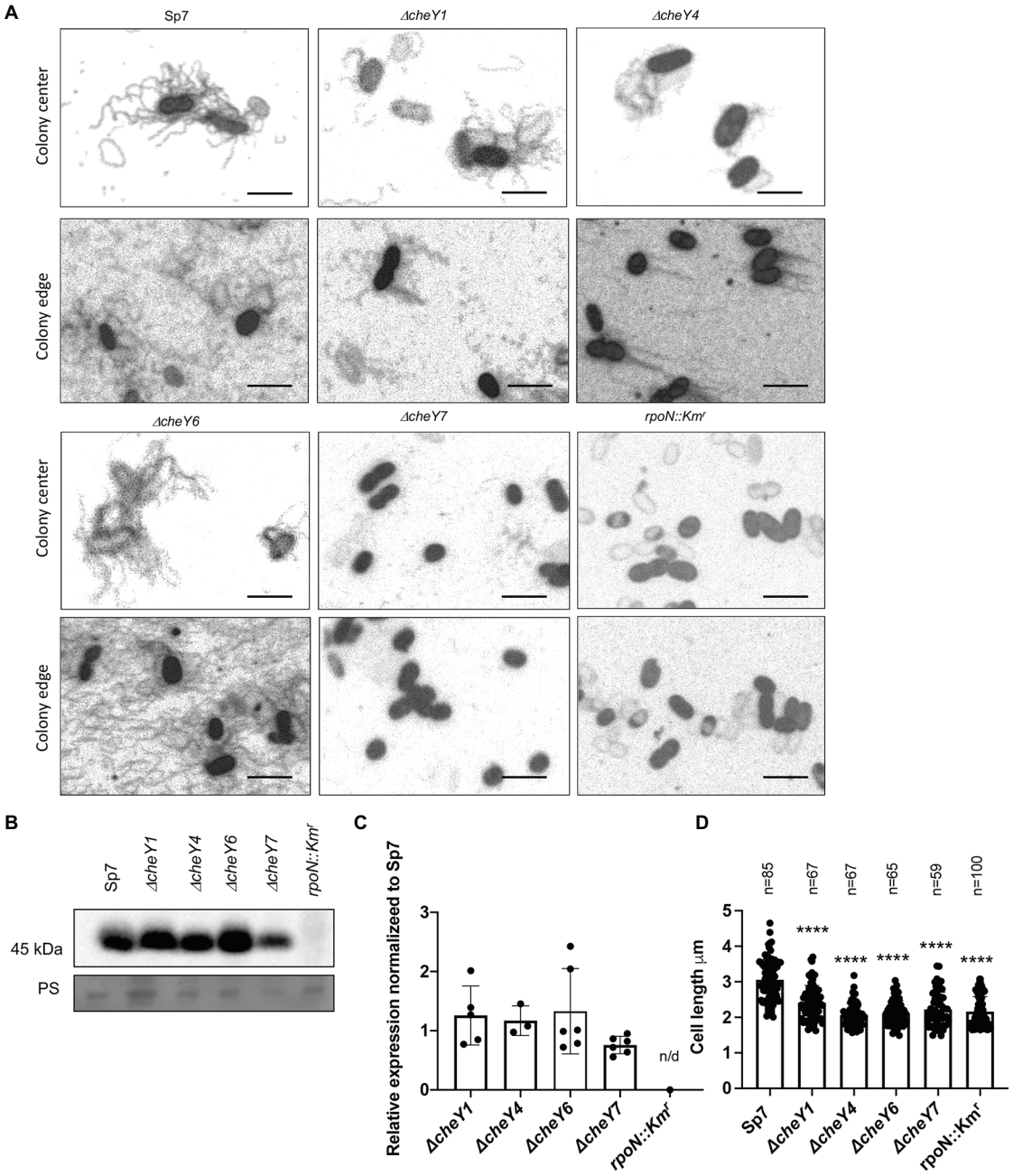

FIGURE 7 | Detection of lateral flagella produced in swarming colonies of *A. brasilense* Sp7 and mutant response regulator strains. **(A)** Representative images of separate cells within and at the edge of a swarming colony. Arrows indicate lateral flagella. **(B)** Western blot analysis with anti-lateral flagellin (1:1,000) polyclonal antisera of whole-cell preparations of *A. brasilense* Sp7, *ΔcheY1*, *ΔcheY4*, *ΔcheY6, ΔcheY7,* and *rpoN::Km^r* mutant strains. Coomassie staining is shown below for the loading control. **(C)** Quantitation of relative lateral flagellin levels normalized to levels in the wild type Sp7 strain. Student *t*-test was used to determine the significance between Sp7 and mutant strains. **(D)** Quantitation of the cell lengths of Sp7, *ΔcheY1*, *ΔcheY4*, *ΔcheY6*, and *ΔcheY7* mutant strains grown under swarming conditions. Student *t*-test was used to determine significance between Sp7 and mutant strains (****$p < 0.005$).

swarming and attachment to surfaces. Specifically, we show that chemotaxis signaling, mediated by the CheY homologs' activity studied here, is required for the ability of colonies to expand within or atop media of varying viscosity, likely in response to gradients generated by cell metabolism during this movement. This is similar to findings reported for the role of chemotaxis in mediating expansion of swarming colonies in gradients in other dually flagellated bacteria such as *Vibrio parahaemolyticus* (Sar et al., 1990), *Vibrio alginolyticus* (Kojima et al., 2007), and *Rhodospirillum centenum* (Jiang et al., 1997). However, this role for chemotaxis in promoting the expansion of swarming colonies is not shared by other species, which increased production of

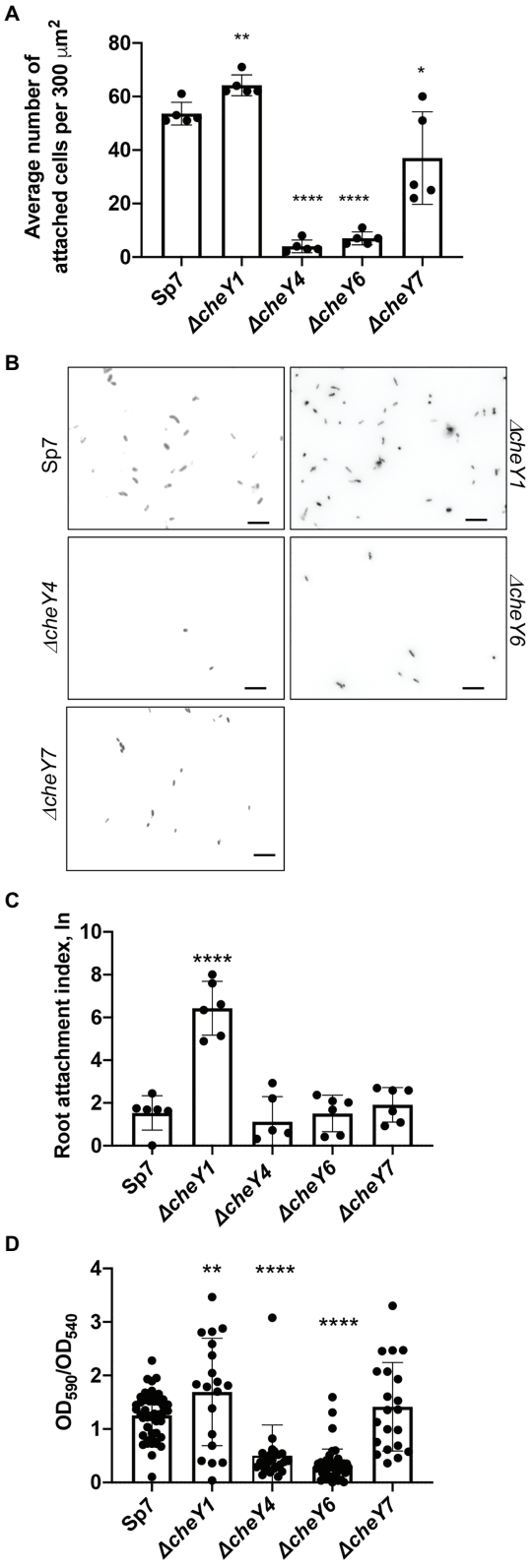

FIGURE 8 | *Azospirillum brasilense* wild type and *cheY* mutant strains attachment to abiotic and biotic surfaces and biofilm formation.

(Continued)

FIGURE 8 | (A) Quantitation of cell attachment of the Sp7, *ΔcheY1*, *ΔcheY4*, *ΔcheY6*, and *ΔcheY7* strains labeled carrying pHRGFP, which constitutively expresses green fluorescent protein (GFP), to glass slides coated with poly-lysine (*$p < 0.05$, **$p < 0.01$, and ****$p < 0.001$). **(B)** Examples of images of the Sp7, *ΔcheY1*, *ΔcheY4*, *ΔcheY6*, and *ΔcheY7* cells attached to poly-lysine coated glass slides. Scale bar is 10 μm. **(C)** Quantitation of cell attachment of the Sp7, *ΔcheY1*, *ΔcheY4*, *ΔcheY6*, and *ΔcheY7* strains carrying pHRGFP, which constitutively expresses GFP, to sterile wheat roots. Student *t*-test was used to determine significance between Sp7 and mutant strains (****$p < 0.005$). **(D)** Quantitative biofilm formation by Sp7, *ΔcheY1*, *ΔcheY4*, *ΔcheY6,* and *ΔcheY7* cells formed in 96 h. Student *t*-test was used to determine significance between Sp7 and mutant strains (**$p < 0.01$ and ****$p < 0.005$).

a single type of flagella during swarming, such as *E. coli* (Burkart et al., 1998) or *Bacillus subtilis* (Kearns and Losick, 2003).

Functional CheYs appear required for the organization of cells in clusters that formed behind the moving edge of a swarming colony in *A. brasilense*. The cell clusters observed in the wild type are reduced or absent in the *cheY* mutant strains. Our data suggest that the formation of these clusters contributes to productive swarming in *A. brasilense* since swarming is diminished or absent in the chemotaxis *cheY* mutants, despite their ability to induce lateral flagella production. However, we recognize that our experimental design was limited and that additional mutants and higher-resolution imaging are needed to conclude on their role during swarming expansion. We note that these clusters could resemble groups of cells, named rafts or packs that have been seen in other bacterial species (Copeland and Weibel, 2009; Partridge and Harshey, 2013). In *E. coli* and *B. subtilis*, these rafts move together, form and reform continuously with collisions leading to realignment of cells along their long axis and the observation of swirling motions (Turner et al., 2010). The role of chemotaxis in mediating cell-to-cell interactions has been previously demonstrated in several motile bacteria, including *A. brasilense* (Bible et al., 2008; Alexandre, 2015), but the exact mechanism(s) are not known. In *E. coli* (Burkart et al., 1998) and other species that use a single type of flagellum for swimming and swarming, such as *B. subtilis* (Kearns and Losick, 2003) and *P. aeruginosa* (Overhage et al., 2008), a basal level of changes in swimming direction (tumble) triggered by chemotaxis signaling is required for proficient swarming, though the tumbling rate is significantly lower than that observed for free-swimming cells (Partridge et al., 2019). This behavior is thought to promote side-by-side cell alignments and coordinated movement of groups of cells within packs as the swarming colony advances (Partridge et al., 2019, 2020). The lateral flagella that power swarming in *A. brasilense* are structurally different from the polar flagellum, and these differences extend to flagellar motors composed of distinct proteins. We have no evidence that the lateral flagella reverse swimming direction during swarming in *A. brasilense* or that the CheY homologs studied here interact with lateral flagella motors. We only have experimental evidence these CheY homologs control the polar flagellum rotational bias (Mukherjee et al., 2019). The polar flagellum is constitutively produced and persists in swarming cells in *A. brasilense* (Hall and Krieg, 1983; Borisov et al., 2009), but its role is unclear. We have not measured motility and

analyzed the motility bias directly from swarming cells. Therefore, how the CheY homologs exert their effects on swarming through control of the polar flagellum rotational bias remains to be elucidated.

The advancing edge of the *A. brasilense* swarming colony suggested it organized as a densely front of cells, similar to the swarm monolayers described in other bacterial species (Partridge and Harshey, 2013). The swarm colony's moving edge appears to include non-motile cells, similar to observations made in other bacterial species (Copeland and Weibel, 2009). The CheY homologs had different effects on this organization: strains lacking CheY6 and CheY7 formed a sharp front of densely packed cells, while strains lacking CheY1 and CheY4 formed a less defined front. These strains have different swimming biases and chemotaxis abilities. These differences could suggest that the role of CheY in this organization is independent from their role during chemotaxis. A similar observation was previously described in *E. coli* (Burkart et al., 1998). Together, the data suggest that CheY homologs are somehow required for motility loss and the formation of an advancing edge of a swarming colony in *A. brasilense*.

Our data also indicate that both CheY4 and CheY7 play a major role in induction of lateral flagella production and initiation of swarming, with CheY7 being essential for this function and CheY4 being required for timely induction of swarming upon surface contact. This is in contrast to the chemotaxis-independent induction of swarmer cell differentiation in *R. centenum* (Jiang et al., 1997) and *V. parahaemolyticus* (Sar et al., 1990), which also possess two types of flagellar systems and somewhat similar to the role of chemotaxis in inducing swarmer cell differentiation in *E. coli* and other species using a single flagellar system for swimming and swarming. *ΔcheY4* and *ΔcheY7* cells are both non-chemotactic suggesting that chemotaxis is required for induction of lateral flagella production and swarming motility. This effect is unlikely to be directly related to the rotational bias of the polar flagellum since CheY6 and CheY4 provoke similar rates of swimming reversals of the polar flagellum but a strain lacking CheY6 shows a greatest defect in swarming differentiation (as observed by changes in cell lengths) compared to a strain lacking CheY4, which swarms at high rates after a prolonged delay. In *A. brasilense*, production of the lateral flagellin (Laf1) which is the major component of the lateral flagella and required for swarming is induced when rotation of the polar flagellum is hindered (Moens et al., 1996). An extracytoplasmic factor (ECF) sigma homolog was recently shown to be at the top of a regulatory cascade that negatively regulates lateral flagellin biogenesis in *A. brasilense* (Dubey et al., 2020). These findings, together, suggest that some form of envelope stress may be a triggering signal for induction of lateral flagella in *A. brasilense*. If this is the case, then our findings suggest that CheY7 and CheY4 play essential roles in this signaling event.

Similar to their role in swarming, our results indicate that the *A. brasilense* CheY homologs, but not chemotaxis, mediate short-term attachment to abiotic surfaces and wheat roots, with these effects leading to similar changes in initial biofilm formation. These effects did not correlate with chemotaxis ability or polar flagellum motor bias. We note that all chemotaxis mutants have lower swimming speed compared to the wild type in the absence of a gradient but they can transiently increase swimming speed in response to attractants, with the exception of a strain lacking CheY1 which is locked at low speeds (Bible et al., 2012; Mukherjee et al., 2016, 2019). A lower swimming speed for this strain would increase its residence time in proximity to surfaces, which could promote enhanced adhesion for this mutant relative to the other strains. Several lines of experimental evidence indicate that chemotaxis signaling regulates non-chemotaxis functions in *A. brasilense*, though the mechanism(s) are not known (Bible et al., 2008; Gullett et al., 2017; Ganusova et al., 2021). It is thus also possible that the *cheY* mutants have different cell surface properties which would modulate their ability to adhere to surfaces.

Collectively, the data obtained here suggest that multiple CheY homologs not only fine tune the rotational bias of flagellar motors and chemotaxis but also promote behaviors that depend on motility such as swarming and attachment to surfaces.

DATA AVAILABILITY STATEMENT

The original contributions presented in the study are included in the article/**Supplementary Material**, further inquiries can be directed to the corresponding author.

AUTHOR CONTRIBUTIONS

EG designed and conducted the experiments, analyzed the data, and wrote the manuscript. LV and TM designed and conducted the experiments, and analyzed the data. GA designed the experiments, analyzed the data, and wrote the manuscript. All authors contributed to the article and approved the submitted version.

FUNDING

This research was supported by a National Science Foundation grant NSF-MCB 1715185 and NSF-MCB 1855066 (to GA). Any opinions, findings, conclusions, or recommendations expressed in this material are those of the authors and do not necessarily reflect the views of the National Science Foundation.

SUPPLEMENTARY MATERIAL

The Supplementary Material for this article can be found online at: https://www.frontiersin.org/articles/10.3389/fmicb.2021.664826/full#supplementary-material

Supplementary Figure 1 | Distribution of the cell sizes of *Azospirillum brasilense* Sp7 grown in the media solidified with 0.2–0.7% (w/vol) agar.

REFERENCES

Alexandre, G. (2015). Chemotaxis control of transient cell aggregation. *J. Bacteriol.* 197, 3230–3237. doi: 10.1128/JB.00121-15

Alexandre, G., Greer, S. E., and Zhulin, I. B. (2000). Energy taxis is the dominant behavior in *Azospirillum brasilense*. *J. Bacteriol.* 182, 6042–6048. doi: 10.1128/JB.182.21.6042-6048.2000

Alexandre, G., Rohr, R., and Bally, R. (1999). A phase variant of *Azospirillum lipoferum* lacks a polar flagellum and constitutively expresses mechanosensing lateral flagella. *Appl. Environ. Microbiol.* 65:4701. doi: 10.1128/AEM.65.10.4701-4704.1999

Alves, L. P., Almeida, A. T., Cruz, L. M., Pedrosa, F. O., de Souza, E. M., Chubatsu, L. S., et al. (2017). A simple and efficient method for poly-3-hydroxybutyrate quantification in diazotrophic bacteria within 5 minutes using flow cytometry. *Br. J. Med. Biol. Res.* 50:e5492. doi: 10.1590/1414-431X20165492

Arruebarrena Di Palma, A., Pereyra, C. M., Moreno Ramirez, L., Xiqui Vázquez, M. L., Baca, B. E., Pereyra, M. A., et al. (2013). Denitrification-derived nitric oxide modulates biofilm formation in *Azospirillum brasilense*. *FEMS Microbiol. Lett.* 338, 77–85. doi: 10.1111/1574-6968.12030

Belyakov, A., Burygin, G., Arbatsky, N., Shashkov, A., Selivanov, N., Matora, L., et al. (2012). Identification of an O-linked repetitive glycan chain of the polar flagellum flagellin of *Azospirillum brasilense* Sp7. *Carbohydr. Res.* 361C, 127–132. doi: 10.1016/j.carres.2012.08.019

Berleman, J. E., and Bauer, C. E. (2005). Involvement of a Che-like signal transduction cascade in regulating cyst cell development in *Rhodospirillum centenum*. *Mol. Microbiol.* 56, 1457–1466. doi: 10.1111/j.1365-2958.2005.04646.x

Bible, A., Russell, M. H., and Alexandre, G. (2012). The *Azospirillum brasilense* Che1 chemotaxis pathway controls swimming velocity, which affects transient cell-to-cell clumping. *J. Bacteriol.* 194, 3343–3355. doi: 10.1128/JB.00310-12

Bible, A. N., Stephens, B. B., Ortega, D. R., Xie, Z., and Alexandre, G. (2008). Function of a chemotaxis-like signal transduction pathway in modulating motility, cell clumping, and cell length in the alphaproteobacterium *Azospirillum brasilense*. *J. Bacteriol.* 190:6365. doi: 10.1128/JB.00734-08

Borisov, I. V., Schelud'ko, A. V., Petrova, L. P., and Katsy, E. I. (2009). Changes in *Azospirillum brasilense* motility and the effect of wheat seedling exudates. *Microbiol. Res.* 164, 578–587. doi: 10.1016/j.micres.2007.07.003

Burkart, M., Toguchi, A., and Harshey, R. M. (1998). The chemotaxis system, but not chemotaxis, is essential for swarming motility in *Escherichia coli*. *Proc. Natl. Acad. Sci. U. S. A.* 95, 2568–2573. doi: 10.1073/pnas.95.5.2568

Chawla, R., Gupta, R., Lele, T. P., and Lele, P. P. (2020). A Skeptic's guide to bacterial mechanosensing. *J. Mol. Biol.* 432, 523–533. doi: 10.1016/j.jmb.2019.09.004

Copeland, M., and Weibel, D. (2009). Bacterial swarming: a model system for studying dynamic self-assembly. *Soft Matter* 5, 1174–1187. doi: 10.1039/b812146j

Croes, C., Moens, S., Bastelaere, E., Vanderleyden, J., and Michiels, K. (1993). Polar flagellum mediates *Azospirillum brasilense* adsorption to wheat roots. *Microbiology* 139, 2261–2269. doi: 10.1099/00221287-139-9-2261

de Oliveira Pinheiro, R., Boddey, L. H., James, E. K., Sprent, J. I., and Boddey, R. M. (2002). Adsorption and anchoring of *Azospirillum* strains to roots of wheat seedlings. *Plant Soil* 246, 151–166. doi: 10.1023/A:1020645203084

Dubey, A. P., Pandey, P., Singh, V. S., Mishra, M. N., Singh, S., Mishra, R., et al. (2020). An ECF41 family σ factor controls motility and biogenesis of lateral flagella in *Azospirillum brasilense* sp245. *J. Bacteriol.* 202, e00231–e00220. doi: 10.1128/JB.00231-20

Edwards, A. N., Siuti, P., Bible, A. N., Alexandre, G., Retterer, S. T., Doktycz, M. J., et al. (2011). Characterization of cell surface and extracellular matrix remodeling of *Azospirillum brasilense* chemotaxis-like 1 signal transduction pathway mutants by atomic force microscopy. *FEMS Microbiol. Lett.* 314, 131–139. doi: 10.1111/j.1574-6968.2010.02156.x

Ferré, A., De La Mora, J., Ballado, T., Camarena, L., and Dreyfus, G. (2004). Biochemical study of multiple CheY response regulators of the chemotactic pathway of *Rhodobacter sphaeroides*. *J. Bacteriol.* 186, 5172–5177. doi: 10.1128/JB.186.15.5172-5177.2004

Figurski, D. H., and Helinski, D. R. (1979). Replication of an origin-containing derivative of plasmid RK2 dependent on a plasmid function provided in trans. *Proc. Natl. Acad. Sci. U. S. A.* 76, 1648–1652. doi: 10.1073/pnas.76.4.1648

Ganusova, E. E., Vo, L. T., Abraham, P. E., O'Neal Yoder, L., Hettich, R. L., and Alexandre, G. (2021). The *Azospirillum brasilense* core chemotaxis proteins CheA1 and CheA4 link chemotaxis signaling with nitrogen metabolism. *mSystems* 6, e01354–e01420. doi: 10.1128/mSystems.01354-20

Gordon, V. D., and Wang, L. (2019). Bacterial mechanosensing: the force will be with you, always. *J. Cell Sci.* 132:jcs227694. doi: 10.1242/jcs.227694

Greer-Phillips, S. E., Stephens, B. B., and Alexandre, G. (2004). An energy taxis transducer promotes root colonization by *Azospirillum brasilense*. *J. Bacteriol.* 186, 6595–6604. doi: 10.1128/JB.186.19.6595-6604.2004

Gullett, J. M., Bible, A., and Alexandre, G. (2017). Distinct domains of CheA confer unique functions in chemotaxis and cell length in *Azospirillum brasilense* Sp7. *J. Bacteriol.* 199, e00189–e00117. doi: 10.1128/JB.00189-17

Gunsolus, I. L., Hu, D., Mihai, C., Lohse, S. E., Lee, C. S., Torelli, M. D., et al. (2014). Facile method to stain the bacterial cell surface for super-resolution fluorescence microscopy. *Analyst* 139, 3174–3178. doi: 10.1039/C4AN00574K

Guttenplan, S. B., and Kearns, D. B. (2013). Regulation of flagellar motility during biofilm formation. *FEMS Microbiol. Rev.* 37, 849–871. doi: 10.1111/1574-6976.12018

Hall, P. G., and Krieg, N. R. (1983). Swarming of *Azospirillum brasilense* on solid media. *Can. J. Microbiol.* 29, 1592–1594. doi: 10.1139/m83-243

Hallez, R., Letesson, J.-J., Vandenhaute, J., and De Bolle, X. (2007). Gateway-based destination vectors for functional analyses of bacterial ORFeomes: application to the Min system in *Brucella abortus*. *Appl. Environ. Microbiol.* 73, 1375–1379. doi: 10.1128/AEM.01873-06

Hauwaerts, D., Alexandre, G., Das, S. K., Vanderleyden, J., and Zhulin, I. B. (2002). A major chemotaxis gene cluster in *Azospirillum brasilense* and relationships between chemotaxis operons in α-proteobacteria. *FEMS Microbiol. Lett.* 208, 61–67. doi: 10.1111/j.1574-6968.2002.tb11061.x

Huang, Z., Wang, Y.-H., Zhu, H.-Z., Andrianova, E. P., Jiang, C.-Y., Li, D., et al. (2019). Cross talk between chemosensory pathways that modulate chemotaxis and biofilm formation. *mBio* 10, e02876–e02818. doi: 10.1128/mBio.02876-18

Hyakutake, A., Homma, M., Austin, M. J., Boin, M. A., Häse, C. C., and Kawagishi, I. (2005). Only one of the five CheY homologs in *Vibrio cholerae* directly switches flagellar rotation. *J. Bacteriol.* 187, 8403–8410. doi: 10.1128/JB.187.24.8403-8410.2005

Jiang, Z. Y., Gest, H., and Bauer, C. E. (1997). Chemosensory and photosensory perception in purple photosynthetic bacteria utilize common signal transduction components. *J. Bacteriol.* 179, 5720–5727. doi: 10.1128/JB.179.18.5720-5727.1997

Kearns, D. B., and Losick, R. (2003). Swarming motility in undomesticated *Bacillus subtilis*. *Mol. Microbiol.* 49, 581–590. doi: 10.1046/j.1365-2958.2003.03584.x

Keen, N. T., Tamaki, S., Kobayashi, D., and Trollinger, D. (1988). Improved broad-host-range plasmids for DNA cloning in gram-negative bacteria. *Gene* 70, 191–197. doi: 10.1016/0378-1119(88)90117-5

Kim, W., Killam, T., Sood, V., and Surette, M. G. (2003). Swarm-cell differentiation in *Salmonella enterica* serovar typhimurium results in elevated resistance to multiple antibiotics. *J. Bacteriol.* 185, 3111–3117. doi: 10.1128/JB.185.10.3111-3117.2003

Kojima, M., Kubo, R., Yakushi, T., Homma, M., and Kawagishi, I. (2007). The bidirectional polar and unidirectional lateral flagellar motors of *Vibrio alginolyticus* are controlled by a single CheY species. *Mol. Microbiol.* 64, 57–67. doi: 10.1111/j.1365-2958.2007.05623.x

Laganenka, L., Colin, R., and Sourjik, V. (2016). Chemotaxis towards autoinducer 2 mediates autoaggregation in *Escherichia coli*. *Nat. Commun.* 7:12984. doi: 10.1038/ncomms12984

Levit, M. N., and Stock, J. B. (2002). Receptor methylation controls the magnitude of stimulus-response coupling in bacterial chemotaxis. *J. Biol. Chem.* 277, 36760–36765. doi: 10.1074/jbc.M204325200

Little, K., Austerman, J., Zheng, J., and Gibbs, K. A. (2019). Cell shape and population migration are distinct steps of *Proteus mirabilis* swarming that are decoupled on high-percentage agar. *J. Bacteriol.* 201, e00726–e00718. doi: 10.1128/JB.00726-18

Michiels, K. W., Croes, C. L., and Vanderleyden, J. (1991). Two different modes of attachment of *Azospirillum brasilense* Sp7 to wheat roots. *Microbiology* 137, 2241–2246. doi: 10.1099/00221287-137-9-2241

Milcamps, A., Van Dommelen, A., Stigter, J., Vanderleyden, J., and de Bruijn, F. J. (1996). The *Azospirillum brasilense rpoN* gene is involved in nitrogen fixation,

nitrate assimilation, ammonium uptake, and flagellar biosynthesis. *Can. J. Microbiol.* 42, 467–478. doi: 10.1139/m96-064

Miller, L. D., Yost, C. K., Hynes, M. F., and Alexandre, G. (2007). The major chemotaxis gene cluster of *Rhizobium leguminosarum* bv. viciae is essential for competitive nodulation. *Mol. Microbiol.* 63, 348–362. doi: 10.1111/j.1365-2958.2006.05515.x

Moens, S., Michiels, K., Keijers, V., Van Leuven, F., and Vanderleyden, J. (1995a). Cloning, sequencing, and phenotypic analysis of *laf1*, encoding the flagellin of the lateral flagella of *Azospirillum brasilense* Sp7. *J. Bacteriol.* 177, 5419–5426. doi: 10.1128/jb.177.19.5419-5426.1995

Moens, S., Michiels, K., and Vanderleyden, J. (1995b). Glycosylation of the flagellin of the polar flagellum of *Azospirillum brasilense*, a Gram-negative nitrogen-fixing bacterium. *Microbiology* 141, 2651–2657. doi: 10.1099/13500872-141-10-2651

Moens, S., Schloter, M., and Vanderleyden, J. (1996). Expression of the structural gene, *laf1*, encoding the flagellin of the lateral flagella in *Azospirillum brasilense* Sp7. *J. Bacteriol.* 178, 5017–5019. doi: 10.1128/jb.178.16.5017-5019.1996

Mukherjee, T., Elmas, M., Vo, L., Alexiades, V., Hong, T., and Alexandre, G. (2019). Multiple CheY homologs control swimming reversals and transient pauses in *Azospirillum brasilense*. *Biophys. J.* 116, 1527–1537. doi: 10.1016/j.bpj.2019.03.006

Mukherjee, T., Kumar, D., Burriss, N., Xie, Z., and Alexandre, G. (2016). *Azospirillum brasilense* chemotaxis depends on two signaling pathways regulating distinct motility parameters. *J. Bacteriol.* 198, 1764–1772. doi: 10.1128/JB.00020-16

O'Neal, L., Gullett, J. M., Aksenova, A., Hubler, A., Briegel, A., Ortega, D., et al. (2019). Distinct chemotaxis protein paralogs assemble into chemoreceptor signaling arrays to coordinate signaling output. *mBio* 10, e01757–e01719. doi: 10.1128/mBio.01757-19

O'Neal, L., Vo, L., and Alexandre, G. (2020). Specific root exudate compounds sensed by dedicated chemoreceptors shape *Azospirillum brasilense* chemotaxis in the rhizosphere. *Appl. Environ. Microbiol.* 86, e01026–e01020. doi: 10.1128/AEM.01026-20

Overhage, J., Bains, M., Brazas, M. D., and Hancock, R. E. W. (2008). Swarming of *Pseudomonas aeruginosa* is a complex adaptation leading to increased production of virulence factors and antibiotic resistance. *J. Bacteriol.* 190:2671. doi: 10.1128/JB.01659-07

Partridge, J. D., and Harshey, R. M. (2013). Swarming: flexible roaming plans. *J. Bacteriol.* 195, 909–918. doi: 10.1128/JB.02063-12

Partridge, J. D., Nhu, N. T. Q., Dufour, Y. S., and Harshey, R. M. (2019). *Escherichia coli* remodels the chemotaxis pathway for swarming. *mBio* 10, e00316–e00319. doi: 10.1128/mBio.00316-19

Partridge, J. D., Nhu, N. T. Q., Dufour, Y. S., and Harshey, R. M. (2020). Tumble suppression is a conserved feature of swarming motility. *mBio* 11, e01189–e01120. doi: 10.1128/mBio.01189-20

Pitzer, J. E., Sultan, S. Z., Hayakawa, Y., Hobbs, G., Miller, M. R., and Motaleb, M. A. (2011). Analysis of the *Borrelia burgdorferi* cyclic-di-GMP-binding protein PlzA reveals a role in motility and virulence. *Infect. Immun.* 79, 1815–1825. doi: 10.1128/IAI.00075-11

Porter, S. L., Wadhams, G. H., Martin, A. C., Byles, E. D., Lancaster, D. E., and Armitage, J. P. (2006). The CheYs of *Rhodobacter sphaeroides*. *J. Biol. Chem.* 281, 32694–32704. doi: 10.1074/jbc.M606016200

Ramos, H. J. O., Roncato-Maccari, L. D. B., Souza, E. M., Soares-Ramos, J. R. L., Hungria, M., and Pedrosa, F. O. (2002). Monitoring *Azospirillum*-wheat interactions using the *gfp* and *gusA* genes constitutively expressed from a new broad-host range vector. *J. Biotechnol.* 97, 243–252. doi: 10.1016/S0168-1656(02)00108-6

Sar, N., McCarter, L., Simon, M., and Silverman, M. (1990). Chemotactic control of the two flagellar systems of *Vibrio parahaemolyticus*. *J. Bacteriol.* 172, 334–341. doi: 10.1128/JB.172.1.334-341.1990

Schmitt, R. (2002). Sinorhizobial chemotaxis: a departure from the enterobacterial paradigm. *Microbiology* 148, 627–631. doi: 10.1099/00221287-148-3-627

Simon, R., Priefer, U., and Pühler, A. (1983). A broad host range mobilization system for in vivo genetic engineering: transposon mutagenesis in gram negative bacteria. *Bio/Technology* 1, 784–791. doi: 10.1038/nbt1183-784

Skerker, J. M., and Laub, M. T. (2004). Cell-cycle progression and the generation of asymmetry in *Caulobacter crescentus*. *Nat. Rev. Microbiol.* 2, 325–337. doi: 10.1038/nrmicro864

Steenhoudt, O., and Vanderleyden, J. (2000). *Azospirillum*, a free-living nitrogen-fixing bacterium closely associated with grasses: genetic, biochemical and ecological aspects. *FEMS Microbiol. Rev.* 24, 487–506. doi: 10.1111/j.1574-6976.2000.tb00552.x

Stephens, B. B., Loar, S. N., and Alexandre, G. (2006). Role of CheB and CheR in the complex chemotactic and aerotactic pathway of *Azospirillum brasilense*. *J. Bacteriol.* 188, 4759–4768. doi: 10.1128/JB.00267-06

Turner, L., Zhang, R., Darnton, N. C., and Berg, H. C. (2010). Visualization of flagella during bacterial swarming. *J. Bacteriol.* 192:3259. doi: 10.1128/JB.00083-10

Viruega-Góngora, V. I., Acatitla-Jácome, I. S., Reyes-Carmona, S. R., Baca, B. E., and Ramírez-Mata, A. (2020). Spatio-temporal formation of biofilms and extracellular matrix analysis in *Azospirillum brasilense*. *FEMS Microbiol. Lett.* 367:fnaa037. doi: 10.1093/femsle/fnaa037

Wu, L., Cui, Y., Hong, Y., and Chen, S. (2011). A CheR/CheB fusion protein is involved in cyst cell development and chemotaxis in *Azospirillum brasilense* Sp7. *Microbiol. Res.* 166, 606–617. doi: 10.1016/j.micres.2010.12.001

Wu, Z., He, R., Zhang, R., and Yuan, J. (2020). Swarming motility without flagellar motor switching by reversal of swimming direction in *E. coli*. *Front. Microbiol.* 11:1042. doi: 10.3389/fmicb.2020.01042

Zamudio, M., and Bastarrachea, F. (1994). Adhesiveness and root hair deformation capacity of Azospirillum strains for wheat seedlings. *Soil Biol. Biochem.* 26, 791–797. doi: 10.1016/0038-0717(94)90275-5

Zhulin, I. B., and Armitage, J. P. (1992). The role of taxis in the ecology of *Azospirillum*. *Symbiosis* 13, 199–206.

Zhulin, I. B., and Armitage, J. P. (1993). Motility, chemokinesis, and methylation-independent chemotaxis in *Azospirillum brasilense*. *J. Bacteriol.* 175, 952–958. doi: 10.1128/JB.175.4.952-958.1993

Zhulin, I. B., Bespalov, V. A., Johnson, M. S., and Taylor, B. L. (1996). Oxygen taxis and proton motive force in *Azospirillum brasilense*. *J. Bacteriol.* 178, 5199–5204. doi: 10.1128/JB.178.17.5199-5204.1996

Conflict of Interest: The authors declare that the research was conducted in the absence of any commercial or financial relationships that could be considered as a potential conflict of interest.

frontiers in Microbiology

ORIGINAL RESEARCH
published: 01 June 2021
doi: 10.3389/fmicb.2021.668892

The Stand-Alone PilZ-Domain Protein MotL Specifically Regulates the Activity of the Secondary Lateral Flagellar System in *Shewanella putrefaciens*

*Anna Pecina[1], Meike Schwan[1], Vitan Blagotinsek[2], Tim Rick[1], Patrick Klüber[1], Tabea Leonhard[1], Gert Bange[2] and Kai M. Thormann[1]**

[1] Department of Microbiology and Molecular Biology, Justus-Liebig-Universität Gießen, Giessen, Germany, [2] Department of Chemistry, SYNMIKRO Research Center, Philipps-University Marburg, Marburg, Germany

OPEN ACCESS

Edited by:
Seiji Kojima, Nagoya University, Japan

Reviewed by:
Keiji Murakami, Tokushima University, Japan
Daniel B. Kearns, Indiana University Bloomington, United States

***Correspondence:**
Kai M. Thormann
kai.thormann@mikro.bio.uni-giessen.de

Specialty section:
This article was submitted to Microbial Physiology and Metabolism, a section of the journal Frontiers in Microbiology

Received: *17 February 2021*
Accepted: *19 April 2021*
Published: *01 June 2021*

Citation:
Pecina A, Schwan M, Blagotinsek V, Rick T, Klüber P, Leonhard T, Bange G and Thormann KM (2021) The Stand-Alone PilZ-Domain Protein MotL Specifically Regulates the Activity of the Secondary Lateral Flagellar System in Shewanella putrefaciens. Front. Microbiol. 12:668892. doi: 10.3389/fmicb.2021.668892

A number of bacterial species control the function of the flagellar motor in response to the levels of the secondary messenger c-di-GMP, which is often mediated by c-di-GMP-binding proteins that act as molecular brakes or clutches to slow the motor rotation. The gammaproteobacterium *Shewanella putrefaciens* possesses two distinct flagellar systems, the primary single polar flagellum and a secondary system with one to five lateral flagellar filaments. Here, we identified a protein, MotL, which specifically regulates the activity of the lateral, but not the polar, flagellar motors in response to the c-di-GMP levels. MotL only consists of a single PilZ domain binding c-di-GMP, which is crucial for its function. Deletion and overproduction analyses revealed that MotL slows down the lateral flagella at elevated levels of c-di-GMP, and may speed up the lateral flagellar-mediated movement at low c-di-GMP concentrations. *In vitro* interaction studies hint at an interaction of MotL with the C-ring of the lateral flagellar motors. This study shows a differential c-di-GMP-dependent regulation of the two flagellar systems in a single species, and implicates that PilZ domain-only proteins can also act as molecular regulators to control the flagella-mediated motility in bacteria.

Keywords: flagella, c-di-GMP, flagellar motor, YcgR, *Shewanella*, PilZ domain, lateral flagella

INTRODUCTION

Numerous species of bacteria in nature are motile by flagella, which allow them to actively move toward more favorable environments. Flagella are long helical proteinaceous filaments, which extend from the cell's surface and are rotated by the membrane-embedded flagellar motor. The flagellar motor is an intricate nanomachine, which is powered by ion gradients. Most flagella depend on H^+ gradients, but numerous bacteria employ Na^+-driven motors (Berg, 2003; Terashima et al., 2017; Nakamura and Minamino, 2019). Torque is created between the stators, transmembrane protein complexes attached to the cell wall, which act as ion-specific channels, and the motor's C-ring within the cytoplasm. The stators are formed by two proteins, commonly referred to as MotA and MotB in H^+-dependent motors and PomA and PomB in Na^+-dependent motors (Kojima, 2015; Lai et al., 2020).

The C-ring is located at the cytoplasmic end of the flagellum and consists of a number of copies of the subunits FliG, located close to the membrane adjacent to the stators, as well as FliM and FliN (Francis et al., 1992, 1994; Zhao et al., 1996). Ion translocation through the stators is thought to result in conformational changes, which are then translated into the rotational movement of the C-ring by electrostatic interaction of the cytoplasmic parts of the stators' A-subunits with the C-terminal domain of FliG (for a cartoon of the flagellar apparatus, see **Figure 1A**). Most flagellar motors are bi-directional and allow counterclockwise and clockwise rotations, which are regulated by one or more associated chemotaxis systems to allow a directed movement by means of a so-called random walk (Sourjik and Wingreen, 2012; Bi and Sourjik, 2018).

A fully assembled flagellum consists of numerous proteins, among which the flagellins, which are the major building blocks of the filament, may add up to several 10,000 copies (Nakamura and Minamino, 2019). Depending on the species and motor, the flagellar rotation rate can reach up to more than 100 Hz, and each rotation is accompanied by a massive influx of the corresponding coupling ion (Meister et al., 1987). Thus, the assembly and operation of a flagellum put a substantial burden on the cell's metabolism, and therefore, under some conditions, such as during biofilm formation or shortage of nutrients, a fast rotation of the motor may not be advantageous. Accordingly, flagella formation and activity are highly regulated, and many bacterial species have developed appropriate systems that, in addition to chemotaxis systems, enable the cells to control the activity of the flagellar motor (Subramanian and Kearns, 2019). Recent studies have demonstrated that some species may even choose to eject major parts of the flagellum when nutrients are lacking (Ferreira et al., 2019; Kaplan et al., 2019; Zhu et al., 2019; Zhuang et al., 2020).

One means to control the activity of the flagellar motors is through the proteins that act as brakes or clutches to slow down the flagellar rotation in response to levels of the secondary messenger molecule c-di-GMP (Brown et al., 2011; Subramanian and Kearns, 2019). Such motor-affecting proteins have been identified in several species, e.g., YcgR in *Escherichia coli* and *Salmonella enterica* (Boehm et al., 2010; Fang and Gomelsky, 2010; Paul et al., 2010), MotI (DgrA) in *Bacillus subtilis* (Chen et al., 2012; Gao et al., 2013; Subramanian et al., 2017), and FlgZ in *Pseudomonas* species (Martinez-Granero et al., 2014; Baker et al., 2016; Wirebrand et al., 2018). All these proteins are characterized by a so-called PilZ domain, which is responsible for binding the effector molecule c-di-GMP upon which the protein directly interacts with the components of the flagellar motor to slow down the rotation. These motor-effector proteins likely function by interfering with normal rotor-stator interactions. In *E. coli*, interaction of YcgR has been mapped to the C-ring proteins FliG and FliM as well as to the stator protein MotA (Boehm et al., 2010; Fang and Gomelsky, 2010; Paul et al., 2010; Hou et al., 2020). MotA has also been demonstrated to be a binding target of *B. subtilis* MotI/DgrA, and similarly for *Pseudomonas* aeruginosa FlgZ, an interaction with an orthologous stator protein, MotC, has been shown (Chen et al., 2012; Baker et al., 2016; Subramanian et al., 2017).

The occurrence of c-di-GMP-dependent motor-regulating proteins in several different and somewhat unrelated bacterial species suggests that they represent a common means for flagellar motor control. However, such functional YcgR-like motor-effector proteins have not yet been described for species belonging to the polarly flagellated gammaproteobacteria of the genus *Vibrio*, *Shewanella*, and others. *Vibrio cholerae* and *Vibrio alginolyticus* possess homologs to YcgR, named PlzD (Pratt et al., 2007; Kojima et al., 2019). *Vc*PlzD has been shown to specifically bind c-di-GMP and the corresponding binding site was identified by crystallization (Benach et al., 2007; Pratt et al., 2007). Overproduction of both *Vc*PlzD and *Va*PlzD in the corresponding species resulted in a negative effect on motility, however, this effect occurred independently of c-di-GMP binding (Pratt et al., 2007; Kojima et al., 2019). So far, it remains unclear by which mechanism *Vibrio* PlzD affects the flagella-mediated motility.

In addition, in *Shewanella* sp., c-di-GMP levels regulate the flagella-mediated motility. In *Shewanella oneidensis* and *S. putrefaciens*, the multidomain transmembrane phosphodiesterase PdeB strongly affects the flagella-mediated swimming in response to the nutrient conditions. Cells lacking *pdeB* exhibit a higher overall c-di-GMP concentration and a drastically decreased spreading through soft agar (Chao et al., 2013; Rossmann et al., 2019). *S. putrefaciens* possesses two distinct flagellar systems, the main Na^+-dependent polar system, which mediates the main propulsion during free swimming, and screw thread motility through structured environments which is controlled by the chemotaxis system (Bubendorfer et al., 2012, 2014; Kühn et al., 2017, 2018). In addition, depending on the media conditions, a secondary lateral flagellar system can be formed, which is powered by H^+ ions and assists in the navigation and spreading through structured environments (Bubendorfer et al., 2012, 2014). We found that, although being localized to the flagellated cell pole, PdeB regulates the lateral flagellar system. Part of this effect is explained by a significant decrease in the lateral flagellar gene expression, but it remains unclear if and how an elevated c-di-GMP level affects both flagellar systems also at the posttranscriptional level (Rossmann et al., 2019). We therefore set out to identify the potential c-di-GMP-dependent factors that regulate the motor activity. Here, we identified and characterized a PilZ-domain protein, MotL, which lacks the N-terminal domain present in YcgR, MotI, or FlgZ, and specifically acts on the lateral flagella in dependence of c-di-GMP.

RESULTS

Identification of a Flagellar Motor Effector Protein in *Shewanella putrefaciens*

To identify the potential c-di-GMP-dependent effectors in *Shewanella putrefaciens*, we started with a genomic screen for homologs of the previously characterized flagellar regulators. The c-di-GMP-dependent functional regulators of the bacterial

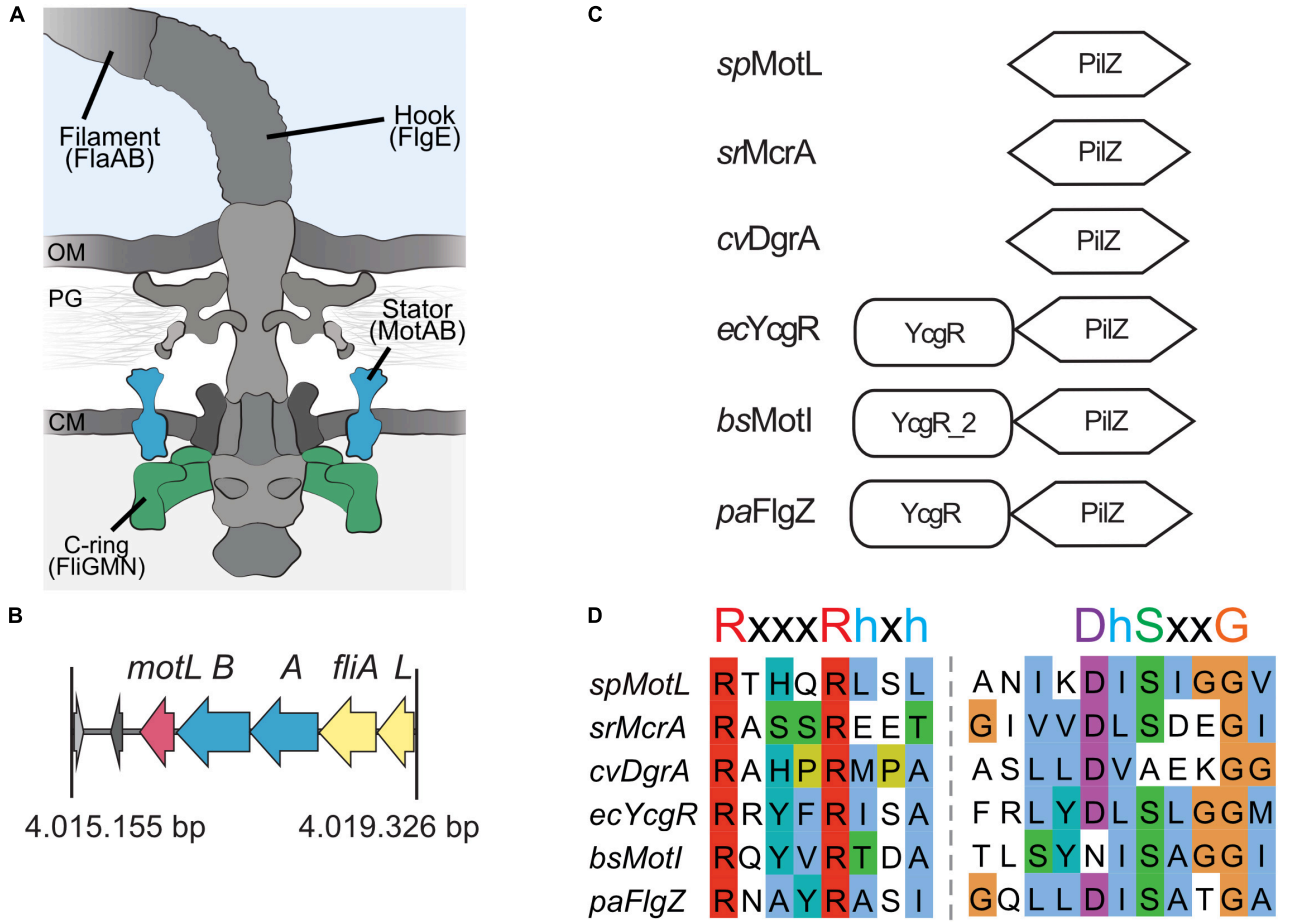

FIGURE 1 | MotL is a putative c-di-GMP-binding PilZ domain-only protein. **(A)** Cartoon of the flagellar motor with the major components (filament, hook, and basal body containing a type III export machinery and the flagellar motor). Torque to drive rotation of the *Shewanella putrefaciens* lateral flagella is created between the stator subunits (proteins MotA and MotB, blue) and the cytoplasmic C-ring (proteins FliG, FliM, and FliN, green). OM, outer membrane; PG, peptidoglycan; CM, cytoplasmic membrane. **(B)** Organization of the *motL* gene region in *S. putrefaciens*, motL is immediately following downstream of the genes *motA* and *motB* that encode the stator subunits. **(C)** Domain organization of PilZ proteins implicated in the regulation of flagella-mediated motility. See text for details. **(D)** Alignment of the PilZ domains of the proteins given in panel **(C)**. The residues critical for c-di-GMP binding are marked above the sequences.

flagellar motors studied so far, *E. coli* YcgR, *Pseudomonas* FlgZ, and *B. subtilis* MotI, all possess a characteristic c-di-GMP-binding PilZ domain and an N-terminal domain referred to as the YcgR domain (Cheang et al., 2019). In *S. putrefaciens,* five proteins are annotated as putative PilZ domain-containing proteins (Sputcn32_2813, Sputcn32_2815, Sputcn32_2212, Sputcn32_1553, and Sputcn32_3446). Apart from possessing a putative PilZ domain, none of these proteins shows noticeable similarities to YcgR, FlgZ, or MotI at the protein level, and so far, none of them has been studied in any detail. Notably, the gene Sputcn32_3446 is located directly downstream of the secondary flagellar gene cluster, immediately following *motA* and *motB*, which encodes the proton-dependent stator of the lateral flagellar motor. We therefore hypothesized that this protein may somehow be involved in the formation and/or activity of the lateral and, potentially, the polar flagella.

Sputcn32_3446, annotated as a PilZ domain, is located 34 bp downstream of *motB* and transcribed in the same direction (**Figure 1B**). The gene is 435 bp in length and encodes a protein of 144 aa with an estimated molecular mass of 16.6 kDa and a theoretical pI of 5.94. The protein is thus much smaller than YcgR (244 aa), FlgZ (263), and MotI (217 aa) as an N-terminal YcgR domain is not present (**Figure 1C**). The predicted c-di-GMP-binding motifs (**RxxxRhxh, DhSxxG**; Galperin and Chou, 2020) are fully conserved (**Figure 1D**). The protein is conserved in a number *Shewanella* species that possess dual flagellar systems, and the gene it is always located downstream of *motB*. Potential homologs of Sputcn32_3446 are also present in some species of *Aeromonas* and *Vibrio*, but absent from the well-characterized *V. parahaemolyticus* and *V. alginolyticus*, which also possess two distinct flagellar systems. We henceforth referred to the protein as MotL, relating to its location within the lateral flagellar gene operon and its differences to YcgR, FlgZ, and MotI with respect to the protein sequence and absence of further domains.

MotL Binds c-di-GMP

The presence of a potential c-di-GMP-binding site in MotL suggested that MotL function may be governed by c-di-GMP. We therefore determined the ability of MotL to bind c-di-GMP *in vitro*. To this end, we aimed at the overproduction of MotL and a corresponding variant bearing alanine substitutions within all conserved residues in the predicted c-di-GMP binding site (*n*o *c*-di-GMP-*b*inding; MotL$_{NCB}$). However, MotL or MotL$_{NCB}$ overproduction and purification was only possible when a fusion protein was added to the proteins' N-termini. For the direct purification from *S. putrefaciens,* we therefore used a variant with a sfGFP fused to the MotL N-terminus (sfGFP-MotL and sfGFP-MotL$_{NCB}$) which was produced from a plasmid. This fusion protein could be stably produced and purified (**Figure 2A**), fully complemented a *motL* deletion mutant (see **Figure 3A** and **Supplementary Figure 1**) and, therefore, also allowed later studies on swimming behavior and localization. MotL and MotL$_{NCB}$ fusion proteins were purified directly from *S. putrefaciens,* and the binding of radioactively labeled c-di-GMP to both variants was determined. However, under these conditions, no significant c-di-GMP binding to MotL was observed. We hypothesized that c-di-GMP may already be bound to MotL and, therefore, both protein variants were purified from a strain also producing the phosphodiesterase (PDE) PdeH, which has previously been shown to effectively lower the c-di-GMP levels in *S. oneidensis* (Thormann et al., 2006). Produced under these conditions, robust c-di-GMP binding to MotL could be observed. In contrast, the MotL$_{NCB}$ variant was unable to bind this second messenger (**Figure 2B**). Based on these findings, we hypothesized that MotL likely functions in a c-di-GMP-dependent fashion.

MotL Exclusively Affects Swimming Mediated by the Lateral Flagella

To determine if MotL has an effect on swimming, we deleted the corresponding gene from the chromosome. The resultant mutant cells were then tested for the ability to spread through soft agar as a measure for the ability of flagella-mediated motility (**Figure 3**).

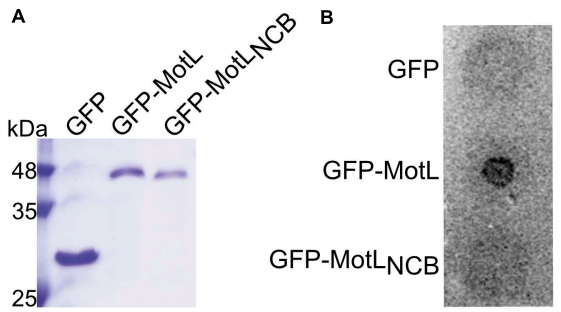

FIGURE 2 | MotL is a c-di-GMP-binding protein. **(A)** Purification of MotL. Shown is a Coomassie-stained SDS gel after separation of His-tagged purified GFP, GFP-MotL, and GFP-MotL$_{NCB}$. **(B)** MotL binds c-di-GMP. Purified protein was applied to a membrane as indicated and exposed to radioactively labeled c-di-GMP. Only the MotL with the predicted binding site is able to bind and retain c-di-GMP.

Loss of *motL* had no significant effect on the spreading of the wild-type cells. However, as swimming motility of *S. putrefaciens* through soft agar is synchronously mediated by both the main polar and secondary lateral flagella (Bubendorfer et al., 2012, 2014), potential effects on only one of the systems may be masked. We therefore introduced the *motL* deletion into strains in which the flagellin-encoding genes of the polar ($\Delta flaAB_1$) or lateral ($\Delta flaAB_2$) systems were deleted, so that these strains only produce one type of functional flagella. Spreading of cells with only the polar flagellum through soft agar was not affected in the absence of MotL. In contrast, cells that only possessed the lateral flagella showed a significant increase in spreading, and this effect could be complemented by the reintegration of *motL* or *sfgfp-motL* into its native gene locus (**Figure 3A**). To determine if the increase in spreading may be caused by an increase in the number of lateral flagella, we introduced the *motL* deletion into a strain in which the lateral flagellar hook structures–as a proxy for an established lateral flagellar system–can be labeled by the coupling of a fluorescent dye to the major hook protein FlgE$_2$ (FlgE$_{2\,T242C}$). Visualization and quantification of the number of cells with lateral hooks by fluorescent microscopy revealed that the population of flagellated cells slightly decreased in the absence of MotL from about 33 to about 26% (**Figure 3C**). Thus, the enhanced spreading in soft agar in Δ*motL* mutants is not due to an increase in flagellation. As previous studies showed that the lateral flagellar system is not controlled by the chemotaxis system of *S. putrefaciens* (Bubendorfer et al., 2012, 2014), an effect of MotL on navigation in cells motile by only lateral flagella was also ruled out.

As the deletion of MotL had a positive effect on the spreading of the *S. putrefaciens* cells with lateral flagellar systems, we hypothesized that overproduction may have the opposite effect. We therefore produced (sfGFP)MotL from a plasmid and determined its effect on spreading (**Figure 3B**). As expected, overproduction of MotL negatively affected the spreading of the wild-type (−15%) and lateral flagella-only cells (−27%), while cells with only the polar flagella exhibited a minor decrease (−4%) in spreading. We have previously observed that the addition of the inducer anhydrotetracycline hydrochloride (AHT) has a negative effect on the flagella-mediated motility due to a yet unknown mechanism (Brenzinger et al., 2018), which may account for the reduction in the spreading seen for the latter strain. We therefore concluded that MotL specifically acts as a regulator on the lateral flagella function.

MotL Controls the Activity of the Lateral Flagella in Response to c-di-GMP

The gain of the lateral flagella-mediated spreading on soft agar upon loss of MotL and the observed c-di-GMP binding by this protein strongly suggested that MotL acts as a c-di-GMP-dependent regulator, such as a brake or clutch, on the lateral flagellar motors. To further investigate this, (GFP)MotL or (GFP)MotL$_{NCB}$ were ectopically produced in a *S. putrefaciens* strain only capable of forming the lateral, but not the polar, flagella ($\Delta flaAB_1$). To determine the direct effect of MotL on the

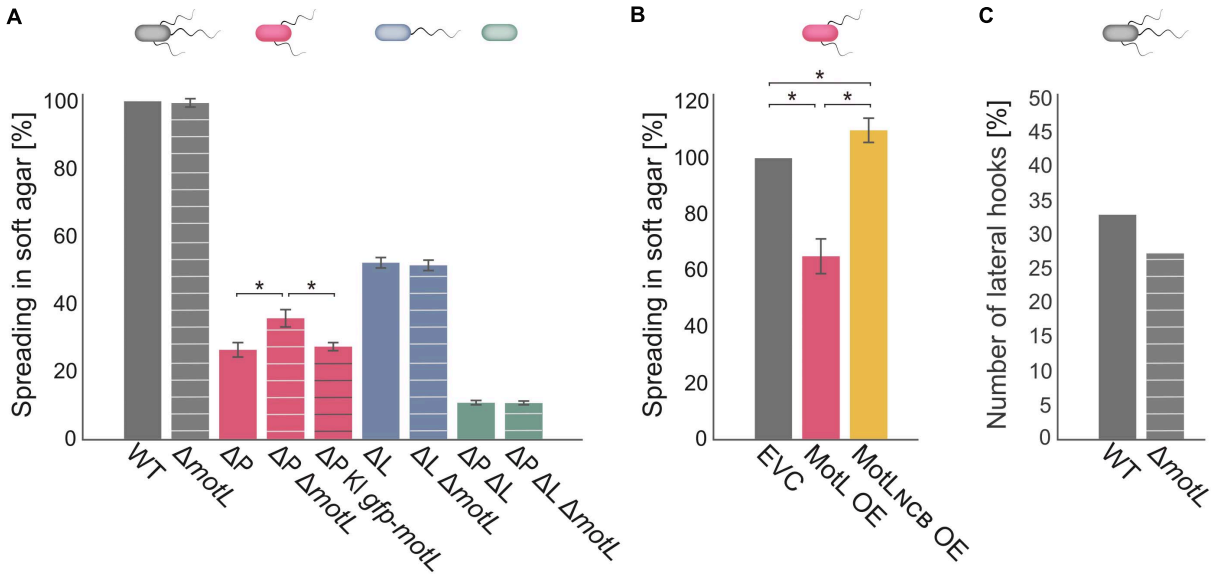

FIGURE 3 | MotL affects the *S. putrefaciens* lateral, but not the polar, flagella. **(A)** Flagella-mediated spreading through soft agar after deletion (and complementation) of *motL*. The corresponding background strains had both the polar and lateral flagella (gray), only one each [ΔP lacking the polar filament (red); ΔL lacking the lateral filament (blue) or no flagella (green) as indicated by the cartoon cells above the bars]. The white cross bands indicate the strains in which *motL* was deleted, black cross bars indicate the strain bearing *gfp-motL*. **(B)** Lateral flagella-mediated spreading upon ectopic overproduction (OE) of GFP-MotL and the corresponding mutant not binding c-di-GMP (GFP-MotL$_{NCB}$). EVC, empty-vector control. **(A,B)** are the results of three independent experiments. The bars with the asterisks indicate significant differences according to ANOVA. **(C)** Effect of *motL* deletion on the presence of lateral hooks as a proxy for the number of functional lateral flagella in cells growing exponentially in the LB medium. See text and methods for the hook staining procedure. The numbers are deduced from observing 430 cells for WT and 431 for *motL* deletion in four independent experiments. The difference is not significant according to the *Pearson's Chi-squared test with Yates' continuity correction*.

performance of the lateral motor, we measured the speed of free-swimming cells upon MotL overproduction by cell tracking using light microscopy (**Figure 4**). The velocities of a strain harboring the vector control (only producing sfGFP) showed a wide speed distribution from about 10 to about 60 $\mu m\ s^{-1}$ with most cells exhibiting a speed between 10 and 40 $\mu m\ s^{-1}$ (**Figure 4A** and **Supplementary Figure 3A**). For the cells overproducing MotL, the subpopulation of the slow swimming cells (in particular, between 10 and 30 $\mu m\ s^{-1}$) increased, and the average speed dropped significantly from 24 to 19 $\mu m\ s^{-1}$. In contrast, the speed distribution of cells producing the MotL$_{NCB}$ variant was highly similar to that of the control strain, suggesting that c-di-GMP binding is required for MotL function.

In the next set of experiments, we therefore determined the effect of high or low c-di-GMP levels on the role of MotL in regulating the lateral flagella function (**Figure 4B**). To this end, we produced MotL together with the phosphodiesterase PdeH from *E. coli* or the diguanylate cyclase DgcA (VCA0956) of *Vibrio cholera*. Both proteins have previously been shown to decrease or increase the intracellular level of c-di-GMP in the closely related *S. oneidensis* (Thormann et al., 2006). To first rule out that the effect of the different c-di-GMP levels on swimming by lateral flagella was mainly due to the effects and mechanisms not mediated by MotL (such as differences in the lateral flagellar gene expression), *pdeH* or *dgcA* were first expressed in the laterally-only flagellated *S. putrefaciens* cells, in which *motL* was deleted, and the spreading of the strains in soft agar was determined (**Supplementary Figure 3C**). Production of PdeH resulted in an increase in spreading of about 30% while DgcA production lowered the spreading to about 80%. In addition, the swimming speeds of the cells were recorded. In contrast to the spreading phenotype, expression of *dgcA* had almost no effect on the swimming speed of the cells compared to those of the cells bearing the empty vector control (**Supplementary Figures 2A,B**). Expression of *pdeH* resulted in a slight shift toward faster cells, but the increase was rather minor (**Supplementary Figures 3A,B**). The results show that production of a diguanylate cyclase (DGC) or a PDE has a notable effect on spreading in soft agar while the swimming speed itself is affected rather little. Thus, other factors than MotL also contribute to the lateral flagella-mediated swimming in dependence of c-di-GMP levels, which is particularly evident in structured environments such as soft agar but less so in the performance of the lateral motors.

In a strain co-producing DgcA and (sfGFP)MotL (high levels of c-di-GMP), the average speed and speed distribution of the cells was similar to that of the cells producing sfGFP–MotL alone (24 versus 26 $\mu m\ s^{-1}$; **Figure 4B**; **Supplementary Figures 3A,B**), while spreading through soft agar was decreased by about 30% (**Supplementary Figure 2C**). This strongly suggested that under the conditions applied (exponential planktonic growth in complex media), a further increase of the c-di-GMP levels within the cells is not relevant for the activity of MotL for free swimming. Thus, the observed diminished spreading through

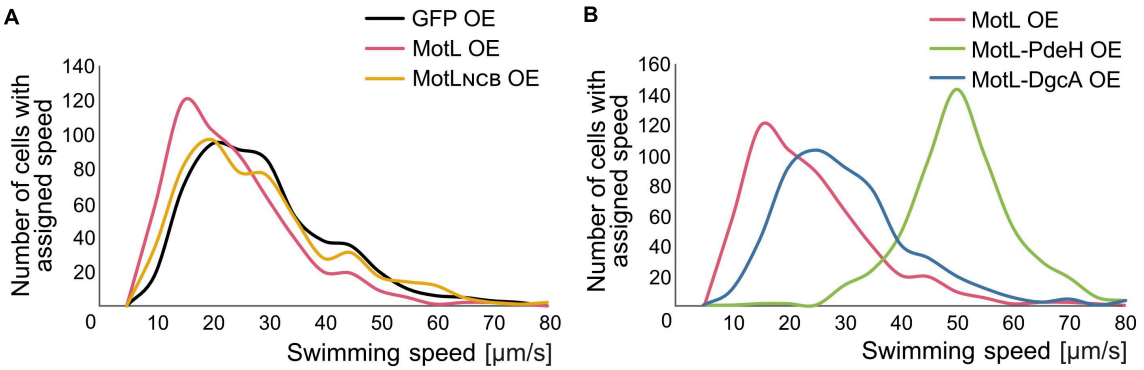

FIGURE 4 | MotL affects the swimming speed mediated by the lateral flagella in a c-di-GMP-dependent fashion. **(A)** Effect of an OE of MotL (red), $MotL_{NCB}$, and GFP (control) on the swimming speed of a strain only possessing the lateral flagella (ΔP). **(B)** Effect of an OE of MotL alone (red) or in concert with the phosphodiesterase PdeH (green) or the diguanylate cyclase DgcA (blue). For both **(A,B)** the swimming speeds of 591 cells per strain were analyzed. See also **Supplementary Figure 3** for the statistical analysis.

soft agar caused by a higher c-di-GMP level is unlikely to be directly mediated by MotL. In sharp contrast, the velocity distribution of the cells at low c-di-GMP levels (MotL co-produced with PdeH) was drastically shifted toward a higher speed (**Figure 4B** and **Supplementary Figures 3A,B**) with an average speed of 50 $\mu m\ s^{-1}$. In addition, the spreading in soft agar doubled compared to that of the strain expressing MotL alone (**Supplementary Figure 2C**). Taken together, the data strongly indicate that MotL specifically regulates the activity of the lateral flagellar in response to low c-di-GMP levels.

MotL Does Not Affect the Lateral Motor Function via the FliL Levels

In the following, we aimed at understanding the mechanism by which FliL mediates its function of the lateral flagellar motor. Previously, another stand-alone PilZ-domain protein, DgrA, had been demonstrated to affect the flagella-mediated swimming in *Caulobacter crescentus* (Christen et al., 2007). In this study, the authors hypothesized that DgrA acts via the flagellar motor protein FliL, as upon the overproduction of DgrA, FliL protein levels were significantly decreased. To determine if MotL functions by a similar mechanism, we quantified the effect of MotL levels on those of the lateral flagella $FliL_2$. To allow the detection of $FliL_2$, the corresponding gene was replaced at its native locus by a mutant version encoding a C-terminal FLAG-tag. Subsequent analysis showed that the tagged version of MotL was stably produced and fully supported the secondary flagella-mediated spreading in soft agar. Absence or overproduction of MotL did not affect the $FliL_2$ levels (**Figure 5A**), suggesting that MotL has a different mode of function as a flagellar regulator.

MotL May Directly Interact With the Components of the Lateral Flagellar Motors

The *in vivo* function of MotL as a regulator of the lateral flagella function suggested that MotL, as other PilZ-domain flagellar brakes or clutches, directly or indirectly interacts with the components of the lateral flagellar motors. We therefore performed localization studies by fluorescence microscopy to determine whether fluorescently tagged MotL may interact with the flagellar basal bodies or with the freely diffusing MotAB stator units not engaged in the flagellar motor.

To visualize the general localization, we used the strain harboring the sfGFP-MotL-encoding hybrid gene in the chromosome replacing native *motL*. Co-localization with the lateral flagellar components was performed in strains in which the C-ring protein $FliM_2$ or the stator component MotB were additionally labeled by mCherry. In addition, the fused MotL protein was overproduced from a plasmid, and/or the cellular levels were increased by the (co-)production of the phosphodiesterase PdeH or the diguanylate cyclase DgcA. However, under no conditions a distinct localization of sfGFP–MotL occurred, and the protein, if present, was always diffusively localized within the cytoplasm (**Supplementary Figure 4**).

In the next step, we performed studies on the direct interactions between MotL and components of the flagellar motor. To this end, we conducted a bacterial two-hybrid (BACTH) analysis for the potential interactions between MotL and $MotL_{NCB}$ on one side, and the C-ring components $FliG_2$, $FliM_2$, and $FliN_2$ and the stator-forming subunits MotA and MotB on the other side (see cartoon of the flagellar motor in **Figure 1A**). To this end, all above-mentioned proteins were produced in an appropriate *E. coli* strain at high or low levels as N- or C-terminal fusion to the T18 and T25 fragments of an adenylate cyclase from *Bordetella pertussis*, which are non-functional when separate. However, interaction of two fusion proteins leading to a close proximity of the T18 and T25 fragments results in the formation of an active adenylate cyclase and raising the cAMP levels, which can be readily visualized on an appropriate media. In this assay, MotL and $MotL_{NCB}$ did not exhibit any interactions with any of the C-ring or stator components (data not shown).

As a third approach to determine a potential interaction of MotL with the flagellar motor, we performed *in vitro* pull-down assays with purified MotL and components of the C-ring of the

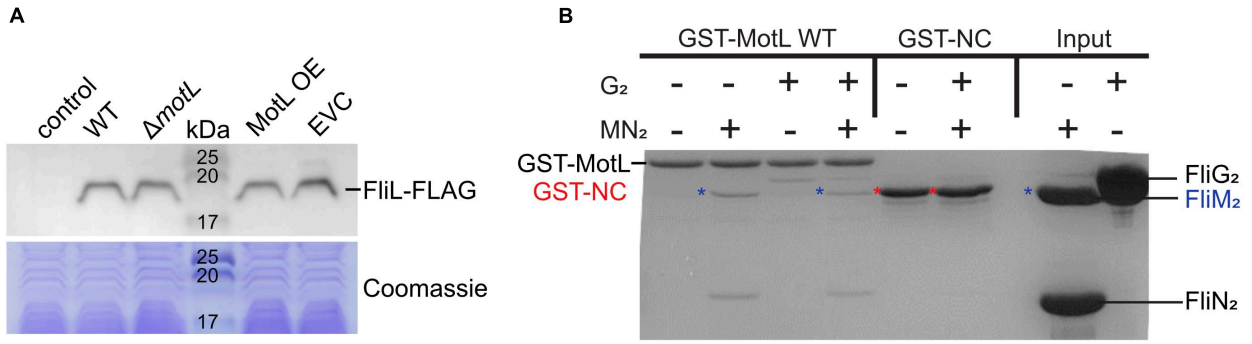

FIGURE 5 | Effect of MotL on FliL levels and MotL interaction with the flagellar C-ring. **(A)** Western blot to determine the levels of (FLAG-tagged) FliL in dependence of MotL levels (upper panel) with the Coomassie-stained polyacrylamide gel as loading control in the panel below. Neither deletion nor overproduction of MotL affects FliL levels. **(B)** Coomassie-stained gel of a GST pulldown with an immobilized MotL protein against the components of the lateral flagellar C-ring (proteins $FliG_2$, $FliM_2$, and $FliN_2$). GST alone (GST-NC) served as the negative control. The position of the proteins in the gel is indicated at the sides of the gel, in addition, blue asterisks indicate the position of FliM2 and red asterisks indicate those of GST-NC.

lateral flagella (**Figure 5B**). To this end, MotL was produced and purified as an N-terminal glutathione-*S*-transferase (GST) fusion to be used as bait. Under the conditions tested, purified $FliG_2$ as well as $FliM_2$ and $FliN_2$ showed binding to MotL, while GST did not display any binding to these C-ring components, which may potentially hint at a functional interaction between MotL and the flagellar motor.

DISCUSSION

For several bacterial species, c-di-GMP has been shown to affect the flagella-mediated motility at the level of motor function by c-di-GMP-binding regulator proteins. Here, we show that in *S. putrefaciens,* such a regulator protein specifically tunes the activity of the lateral, but not the polar, flagellar system. This regulator, now referred to as MotL, basically consists of a single PilZ domain, which has previously been shown to be involved in c-di-GMP binding and, which, accordingly occurs in a number of c-di-GMP-dependent effector proteins (Amikam and Galperin, 2006; Cheang et al., 2019).

We showed that MotL binds c-di-GMP and that binding of this second messenger affects the MotL function, suggesting that rising levels of c-di-GMP decrease the flagella rotation. However, when MotL was produced together with the DGC DgcA, the effect on the swimming speed provided by the lateral flagella was surprisingly small. As we have previously shown that DgcA is an active DGC in *Shewanella* (Thormann et al., 2006) and spreading in soft agar was noticeably reduced upon DgcA production (**Supplementary Figures 2C,3C**), we assume that DgcA actually raises the level of cellular c-di-GMP. This suggests that the level of c-di-GMP in *S. putrefaciens* under the conditions used for the swimming assays was already sufficiently high to achieve the maximum effect of MotL on the flagellar motors. This hypothesis was corroborated by the finding that c-di-GMP binding to MotL *in vitro* was only achieved when the protein was purified from an *S. putrefaciens* strain in which the PDE PdeH was additionally produced. The effect of DgcA production on spreading in soft agar may thus be rather due to other c-di-GMP-mediated processes such as the downregulation of the lateral flagella and activation of adhesion factors (Rossmann et al., 2019). In contrast, we found a huge effect of MotL on the lateral motors at a low c-di-GMP concentration, where the cells moved at an even higher speed as under the same conditions in the absence of MotL and exhibited a massive increase in spreading. This finding suggests that MotL may not only slow down flagellar rotation but may also speed up swimming mediated by the lateral flagella in response to lower c-di-GMP levels. Generally, marine bacteria, among them, *S. putrefaciens*, have been reported to accelerate to a higher speed in the presence of various amino acids (Barbara and Mitchell, 2003). This process, referred to as chemokinesis, enhances the chemotactic precision as shown for *V. alginolyticus* (Son et al., 2016). The underlying mechanism is yet unknown, and it is also unclear if another protein component is required, e.g., for rotor-stator stabilization, and if MotL may play a role in this process.

The mechanism by which MotL affects the lateral flagella motors remains elusive so far. Several of the c-di-GMP-dependent flagellar motor effectors have been studied in more detail, namely YcgR of *E. coli* and *Salmonella*, MotI (formerly YpfA or DgrA) in *B. subtilis*, and FlgZ in *Pseudomonas*. MotI and FlgZ are thought to predominantly or even exclusively function through interactions with stator units to inhibit proper rotor-stator interactions. MotI (YpfA) was shown to interact with the stator subunit MotA in the BACTH analysis, by the co-purification of MotA with an ectopically overproduced MotI (YpfA), identification and analysis of suppressor mutants in MotA, and localization pattern of fluorescently labeled MotI (Chen et al., 2012; Subramanian et al., 2017). Similarly, *P. aeruginosa* FlgZ was demonstrated to interact with the stator subunit MotC by the BACTH analysis and co-precipitation experiments (Baker et al., 2016). MotCD is the stator that is employed by *P. aeruginosa* during swarming motility. No interaction was found with any of the tested C-ring components and, notably, also none with the subunits of the second stator system MotAB, which inhibits swarming and rather promotes

free swimming motility (Doyle et al., 2004; Toutain et al., 2005). Also, fluorescence microscopy on the fluorescently labeled FlgZ showed the expected localization to the single polar flagellar motor in swarming cells. Thus, in *P. aeruginosa,* FlgZ regulates swarming motility in dependence of c-di-GMP levels likely by specifically uncoupling the MotCD stator from the motor.

In contrast, flagellar motor regulation by YcgR of *E. coli* and *Salmonella* does involve both the flagellar stators as well as the flagellar C-ring. Förster resonance transfer studies revealed a c-di-GMP-dependent interaction with the MotAB stator and suppressor mutants in MotA were isolated (Boehm et al., 2010). In addition, FliG and FliM could be co-isolated with overproduced YcgR (Fang and Gomelsky, 2010; Paul et al., 2010), and BACTH studies suggested a direct interaction of YcgR with FliG and FliM (Fang and Gomelsky, 2010). Furthermore, mutations in FliG and FliM affected YcgR binding and inhibition of motility, and the localization of YcgR–GFP as punctae was shown to depend on the presence of FliG and FliM (Paul et al., 2010). Notably, the general interaction of YcgR with the flagellar C-ring appears to be independent of c-di-GMP binding (Fang and Gomelsky, 2010; Paul et al., 2010). Accordingly, a recent study provides evidence that YcgR functions at the interface between MotA and FliG to slow down the flagellar rotation (Hou et al., 2020). In addition, to act as the uncoupler of flagellar rotor and stator, YcgR has been proposed to also regulate chemotaxis by affecting the counterclockwise-clockwise bias of the flagellar motor (Girgis et al., 2007; Fang and Gomelsky, 2010; Paul et al., 2010).

Notably, in contrast to YcgR and other motor regulating proteins, MotL consists of only a PilZ domain. Studies on crystal structures of YcgR-like proteins, MotI, PlzD, and PP4397, showed that for these proteins, c-di-GMP binding involves both the PilZ as well as the N-terminal YcgR domains. This leads to an extensive conformational change, which is assumed to enable the functional interaction (Benach et al., 2007; Ko et al., 2010; Subramanian et al., 2017). Accordingly, the N-terminal domain of YcgR has been suggested to be important for the specificity of YcgR–FliG interactions (Fang and Gomelsky, 2010). However, as MotL does not possess such an N-terminal YcgR domain, interaction with its target protein has to occur in a different fashion. Single PilZ-domain proteins, such as MotL, are thought to serve as c-di-GMP adaptors to control target systems (Christen et al., 2007; Cheang et al., 2019). Even in the absence of a YcgR domain, our *in vitro* assays hint at an interaction of *S. putrefaciens* MotL and FliG, FliM, and FliN of the lateral flagella (see **Figure 1A**), and we thus suggest that MotL functions include an interaction with the C-ring of the lateral flagellar motors, e.g., by directly or indirectly altering the rotor-stator interactions. Although we were unable, so far, to demonstrate the *in vitro* or *in vivo* interactions of MotL and the MotAB stator, we cannot rule out the possibility that the regulatory MotL function includes a (transient) binding to MotA or MotB, e.g., to weaken or to strengthen the rotor-stator interactions. Further studies are required to elucidate if MotL acts on the flagellar motor directly via FliG and/or the MotAB stators upon c-di-GMP binding and if this involved further factors. A direct effect of MotL on chemotaxis is rather unlikely, as previous studies have indicated that the lateral flagellar motors of *S. putrefaciens* are not responding to the chemotaxis system (Bubendorfer et al., 2012, 2014). However, as the lateral flagella affect the turning angles of the cells during the reorientation events (Bubendorfer et al., 2014), an indirect effect on cell navigation is conceivable.

In addition to MotL, other PilZ domain-only proteins have been implicated in the regulation of the flagella-mediated motility (see **Figure 1C**). The single PilZ domain protein DgrA was shown to be a c-di-GMP-dependent negative regulator of the flagella-mediated motility in *C. crescentus* (Christen et al., 2007), although the overall homology to the PilZ domains of other flagellar regulators is rather small. The mechanism by which DgrA exerts this control remains obscure so far, but it is suggested to occur via the levels of the motor protein FliL, which we have shown to be not the case for MotL. In addition, also in *Sinorhizobium meliloti*, a PilZ domain-only protein, McrA, has been demonstrated to negatively affect swimming in dependence of c-di-GMP binding, however, also for McrA, the mechanism is still unsolved (Schäper et al., 2016). Thus, MotL/DgrA/McrA-like flagellar motor regulators may be common among bacteria but further studies are required to determine their exact underlying mechanism.

MATERIALS AND METHODS

Bacterial Strains, Growth Conditions, and Media

Bacterial strains used in this study are summarized in **Supplementary Table 1**. *Shewanella putrefaciens* CN-32 (CN-32) strains were cultivated at 30°C in LB, and *E. coli* strains were cultured at 37°C in LB. When appropriate, media were supplemented with 50 μg ml^{-1} of kanamycin, 40 ng ml^{-1} of anhydrotetracyclin, 10% (w/v) sucrose, or 1.5% (w/v) agar. Soft agar plates were prepared with LB and 0.3% (w/v) agar, and when necessary, 50 μg ml^{-1} of kanamycin and 40 ng ml^{-1} of anhydrotetracyclin was added. *E. coli* WM3064 cultures were supplemented with 2,6-diamino-pimelic acid (DAP) to a final concentration of 300 μM.

Strain and Vector Constructions

Bacterial strains and plasmids used in this study are listed in **Supplementary Tables 1 2**. Construction of Plasmids was performed using the method of Gibson assembly (Gibson et al., 2009). The corresponding oligonucleotides (Sigma-Aldrich, Taufkirchen, Germany) used for cloning are listed in **Supplementary Table 3**. All kits for preparation and purification of nucleic acids (VWR International GmbH, Darmstadt, Germany) and enzymes (Fermentas, St. Leon-Rot, Germany) were used according to the standard manufacturers' protocols. In-frame deletions or chromosomal integration of fusions in *S. putrefaciens* CN-32 were generated using the suicide vector pNTPS-138-R6K as previously described (Lassak et al., 2010). Plasmids were transferred into *S. putrefaciens* cells via conjugation using *E. coli* WM3064 as a donor. To generate markerless in-frame deletions, 500–700 bp fragments flanking the target gene were amplified and fused to create a deletion

leaving only eight codons of the 5′- and 3′-termini of the corresponding gene. To complement the deletion mutant, full-length *motL* was reinserted into its native chromosomal position. To generate a c-di-GMP-insensitive version of MotL, the highly conserved c-di-GMP-binding residues in the PilZ domain (R29A; R33A; D73A; S75A; and G78A) were substituted by alanine, and the resulting protein was named $MotL_{NCB}$ (for *n*o *c*-di-GMP-*b*inding). For N-terminal fluorescent fusions the genes of *motL* (or $motL_{NCB}$) and *mcherry* (or *sfgfp*) with a flexible GSGS linker-encoding sequence between these genes were re-integrated into the appropriate deletion strains. In order to overproduce a fluorescent version of MotL (or $MotL_{NCB}$), the vector pBTOK (Rossmann et al., 2015) with the same GSGS linker between the protein and fluorescent tags was used.

Fluorescence Microscopy

Strains were cultivated overnight in the LB medium and sub cultured the next day until they reached the exponential growth phase (OD_{600} = 0.2–0.3). Then, 5 μl of culture were spotted on an agarose pad [PBS buffer solified with 1% (w/v) agarose]. Fluorescence images were acquired using a Leica DMI 6000 B inverse microscope (Leica, Wetzlar, Germany) equipped with an SCMOS camera (Visitron Systems, Puchheim, Germany) and a HC PL APO 100×/1.4 oil PH3 objective. Image processing and analysis was carried out using the ImageJ-based Fiji tool (Schindelin et al., 2012).

Hook Stain

Fluorescent staining of lateral hook structures ($FlgE_2$–Cys) (Schuhmacher et al., 2015) were prepared as previously described (Guttenplan et al., 2013; Rossmann et al., 2015) using Alexa Fluor 488-maleimide (Molecular Probes, Life Technologies) or iFluor 568-maleimide (AAT Bioquest) for staining.

Motility Assays

Determination of Swimming Speed

Cells of CN-32 strains from overnight cultures were sub inoculated in 10 ml of LB with an OD_{600} of 0.05. After reaching the exponential growth phase (OD_{600} = 0.2–0.3), a 100 μl aliquot was placed under a coverslip fixed by four droplets of silicone (baysilone, VWR International GmbH, Darmstadt, Germany) to generate a space of 1–2 mm width. Movies of 120 frames were taken at room temperature with a Leica DMI 6000 B inverse microscope (Leica, Wetzlar, Germany) equipped with an SCMOS camera (Visitron Systems, Puchheim, Germany) and a HCX PL APO 100×/1.4 objective. The speed of at least 500 cells per strain was quantified using the MTrackJ plugin of Fiji (Meijering et al., 2012). Significance was tested using ANOVA (p = 0.05) in R version 3.0.1.

Spreading on Soft-Agar Plates

Spreading ability in semi-solid environments was analyzed by placing 4 μl of an exponentially grown planktonic culture on soft agar plates [LB supplemented with 0.3% (w/v) agar and, if applicable, 50 μg ml^{-1} of kanamycin and 40 ng ml^{-1} of anhydrotetracyclin) followed by an incubation period of 24 h at room temperature. Strains that were to be directly compared were always placed on the same plate. Plates were scanned for documentation using an Epson V700 Photo Scanner.

Western Blotting

Production and stability of proteins fused to a fluorophore were determined by immunoblot analysis. Protein lysates were prepared from exponentially growing cultures and uniformly adjusted to an OD_{600} of 10. Protein separation and immunoblot detection were carried out as previously described (Bubendorfer et al., 2012; Binnenkade et al., 2014) using polyclonal antibodies raised against the FLAG-tag (Sigma-Aldrich/Merck, Darmstadt, Germany). Signal detection was carried out using the SuperSignal® West Pico Chemiluminescent Substrate (Thermo Scientific, Schwerte, Germany), and was documented using a FUSION-SL chemiluminescence imager (Peqlab, Erlangen, Germany).

In vitro Interaction Studies on MotL and the Flagellar C-Ring

Protein Purification

The protein constructs of interest (with either His or GST tags) were overproduced in *E. coli* BL21 (DE3) competent cells. Cell cultures were grown in the LB medium at 30°C overnight, and shaken at 180 rpm. 1% (w/v) lactose monohydrate was used for induction. Cells were harvested, lysed by microfluidizer (M110-L, Microfluidics), and centrifuged to pellet cell debris. The supernatant was then loaded onto a GE Healthcare HisTrapFF affinity column (for His-tagged proteins) or a GSTrap affinity column (for GST-tagged proteins). For the His-tagged proteins, the lysis and wash buffer contained 20 mM HEPES pH 8.0, 250 mM NaCl, 20 mM KCl, 20 mM $MgCl_2$, and 40 mM imidazole, while the imidazole concentration in the elution buffer was increased to 500 mM. For the GST-tagged proteins, the lysis and wash buffer contained 20 mM HEPES pH 7.5, 200 mM NaCl, 20 mM KCl, 20 mM $MgCl_2$, and the elution buffer additionally contained 50 mM *Tris*-HCl pH 8.0 and 20 mM of L-glutathione. After elution, the protein was purified by size exclusion chromatography (SEC) using an S200 Sepharose column and GE Lifesciences ÄKTA Prime and Purifier systems. After purification, the proteins were concentrated using the Amicon Ultra-15 spin concentrators (10 kDa cutoff point) and flash-frozen to be used in *in vitro* GST pulldown assays.

In vitro GST Pulldown Assays

The assays were performed using spin columns from the company MobiTec. After assembly of the columns, 500 μL of GST-pulldown buffer (20 mM HEPES pH 7.5, 200 mM NaCl, 20 mM KCl, 20 mM $MgCl_2$, and 0.6 μM Tween20) was added into each column, and then 30 μl of resuspended bead slurry was pipetted in (GST-Sepharose beads). The resulting suspension was centrifuged for 1 min at 4,000 rpm to wash the beads, which were then resuspended in 500 μL of the GST-pulldown buffer. The beads were exposed to 1 nmol of a GST-tagged protein, incubated with the protein on a rotation machine for 15 min and centrifuged under the same conditions as above. The interaction partner protein was then added (10 nmol), and incubation period on the rotation machine was carried out for 30 min. The sample

was centrifuged again and then washed three times with 500 µl of the GST-pulldown buffer. The elution was carried out with 40 µl of the GSH elution buffer (containing 50 mM *Tris*-HCl pH 8.0 and 20 mM L-glutathione). The samples were then analyzed by the SDS-PAGE gel separation and staining.

Bacterial Two-Hybrid Assays

To determine the potential interaction between MotL and proteins of the lateral flagellar motor, we used a bacterial two-hybrid (BACTH) system (Euromedex) essentially as previously described (Karimova et al., 1998, 2005). The proteins of interest were genetically fused N- and C-terminally to the T25 and T18 fragments of the adenylate cyclase catalytic domain from *B. pertussis*. If an *in vivo* interaction of the fusion proteins occurs, the two adenylate cyclase fragments T18 and T25 will come into a sufficiently close proximity to become active and produce cAMP. The according hybrid genes were assembled in the expression plasmids pKT25, pKNT25, pUT18, and pUT18C. Appropriate plasmid pairs were co-transformed in *E. coli* BTH101, which lacks adenylate cyclase activity. The cells were grown and plated on LB_{AmpKm} plates containing isopropyl β-*D*-1-thiogalactopyranoside (IPTG; 0.5 mM) for induction of protein production and 5-bromo-4-chloro-3-indolyl β-*D*-galactopyranoside (X-Gal; 40 µg ml^{-1}) and for simple detection of adenylate cyclase activity. The plates were incubated for 48 h at 30°C, and protein interaction was scored by the blue coloration of the corresponding colonies. The empty plasmids were used as a negative control while the plasmid pair pKT25-ZIP and pUT18C-ZIP served as a positive control, and both were present on any assay plate.

c-di-GMP Binding Assays

Enrichment of MotL Variants by Magnetic Beads Pulldown

GFP-tagged variants of MotL were directly isolated from *S. putrefaciens* CN-32 cell lysate through protein-protein interaction with GFP-Trap_MA beads (ChromoTek GmbH, Planegg, Germany). Cells were cultivated overnight in the LB medium containing 50 µg ml^{-1} kanamycin and sub cultured and induced with 40 ng ml^{-1} anhydrotetracyclin the next day. The entire culture was harvested after reaching an OD_{600} = 1 and the immunoprecipitation was carried out according to the manufacturer's protocol.

Production of Radioactively Labeled c-di-GMP

Radiolabeled c-di-GMP was synthesized from [α^{32}-P]-GTP (Hartmann Analytik, Germany) by the mutated diguanylatecyclase WspR (R242A) as previously described (Sambanthamoorthy et al., 2012; Srivastava and Waters, 2015). For the heterologous production of WspR (R242A), *E. coli* BL21 (DE3) (New England Biolabs, Frankfurt, Germany) cells harboring the applicable pET24C overexpression plasmid were grown at 37°C in the LB medium containing 50 µg ml^{-1} kanamycin to an OD_{600} = 0.3. Then, the cells were induced with D-(+)-lactose-monohydrate (12.5 g·l^{-1}) and incubated overnight at 15°C. The entire culture was harvested and the cell pellet was resuspended in buffer A [50 mM *Tris*-HCl, 250 mM NaCl, 25 mM KCl, 5 mM MgCl2, 0.5 mM dithiothreitol (DTT), 0.01% sodium azide, 5% glycerol, and 40 mM imidazole] and lysed by sonification (Bandelin Sonoplus). After centrifugation (20,000 rpm, 30 min, 4°C), the supernatant was filtered and loaded on a 5-ml HisTrap column (GE Healthcare), equilibrated with five column volumes (CV) of buffer A. The column was washed with 5 CV of buffer A before the protein was eluted with 5 CV of buffer B (buffer A with an imidazole concentration of 300 mM). Protein concentration was determined by spectrophotometry (NanoDrop Lite, Thermo Scientific) and the proteins were used immediately or stored for a short time at 4°C.

Binding Assays

For binding assays, 1.5 µM of the appropriate protein was incubated together with 2 µl of radiolabeled c-di-GMP or GTP in a binding buffer (5 mM *Tris*-HCl, 12.5 mM NaCl, 2.5 mM $MgCl_2$; and final volume of 50 µl) for 5 min at RT before 10 µl were spotted on a nitrocellulose membrane (in triplicates). After drying, the membrane was washed three times with the binding buffer, tried, and exposed on phosphorimaging screens (Bio-Rad) and analyzed with the 1D-Quantity One software (Bio-Rad).

DATA AVAILABILITY STATEMENT

The original contributions presented in the study are included in the article/**Supplementary Material**, further inquiries can be directed to the corresponding author.

AUTHOR CONTRIBUTIONS

KT and GB conceptualized the study and provided resources and funding. AP, MS, VB, TR, PK, and TL conducted the experiments. AP, MS, VB, and KT wrote the manuscript. All authors read and commented on the manuscript.

FUNDING

The work was supported by a grant from the Deutsche Forschungsgemeinschaft (DFG, TH831/5-2) to KT. GB acknowledges support through the DFG priority program 1879.

ACKNOWLEDGMENTS

We are grateful to Ulrike Ruppert for the excellent technical support.

SUPPLEMENTARY MATERIAL

The Supplementary Material for this article can be found online at: https://www.frontiersin.org/articles/10.3389/fmicb.2021.668892/full#supplementary-material

REFERENCES

Amikam, D., and Galperin, M. Y. (2006). PilZ domain is part of the bacterial c-di-GMP binding protein. *Bioinformatics* 22, 3–6. doi: 10.1093/bioinformatics/bti739

Baker, A. E., Diepold, A., Kuchma, S. L., Scott, J. E., Ha, D. G., Orazi, G., et al. (2016). PilZ domain protein FlgZ mediates cyclic di-GMP-dependent swarming motility control in *Pseudomonas aeruginosa*. *J. Bacteriol.* 198, 1837–1846. doi: 10.1128/JB.00196-16

Barbara, G. M., and Mitchell, J. G. (2003). Bacterial tracking of motile algae. *FEMS Microbiol. Ecol.* 44, 79–87. doi: 10.1111/j.1574-6941.2003.tb01092.x

Benach, J., Swaminathan, S. S., Tamayo, R., Handelman, S. K., Folta-Stogniew, E., Ramos, J. E., et al. (2007). The structural basis of cyclic diguanylate signal transduction by PilZ domains. *EMBO J.* 26, 5153–5166. doi: 10.1038/sj.emboj.7601918

Berg, H. C. (2003). The rotary motor of bacterial flagella. *Annu. Rev. Biochem.* 72, 19–54. doi: 10.1146/annurev.biochem.72.121801.161737

Bi, S., and Sourjik, V. (2018). Stimulus sensing and signal processing in bacterial chemotaxis. *Curr. Opin. Microbiol.* 45, 22–29. doi: 10.1016/j.mib.2018.02.002

Binnenkade, L., Teichmann, L., and Thormann, K. M. (2014). Iron triggers lambdaSo prophage induction and release of extracellular DNA in *Shewanella oneidensis* MR-1 biofilms. *Appl. Environ. Microbiol.* 80, 5304–5316. doi: 10.1128/AEM.01480-14

Boehm, A., Kaiser, M., Li, H., Spangler, C., Kasper, C. A., Ackermann, M., et al. (2010). Second messenger-mediated adjustment of bacterial swimming velocity. *Cell* 141, 107–116. doi: 10.1016/j.cell.2010.01.018

Brenzinger, S., Pecina, A., Mrusek, D., Mann, P., Völse, K., Wimmi, S., et al. (2018). ZomB is essential for flagellar motor reversals in *Shewanella putrefaciens* and *Vibrio parahaemolyticus*. *Mol. Microbiol.* 109, 694–709. doi: 10.1111/mmi.14070

Brown, M. T., Delalez, N. J., and Armitage, J. P. (2011). Protein dynamics and mechanisms controlling the rotational behaviour of the bacterial flagellar motor. *Curr. Opin. Microbiol.* 14, 734–740. doi: 10.1016/j.mib.2011.09.009

Bubendorfer, S., Held, S., Windel, N., Paulick, A., Klingl, A., and Thormann, K. M. (2012). Specificity of motor components in the dual flagellar system of *Shewanella putrefaciens* CN-32. *Mol. Microbiol.* 83, 335–350. doi: 10.1111/j.1365-2958.2011.07934.x

Bubendorfer, S., Koltai, M., Rossmann, F., Sourjik, V., and Thormann, K. M. (2014). Secondary bacterial flagellar system improves bacterial spreading by increasing the directional persistence of swimming. *Proc. Natl. Acad. Sci. U.S.A.* 111, 11485–11490. doi: 10.1073/pnas.1405820111

Chao, L., Rakshe, S., Leff, M., and Spormann, A. M. (2013). PdeB, a cyclic Di-GMP-specific phosphodiesterase that regulates *Shewanella oneidensis* MR-1 motility and biofilm formation. *J. Bacteriol.* 195, 3827–3833. doi: 10.1128/JB.00498-13

Cheang, Q. W., Xin, L., Chea, R. Y. F., and Liang, Z. X. (2019). Emerging paradigms for PilZ domain-mediated c-di-GMP signaling. *Biochem. Soc. Trans.* 47, 381–388. doi: 10.1042/BST20180543

Chen, Y., Chai, Y., Guo, J. H., and Losick, R. (2012). Evidence for cyclic di-GMP-mediated signaling in *Bacillus subtilis*. *J. Bacteriol.* 194, 5080–5090. doi: 10.1128/JB.01092-12

Christen, M., Christen, B., Allan, M. G., Folcher, M., Jeno, P., Grzesiek, S., et al. (2007). DgrA is a member of a new family of cyclic diguanosine monophosphate receptors and controls flagellar motor function in *Caulobacter crescentus*. *Proc. Natl. Acad. Sci. U.S.A.* 104, 4112–4117. doi: 10.1073/pnas.0607738104

Doyle, T. B., Hawkins, A. C., and McCarter, L. L. (2004). The complex flagellar torque generator of *Pseudomonas aeruginosa*. *J. Bacteriol.* 186, 6341–6350. doi: 10.1128/JB.186.19.6341-6350.2004

Fang, X., and Gomelsky, M. (2010). A post-translational, c-di-GMP-dependent mechanism regulating flagellar motility. *Mol. Microbiol.* 76, 1295–1305. doi: 10.1111/j.1365-2958.2010.07179.x

Ferreira, J. L., Gao, F. Z., Rossmann, F. M., Nans, A., Brenzinger, S., Hosseini, R., et al. (2019). Gamma-*proteobacteria* eject their polar flagella under nutrient depletion, retaining flagellar motor relic structures. *PLoS Biol.* 17:e3000165. doi: 10.1371/journal.pbio.3000165

Francis, N. R., Irikura, V. M., Yamaguchi, S., DeRosier, D. J., and Macnab, R. M. (1992). Localization of the *Salmonella typhimurium* flagellar switch protein FliG to the cytoplasmic M-ring face of the basal body. *Proc. Natl. Acad. Sci. U.S.A.* 89, 6304–6308. doi: 10.1073/pnas.89.14.6304

Francis, N. R., Sosinsky, G. E., Thomas, D., and DeRosier, D. J. (1994). Isolation, characterization and structure of bacterial flagellar motors containing the switch complex. *J. Mol. Biol.* 235, 1261–1270. doi: 10.1006/jmbi.1994.1079

Galperin, M. Y., and Chou, S. H. (2020). Structural conservation and diversity of PilZ-related domains. *J. Bacteriol.* 202:e00664-19. doi: 10.1128/JB.00664-19

Gao, X., Mukherjee, S., Matthews, P. M., Hammad, L. A., Kearns, D. B., and Dann, C. E. III (2013). Functional characterization of core components of the *Bacillus subtilis* cyclic-di-GMP signaling pathway. *J Bacteriol.* 195, 4782–4792. doi: 10.1128/JB.00373-13

Gibson, D. G., Young, L., Chuang, R. Y., Venter, J. C., Hutchison, C. A. III, and Smith, H. O. (2009). Enzymatic assembly of DNA molecules up to several hundred kilobases. *Nat. Methods* 6, 343–345. doi: 10.1038/nmeth.1318

Girgis, H. S., Liu, Y., Ryu, W. S., and Tavazoie, S. (2007). A comprehensive genetic characterization of bacterial motility. *PLoS Genet.* 3, 1644–1660. doi: 10.1371/journal.pgen.0030154

Guttenplan, S. B., Shaw, S., and Kearns, D. B. (2013). The cell biology of peritrichous flagella in *Bacillus subtilis*. *Mol. Microbiol.* 87, 211–229. doi: 10.1111/mmi.12103

Hou, Y. J., Yang, W. S., Hong, Y., Zhang, Y., Wang, D. C., and Li, D. F. (2020). Structural insights into the mechanism of c-di-GMP-bound YcgR regulating flagellar motility in *Escherichia coli*. *J. Biol. Chem.* 295, 808–821. doi: 10.1074/jbc.RA119.009739

Kaplan, M., Subramanian, P., Ghosal, D., Oikonomou, C. M., Pirbadian, S., Starwalt-Lee, R., et al. (2019). In situ imaging of the bacterial flagellar motor disassembly and assembly processes. *EMBO J.* 38:e100957. doi: 10.15252/embj.2018100957

Karimova, G., Dautin, N., and Ladant, D. (2005). Interaction network among *Escherichia coli* membrane proteins involved in cell division as revealed by bacterial two-hybrid analysis. *J. Bacteriol.* 187, 2233–2243. doi: 10.1128/JB.187.7.2233-2243.2005

Karimova, G., Pidoux, J., Ullmann, A., and Ladant, D. (1998). A bacterial two-hybrid system based on a reconstituted signal transduction pathway. *Proc. Natl. Acad. Sci. U.S.A.* 95, 5752–5756. doi: 10.1073/pnas.95.10.5752

Ko, J., Ryu, K. S., Kim, H., Shin, J. S., Lee, J. O., Cheong, C., et al. (2010). Structure of PP4397 reveals the molecular basis for different c-di-GMP binding modes by PilZ domain proteins. *J. Mol. Biol.* 398, 97–110. doi: 10.1016/j.jmb.2010.03.007

Kojima, S. (2015). Dynamism and regulation of the stator, the energy conversion complex of the bacterial flagellar motor. *Curr. Opin. Microbiol.* 28, 66–71. doi: 10.1016/j.mib.2015.07.015

Kojima, S., Yoneda, T., Morimoto, W., and Homma, M. (2019). Effect of PlzD, a YcgR homologue of c-di-GMP-binding protein, on polar flagellar motility in *Vibrio alginolyticus*. *J. Biochem.* 166, 77–88. doi: 10.1093/jb/mvz014

Kühn, M. J., Schmidt, F. K., Eckhardt, B., and Thormann, K. M. (2017). Bacteria exploit a polymorphic instability of the flagellar filament to escape from traps. *Proc. Natl. Acad. Sci. U.S.A.* 114, 6340–6345. doi: 10.1073/pnas.1701644114

Kühn, M. J., Schmidt, F. K., Farthing, N. E., Rossmann, F. M., Helm, B., Wilson, L. G., et al. (2018). Spatial arrangement of several flagellins within bacterial flagella improves motility in different environments. *Nat. Commun.* 9:5369. doi: 10.1038/s41467-018-07802-w

Lai, Y. W., Ridone, P., Peralta, G., Tanaka, M. M., and Baker, M. A. B. (2020). Evolution of the stator elements of rotary prokaryote motors. *J. Bacteriol.* 202, e00557-19. doi: 10.1128/JB.00557-19

Lassak, J., Henche, A. L., Binnenkade, L., and Thormann, K. M. (2010). ArcS, the cognate sensor kinase in an atypical Arc system of *Shewanella oneidensis* MR-1. *Appl. Environ. Microbiol.* 76, 3263–3274. doi: 10.1128/AEM.00512-10

Martinez-Granero, F., Navazo, A., Barahona, E., Redondo-Nieto, M., Gonzalez de Heredia, E., Baena, I., et al. (2014). Identification of *flgZ* as a flagellar gene encoding a PilZ domain protein that regulates swimming motility and biofilm formation in *Pseudomonas*. *PLoS One* 9:e87608. doi: 10.1371/journal.pone.0087608

Meijering, E., Dzyubachyk, O., and Smal, I. (2012). Methods for cell and particle tracking. *Methods Enzymol.* 504, 183–200. doi: 10.1016/B978-0-12-391857-4.00009-4

Meister, M., Lowe, G., and Berg, H. C. (1987). The proton flux through the bacterial flagellar motor. *Cell* 49, 643–650. doi: 10.1016/0092-8674(87)90540-x

Nakamura, S., and Minamino, T. (2019). Flagella-driven motility of bacteria. *Biomolecules* 9:279. doi: 10.3390/biom9070279

Paul, K., Nieto, V., Carlquist, W. C., Blair, D. F., and Harshey, R. M. (2010). The c-di-GMP binding protein YcgR controls flagellar motor direction and speed to affect chemotaxis by a "backstop brake" mechanism. *Mol. Cell.* 38, 128–139. doi: 10.1016/j.molcel.2010.03.001

Pratt, J. T., Tamayo, R., Tischler, A. D., and Camilli, A. (2007). PilZ domain proteins bind cyclic diguanylate and regulate diverse processes in *Vibrio cholerae*. *J. Biol. Chem.* 282, 12860–12870. doi: 10.1074/jbc.M611593200

Rossmann, F., Brenzinger, S., Knauer, C., Dörrich, A. K., Bubendorfer, S., Ruppert, U., et al. (2015). The role of FlhF and HubP as polar landmark proteins in *Shewanella putrefaciens* CN-32. *Mol. Microbiol.* 98, 727–742. doi: 10.1111/mmi.13152

Rossmann, F. M., Rick, T., Mrusek, D., Sprankel, L., Dorrich, A. K., Leonhard, T., et al. (2019). The GGDEF domain of the phosphodiesterase PdeB in *Shewanella putrefaciens* mediates recruitment by the polar landmark protein HubP. *J. Bacteriol.* 201, e00534-18. doi: 10.1128/JB.00534-18

Sambanthamoorthy, K., Sloup, R. E., Parashar, V., Smith, J. M., Kim, E. E., Semmelhack, M. F., et al. (2012). Identification of small molecules that antagonize diguanylate cyclase enzymes to inhibit biofilm formation. *Antimicrob. Agents Chemother.* 56, 5202–5211. doi: 10.1128/AAC.01396-12

Schäper, S., Krol, E., Skotnicka, D., Kaever, V., Hilker, R., Søgaard-Andersen, L., et al. (2016). Cyclic di-GMP regulates multiple cellular functions in the symbiotic alphaproteobacterium *Sinorhizobium meliloti*. *J. Bacteriol.* 198, 521–535. doi: 10.1128/JB.00795-15

Schindelin, J., Arganda-Carreras, I., Frise, E., Kaynig, V., Longair, M., Pietzsch, T., et al. (2012). Fiji: an open-source platform for biological-image analysis. *Nat. Methods* 9, 676–682. doi: 10.1038/nmeth.2019

Schuhmacher, J. S., Rossmann, F., Dempwolff, F., Knauer, C., Altegoer, F., Steinchen, W., et al. (2015). MinD-like ATPase FlhG effects location and number of bacterial flagella during C-ring assembly. *Proc. Natl. Acad. Sci. U.S.A.* 112, 3092–3097. doi: 10.1073/pnas.1419388112

Son, K., Menolascina, F., and Stocker, R. (2016). Speed-dependent chemotactic precision in marine bacteria. *Proc. Natl. Acad. Sci. U.S.A.* 113, 8624–8629. doi: 10.1073/pnas.1602307113

Sourjik, V., and Wingreen, N. S. (2012). Responding to chemical gradients: bacterial chemotaxis. *Curr. Opin. Cell Biol.* 24, 262–268. doi: 10.1016/j.ceb.2011.11.008

Srivastava, D., and Waters, C. M. (2015). A filter binding assay to quantify the association of cyclic di-GMP to proteins. *Bio Protoc.* 5:e1394. doi: 10.21769/bioprotoc.1394

Subramanian, S., Gao, X., Dann, C. E. III, and Kearns, D. B. (2017). MotI (DgrA) acts as a molecular clutch on the flagellar stator protein MotA in *Bacillus subtilis*. *Proc. Natl. Acad. Sci. U.S.A.* 114, 13537–13542. doi: 10.1073/pnas.1716231114

Subramanian, S., and Kearns, D. B. (2019). Functional regulators of bacterial flagella. *Annu. Rev. Microbiol.* 73, 225–246. doi: 10.1146/annurev-micro-020518-115725

Terashima, H., Kawamoto, A., Morimoto, Y. V., Imada, K., and Minamino, T. (2017). Structural differences in the bacterial flagellar motor among bacterial species. *Biophys. Physicobiol.* 14, 191–198. doi: 10.2142/biophysico.14.0_191

Thormann, K. M., Duttler, S., Saville, R. M., Hyodo, M., Shukla, S., Hayakawa, Y., et al. (2006). Control of formation and cellular detachment from *Shewanella oneidensis* MR-1 biofilms by cyclic di-GMP. *J. Bacteriol.* 188, 2681–2691. doi: 10.1128/JB.188.7.2681-2691.2006

Toutain, C. M., Zegans, M. E., and O'Toole, G. A. (2005). Evidence for two flagellar stators and their role in the motility of *Pseudomonas aeruginosa*. *J. Bacteriol.* 187, 771–777. doi: 10.1128/JB.187.2.771-777.2005

Wirebrand, L., Osterberg, S., Lopez-Sanchez, A., Govantes, F., and Shingler, V. (2018). PP4397/FlgZ provides the link between PP2258 c-di-GMP signalling and altered motility in *Pseudomonas putida*. *Sci. Rep.* 8:12205. doi: 10.1038/s41598-018-29785-w

Zhao, R., Pathak, N., Jaffe, H., Reese, T. S., and Khan, S. (1996). FliN is a major structural protein of the C-ring in the *Salmonella typhimurium* flagellar basal body. *J. Mol. Biol.* 261, 195–208. doi: 10.1006/jmbi.1996.0452

Zhu, S., Schniederberend, M., Zhitnitsky, D., Jain, R., Galan, J. E., Kazmierczak, B. I., et al. (2019). In situ structures of polar and lateral flagella revealed by cryo-electron tomography. *J. Bacteriol.* 201, e117–e119. doi: 10.1128/JB.00117-19

Zhuang, X. Y., Guo, S., Li, Z., Zhao, Z., Kojima, S., Homma, M., et al. (2020). Live-cell fluorescence imaging reveals dynamic production and loss of bacterial flagella. *Mol. Microbiol* 114, 279–291. doi: 10.1111/mmi.14511

Conflict of Interest: The authors declare that the research was conducted in the absence of any commercial or financial relationships that could be construed as a potential conflict of interest.

frontiers in Microbiology

PERSPECTIVE
published: 15 July 2021
doi: 10.3389/fmicb.2021.655942

How Can a Histidine Kinase Respond to Mechanical Stress?

*Linda J. Kenney**

Department of Biochemistry and Molecular Biology, University of Texas Medical Branch, Galveston, TX, United States

Bacteria respond to physical forces perceived as mechanical stress as part of their comprehensive environmental sensing strategy. Histidine kinases can then funnel diverse environmental stimuli into changes in gene expression through a series of phosphorelay reactions. Because histidine kinases are most often embedded in the inner membrane, they can be sensitive to changes in membrane tension that occurs, for example, in response to osmotic stress, or when deformation of the cell body occurs upon encountering a surface before forming biofilms, or inside the host in response to shear stress in the kidney, intestine, lungs, or blood stream. A summary of our recent work that links the histidine kinase EnvZ to mechanical changes in the inner membrane is provided and placed in a context of other bacterial systems that respond to mechanical stress.

Keywords: mechanosignaling, lipid allostery, EnvZ, histidine kinase, nanodiscs, catch bonds, mechanosensitive channels, biofilms

OPEN ACCESS

Edited by:
Seiji Kojima,
Nagoya University, Japan

Reviewed by:
Claudia Studdert,
CONICET Santa Fe, Argentina
Md. Motaleb,
The Brody School of Medicine at East Carolina University, United States

***Correspondence:**
Linda J. Kenney
Likenney@utmb.edu

Specialty section:
This article was submitted to Microbial Physiology and Metabolism, a section of the journal Frontiers in Microbiology

Received: *19 January 2021*
Accepted: *08 June 2021*
Published: *15 July 2021*

Citation:
Kenney LJ (2021) How Can a Histidine Kinase Respond to Mechanical Stress? Front. Microbiol. 12:655942. doi: 10.3389/fmicb.2021.655942

INTRODUCTION

Bacteria are sensitive to physical forces and experience them as part of their environmental sensing strategies, for example during growth and elongation, cell division or cell envelope remodeling, or as they adhere to a surface in order to form biofilms, and as they experience shear stress during colonization and infection as pathogens [see Harper and Hernandez (2020) for a recent review]. Although bacteria have long been known to be sensitive to their mechanical environment (Koch et al., 1982), understanding the effects of physical forces on bacterial physiology has been limited by their small size ($\sim 1\,\mu m$). Herein, I first summarize some well-characterized examples of force effects on bacterial systems (**Figure 1**) and then describe some recent advances in understanding the effects of membrane tension and lipids on bacterial two-component signaling systems, with an emphasis on the EnvZ/OmpR two-component signaling system.

BILAYER-MEDIATED GATING OF MECHANOSENSITIVE CHANNELS

Effects of membrane tension are probably best described on mechanosensitive channels, in which the bilayer mediates channel gating. The major mechanosensitive channels MscS, MscL protect bacteria from hypoosmotic shock [see Kung et al. (2010) for a review]. When cells experience a hypoosmotic downshift, mechanosensitive channels act as emergency valves to release cytoplasmic solutes to enable a rapid decrease in osmolality (Levina et al., 1999). Mechanosensitive channels directly interact with the membrane phospholipids (Nomura et al., 2012), and are gated in response

Abbreviations: HK, histidine kinase; RR, response regulator; HDXMS, amide hydrogen deuterium exchange mass spectrometry.

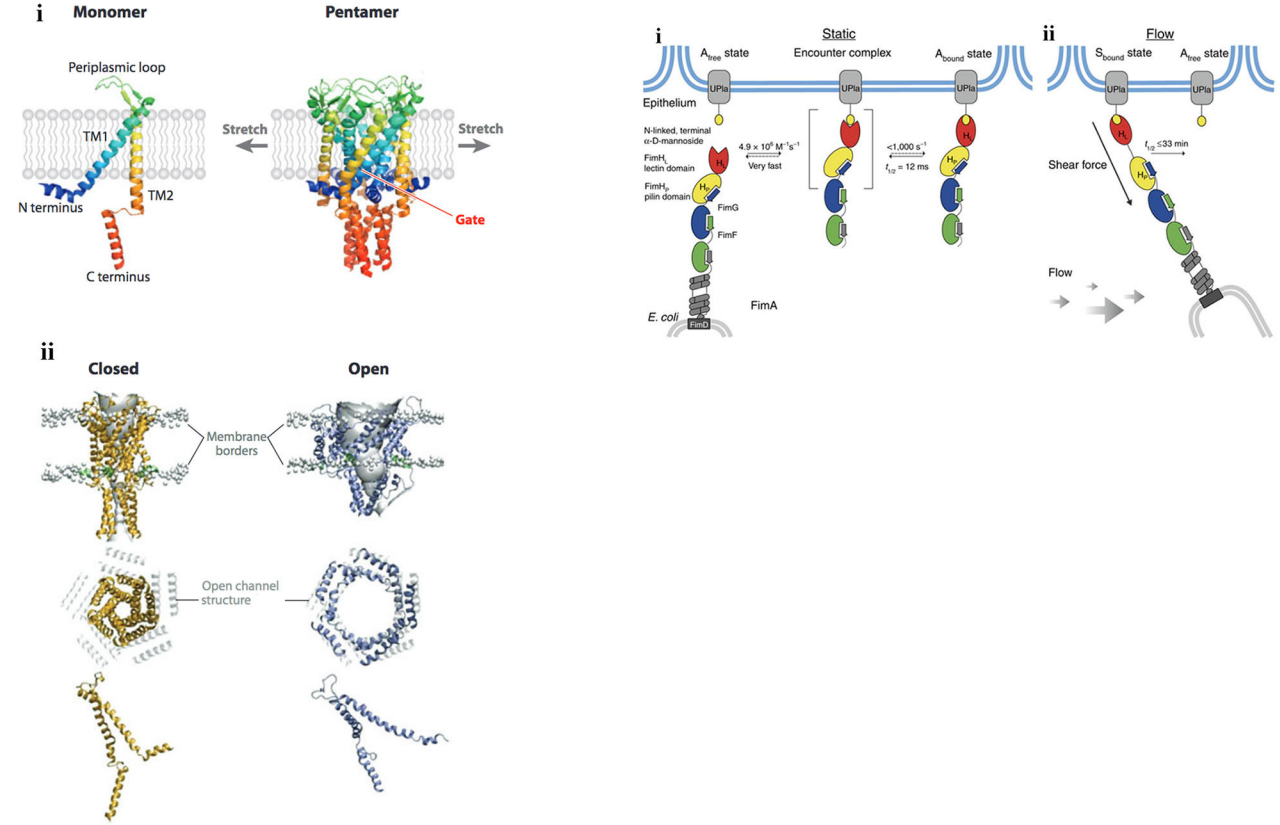

FIGURE 1 | Mechanisms of mechanosignaling in bacteria. **(A)** Structure and gating mechanism of MscL. (i) X-ray structure of the MscL from *Mycobacterium tuberculosis.* The channel monomer (left) is composed of two α-helical TM domains, TM1 and TM2; cytoplasmic N- and C-terminal domains; and a central periplasmic loop. The five TM1 domains form a tightly packed bundle funneling to a hydrophobic constriction, functioning as the gate (right). (ii) Three-dimensional reconstruction of the pentameric MscL of *E. coli* viewed in the plane of the membrane (top) and from above (middle). The channel is shown in its closed (left) and open (right) states. In the top row, lipid phosphate headgroups are shown as gray balls to indicate the outer and inner borders of the membrane. The extent of rearrangement of a single MscL subunit from the closed to the open conformation is depicted at the bottom. Membrane tension flattens MscL in the direction of the pore axis due to an increased tilt in the TM1 and TM2 helices. Closed and open structures of MscL (middle) are superimposed on the open channel structure (depicted in gray). TM, transmembrane. Reprinted with permission from Kung et al. (2010). **(B)** Catch-bond mechanism of FimH-mediated cell adhesion. (i) In the absence of tensile mechanical force, formation of the FimH-Uroplakin 1a (UPIa) complex comprises the highly dynamic transition of the $\mathbf{A_{free}}$ to the $\mathbf{A_{bound}}$ state. Dissociation of the receptor from the FimH lectin domain in the $\mathbf{A_{bound}}$ state is promoted via dynamic allostery by the pilin domain that acts as a negative allosteric regulator. (ii) Shear force increases the population of the $\mathbf{S_{bound}}$ state of FimH, in which the pilin and lectin domains are separated. The dissociation of $\mathbf{S_{bound}}$ under shear force is slowed down up to 100,000-fold compared with $\mathbf{A_{bound}}$. The indicated rate constants and half-lives correspond to the interaction between $FimH^{F18}$ and the model ligand HM. Rate limiting reactions are indicated by solid arrows, and fast, non-limiting reactions by dashed arrows. Reprinted with permission from Sauer et al. (2016).

to changes in membrane tension. Reconstitution of purified channel proteins into liposomes of varying lipid composition enabled the analysis of mechanosensitive channels by patch-clamp electrophysiology (Nomura et al., 2012). Membranes that were thicker, by being composed of phospholipids having longer acyl chain lengths (Perozo et al., 2002), or containing cholesterol (Nomura et al., 2012), raised the activation threshold, whereas thinner membranes composed of phospholipids of shorter acyl chain lengths lowered the activation barrier (Perozo et al., 2002). An N-terminal amphipathic helix of MscL acts as a crucial structural element by stabilizing the closed state and coupling the channel to the membrane (Bavi et al., 2016). This horizontal helix directly links membrane bilayer fluctuations to protein conformation (Iscla et al., 2008), exquisitely coupling membrane dynamics to channel open or closed states (see **Figure 1A**), as first suggested by Segrest et al. (1974).

PROTEIN ALLOSTERY MEDIATES CATCH BOND STRENGTH

Catch bonds play a significant role in bacterial adhesion, especially during transit of *E. coli* in the intestinal tract or uropathogenic *E. coli* in the renal tubules, where firm adhesion of bacteria in the face of hydrodynamic flow is required. Mechanosensitive catch bonds are a non-covalent bond whose

dissociation constant increases upon application of tensile force. The concept of a catch bond is similar to a Chinese finger trap, where the bond strengthens when force is applied and weakens when force is released (Thomas, 2009). The bacterial adhesion FimH is a two-domain protein at the tip of Type I pili that recognizes terminal mannoses on epithelial glycoproteins. In the absence of tensile force, the FimH pilin domain allosterically accelerates (by 100,000-fold) spontaneous ligand dissociation from the FimH lectin domain, resulting in weak affinity (Sauer et al., 2016). Mechanical stress physically separates the FimH domains and abolishes the interdomain allostery, and the affinity of FimH for the lectin is increased (see **Figure 1B**). Thus, protein allostery contributes to mechanotransduction in catch bonds by altering bond strength.

Signal transduction in bacteria is largely perceived by two-component signaling systems that respond to environmental stress coupled to a phosphorelay that usually results in changes in gene expression. Thus, it seems logical that two-component systems would also be sensitive to changes in membrane tension. In the remaining sections, we focus on what is currently known regarding mechanosignaling in gram-negative bacterial two-component systems.

MECHANICAL EFFECTS ON TWO COMPONENT SIGNALING SYSTEMS

Bacteria sense and respond to their environment largely through the use of two-component regulatory systems that function as a histidine kinase (HK)-response regulator (RR) pair. The HK is typically an inner membrane protein and the RR is most often a cytoplasmic two-domain DNA binding protein [see Hoch and Silhavy (1995) for numerous examples]. The two components function in a phosphorelay that involves ATP binding by the HK and autophosphorylation on a conserved histidine residue. The phosphoryl group is subsequently transferred to a conserved aspartic acid in the N-terminal phosphorylation domain of the RR. Phosphorylation in the N-terminus of the RR stimulates dimerization and communicates with the C-terminus for enhanced DNA binding and transcriptional activation. In *E. coli*, the EnvZ/OmpR two-component system functions to regulate many genes in response to acid and osmotic stress (Chakraborty et al., 2017; Chakraborty and Kenney, 2018), including the differential expression of outer membrane porins OmpF and OmpC [reviewed in Kenney and Anand (2020)]. In *Salmonella enterica* serovars Typhi and Typhimurium, EnvZ/OmpR is stimulated by acid stress (Chakraborty et al., 2015; Kenney, 2019) to up-regulate the SsrA/B two-component system (Liew et al., 2019) required for intracellular survival and virulence (Lee et al., 2000; Feng et al., 2003).

HKs are typically organized with their N-and C-termini in the cytoplasm, with two transmembrane domains, a periplasmic loop and a large C-terminal portion that is subdivided into a four-helix bundle containing the phosphorylated histidine and an ATP binding domain [see Kenney and Anand (2020)]. In general, HKs are much less abundant compared to their cognate RRs (Cai and Inouye, 2002; Liew et al., 2019). The low copy number of the HKs coupled with their usual location in the inner membrane makes studying their activation mechanisms difficult. To circumvent this problem, we initially explored the protein dynamics of the C-terminus that was liberated from the membrane (EnvZc, comprising residues 180–450) using amide hydrogen deuterium exchange mass spectrometry (HDXMS) (Wang et al., 2012). A 17-amino acid peptide flanking the phosphorylatable histidine was exquisitely sensitive to osmolytes and defined a cytoplasmic locus for osmosensing (see **Figure 2A**). At low osmolality, the peptide containing the phosphorylatable histidine had higher rates of exchange and the helix was locally disordered. The presence of osmolytes reduced exchange and promoted helical stabilization through the addition of several H-bonds (**Figure 2B**; Wang et al., 2012). These events increased autophosphorylation and subsequent OmpR activation. It was surprising that EnvZc, which was no longer located in the inner membrane, was still capable of osmosensing, as reported by the upregulation of an *ompC-lacZ* transcriptional fusion at high osmolality. This finding raised the question then as to what role (if any) does the membrane and the transmembrane domains of EnvZ play in controlling EnvZ activity?

The answer came in part from the use of purified, full-length detergent-solubilized EnvZ protein that was embedded into phospholipid bilayer nanodiscs (**Figure 2C**; Ghosh et al., 2017). Nanodiscs were useful for this purpose, because they are monodisperse, exhibit long term stability compared to proteoliposomes, and have a wide range of membrane protein applications (Nath et al., 2007). Although the use of nanodiscs eliminated the sidedness compared to the native protein *in situ*, their use enabled us to manipulate the membrane lipid composition, and to examine the effect of membrane lipids in regulating EnvZ receptor function through an interaction with the transmembrane segments (TMs) or the HAMP domain (**Figure 2D**), which were lacking in the EnvZc construct (Wang et al., 2012). With every construct that we explored, phosphorylation of EnvZ was stimulated in response to increasing osmolality by about 4-fold. Surprisingly, however, the addition of *E. coli* lipids to EnvZc (**Figure 2E**) dramatically increased ATP turnover at both low and high osmolality (25- or 14-fold, respectively), compared to EnvZc alone (see **Table 1**). A similar level of stimulation of ATP turnover (14- to 15-fold) was also observed with the full-length EnvZ protein embedded into nanodiscs, indicating that membrane lipid effects on the ATP binding domain was indeed the manifestation of membrane tension on EnvZ.

The subsequent application of HDXMS enabled us to determine which region of EnvZ was susceptible to lipids. The highly conserved glycine-rich motif of the ATP binding domain showed increased exchange in the presence of lipids with both EnvZc and with full-length EnvZ, exposing a previously unobserved effect of lipids on an HK. We speculated that as cells reduce their volume when they encounter a high osmotic environment, mechanical effects on the membrane lipids would exert an effect on the ATP binding domain of EnvZ, stimulating an increase in EnvZ autophosphorylation. Thus, lipids exert allosteric effects mediated through the ATP binding domain that drive HK signaling in response to osmotic stress.

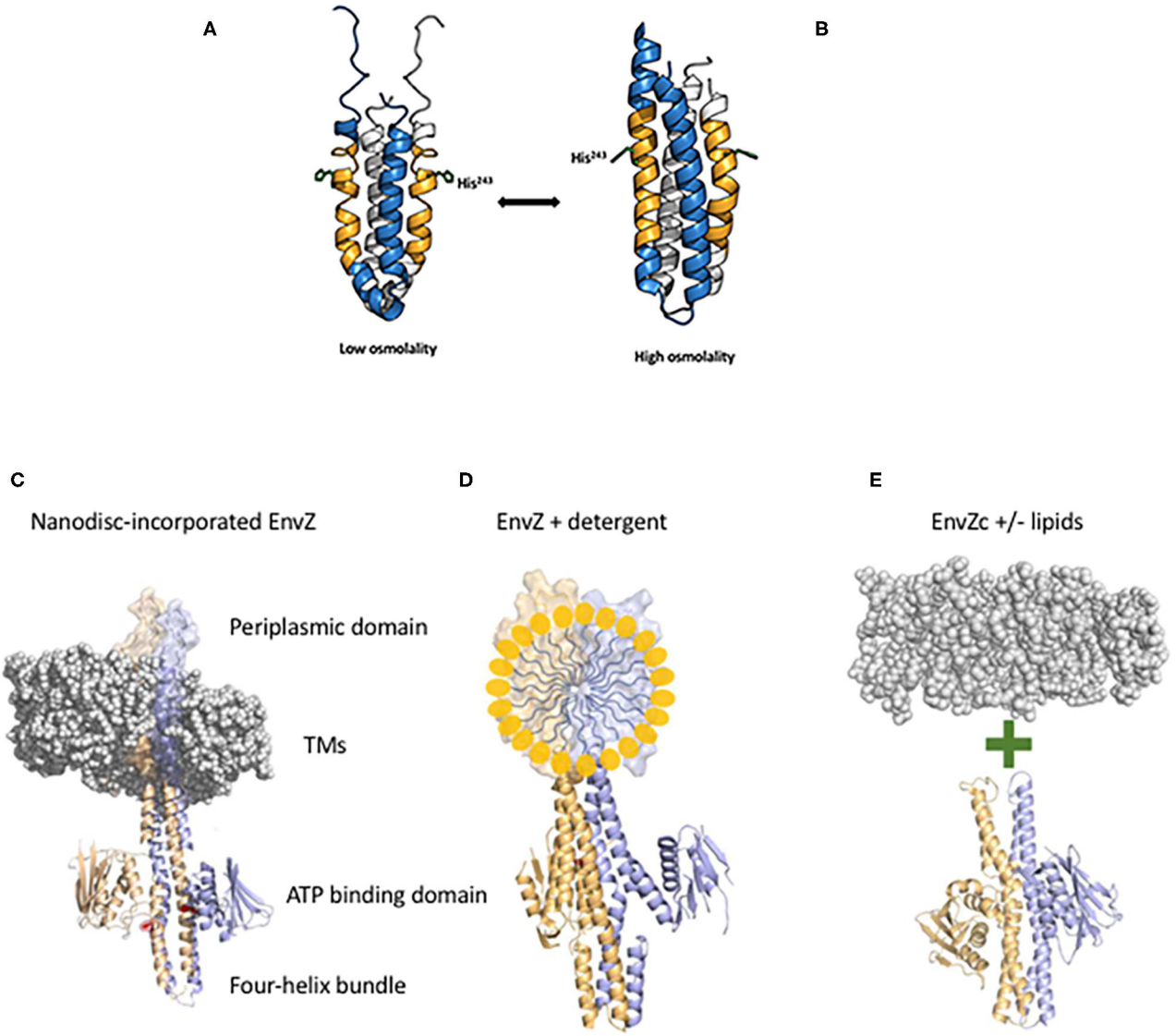

FIGURE 2 | EnvZc four-helix bundle subdomain structure at low osmolality **(A)** and at high osmolality **(B)**. The low osmolality structure was composed of residues 223–289 and was solved by NMR (PDB ID:1JOY) (Tanaka et al., 1998), the high osmolality structure was a chimera of EnvZ with the *Archaeoglobus fulgidus* Af1503 HAMP domain (PDB ID:4CTI) (Ferris et al., 2014). The amber peptide was identified from HDXMS analysis highlighting the change from poorly ordered to highly ordered during the switch from low to high osmolality (Wang et al., 2012). The sidechain of the histidine that is phosphorylated (His^{243}) is shown in stick form. At low osmolality, His^{243} is positioned by a coordinated relay of interactions from the backbone carbonyl of Ala^{239} (one helical turn above His^{243}) through the imidazole side chain of His^{243} to the carboxylic acid side chain of Asp^{244}. Intrinsic disorder within the amber peptide affords a low basal level of autophosphorylation. High osmolality stabilizes the helical backbone and relieves the Ala^{239} carbonyl link to anchor the His^{243} imidazole by a H-bond with Asp^{244} at the Nδ of His^{243}. This enables phosphotransfer to the Nε of His^{243} [see Kenney and Anand (2020) for more details]. Thus, the core of osmosensing is a His-Asp/Glu dyad positioned within a flexible helix. Various EnvZ constructs employed in the study. **(C)** The EnvZ periplasmic domain protrudes above the membrane (shown as a space filling model PDB ID:3J00, the EnvZ dimer is from PDB ID:4CTI). The transmembrane domains (TMs) connect to the four-helix bundle formed from a dimer of two monomers shown in lavender and pale orange. A single His^{243} side chain is highlighted in red (phosphorylation site) and the ATP binding domains flank His^{243} [from Kenney and Anand (2020)]. **(D)** Full-length EnvZ solubilized in detergent micelles for comparison with nanodiscs and *E. coli* lipids. **(E)** The activity of EnvZc alone (bottom) was compared with EnvZc in the presence of lipids (see **Table 1**).

Local anesthetics such as procaine and phenylethyl alcohol (PEA) partition into the inner membrane, yet they lead to a reduction in the level of OmpF and an increase in OmpC in the outer membrane of *E. coli,* mimicking a high osmolality phenotype (Granett and Villarejo, 1982; Pages and Lazdunski, 1982). In the case of procaine, its action was reported to be dependent upon EnvZ (Granett and Villarejo, 1982; Taylor et al., 1983). Until recently, it was not possible to directly connect lipid effects to HK signaling. The observation that membrane lipids altered ATP turnover of EnvZ and stimulated phosphorylation

TABLE 1 | Lipid interactions enhance EnvZ autophosphorylation [adapted from Ghosh et al. (2017)].

Fold-Stimulation compared to EnvZc	ADP produced (Mole/Min per Mole of EnvZ)	
	Low osmolality	High osmolality
EnvZc + *E. coli* lipids	24	14
EnvZ + *E. coli* lipid nanodiscs	14	15

EnvZ autophosphorylation was measured using an in vitro ADP Glo kinase assay (Promega, Madison WI), which uses luminescence to quantify the amount of ADP produced over time. Measurements were performed at low osmolality (100 mOsm/kg) and high osmolality (780 mOsm/kg). The activity of EnvZc alone was 0.09 mole ADP/mol EnvZc per minute at low osmolality and 0.32 mole ADP/mol EnvZc per minute at high osmolality. See Ghosh et al. (2017) for more details.

(Ghosh et al., 2017) provided an explanation for how local anesthetics such as procaine (Granett and Villarejo, 1982) and other membrane perturbants (Rampersaud and Inouye, 1991) affect EnvZ signaling. By altering the lipids (Papahadjopoulos, 1972), these agents can exert an indirect effect on the glycine-rich loop of the ATP binding domain, stimulating ATP turnover and subsequent autophosphorylation of EnvZ at His^{243}. Increasing EnvZ autophosphorylation subsequently increases OmpR∼P levels, driving repression of *ompF* and activation of *ompC* transcription (Granett and Villarejo, 1981, 1982; Rampersaud et al., 1994). Thus, modification of the lipid bilayer by local anesthetics can be understood in terms of direct mechanical effect of lipids on the ATP binding domain of EnvZ.

To obtain a comprehensive understanding of downstream signaling events, a comparison with the much-studied chemotaxis system is informative. Although the bacterial chemotaxis system is an atypical "two-component" system, the common features include the HK CheA and the single domain RR CheY. Significant differences include the cytoplasmic location of the kinase CheA (Stock et al., 1989), although gram-positive organisms have soluble, cytoplasmic HKs as well [described in Hoch and Silhavy (1995)], and the histidine that is phosphorylated is in a different location (the P1 domain) from the more classical membrane-bound kinases (Hess et al., 1988). Changes in membrane tension resulting from osmotic shock act as a repellant by mechanically perturbing chemoreceptors, driving enhanced activity of the CheA kinase (Vaknin and Berg, 2006). The CheA kinase then phosphorylates the CheY RR to switch the direction of rotation of the flagellar motor from counterclockwise (smooth swimming), to clockwise (tumbling). In this example, the chemoreceptors act as a mediator between membrane tension and the soluble kinase CheA. Thus, both EnvZ and CheA are activated by membrane tension (compared in **Figure 3A**).

Similarly, a role of the ATP binding domain in HK signaling has been described in both the EnvZ/OmpR system (see above) and the chemotaxis system. ATP binding orders the "ATP lid" and creates a binding site for P1, the domain that contains the phosphorylated histidyl residue of CheA (Jun et al., 2020). Similarly, membrane lipid interactions with the ATP binding domain of EnvZ increase autophosphorylation of His^{243}. EnvZc is as sensitive to lipids as the full-length EnvZ, suggesting that it may localize in proximity to the inner membrane (Ghosh et al., 2017). Thus, at least in these two systems, kinase control by environmental stimuli appears to be exclusively at the level of autophosphorylation and is sensitive to membrane tension.

MECHANICAL STRESS/SURFACE SENSING

During biofilm formation, it is believed that sessile bacteria first interact with a surface via appendages such as pili and flagella (Zhang and Normark, 1996; Otto et al., 2001; Bhomkar et al., 2010; Lele et al., 2013; Tipping et al., 2013; Lee and Belas, 2015), and then eventually the bacterial cell body encounters the surface. Physical contact between the surface and the cell body is presumably sensed as envelope stress that leads to downstream changes in gene expression (**Figure 3**). When planktonic, motile bacteria approach a surface, flagellar rotation decreases, presumably due to either a change in viscosity or through the physical interaction with the surface (McCarter et al., 1988). This virulence/biofilm lifestyle switch has been most thoroughly studied in *Pseudomonas aeruginosa*. A complete proteomic analysis was obtained from *P. aeruginosa* immobilized on glass wool comparing attached and unattached populations. Six hundred sixteen proteins showed modified abundance, including several two-component systems (Crouzet et al., 2017). Two-component systems that are intricately involved in the sessile-motile switch and may be good candidates for surface sensors include the chemosensory signaling system Wsp (Huangyutitham et al., 2013) in *P. aeruginosa* and the RcsCDB system in *E. coli* (Ferrieres and Clarke, 2003).

In the Wsp chemosensory signaling system, the membrane bound receptor WspA responds to surface signals and activates the soluble, cytoplasmic HK WspE, which in turn phosphorylates the hybrid RR WspR. Instead of coupling phosphorylation in the N-terminal receiver domain to a DNA binding domain in the C-terminus, WspR contains a guanylate cyclase domain that produces cyclic di-GMP, stimulating biofilm formation. When *P. aeruginosa* encounters a surface, phospho-WspR forms clusters in the cytoplasm that stimulate the cyclase activity (Huangyutitham et al., 2013). WspA localizes laterally along the cell, and the periplasmic and transmembrane domains of WspA are not essential for surface sensing, although the system performed better when they were present (O'Connor et al., 2012). Additional components do not appear to be required, since surface sensing could be reconstituted in *E. coli* (M. R. Parsek and C. S. Harwood, personal communication). More recently, it was reported that ethanol, produced during co-infections of *C. albicans* and *P. aeruginosa,* stimulated biofilm production in a process requiring WspR and the chemosensory receptor WspA (Chen et al., 2014). The authors proposed that ethanol and other alcohols can increase the rigidity of cell membranes by promoting an altered composition of fatty acids (Ingram and Buttke, 1984). It will now be worthwhile to determine whether the membrane-localized WspA can be activated by changes in lipid composition or physical changes

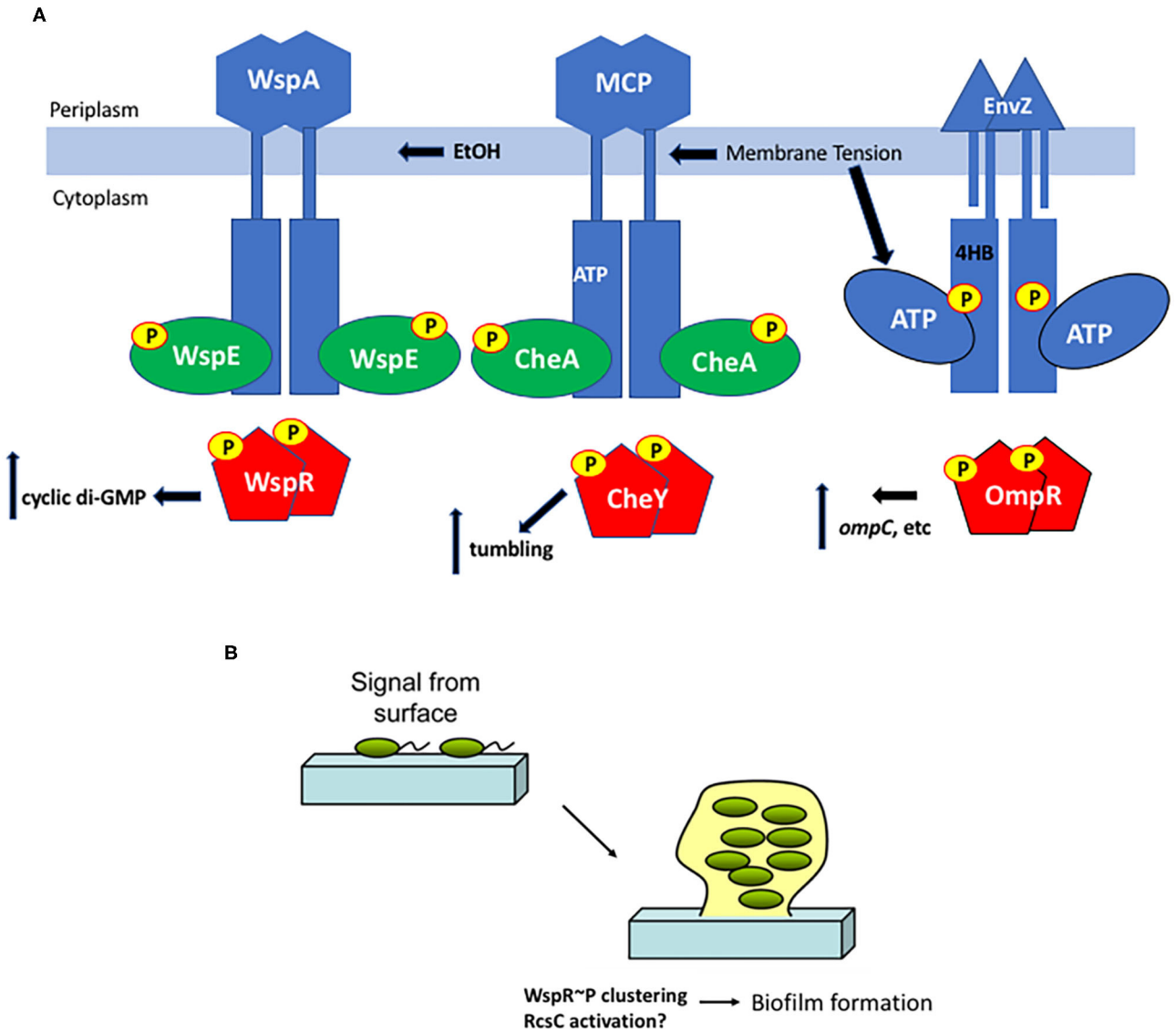

FIGURE 3 | Surface sensing in bacteria. **(A)** Membrane tension from osmotic stress, altered lipids or EtOH produced from a co-infection with *C. albicans* alters the chemoreceptors WspA and MCPs and/or the EnvZ HK directly and stimulates ATP turnover, increasing RR phosphorylation in turn, resulting in a change in output, depending on the RR. **(B)** Interaction with a surface is an early step in biofilm formation. Cells transition from the motile, planktonic state to interact with a surface via pili or other appendages and then begin the biofilm process. Deformation of the bacterial cell as it encounters a surface could then drive signaling steps that eventually lead to aggregation and production of matrix proteins.

in *P. aeruginosa* membranes (see **Figure 3A**). Perhaps even more interesting was the observation that cell surface-sensing resulted in a heterogeneous population of low cyclic di-GMP cells and high cyclic di-GMP cells that perform complementary tasks in the early stages of biofilm production (Armbruster et al., 2019). The Wsp chemosensory system was essential for establishing the heterogeneity that then creates a division of labor between cells involved in surface exploration and cells involved in polysaccharide production.

In *E. coli,* bacterial signaling systems that were reported to be involved in surface sensing are the RcsCDB phosphorelay and the CpxA/R system. The sensor kinase RcsC plays an important role in controlling the remodeling of the *E. coli* surface in response to growth on a solid surface and during biofilm formation (Ferrieres and Clarke, 2003). The Cpx two-component signal transduction pathway responds specifically to stress caused by disturbances in the cell envelope and CpxA then activates CpxR to express genes encoding periplasmic protein folding and degrading factors. The outer membrane lipoprotein NlpE was reported to discriminate between surface adhesion vs. the misfolded protein pathway in that it was essential for the activation of Cpx specifically during surface adhesion, but not in the response to misfolded

proteins in the cell envelope (Otto and Silhavy, 2002). This finding was disputed by a more recent study that used single cell analysis of cells in a microfluidic device and reported that the RcsCDB system was activated upon surface attachment, but the CpxA/R system was not (Kimkes and Heinemann, 2018), confirming an earlier study that implicated RcsC in surface sensing (Ferrieres and Clarke, 2003). At the present time, it still remains a mystery as to how RcsC functions to sense surfaces to drive downstream activation of the biofilm pathway (Kimkes and Heinemann, 2020). Sensing may involve a disruption of the membrane lipoprotein RcsF and its interaction with outer membrane proteins (Konovalova et al., 2014).

CONCLUDING REMARKS

Although much remains to be understood in molecular terms as to how bacteria respond to mechanical stress, it is clear that some progress has been achieved. Bacteria respond to changes in membrane tension via a combination of mechanical events, including both lipid allostery and protein allostery. In the examples of lipid allostery, direct interaction with membrane phospholipids leads to bilayer-mediated gating in the case of mechanosensitive channels, or to direct effects on ATP binding and subsequent HK phosphorylation in the case of EnvZ and CheA (and possibly WspA) (summarized in **Figure 3A**). Cell body deformation when bacteria encounter a surface is also sensed as "envelope stress", activating RcsC in an unknown series of events and driving early steps in the biofilm pathway (**Figure 3B**). In the case of FimH-mediated catch bonds, protein allostery is abolished as force separates protein domains, and the catch bond is strengthened. New tools such as membrane tension sensors (Dal Molin et al., 2015; Soleimanpour et al., 2016; Colom et al., 2018), and new applications of existing methods including: gel encapsulation (Tuson et al., 2012), optical traps (Wang et al., 2010), microfluidic devices (Amir et al., 2014; Sun et al., 2014; Chang et al., 2018; Sanfilippo et al., 2019), atomic force microscopy (Yao et al., 1999; Deng et al., 2011; Mularski et al., 2015), and the ability to study single cells within a population will provide useful tools in defining additional mechanisms of mechanotransduction in bacteria.

DATA AVAILABILITY STATEMENT

The original contributions presented in the study are included in the article/supplementary material, further inquiries can be directed to the corresponding author/s.

AUTHOR CONTRIBUTIONS

The author confirms being the sole contributor of this work and has approved it for publication.

FUNDING

The work was supported by grants VA 5IOBX-000372 and NIH R21-123640 to LJK and MOE2012-T3-1-008 to Ganesh S. Anand.

ACKNOWLEDGMENTS

LJK is grateful to Prof. Boris Martinac (Victor Chang Cardiac Research Institute, Sydney, AU), Ganesh S. Anand (Pennsylvania State University, USA), Caroline S. Harwood (University of Washington), Matthew R. Parsek (University of Washington), and Zemer Gitai (Princeton University) for helpful discussions.

REFERENCES

Amir, A., Babaeipour, F., McIntosh, D. B., Nelson, D. R., and Jun, S. (2014). Bending forces plastically deform growing bacterial cell walls. *Proc. Natl. Acad. Sci. U.S.A.* 111, 5778–5783. doi: 10.1073/pnas.1317497111

Armbruster, C. R., Lee, C. K., Parker-Gilham, J., de Anda, J., Xia, A., Zhao, K., et al. (2019). Heterogeneity in surface sensing suggests a division of labor in *Pseudomonas aeruginosa* populations. *Elife* 8:e45084. doi: 10.7554/eLife.45084

Bavi, N., Cortes, D. M., Cox, C. D., Rohde, P. R., Liu, W., Deitmer, J. W., et al. (2016). The role of MscL amphipathic N terminus indicates a blueprint for bilayer-mediated gating of mechanosensitive channels. *Nat. Commun.* 7:11984. doi: 10.1038/ncomms11984

Bhomkar, P., Materi, W., Semenchenko, V., and Wishart, D. S. (2010). Transcriptional response of E. *coli* upon FimH-mediated fimbrial adhesion. *Gene Regu. Syst. Bio.* 4, 1–17. doi: 10.4137/GRSB.S4525

Cai, S. J., and Inouye, M. (2002). EnvZ-OmpR interaction and osmoregulation in *Escherichia coli*. *J. Biol. Chem.* 277, 24155–24161. doi: 10.1074/jbc.M110715200

Chakraborty, S., and Kenney, L. J. (2018). A new role of OmpR in acid and osmotic stress in salmonella and *E. coli*. *Front. Microbiol.* 9:2656. doi: 10.3389/fmicb.2018.02656

Chakraborty, S., Mizusaki, H., and Kenney, L. J. (2015). A FRET-based DNA biosensor tracks OmpR-dependent acidification of salmonella during macrophage infection. *PLoS Biol.* 13:e1002116. doi: 10.1371/journal.pbio.1002116

Chakraborty, S., Winardhi, R. S., Morgan, L. K., J., and Yan, and, L. J., Kenney. (2017). Non-canonical activation of OmpR drives acid and osmotic stress responses in sngle bacterial cells. *Nat. Commun.* 8:1587. doi: 10.1038/s41467-017-02030-0

Chang, D., Sakuma, S., Kera, K., Uozumi, N., and Arai, F. (2018). Measurement of the mechanical properties of single synechocystis sp. strain PCC6803 cells in different osmotic concentrations using a robot-integrated microfluidic chip. *Lab Chip* 18, 1241–1249. doi: 10.1039/C7LC01245D

Chen, A. I., Dolben, E. F., Okegbe, C., Harty, C. E., Golub, Y., Thao, S., et al. (2014). Candida albicans ethanol stimulates *Pseudomonas aeruginosa* WspR-controlled biofilm formation as part of a cyclic relationship involving phenazines. *PLoS Pathog.* 10:e1004480. doi: 10.1371/journal.ppat.1004480

Colom, A., Derivery, E., Soleimanpour, S., Tomba, C., Molin, M. D., Sakai, N., et al. (2018). A fluorescent membrane tension probe. *Nat. Chem.* 10, 1118–1125. doi: 10.1038/s41557-018-0127-3

Crouzet, M., Claverol, S., Lomenech, A. M., Le Senechal, C., Costaglioli, P., Barthe, C., et al. (2017). Pseudomonas aeruginosa cells attached to a surface display a typical proteome early as 20 minutes of incubation. *PLoS ONE* 12:e0180341. doi: 10.1371/journal.pone.0180341

Dal Molin, M., Verolet, Q., Colom, A., Letrun, R., Derivery, E., Gonzalez-Gaitan, M., et al. (2015). Fluorescent flippers for mechanosensitive membrane probes. *J. Am. Chem. Soc.* 137, 568–571. doi: 10.1021/ja5107018

Deng, Y., Sun, M., and Shaevitz, J. W. (2011). Direct measurement of cell wall stress stiffening and turgor pressure in live bacterial cells. *Phys. Rev. Lett.* 107:158101. doi: 10.1103/PhysRevLett.107.158101

Feng, X., Oropeza, R., and Kenney, L. J. (2003). Dual regulation by phospho-OmpR of ssrA/B gene expression in salmonella pathogenicity island 2. *Mol. Microbiol.* 48, 1131–1143. doi: 10.1046/j.1365-2958.2003.03502.x

Ferrieres, L., and Clarke, D. J. (2003). The RcsC sensor kinase is required for normal biofilm formation in *Escherichia coli* K-12 and controls the expression of a regulon in response to growth on a solid surface. *Mol. Microbiol.* 50, 1665–1682. doi: 10.1046/j.1365-2958.2003.03815.x

Ferris, H. U., Coles, M., Lupas, A. N., and Hartmann, M. D. (2014). Crystallographic snapshot of the *Escherichia coli* EnvZ histidine kinase in an active conformation. *J. Struct. Biol.* 186, 376–379. doi: 10.1016/j.jsb.2014.03.014

Ghosh, M., Wang, L. C., Ramesh, R., Morgan, L. K., Kenney, L. J., and Anand, G. S. (2017). Lipid-Mediated regulation of embedded receptor kinases via parallel allosteric relays. *Biophys. J.* 112, 643–654. doi: 10.1016/j.bpj.2016.12.027

Granett, S., and Villarejo, M. (1981). Selective inhibition of carbohydrate transport by the local anesthetic procaine in *Escherichia coli*. *J. Bacteriol.* 147, 289–296. doi: 10.1128/jb.147.2.289-296.1981

Granett, S., and Villarejo, M. (1982). Regulation of gene expression in *Escherichia coli* by the local anesthetic procaine. *J. Mol. Biol.* 160, 363–367. doi: 10.1016/0022-2836(82)90181-4

Harper, C. E., and Hernandez, C. J. (2020). Cell biomechanics and mechanobiology in bacteria: challenges and opportunities. *APL Bioeng.* 4:021501. doi: 10.1063/1.5135585

Hess, J. F., Bourret, R. B., and Simon, M. I. (1988). Histidine phosphorylation and phosphoryl group transfer in bacterial chemotaxis. *Nature* 336, 139–143. doi: 10.1038/336139a0

Hoch, J. A., and Silhavy, T. J (Eds). (1995). *Two-Component Signal Transduction*. Washington, DC: ASM Press. doi: 10.1128/9781555818319

Huangyutitham, V., Guvener, Z. T., and Harwood, C. S. (2013). Subcellular clustering of the phosphorylated WspR response regulator protein stimulates its diguanylate cyclase activity. *MBio* 4, e00242–e00213. doi: 10.1128/mBio.00242-13

Ingram, L. O., and Buttke, T. M. (1984). Effects of alcohols on micro-organisms. *Adv. Microb. Physiol.* 25, 253–300. doi: 10.1016/S0065-2911(08)60294-5

Iscla, I., Wray, R., and Blount, P. (2008). On the structure of the N-terminal domain of the MscL channel: helical bundle or membrane interface. *Biophys. J.* 95, 2283–2291. doi: 10.1529/biophysj.107.127423

Jun, S. Y., Pan, W., and Hazelbauer, G. L. (2020). ATP binding as a key target for control of the chemotaxis kinase. *J. Bacteriol.* 202:e00095–20. doi: 10.1128/JB.00095-20

Kenney, L. J. (2019). The role of acid stress in salmonella pathogenesis. *Curr. Opin. Microbiol.* 47, 45–51. doi: 10.1016/j.mib.2018.11.006

Kenney, L. J., and Anand, G. S. (2020). EnvZ/OmpR Twp-component signaling: an archetype system that can function non-canonically. *EcoSalPlus* 9, 1–31. doi: 10.1128/ecosalplus.ESP-0001-2019

Kimkes, T. E. P., and Heinemann, M. (2018). Reassessing the role of the *Escherichia coli* CpxAR system in sensing surface contact. *PLoS ONE* 13:e0207181. doi: 10.1371/journal.pone.0207181

Kimkes, T. E. P., and Heinemann, M. (2020). How bacteria recognise and respond to surface contact. *FEMS Microbiol. Rev.* 44, 106–122. doi: 10.1093/femsre/fuz029

Koch, A. L., Higgins, M. L., and Doyle, R. J. (1982). The role of surface stress in the morphology of microbes. *J. Gen. Microbiol.* 128, 927–945. doi: 10.1099/00221287-128-5-927

Konovalova, A., Perlman, D. H., Cowles, C. E., and Silhavy, T. J. (2014). Transmembrane domain of surface-exposed outer membrane lipoprotein RcsF is threaded through the lumen of beta-barrel proteins. *Proc. Natl. Acad. Sci. U.S.A.* 111, E4350–E4358. doi: 10.1073/pnas.1417138111

Kung, C., Martinac, B., and Sukharev, S. (2010). Mechanosensitive channels in microbes. *Annu. Rev. Microbiol.* 64, 313–329. doi: 10.1146/annurev.micro.112408.134106

Lee, A. K., Detweiler, C. S., and Falkow, S. (2000). OmpR regulates the two-component system SsrA-ssrB in salmonella pathogenicity island 2. *J. Bacteriol.* 182, 771–781. doi: 10.1128/JB.182.3.771-781.2000

Lee, Y. Y., and Belas, R. (2015). Loss of FliL alters proteus mirabilis surface sensing and temperature-dependent swarming. *J. Bacteriol.* 197, 159–173. doi: 10.1128/JB.02235-14

Lele, P. P., Hosu, B. G., and Berg, H. C. (2013). Dynamics of mechanosensing in the bacterial flagellar motor. *Proc. Natl. Acad. Sci. U.S.A.* 110: 11839–11844. doi: 10.1073/pnas.1305885110

Levina, N., Totemeyer, S., Stokes, N. R., Louis, P., Jones, M. A., and Booth, I. R. (1999). Protection of *Escherichia coli* cells against extreme turgor by activation of MscS and MscL mechanosensitive channels: identification of genes required for MscS activity. *EMBO J.* 18: 1730–1737. doi: 10.1093/emboj/18.7.1730

Liew, A. T. F., Foo, Y. H., Gao, Y., Zangoui, P., Singh, M. K., Gulvady, R., et al. (2019). Single cell, super-resolution imaging reveals an acid pH-dependent conformational switch in SsrB regulates *SPI*-2. Elife 8:e51912. doi: 10.7554/eLife.45311.043

McCarter, L., Hilmen, M., and Silverman, M. (1988). Flagellar dynamometer controls swarmer cell differentiation of *V. parahaemolyticus*. *Cell* 54, 345–351. doi: 10.1016/0092-8674(88)90197-3

Mularski, A., Wilksch, J. J., Wang, H., Hossain, M. A., Wade, J. D., Separovic, F., et al. (2015). Atomic force microscopy reveals the mechanobiology of lytic peptide action on bacteria. *Langmuir* 31, 6164–6171. doi: 10.1021/acs.langmuir.5b01011

Nath, A., Atkins, W. M., and Sligar, S. G. (2007). Applications of phospholipid bilayer nanodiscs in the study of membranes and membrane proteins. *Biochemistry* 46, 2059–2069. doi: 10.1021/bi602371n

Nomura, T., Cranfield, C. G., Deplazes, E., Owen, D. M., Macmillan, A., Battle, A. R., et al. (2012). Differential effects of lipids and lyso-lipids on the mechanosensitivity of the mechanosensitive channels MscL and MscS. *Proc. Natl. Acad. Sci. U.S.A.* 109, 8770–8775. doi: 10.1073/pnas.1200051109

O'Connor, J. R., Kuwada, N. J., Huangyutitham, V., Wiggins, P. A., and Harwood, C. S. (2012). Surface sensing and lateral subcellular localization of WspA, the receptor in a chemosensory-like system leading to c-di-GMP production. *Mol. Microbiol.* 86, 720–729. doi: 10.1111/mmi.12013

Otto, K., Norbeck, J., Larsson, T., Karlsson, K. A., and Hermansson, M. (2001). Adhesion of type 1-fimbriated *Escherichia coli* to abiotic surfaces leads to altered composition of outer membrane proteins. *J. Bacteriol.* 183, 2445–2453. doi: 10.1128/JB.183.8.2445-2453.2001

Otto, K., and Silhavy, T. J. (2002). Surface sensing and adhesion of *Escherichia coli* controlled by the Cpx-signaling pathway. *Proc. Natl. Acad. Sci. USA.* 99, 2287–2292. doi: 10.1073/pnas.042521699

Pages, J. M., and Lazdunski, C. (1982). Transcriptional regulation of ompF and lamB genetic expression by local anesthetics. *FEMS Microbiol. Lett.* 15, 153–157. doi: 10.1111/j.1574-6968.1982.tb00058.x

Papahadjopoulos, D. (1972). Studies on the mechanism of action of local anesthetics with phospholipid model membranes. *Biochim. Biophys. Acta* 265, 169–186. doi: 10.1016/0304-4157(72)90001-9

Perozo, E., Kloda, A., Cortes, D. M., and Martinac, B. (2002). Physical principles underlying the transduction of bilayer deformation forces during mechanosensitive channel gating. *Nat. Struct. Biol.* 9, 696–703. doi: 10.1038/nsb827

Rampersaud, A., Harlocker, S. L., and Inouye, M. (1994). The OmpR protein of *Escherichia coli* binds to sites in the *ompF* promoter region in a hierarchical manner determined by its degree of phosphorylation. *J. Biol. Chem.* 269, 12559–12566. doi: 10.1016/S0021-9258(18)99912-6

Rampersaud, A., and Inouye, M. (1991). Procaine, a local anesthetic, signals through the EnvZ receptor to change the DNA binding affinity of the transcriptional activator protein OmpR. *J. Bacteriol.* 173, 6882–6888. doi: 10.1128/jb.173.21.6882-6888.1991

Sanfilippo, J. E., Lorestani, A., Koch, M. D., Bratton, B. P., Siryaporn, A., Stone, H. A., et al. (2019). Microfluidic-based transcriptomics reveal force-independent bacterial rheosensing. *Nat. Microbiol.* 4, 1274–1281. doi: 10.1038/s41564-019-0455-0

Sauer, M. M., Jakob, R. P., Eras, J., Baday, S., Eris, D., Navarra, G., et al. (2016). Catch-bond mechanism of the bacterial adhesin FimH. *Nat. Commun.* 7:10738. doi: 10.1038/ncomms10738

Segrest, J. P., Jackson, R. L., Morrisett, J. D., and Gotto, A. M. Jr. (1974). A molecular theory of lipid-protein interactions in the plasma lipoproteins. *FEBS Lett.* 38:247–258. doi: 10.1016/0014-5793(74)80064-5

Soleimanpour, S., Colom, A., Derivery, E., Gonzalez-Gaitan, M., Roux, A., Sakai, N., et al. (2016). Headgroup engineering in mechanosensitive membrane probes. *Chem. Commun.* 52, 14450–14453. doi: 10.1039/C6CC08771J

Stock, J. B., Ninfa, A. J., and Stock, A. M. (1989). Protein phosphorylation and regulation of adaptive responses in bacteria. *Microbiol. Rev.* 53, 450–490. doi: 10.1128/MMBR.53.4.450-490.1989

Sun, X., Weinlandt, W. D., Patel, H., Wu, M., and Hernandez, C. J. (2014). A microfluidic platform for profiling biomechanical properties of bacteria. *Lab Chip* 14, 2491–2498. doi: 10.1039/C3LC51428E

Tanaka, T., Saha, S. K., Tomomori, C., Ishima, R., Liu, D., Tong, K. I., et al. (1998). NMR structure of the histidine kinase domain of the E. *coli* osmosensor EnvZ. *Nature* 396, 88–92. doi: 10.1038/23968

Taylor, R. K., Hall, M. N., and Silhavy, T. J. (1983). Isolation and characterization of mutations altering expression of the major outer membrane porin proteins using the local anaesthetic procaine. *J. Mol. Biol.* 166, 273–282. doi: 10.1016/S0022-2836(83)80085-0

Thomas, W. E. (2009). Mechanochemistry of receptor-ligand bonds. *Curr. Opin. Struct. Biol.* 19, 50–55. doi: 10.1016/j.sbi.2008.12.006

Tipping, M. J., Delalez, N. J., Lim, R., Berry, R. M., and Armitage, J. P. (2013). Load-dependent assembly of the bacterial flagellar motor. *MBio* 4, e00551–13. doi: 10.1128/mBio.00551-13

Tuson, H. H., Auer, G. K., Renner, L. D., Hasebe, M., Tropini, C., Salick, M., et al. (2012). Measuring the stiffness of bacterial cells from growth rates in hydrogels of tunable elasticity. *Mol. Microbiol.* 84, 874–891. doi: 10.1111/j.1365-2958.2012.08063.x

Vaknin, A., and Berg, H. C. (2006). Osmotic stress mechanically perturbs chemoreceptors in *Escherichia coli*. *Proc. Natl. Acad. Sci. U.S.A.* 103, 592–596. doi: 10.1073/pnas.0510047103

Wang, L. C., Morgan, L. K., Godakumbura, P., Kenney, L. J., and Anand, G. S. (2012). The inner membrane histidine kinase EnvZ senses osmolality via helix-coil transitions in the cytoplasm. *EMBO J.* 31, 2648–2659. doi: 10.1038/emboj.2012.99

Wang, S., Arellano-Santoyo, H., Combs, P. A., and Shaevitz, J. W. (2010). Actin-like cytoskeleton filaments contribute to cell mechanics in bacteria. *Proc. Natl. Acad. Sci. U.S.A.* 107, 9182–9185. doi: 10.1073/pnas.0911517107

Yao, X., Jericho, M., Pink, D., and Beveridge, T. (1999). Thickness and elasticity of gram-negative murein sacculi measured by atomic force microscopy. *J. Bacteriol.* 181, 6865–6875. doi: 10.1128/JB.181.22.6865-6875.1999

Zhang, J. P., and Normark, S. (1996). Induction of gene expression in *Escherichia coli* after pilus-mediated adherence. *Science* 273, 1234–1236. doi: 10.1126/science.273.5279.1234

Conflict of Interest: The author declares that the research was conducted in the absence of any commercial or financial relationships that could be construed as a potential conflict of interest.

frontiers in Microbiology

ORIGINAL RESEARCH
published: 01 October 2021
doi: 10.3389/fmicb.2021.692707

BB0259 Encompasses a Peptidoglycan Lytic Enzyme Function for Proper Assembly of Periplasmic Flagella in *Borrelia burgdorferi*

Hui Xu[1], Bo Hu[2], David A. Flesher[3,4], Jun Liu[3,5] and Md A. Motaleb[1]**

[1]Department of Microbiology and Immunology, Brody School of Medicine, East Carolina University, Greenville, NC, United States, [2]Department of Microbiology and Molecular Genetics, McGovern Medical School, The University of Texas Health Science Center at Houston, Houston, TX, United States, [3]Department of Microbial Pathogenesis, Yale University School of Medicine, New Haven, CT, United States, [4]Department of Molecular Biophysics and Biochemistry, Yale University, New Haven, CT, United States, [5]Microbial Sciences Institute, Yale University, West Haven, CT, United States

OPEN ACCESS

Edited by:
Matthew Arthur Baker, University of New South Wales, Australia

Reviewed by:
Eli Cohen, Imperial College London, United Kingdom
Steven Johnson, National Cancer Institute (NCI), Frederick, United States

***Correspondence:**
Md A. Motaleb
motalebm@ecu.edu
Jun Liu
jliu@yale.edu

Specialty section:
This article was submitted to Microbial Physiology and Metabolism, a section of the journal Frontiers in Microbiology

Received: *09 April 2021*
Accepted: *19 August 2021*
Published: *01 October 2021*

Citation:
Xu H, Hu B, Flesher DA, Liu J and Motaleb MA (2021) BB0259 Encompasses a Peptidoglycan Lytic Enzyme Function for Proper Assembly of Periplasmic Flagella in Borrelia burgdorferi. Front. Microbiol. 12:692707. doi: 10.3389/fmicb.2021.692707

Assembly of the bacterial flagellar rod, hook, and filament requires penetration through the peptidoglycan (PG) sacculus and outer membrane. In most β- and γ-proteobacteria, the protein FlgJ has two functional domains that enable PG hydrolyzing activity to create pores, facilitating proper assembly of the flagellar rod. However, two distinct proteins performing the same functions as the dual-domain FlgJ are proposed in δ- and ε-proteobacteria as well as spirochetes. The Lyme disease spirochete *Borrelia burgdorferi* genome possesses a FlgJ and a PG lytic SLT enzyme protein homolog (BB0259). FlgJ in *B. burgdorferi* is crucial for flagellar hook and filament assembly but not for the proper rod assembly reported in other bacteria. However, BB0259 has never been characterized. Here, we use cryo-electron tomography to visualize periplasmic flagella in different *bb0259* mutant strains and provide evidence that the E580 residue of BB0259 is essential for PG-hydrolyzing activity. Without the enzyme activity, the flagellar hook fails to penetrate through the pores in the cell wall to complete assembly of an intact periplasmic flagellum. Given that FlgJ and BB0259 interact with each other, they likely coordinate the penetration through the PG sacculus and assembly of a functional flagellum in *B. burgdorferi* and other spirochetes. Because of its role, we renamed BB0259 as flagellar-specific lytic transglycosylase or LTase^{Bb}.

Keywords: Lyme disease, flagella, peptidoglycan hydrolases, cryo-elecron tomography, spirochete, *Borrelia*

INTRODUCTION

In most bacterial species, the flagellum is a rotary nanomachine framed in a supramolecular structure that initiates assembly from the cell envelope and extends into the extracellular space. However, in motile spirochetes, this migratory organelle resides in the periplasmic space and is therefore called the periplasmic flagellum (Wolgemuth et al., 2006; Charon et al., 2009, 2012). Despite differences in location, the external flagella found in the model organisms *Escherichia coli* and *Salmonella enterica* serovar Typhimurium share a remarkably high degree of similarity with respect to overall structure, as the key components are conserved among the external flagella and the periplasmic flagella of spirochetes (Liu et al., 2009; Chen et al.,

2011; Zhao et al., 2013; Terashima et al., 2017; Carroll and Liu, 2020). The supramolecular structure is composed of more than 25 distinct protein subunits and self-assembles to final lengths of up to 20 μm in the model organisms. The individual flagellum consists of three major substructures: a basal body, hook, and filament (reviewed in Nakamura and Minamino, 2019; Carroll and Liu, 2020). Synthesis of the flagellum begins with the assembly of a basal body composed of an MS ring embedded in the cell membrane and a rod. The MS ring is comprised of multiple copies of FliF and acts as a platform for assembly of the rod, C-ring, torque-generating stator, and flagellum-specific type III secretion system (fT3SS). The rod is composed of five proteins, FliE, FlgB, FlgC, FlhO/FlgF, and FlgG. These rod proteins are transported from the cytoplasm to the periplasmic space *via* the fT3SS (Saijo-Hamano et al., 2019) and then assemble onto the MS ring—in an ordered fashion from the proximal rod to the distal rod (Zhao et al., 2013; Terashima et al., 2017; Carroll and Liu, 2020). The distal rod serves as the template for subsequent assembly of the P-ring and hook (*B. burgdorferi* lacks the L-ring; Zhao et al., 2013). The filaments are subsequently polymerized onto the hook to complete assembly of a flagellum. Hook and filament assembly is mediated by the hook cap FlgD and filament cap FliD protein, respectively (Homma and Iino, 1985; Ohnishi et al., 1994; Yonekura et al., 2000).

In order for the assembly of the rod with 30 nm × 4 nm to penetrate the outer membrane in *E. coli* or *S. enterica*, a hole must be created in the peptidoglycan sacculus, as its mesh diameter is narrower than 2 nm (Demchick and Koch, 1996; Herlihey et al., 2014). This PG hydrolytic activity is accomplished by a dual-domain protein FlgJ of *S. enterica* and *E. coli*. FlgJ is composed of an N-terminal scaffolding domain required for polymerization of the distal rod and a C-terminal domain required to form a hole in the PG sacculus. The C-terminal domain of FlgJ proteins belongs to the glycoside hydrolase family in which these β-N-acetyl-glucosaminidases cleave the β-1,4 glycosidic linkage between the N-acetylglucosamine and N-acetylmuramic acid residues of bacterial cell wall peptidoglycan, with Glu184 and Glu223 serving as the catalytic residues (Nambu et al., 1999; Herlihey et al., 2014; Zaloba et al., 2016).

Once the enzyme has made a hole in the cell wall, FlgG proteins are secreted and assemble in two stacks to make an 11 nm-long rod just underneath the FlgJ rod cap, thereby spanning the remaining distance between the cell wall and outer membrane (Jones and Macnab, 1990; Cohen and Hughes, 2014). The ejection of the FlgJ rod cap allows the FlgD hook cap to assemble at the tip of the rod and results in the transition from rod to hook polymerization (Nambu et al., 1999; Cohen and Hughes, 2014). While dual-domain FlgJ proteins are found in most β- and γ-proteobacteria, two distinct proteins performing similar functions as the dual-domain FlgJ are reported in diverse bacterial genomes, including δ- and ε-proteobacteria as well as spirochete species *B. burgdorferi*, *Leptospira interrogans*, and *Treponema* (Nambu et al., 1999, 2006; Gonzalez-Pedrajo et al., 2002; Zaloba et al., 2016; Garcia-Ramos et al., 2018). Moreover, the single-domain flagellar scaffolding protein FlgJ is reported to interact with PG-lytic enzymes, such as soluble lytic transglycosylases (SLT) proteins (Garcia-Ramos et al., 2018). These specialized cell wall-degrading enzymes allow the efficient assembly and anchoring of supramolecular structures in the cell envelope. The SLTs represent one class of autolysins that act like a lysozyme (muramidase) to cleave the β-(1→4) glycosidic linkage between N-acetylmuramyl and N-acetylglucosaminyl residues of cell wall peptidoglycan. Unlike lysozymes, however, SLTs are not hydrolases but cleave the β-glycosidic linkages, with simultaneous production of 1,6-anhydromuramyl residues (Holtje et al., 1975; van Asselt et al., 1999; Blackburn and Clarke, 2001; Koraimann, 2003).

As *B. burgdorferi* FlgJ is reported to be a single-domain protein that lacks a PG-hydrolyzing enzymatic domain, we sought to investigate the genome to identify a protein that harbors this domain (Zhang et al., 2012). BB0531 and BB0259 identified in this communication are both predicted to possess PG-hydrolyzing enzyme activities. BB0531 possesses a glucosaminidase domain; however, subsequent analysis indicates that this protein is not involved in flagellar pore-forming activities. BB0259 possesses an SLT homolog at its C-terminal domain, and further analyses indicate that FlgJ specifically interacts with BB0259. Because of its apparent flagellar specific peptidoglycan lytic enzyme function in the spirochete, BB0259 is renamed as LTase^{Bb}. FlgJ and LTase^{Bb} appear to function distinctively compared to their counterparts from other bacteria. Our model describes how *B. burgdorferi* FlgJ and LTase^{Bb} work synchronously to form a functional periplasmic flagellum.

MATERIALS AND METHODS

Bacterial Strains and Growth Conditions

Borrelia burgdorferi B31-A is a high-passage noninfectious clone used as the wild-type (WT) strain (Bono et al., 2000; Tilly et al., 2001). The isogenic *bb0259* mutant and complemented strains were constructed as described below. All *B. burgdorferi* strains were grown in Barbour–Stoenner–Kelly II (BSK-II) liquid medium or on soft agarose plates at 35°C in the presence of 2.5% CO_2 (Motaleb et al., 2007). Antibiotics, when needed, were supplied in BSK-II medium at proper concentrations: 200 μg/ml kanamycin and/or 40 μg/ml gentamycin. All *Escherichia coli* strains were cultured in Luria-Bertani (LB) liquid medium or on LB agar plates (Bertani, 1951, 2004). When required, 100 μg/ml ampicillin or 4 μg/ml gentamycin was supplemented into the LB medium.

Bioinformatics

Basic local alignment search tool (BLAST) was used to determine protein homologs from the sequence database (Altschul et al., 1990, 1997). For the BLAST analysis, a significant homolog is determined based on their E-value [the lower an E-value (the closer it is to zero), the more significant the score is]. Signal peptide was predicted using SignalP 5.0 (Almagro Armenteros et al., 2019) and Phobius

(Kall et al., 2004, 2005, 2007). Analysis of bacterial lipoprotein was performed using DOLOP (Madan Babu and Sankaran, 2002; Babu et al., 2006). Clustal Omega was utilized to align multiple amino acid sequences (Sievers et al., 2011). FFAS server was used as described elsewhere.

Overexpression and Purification of Recombinant Proteins in *Escherichia coli*

Multiple attempts to express soluble *B. burgdorferi* BB0259 with variable lengths using short-affinity tags (His6 or Strep) failed, as all these recombinant BB0259 proteins with short affinity tags formed inclusion bodies in the *E. coli* host. In order to produce soluble recombinant BB0259 protein, a DNA fragment harboring the BB0259 open reading frame (ORF) without signal peptide (1-49 aa) was polymerase chain reaction (PCR)-amplified from chromosomal DNA of *B. burgdorferi* B31-A using the primers PF rBB0259-BamHI (GGATCC TGGTTATGGAATTTTGATTATAC) and PR rBB0259-PstI (CTGCAGTTAATTTTTGGGGAATTCGCCC; restriction sites are underlined) and cloned into the pMAL c5x (NEB Inc.) through *Bam*HI and *Pst*I restriction sites to produce maltose binding protein (MBP)-tagged BB0259. Similarly, the 1xFLAG (DYKDDDDK) tagged FlgJ with gene locus number (BB0771a, also named BB0858) was constructed for far-western or affinity blotting. A DNA fragment of full-length *flgJ* fused with 1xFLAG tag coding sequence (GACTACAAAGACGATGACGACAAG) at C-terminus was amplified by PCR with primers PF MBPFlgJBamHI (CGTCGACGGATCCGAAACCAAAATTAAT TCACAAAATC) and PR MBPFlgJPstI (TAATTACCTGCAG TTACTTGTCGTCATCGTCTTTGTAGTCTTTACTTTTTTGTA ATTGATTGTA) and cloned into the pMAL c5x using *Bam*HI and *Pst*I restriction sites. MBP tagged FlaB (BB0147), FlgE (BB0283), FlgD (BB0284), FlgG (BB0774), and FlgL (BB0182) were also prepared to determine protein–protein interactions. The coding regions of FlaB, FlgE, FlgG, and FlgL were amplified by PCR with primers PF MBPflaB_NotI (GTCCATGGGCGG CCGCATGATTATCAATCATAATACATC) and PR MBPflaB_ BamHI (GGAATTCGGATCCTTATCTAAGCAATGACAAAA CATATTG), PF MBPflgE_NotI (GTCCATGGGCGGCCGC ATGAT GAGGTCTTTATATTCTGG) and PR MBPflgE_BamHI (GGAATTCGGATCCTTAATTTTTCAATCTTACAAGTTCTTG), PF MBPflgG_NotI (GTCCA TGGGCG GCCGCATGATGAGA GCATTATGGACAGC) and PR MBPflgG_BamHI (GGAATTC GGATCC TTATTGCCTTTTTAAGTTATTTGC), PF MBPflgL_ NotI (GTCCATGGGCGGCCGCATGATAAATAGAGTAAGTCA TCC) and PR MBPflgL_BamHI (GGAATTCGGATCCTTATTT TATAAAATCTAATAAAGTCG), respectively, and cloned into the pMAL c5x (NEB Inc.) using *Not*I and *Bam*HI restriction sites. Recombinant FlgD construct was similarly prepared using *Nde*I-*Nco*I restriction enzymes with primers PF MBPflgD_NdeI (GCTGGACGACATATGAATAAAATAAACGGTGTTGAAAATG) and PR MBPflgD_NcoI (TGCTGGGCACCATGG TTATTCC TCCAAACCTACCGATAAT). All *E. coli* DH5α strains carrying the pMAL c5x constructs for expressing BB0259, FlaB, FlgE, FlgG, FlgL, FlgD, 1xFLAG tagged FlgJ were induced with 0.25 mM Isopropyl β-D-1-thiogalactopyranoside (IPTG) at room temperature, and purifications of recombinant proteins were performed with amylose resin (NEB Inc.) according to the manufacturer's protocol.

SDS-PAGE, Immunoblot, and Affinity Blotting

Sodium dodecyl sulfate–polyacrylamide gel electrophoresis (SDS-PAGE) was carried out as mentioned previously (Motaleb et al., 2000). Exponentially growing *B. burgdorferi* cells were harvested and washed with phosphate-buffered saline (PBS) and resuspended in the same buffer to process the preparation of cell lysate for SDS-PAGE. Immunoblotting was performed with *B. burgdorferi* FlaB, FlgE, MotB, FliL, and DnaK-specific antibodies (Motaleb et al., 2000, 2011; Sal et al., 2008; Sultan et al., 2015) and Pierce™ ECL or ECL 2 substrate (Thermo Fisher Scientific Inc.). Concentration of the proteins was determined using a Bio-Rad protein assay kit with bovine serum albumin (BSA) as the standard. Unless specified, approximately 10 μg of cell lysates was subjected to SDS-PAGE.

Far-western or affinity blotting assay with recombinant proteins was performed as described previously (Toker and Macnab, 1997; Kariu et al., 2015; Moon et al., 2016, 2018; Xu et al., 2019). Briefly, 1 μg purified recombinant proteins was subjected to SDS-PAGE and Coomassie blue staining or transferred to polyvinylidene difluoride (PVDF) membrane. The PVDF membranes were blocked in the blocking solution (5% BSA, 10 mM Tris, 150 mM NaCl and 0.3% Tween 20, pH 7.4) with gentle shaking for 4 to 6 h at room temperature, and then the membranes were incubated with or without the purified FLAG-FlgJ protein at the concentration 2 μg/ml in blocking solution overnight. The membranes were washed 3 times with the washing buffer (10 mM Tris, 150 mM NaCl and 0.3% Tween 20, pH 7.4) and then immunoblotted with monoclonal anti-FLAG® M2 antibody (Sigma-Aldrich Co. LLC) followed by ECL 2 detection, as mentioned above. The X-ray films were exposed to the membranes for less than a minute.

Construction of the *Borrelia burgdorferi* Mutants and Complemented Strains

Construction of the *bb0259* and *bb0531* inactivation plasmids, electroporation, and plating of *B. burgdorferi* were as described earlier (Motaleb et al., 2000; Sultan et al., 2010, 2013; Moon et al., 2016; Xu et al., 2017). *bb0259* was inactivated by P_{flgB}-kanamycin resistance cassette (P_{flgB}-*aph1*), which possessed the *flgB* promoter driving kanamycin resistance gene (Ge et al., 1997; Bono et al., 2000; Li et al., 2010; Zhang et al., 2012; Moon et al., 2016; Xu et al., 2017, 2019). In short, DNA fragment including upstream 394-bp region of *bb0259*, *bb0259* containing five *Hind*III sites, and downstream 324-bp region of *bb0259* was amplified by PCR from chromosomal DNA of wild-type *B. burgdorferi* strain B31-A through Expand™ High Fidelity PCR System (Sigma-Aldrich Inc.) using primers BB0259-KO-F (GTTGAGTATATTGACGAGAAG) and BB0259-KO-R (TCCCAACAA CTCCGGTAACA), which was further TA cloned into pGEM-T Easy (Promega Inc.), yielding pGEM-T Easy::*bb0259*. P_{flgB}-*Kan* was introduced into pGEM-T Easy::*bb0259*

through the first and last *HindIII* sites located within *bb0259* gene, creating pGEM-T Easy::*bb0259KO-*P_{flgB}*-Kan*, of which the direction of transcription of P_{flgB}*-Kan* was confirmed to be the same as that of *bb0259*. Plasmid pGEM-T Easy::*bb0259KO-*P_{flgB}*-Kan* was linearized by *Not*I restriction digestion and electroporated into competent *B. burgdorferi* B31-A cells to create Δ*bb0259* mutant cells. *bb0531* mutant was similarly prepared using a promoter-less kanamycin cassette (*Pl-Kan*), as described (Sultan et al., 2010). Kanamycin-resistant transformants were screened by PCR to confirm the genotypes of the mutants.

The *bb0259* mutant was complemented *in trans* using the *B. burgdorferi-E. coli* shuttle vector pBSV2G (Elias et al., 2003). In short, *bb0259* was PCR amplified using primers BB0259 Comp F (GATCCATATGTTTAATAGAAGTTCTTG; underlined sequence is *NdeI* site) and BB0259 Comp R (CTGCAGTTAATTT TTGGGGAATTCGCCC) and ligated into pGEM-T Easy, yielding plasmid *bb0259*ORF-Easy. DNA fragment containing *bb0259* ORF was then released using *NdeI* restriction digestion from *bb0259*ORF-Easy, and further ligated into *NdeI*-treated P_{flgB}-motB-Easy vector (Sultan et al., 2015), creating plasmid P_{flgB}-bb0259-Easy. Finally, this plasmid was digested with *NotI* and cloned into the same restriction site of the shuttle vector pBSV2G, generating pBSV2G::P_{flgB}*-bb0259*. The newly constructed shuttle vector pBSV2G::P_{flgB}*-bb0259* was electroporated into the Δ*bb0259* mutant cells, followed by selection with both kanamycin and gentamycin. The resistant clones, namely *bb0259*^{com}, were analyzed by PCR for confirmation of the presence of plasmid pBSV2G::P_{flgB}*-bb0259*.

Borrelia burgdorferi bb0259-E580Q (E glutamate to Q glutamine) and *bb0259*-D606N (D aspartate to N asparagine) point-mutated strains were constructed through allelic exchange mutagenesis (Yang et al., 2003). Simply, using B31-A chromosomal DNA as the template, the left arm (882 bp, partial *bb0259* gene), promoter-less kanamycin cassette (*Pl-Kan*; 846 bp), and right arm (564 bp, including 88 bp leftover from *bb0259* gene for potential ribosome binding and 476 bp of partial *bb0258* gene) were PCR amplified, respectively, using primer pairs P1F BB0259PointMuKOplKan (CCTAACGTAAGCGGAGAATACA AGAGTCTTTTGCATTCTG) and P1R BB0259Point MuKO plKan (TAAAATTGCTTTTAACTATTAATTTTTGGGGAATTC GCCC), P2F BB0259PointMuKOplKan (GGGCGAATTCCCC AAAAATTAATAGTTAAAAGCAATTTTA) and P2R BB0259 PointMuKOplKan (CTTTTCATACAAAGCATCATTTAGAAA AACTCATCGAGC), P3F BB0259PointMuKOplKan (GCTCGA TGAGTTTTTCTAAATGATGCTTTGTATGAAAAG) and P3R BB0259PointMuKOplKan (CCCAAGCCTTGCATCAGCCCCA TAAAAATTCCTGCTAAC). Through overlapping PCR, *Pl-Kan* was inserted between the left arm and right arm, and further cloned into pGEM-T Easy, creating vector pGEM-T Easy:: bb0259PointMuKO-Pl-Kan. Using pGEM-T Easy::bb0259 PointMuKO-Pl-Kan as the template, point mutations of BB0 259E580Q were introduced by QuikChange II Site-Directed Mutagenesis Kit (Agilent Technologies Inc.) using the primers PF BB0259E580Q (CTTTAAT AAAAGCA**CAA** AGTAG CTTTG AAAAAAATG) and PR BB0259E580Q (CATTTTTTTCAA AGCTACT**TTG**T GCTTTTATTAAAG; bold and underlined sequences indicate the point mutation), to create pGEM-T Easy::bb0259E580QKO-Pl-Kan. Similarly, through site-directed mutagenesis pGEM-T Easy::bb0259D606NKO-Pl-Kan was generated with primers PF BB0259D606N (GCCATCAACAGC AAAT**AAT**ATTTCTAAA GAACTTAAG) and PR BB0259D606N (CTTAAGTTCTTTA GAAAT**ATT**ATTTGC TGTTGATGGC). These two vectors were linearized by *Not*I digestion and electroporated into the competent *B. burgdorferi* B31 A cells to generate *bb0259*-E590Q and *bb0259*-D606N mutant strains, of which the point mutations of *bb0259* were further verified by sequencing.

Dark-Field Microscopy and Swarm Plate Motility Assays

Exponentially growing *B. burgdorferi* cells were observed using a Zeiss Axio Imager M1 dark-field microscope to determine bacterial morphology and motility. To evaluate the motility of *B. burgdorferi* cells, swarm plate assays were performed following our well-established protocol (Motaleb et al., 2000, 2007, 2011).

Cryo-ET Analysis of *bb0259* and *bb0531* Mutant Cells

Frozen-hydrated *B. burgdorferi* specimens were prepared as described previously (Zhao et al., 2013). In short, the bacterial culture was centrifuged at 5,000 × *g* for 5 min, and the resulting pellets were suspended in PBS to achieve a cell concentration ~1×10^8/ml. After adding 10-nm gold marker solution, 5 μl of the cell suspension was placed on freshly glow-discharged holey carbon grid (Quantifoil Cu R2/2, 200 mesh) for 25 s. The grids were blotted with filter paper for 3 to 5 s and rapidly frozen in liquid ethane, using a homemade plunger apparatus as described previously (Zhao et al., 2013).

The Δ*bb0531*, Δ*bb0259*, and complemented *bb0259*^{com} strains were imaged at −170°C using a Polara G2 electron microscope (FEI Company) equipped with a field emission gun and a 4,096-by-4,096 charge-coupled device (16-megapixel) camera (TVIPS Gmbh, Germany). The microscope was operated at 300 kV with a magnification of ×31,000, resulting in an effective pixel size of 5.7 Å. Using the FEI batch tomography program, low-dose single-axis tilt series were collected from each bacterium at ~8 μm defocus with a cumulative dose of ~100 $e^-/Å^2$ distributed over 65 images. In total, 80 tomographic reconstructions of Δ*bb0259* cell tips and 10 tomographic reconstructions of complemented *bb0259* cells were generated.

The *bb0259* point mutants (*bb0259*-E580Q and *bb0259*-D606N) were imaged with Krios electron microscope (Thermo Fisher) with a field emission gun, a volta phase plate, and a direct electron detector (Gatan K3 Summit). SerialEM was used to collect tilt series at focus. A total dose of 55 $e^-/Å^2$ is distributed among 35 tilt images covering angles from −51° to +51° at tilt steps of 3°. For every single tilt series collection, dose-fractionated mode was used to generate 11 frames per projection image. Collected dose-fractionated data were first subjected to the MotionCor2 to generate drift-corrected files (Zheng et al., 2017). IMOD software was used to align the tilt series and to generate tomograms (Kremer et al., 1996).

In total, 240 tomographic reconstructions of *bb0259*-E580Q cells and 10 tomographic reconstructions of *bb0259*-D606N cells were generated.

Subtomogram Averaging

A total of 646 flagellar motor subtomograms were picked from Δ*bb0259* tomograms. The initial orientation of each particle was manually estimated by the C-ring and hook. The subtomograms were used to generate the averaged structure as described previously (Zhao et al., 2013).

Three-Dimensional Visualization

The software package EMAN2 was used for 3D segmentation (Chen et al., 2017). Segmentation of tomograms was performed using supervised machine learning to segment features of interest. The outer membrane, inner membrane, peptidoglycan layer, and flagella were segmented in this manner and manually cleaned using ChimeraX (Goddard et al., 2018). An existing motor model derived from subtomogram averaging was manually inserted into the segmented model. ChimeraX was used for visualization.

RESULTS

An Open Reading Frame Encompasses a Peptidoglycan-Hydrolyzing Enzymatic Domain

The single-domain FlgJ of *B. burgdorferi* plays roles in hook and filament assembly but not in rod assembly in *S. enterica* (Nambu et al., 1999; Cohen and Hughes, 2014; Zaloba et al., 2016), as *flgJ* mutant cells possess an intact rod and P-ring but form partial hook and filament structures (Zhang et al., 2012). Given that an enzymatic activity is required for pore formation in the PG layer for assembly of the flagellar hook and filament, and that *B. burgdorferi* FlgJ lacks a peptidoglycan-hydrolyzing enzyme domain, we sought to determine an ORF containing an enzymatic domain in the Lyme disease spirochetal genome. Using the *S. enterica* FlgJ with GenBank accession number NP_460153 as a query in BLAST search, we found no significant homologs in *B. burgdorferi* (not shown; Nambu et al., 1999; Hirano et al., 2001; Cohen and Hughes, 2014). However, using the FFAS server,[1] BB0531 was identified as the only significant homolog of FlgJ (homology score −41.70; a lower FFAS score indicates higher confidence of the prediction; Rychlewski et al., 2000; Jaroszewski et al., 2005, 2011). BB0531 is annotated as a hypothetical protein with unknown function in the *B. burgdorferi* genome; however, it is predicted to possess a mannosyl-glycoprotein endo-β-N-acetylglucosaminidase domain responsible for peptidoglycan remodeling or hydrolyzing activity (Pfam: PF01832). BB0531 shares only 15% amino acid sequence identity with *S. enterica* FlgJ and alignment of amino acid sequences of *S. enterica* FlgJ and BB0531 from FFAS shows that the catalytic residues of FlgJ are not well conserved in BB0531 leading us to speculate that BB0531 is not involved in peptidoglycan hydrolyzing activity for flagellar penetration (not shown).

Because *B. burgdorferi* lacks a significant homolog of *S. enterica* FlgJ, we used the model organism's SLT domain as a query in the BLAST search and identified BB0259 as a homolog in *B. burgdorferi*. BB0259 shares 35–41% amino acid sequence identity with significant E-value at the SLT domain (**Figure 1**; Pfam: PF01464; Thunnissen et al., 1994; van Asselt et al., 1999; Koraimann, 2003). Importantly, the motifs and amino acid residues required for peptidoglycan lytic enzymatic activity are highly conserved in BB0259 (**Figure 1**). BB0259 possesses a signal sequence (1-24 aa) with lipobox consensus residues LVSC, an unknown domain with no homologs (25-558 aa), and an SLT domain at the C-terminal region (559-717 aa; **Figure 1**). The presence of these features led us to hypothesize that BB0259 is secreted into the periplasmic space using its signal sequence to create pores in the PG layer, thereby completing assembly of the flagellar hook–filament.

Mutants in *bb0259*, but Not *bb0531*, Exhibit Defective Motility and Altered Morphology

Completion of the appropriately assembled flagellar rod, hook, and filament is critical for the spirochete motility and morphology (Motaleb et al., 2000, 2015; Sal et al., 2008; Sultan et al., 2013; Zhao et al., 2013). If the SLT domain of BB0259 or the glucosaminidase domain of BB0531 displays PG-hydrolyzing activities, which are specific for flagellar assembly, then a deletion mutant in *bb0259* or *bb0531* is expected to be unable to create pores in the PG layer, resulting in defective rod/hook/filament assembly and a motility-deficient phenotype. To test this proposition, we created deletion mutants Δ*bb0259* and Δ*bb0531* (**Supplementary Figures S1, S2, and S5**). While the Δ*bb0531* cells lack any observable phenotype with respect to motility and morphology, the Δ*bb0259* mutant cells observed under a dark-field microscope are completely non-motile (**Figure 2A** and not shown). Swarm plate motility assays also indicated that Δ*bb0259* mutant cells are deficient in swarming out from the initial site of inoculation in soft agarose plates (**Figure 2B**). Furthermore, while wild-type cells show characteristic flat-wave morphology, Δ*bb0259* mutant cells are rod-shaped (**Figure 2A**). To demonstrate that the phenotypes described here are devoid of a polar effect on downstream gene expression or a secondary mutation elsewhere in the genome, we complemented the mutant *in trans* using a shuttle vector (**Supplementary Figures S1, S2**). Complemented *bb0259* (*bb0259*^{com}) cells observed under a microscope as well as in swarm plate motility assays indicated morphology and motility phenotypes restored to wild-type level (**Figures 2A**,**B**). Furthermore, SLT proteins important for hydrolyzing the PG sacculus for flagellar insertion and subsequent assembly of an intact flagellum are reported to be secreted in the periplasm using their Sec-signal peptide (Garcia-Ramos et al., 2018). Consistent with this observation, a recent study reported that BB0259 is associated with the inner membrane (Toledo et al., 2018). To determine whether the Sec-signal sequence is required

[1]https://ffas.godziklab.org/ffas-cgi/cgi/ffas.pl

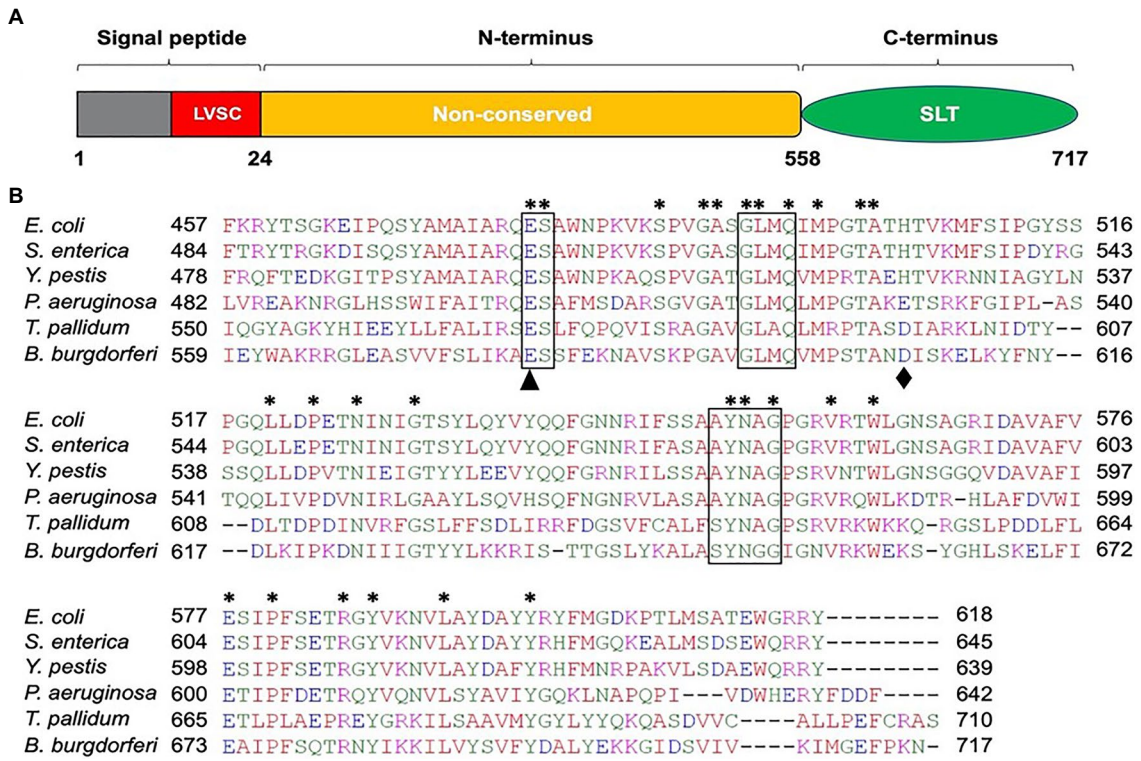

FIGURE 1 | Amino acid sequence analysis of *B. burgdorferi* BB0259 (GenBank accession no. NP_212393). **(A)** Domain architecture of BB0259. BB0259 consists of 717 amino acids and is predicted to contain a lipobox consensus sequence (LVSC) in the signal peptide region (1-24 aa) determined by DOLOP program: https://www.mrc-lmb.cam.ac.uk/genomes/dolop/analysis.shtml. BB0259 also possesses a non-conserved N-terminal domain (25-558 aa) and a conserved C-terminal soluble lytic transglycosylase (SLT) domain (559-717 aa). Diagram is not in scale. **(B)** Multiple sequence alignment of SLT domains with GenBank accession no. 1QSA_A from *E. coli*, APW71272 from *S. enterica*, ANW15826 from *Y. pestis*, AID74248 from *P. aeruginosa*, and WP_010881492 from *Treponema pallidum* using Clustal Omega program: https://www.ebi.ac.uk/Tools/msa/clustalo/. Asterisks indicate identical residues. Boxed regions denote the conserved motifs ES-GLMQ-AYNAG among the SLT-domain proteins. *S. enterica* SLT domain shares 35% identity with the SLT domain of BB0259 with E-value 6e−25. Black triangle and diamond demonstrate the catalytic (E580) and non-conserved (D606) residues, respectively.

for BB0259 proteins to be secreted in the periplasm, where they create pores in the PG sacculus for flagellar assembly and thereby provide motility to the cell, we complemented the non-motile Δ*bb0259* mutant without the signal sequence (*bb0259*Δsec). As described above, while the full-length *bb0259* was able to complement the Δ*bb0259* mutant and therefore restored the morphology and motility phenotypes (**Figures 2A**,**B**), the Sec-signal sequence-deleted variant *bb0259*Δsec was unable to restore any of the phenotypes (data not shown). These results suggest that the signal sequence is essential for BB0259 proteins to be secreted in the periplasm.

The altered motility and morphology phenotypes exhibited by the deletion mutant suggest that the rod/hook/filament structure was not properly assembled due to a lack of the SLT enzymatic activity of BB0259 that would hydrolyze the PG layer for flagellar structures to assemble through the PG sacculus and provide motility to the bacterial cell. *B. burgdorferi* cells lacking the gene-encoding filament FlaB or hook FlgE were reported to be non-motile and rod-shaped (Motaleb et al., 2000; Sal et al., 2008; Sultan et al., 2013). We therefore tested whether these gene products were synthesized in the Δ*bb0259* cells. Western blotting results (**Supplementary Figure S3**) indicate that the mutant cells synthesized very few FlaB proteins, with no effect on synthesis of the hook protein FlgE. Lack of the filaments in the Δ*bb0259* cells may thus have resulted in the motility-deficient and rod-shaped morphology (**Figures 2A**,**B**).

Glutamate E580 of BB0259 Is the Catalytic Site Residue

The SLT enzyme domain proteins possess a conserved ES-GLMQ-AYNAG motif in which the glutamate [E] residue is reported to be the catalytic residue (**Figure 1**; Thunnissen et al., 1994; van Asselt et al., 1999; Koraimann, 2003). The SLT domain identified in the C-terminal region of BB0259 possesses an E residue at position 580. To determine whether the E residue is the catalytic site, we created a point mutant in E580 of BB0259, resulting in *bb0259*-E580Q *B. burgdorferi* (**Supplementary Figures S1, S2**). Furthermore, the E223 and D248 residues of the *S. enterica* FlgJ enzymatic domain were reported to be important for PG-hydrolyzing activities (Nambu et al., 1999), and we noticed that the BB0259 SLT domain also encompasses similarly distanced E580 and D606 residues

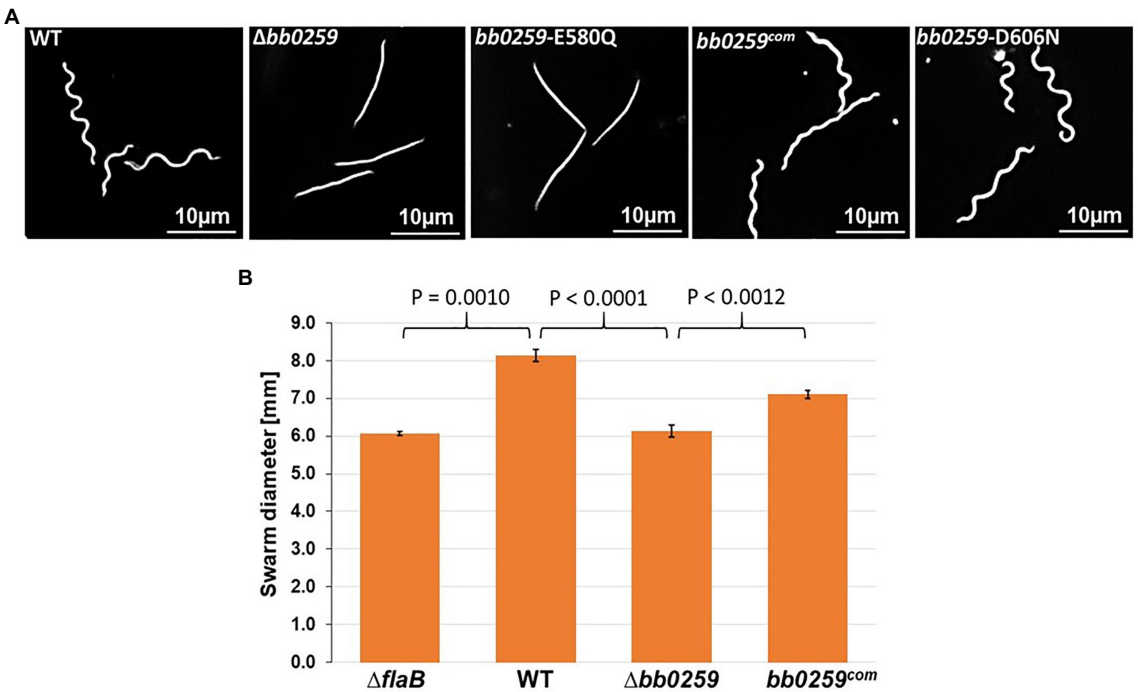

FIGURE 2 | Morphology and motility phenotypes of the *bb0259* mutant cells. **(A)** Dark-field microscopic images showing the characteristic flat-wave morphology of the WT, complemented *bb0259*^{com} and *bb0259*-D606N cells and rod-shaped morphology of the Δ*bb0259* and *bb0259*-E580Q mutants. **(B)** Average swarm diameters from three swarm plates are shown in millimeter scale. *bb0259*-E580Q and *bb0259*-D606N mutants show motility phenotypes similar to the Δ*bb0259* and WT cells, respectively, and are not shown. A non-motile flagellar filament mutant Δ*flaB* was used as a control. Bars represent mean ± standard deviation of the mean from three plates. Values of p between samples are shown at the top. A value of $p < 0.05$ was considered as significantly different.

(**Figure 1**). Even though BB0259 shares limited homology with *S. enterica* FlgJ, and E580 and D606 do not align with E223 and D248 residues of FlgJ (not shown), we created a *bb0259*-D606N *B. burgdorferi* point mutant to determine whether this non-conserved D606 residue codes for any enzyme function (**Supplementary Figures S1, S2**). The *bb0259*-E580Q point mutant *B. burgdorferi* cells exhibited phenotypes identical to those of the deletion mutant Δ*bb0259* with respect to morphology and motility, whereas the *bb0259*-D606N cells were devoid of any detectable phenotype (**Figures 2A**,**B**). These results indicate that E580 of BB0259 is the catalytic site residue required for BB0259 function, while the D606 residue is not important for PG-hydrolyzing activities.

Rod/Hook Structures of *bb0259* Mutant Cells Lie Underneath the PG Layer

The morphology and motility phenotypes of the mutant cells led us to speculate that the periplasmic flagellar rod/hook/filament is not able to assemble properly due to the lack of PG-hydrolyzing activity of the Δ*bb0259* and *bb0259*-E580Q cells. Despite using the best possible assays to determine whether BB0259 is able to hydrolyze PG, as this protein possesses an SLT domain, our numerous attempts to demonstrate such activity resulted in little success. Attempts to determine the PG-hydrolyzing enzyme assays using various published assay conditions were unsuccessful even when utilizing the purified *B. burgdorferi* PG as a substrate (Jutras et al., 2016). As an alternative to enzyme assays, we used cryo-electron tomography (cryo-ET) to directly visualize the mutant's flagella *in situ* to determine whether the rod/hook/filament assembles or whether the flagella are able to penetrate the PG-layer in the mutant cells. As shown in cryo-ET images (**Supplementary Figure S4**), the Δ*bb0259* mutant cells appear able to synthesize or assemble the rod, P-ring, and hook structures but lack the filament structure (**Supplementary Figures S4A,B**). The hook length of the Δ*bb0259* mutant cells was measured to be the same as that of wild-type cells (~51 nm; $n = 20$), and the hooks of the mutant cells look to be underneath the peptidoglycan layer (**Figures 3E–H, 4D**). However, similar cryo-ET data from the wild-type and complemented *bb0259*^{com} cell tips show the intact rod, P-ring, and hook as well as filament (**Supplementary Figures S4D,E,G**). The averaged motor structure from the mutant cells appears to be identical to the wild-type motor structure, without any visible defect in the rod, P-ring, stator, C-ring, export apparatus, or collar structure (**Supplementary Figures S4C,F**). Importantly, the hooks from the *bb0259*-E580Q or Δ*bb0259* cells were found to be underneath the peptidoglycan layer (**Figures 3E–H, 4D**), whereas an intact rod-hook–filament structure was clearly assembled in the wild-type, *bb0259*-D606N point mutant, and complemented *bb0259*^{com} cells (**Figures 3A–D, 4C**). The Δ*bb0259* or *bb0259*-E580Q mutant completed assembly of all the components of the flagella except the filament, and its hooks were not able to penetrate

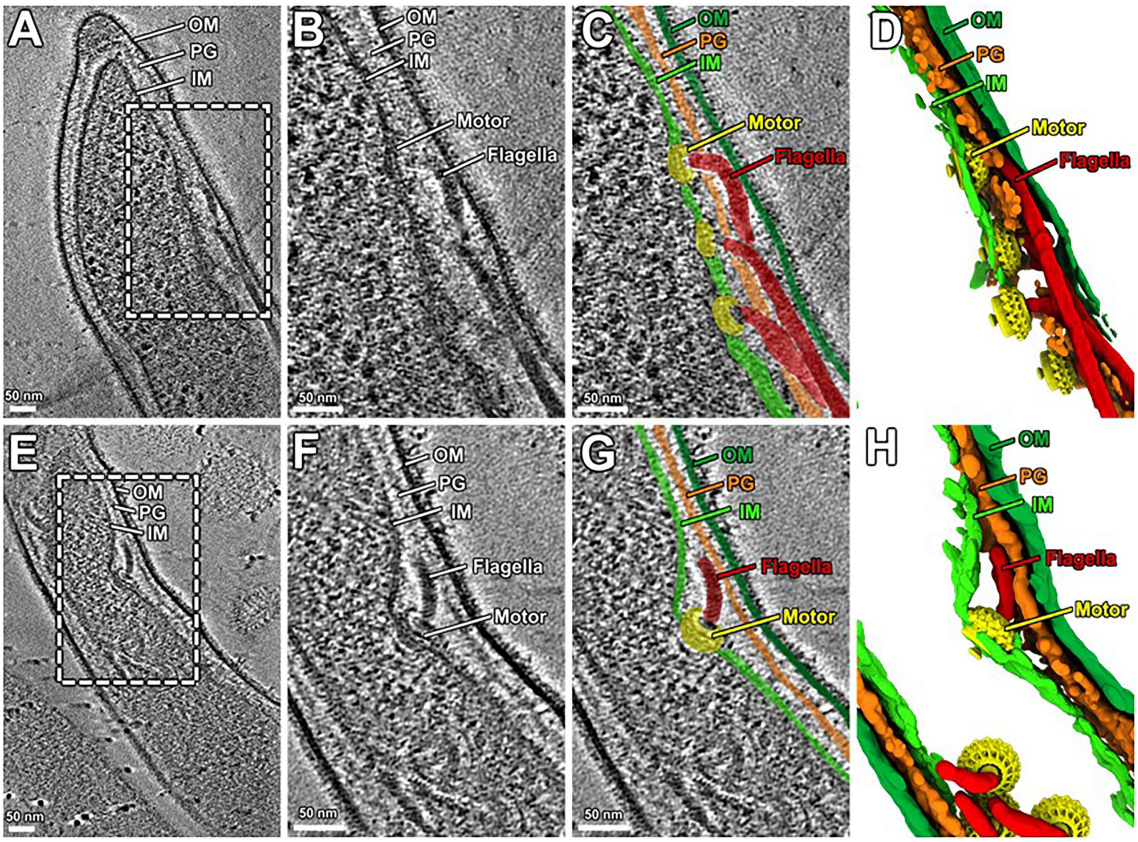

FIGURE 3 | Cryo-ET analysis of *bb0259*-D606N and *bb0259*-E580Q. **(A)** A representative tomographic slice from a *bb0259*-D606N cell tip shows multiple intact flagella, including the motor, hook, and the filament. **(B)** A zoom-in view. **(C)** The motors are colored in yellow, and the hooks and filaments are in red. The inner membrane (light green), outer membrane (dark green), and PG (orange) are colored differently. **(D)** A 3D view shows the motors (yellow) and the hooks and filaments (red). **(E)** A representative tomographic slice from a *bb0259*-E580Q cell tip shows multiple flagella without filament. **(F)** A zoom-in view of one motor and its hook. **(G)** The motor is colored in yellow, and the hook is in red. **(H)** A 3D view shows the motors (yellow) and the hooks (red).

through the PG (**Figures 3E–H, 4D**). These results suggest that BB0259 possesses PG-lytic activity; that residue E580, but not D606, is essential for the catalytic activity of the enzyme; and that hydrolyzing the PG sacculus to allow the hook to penetrate through the cell wall is essential for completion of the assembly of an intact flagellum. We therefore renamed the BB0259 protein flagellar-specific LTase^{Bb}. On the other hand, cryo-ET images of the Δ*bb0531* mutant cells show that the periplasmic flagella are completely assembled like the wild-type cells without any detectable defect in penetrating the PG layer or assembly of the flagella indicating that BB0531 is not involved in PG hydrolytic activity for flagellar penetration (**Supplementary Figure S6**).

BB0259 or LTase^{Bb} Interacts With the Single-Domain Protein FlgJ

The requirement of PG-hydrolyzing activity for proper assembly of periplasmic flagella and consequently for motility suggests that LTase^{Bb} is essential for creating space within the peptidoglycan sacculus for insertion of cell-envelope spanning structures such as flagella. Given that the single-domain FlgJ protein lacks a PG-hydrolyzing enzyme domain, LTase^{Bb} is postulated to interact with FlgJ as the enzyme creates pores in the PG sacculus for the hook to assemble through the layer, subsequently allowing the completion of hook–filament structures for cells to be mobile. To test this proposition or to determine which proteins FlgJ interacts with, we performed far-western or affinity blotting. Recombinant FlgJ protein was used as a probe to incubate a PVDF membrane transferred with the distal rod protein FlgG, hook protein FlgE, hook cap protein FlgD, hook–filament junction protein FlgL, filament protein FlaB, and LTase^{Bb}. As shown in **Figure 5**, FlgJ specifically interacts with LTase^{Bb} and the hook cap protein FlgD.

DISCUSSION

Soluble lytic transglycosylases cleave the glycosidic linkage between N-actetylmuramoyl and N-acetylglucosaminyl residues with the simultaneous production of a 1,6-anydromuramoyl product (Holtje et al., 1975; Herlihey et al., 2014). These enzymes, transglycosylases, are abundant in bacteria, found in different forms, and crucial for generating pores by

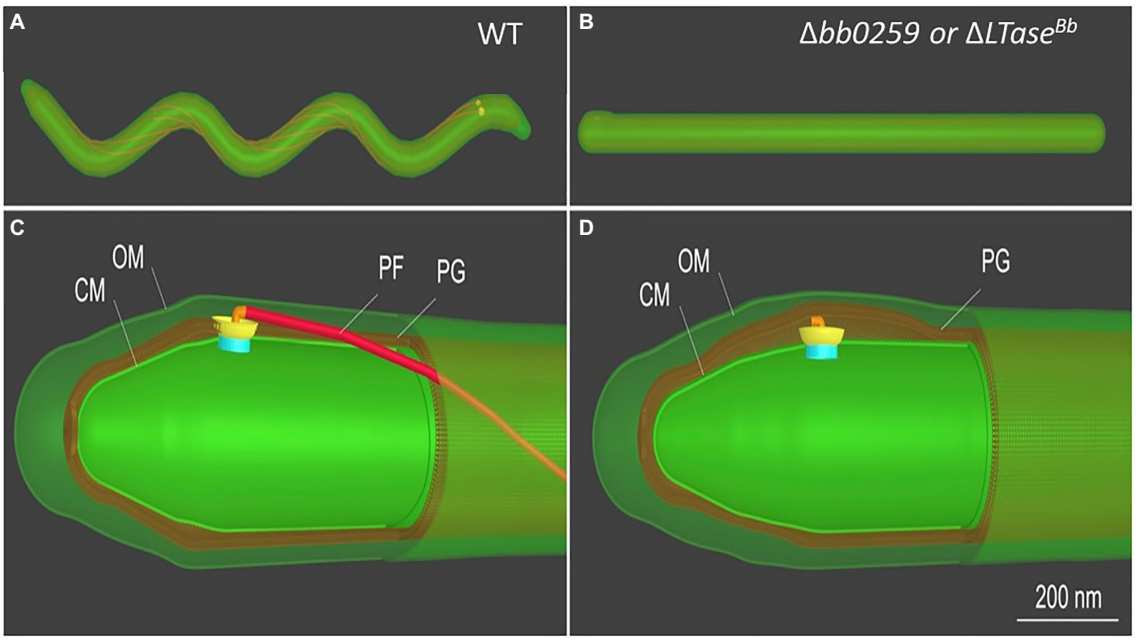

FIGURE 4 | Schematic of *B. burgdorferi* WT and Δ*bb0259* mutant cells. *B. burgdorferi* cells summarizing the results from **Figure 3**. Δ*bb0259* is alternatively called *ΔLTaseBb*. **(A)** A WT *B. burgdorferi* cell has a flat-wave shape with multiple periplasmic flagella, which reside and rotate in the periplasmic space. **(B)** A *ΔLTaseBb* mutant cell is rod-shaped because of the lack of flagellar filaments. **(C)** A zoom-in view of the WT cell tip shows one motor and its long flagellar filament in the periplasmic space as its hook was able to penetrate the PG sacculus to complete assembly of an intact flagellum. **(D)** A zoom-in view of the *ΔLTaseBb* mutant cell shows a hook underneath the PG layer lacking the filament as its hook failed to penetrate the cell wall.

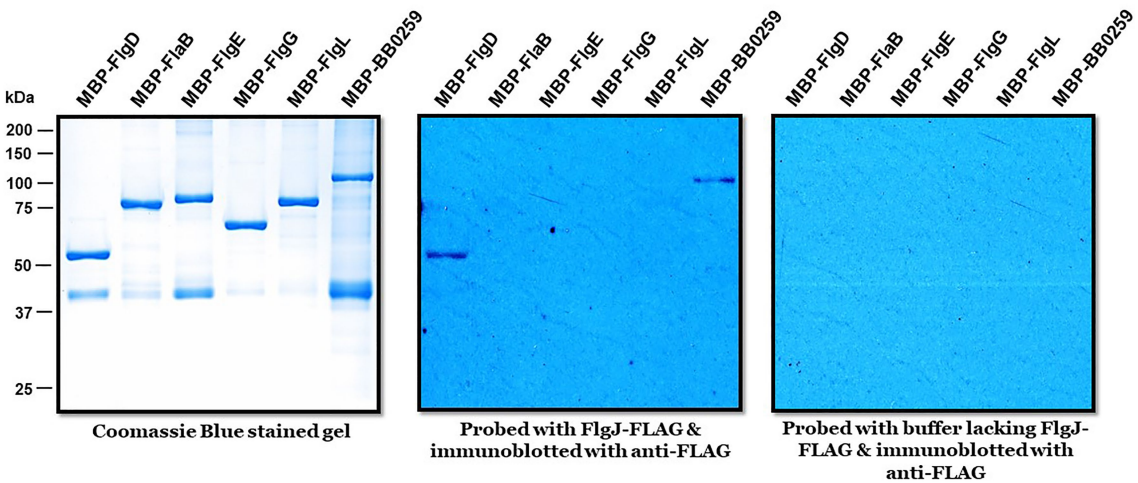

FIGURE 5 | Biophysical interactions of FlgJ with BB0259/LTase^{Bb} and FlgD. Approximately 1 μg of maltose binding protein (MBP)-tagged proteins shown on top of each panel were subjected to sodium dodecyl sulfate–polyacrylamide gel electrophoresis and stained with Coomassie blue (left) or transferred to a polyvinylidene difluoride membrane (middle & right panels). The membranes were incubated with or without FLAG-FlgJ and then immunoblotted with anti-FLAG monoclonal antibodies.

hydrolyzing the PG sacculus for biosynthesis and recycling of PG, bacterial cell division, and the insertion of cell membrane-spanning structures such as flagella (Herlihey et al., 2014). *B. burgdorferi* LTase^{Bb} appears similar to the *S. enterica* and *E. coli* SLT proteins as it possesses the conserved ES-GLMQ-AYNAG motif, with E580 being the catalytic residue (**Figure 1**). Furthermore, the C-terminal domain with the enzymatic motif encompassing the amino acid residues 559-717 is also similar in size to the PG-hydrolytic domains of other bacteria (de la Mora et al., 2012). While a confirmatory enzymatic assay is required to state whether BB0259 in fact possesses any enzymatic activity, our numerous attempts at such an assay

were unsuccessful. It is noteworthy that measuring the peptidoglycan-degrading or lytic activity of FlgJ/SLT proteins poses significant technical drawbacks. The lack of a defined substrate, the heterogeneity of both the substrate and resulting hydrolyzing products in terms of peptide chain composition and extent of PG sacculus cross-linking, and any modification to the glycan chains contribute to the complexity of analysis of the peptidoglycan. However, genetic studies concomitant with direct visualization of the flagella *in situ* by cryo-ET enabled us to propose that BB0259 possesses peptidoglycan pore-forming activities and that E580 is the catalytic residue for the peptidoglycan lytic activities, as the *bb0259*-E580Q mutant's hooks were unable to penetrate the peptidoglycan sacculus (**Figure 3**).

LTase^{Bb} possesses an N-terminal peptide with unknown function (25-558 aa). As the C-terminal domain possesses the enzymatic motif, we speculate that the N-terminal domain is involved in binding to FlgJ, as LTase^{Bb} secretes into the periplasm using its Sec-signaling sequence. Since LTase^{Bb} appears to possess peptidoglycan lytic activities and FlgG and FlgJ are required for proper rod/hook/filament assembly (Zhang et al., 2012; Zhao et al., 2013), we propose that these proteins physically interact to facilitate the insertion of the flagella through the PG layer as the enzyme creates pores in the sacculus (**Figure 6**). Our direct visualization of the mutant's flagella *in situ* by cryo-ET shows that the hooks are unable to pass through the PG sacculus, and therefore, these structures were detected just underneath the PG layer (**Figures 3E–H, 4D**). Consequently, the flagella did not assemble properly, leading to the non-motile and rod-shaped morphology (**Figures 2A**,**B**).

Borrelia burgdorferi FlgJ and the SLT domain-containing LTase^{Bb} are distinct from their counterparts in *S. enterica*. For example, FlgJ from *S. enterica* is involved in flagellar rod formation or required for the transition from rod to hook formation (Cohen and Hughes, 2014). However, cryo-ET data from the *B. burgdorferi* Δ*flgJ* mutant show that the mutant completed assembly of the rod and P-ring but assembled a partial hook and filament structures (Zhang et al., 2012). It is noteworthy that, unlike the model organisms, the rod and P-ring in this spirochete are not able to contact the PG layer, as the rod is significantly smaller than in the model organisms (17 nm vs. 30 nm in *E. coli*; Zhao et al., 2013; Saijo-Hamano et al., 2019). It is the spirochete-specific collar that contacts the PG sacculus, while the hook penetrates the peptidoglycan layer to complete assembly and formation of the filament in *B. burgdorferi* (Zhao et al., 2013). FlgJ in the spirochete is therefore likely important for assembly of the hook/filament during the hook-to-filament transition (Zhang et al., 2012). The mutants of *bb0259* (or *LTase*^{Bb}) also assemble the rod, P-ring, and hook but are unable to synthesize/assemble the filament (**Figures 3, 4, Supplementary Figure S3**). The hooks are not able to penetrate the PG layer due to the lack of PG lytic activity in Δ*bb0259* or *bb0259*-E580Q mutants (Δ*LTase*^{Bb} or *LTase*^{Bb}-E580Q, respectively). This result also enforces the

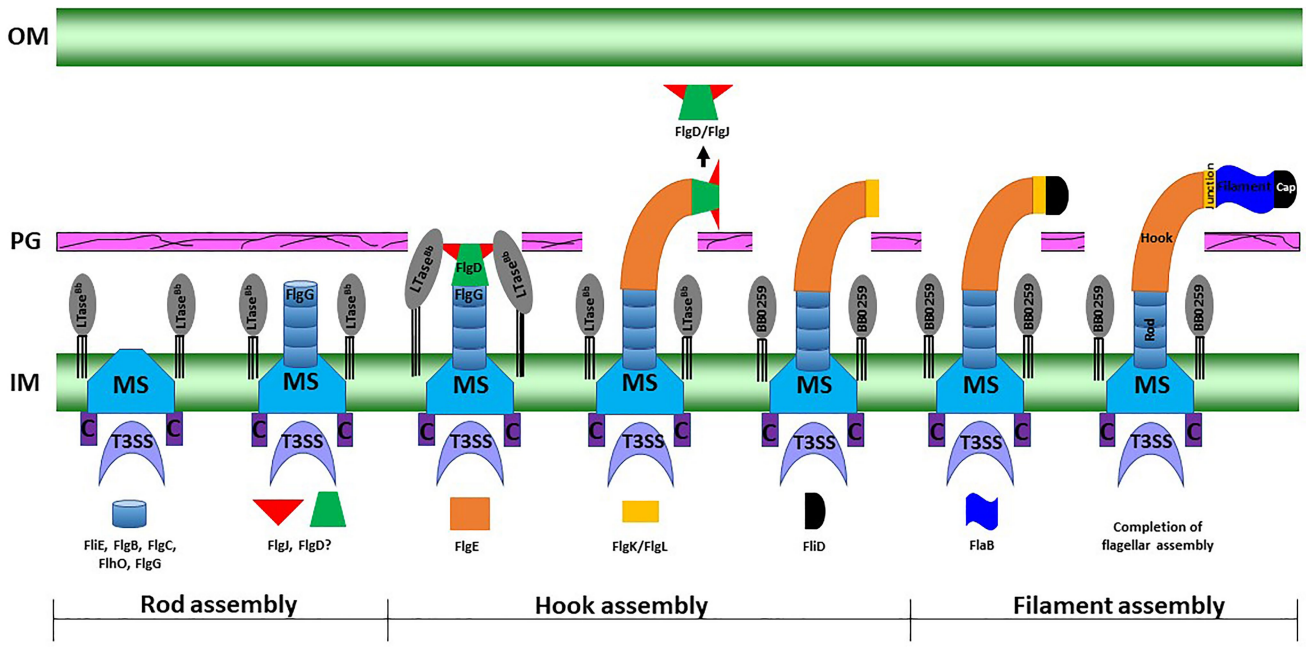

FIGURE 6 | A working model of periplasmic flagellar hook–filament assembly in the spirochete *B. burgdorferi*. At the onset of rod assembly, many flagellar components assemble, such as the MS ring, C ring, export apparatus, stators, and collar. Subsequently, the rod components (FliE, FlgB, FlgC, FlhO/FlgF, and FlgG) are sequentially secreted into the periplasmic space through flagellar T3SS and assemble (Zhao et al., 2013). The hook cap protein FlgD and its chaperone or interacting protein FlgJ form at the distal end of the rod and initiate hook assembly. Binding of FlgJ with the pre-localized SLT enzyme BB0259 or LTase^{Bb} in the periplasmic leaflet of the cell wall promotes hydrolysis of the sacculus as the hook completes assembly through the cell wall. Assembly of the filament (FlaA and FlaB) is promoted by the filament cap.

notion that FlgJ and LTase^{Bb} are crucial for hook/filament assembly and/or for hook-to-filament transition (**Figure 6**).

Δ*bb0259*/Δ*LTase*^{Bb} or *bb0259*-E580Q/*LTase*^{Bb}-E580Q mutant phenotypes appear to be very similar to that of the Δ*flaB* mutant (Zhao et al., 2013). In both cases, the mutants complete assembly and formation of the motor, rod, P-ring, and hook but lack the filament (compare **Figures 3F**,**G** with **Supplementary Figure S4H** or Figure 5A from ref. Zhao et al., 2013). However, in the *flaB* mutant, the hook is able to penetrate the PG layer (**Supplementary Figure S4H**) as the PG enzyme activity of BB0259 is believed to be retained in Δ*flaB* cells, again reinforcing that BB0259 or LTase^{Bb} is a PG hydrolyzing enzyme. Moreover, the hook length of the Δ*LTase*^{Bb}, Δ*flaB*, and wild-type cells is the same (~51 nm; $n = 20$) and consistent with the previously reported hook length (Zhao et al., 2013), suggesting that LTase^{Bb} is not involved in hook assembly. All these data suggest that FlgJ and LTase^{Bb} are distinct from their counterparts in other flagellated bacteria reported to date. Importantly, in *S. enterica*, FlgJ interacts with the rod proteins including the distal rod FlgG as FlgJ is considered a rod-capping or scaffolding protein (Hirano et al., 2001; Cohen and Hughes, 2014). However, that is not the case in *B. burgdorferi*. FlgJ interaction with FlgG is undetectable (**Figure 5**), and the Δ*flgJ* mutant's rod structures are intact in *B. burgdorferi* (Zhang et al., 2012).

Based on reports of FlgJ and this communication, we propose a model for how LTase^{Bb} and FlgJ work synergistically with the hook cap protein FlgD to complete assembly of the hook–filament in *B. burgdorferi* (**Figure 6**). In this model, LTase^{Bb} uses Sec-dependent pathway to be secreted into the periplasm. Using the flagellar type III secretion system, FlgJ and hook-capping protein FlgD compile onto the rod as the rod completes assembly onto the MS-ring. Interactions of FlgJ with BB0259 or LTase^{Bb} and FlgD (**Figure 5**) enable the hook to initiate and complete its assembly through the PG holes created by LTase^{Bb} wherein FlgJ chaperones or interacts with FlgD for the hook to complete its assembly in the periplasm (**Figure 6**). Without the FlgJ, the hook FlgE synthesis or assembly is therefore incomplete (Zhang et al., 2012) due to a lack of interaction between FlgD and FlgJ or lack of chaperone functions of FlgJ for FlgD. We speculate that the hook-to-filament assembly occurs as in other bacteria, as we have reported (Zhao et al., 2013). Additional in-depth analysis is warranted to better understand the spatiotemporal synthesis of the FlgJ, FlgD, and LTase^{Bb} proteins and hook–filament assemblies in *B. burgdorferi*.

DATA AVAILABILITY STATEMENT

The raw data supporting the conclusions of this article will be made available by the authors, without undue reservation.

AUTHOR CONTRIBUTIONS

HX, BH, and DAF conducted the experiments. JL and MM designed the experiments. All authors contributed to the article and approved the submitted version.

FUNDING

JL was supported by grants GM107629 and R01AI087946. MM was supported by R01AI132818 from National Institutes of Health (NIH). Part of cryo-ET data were collected at Yale CryoEM resource that is funded in part by the NIH grant 1S10OD023603-01A1.

ACKNOWLEDGMENTS

We thank Jennifer Aronson for critical reading of the manuscript. We thank David Burton for modeling and illustration and Michelle LaHair for technical helps.

SUPPLEMENTARY MATERIAL

The Supplementary Material for this article can be found online at: https://www.frontiersin.org/articles/10.3389/fmicb.2021.692707/full#supplementary-material

REFERENCES

Almagro Armenteros, J. J., Tsirigos, K. D., Sonderby, C. K., Petersen, T. N., Winther, O., Brunak, S., et al. (2019). SignalP 5.0 improves signal peptide predictions using deep neural networks. *Nat. Biotechnol.* 37, 420–423. doi: 10.1038/s41587-019-0036-z

Altschul, S. F., Gish, W., Miller, W., Myers, E. W., and Lipman, D. J. (1990). Basic local alignment search tool. *J. Mol. Biol.* 215, 403–410. doi: 10.1016/S0022-2836(05)80360-2

Altschul, S. F., Madden, T. L., Schaffer, A. A., Zhang, J., Zhang, Z., Miller, W., et al. (1997). Gapped BLAST and PSI-BLAST: a new generation of protein database search programs. *Nucleic Acids Res.* 25, 3389–3402. doi: 10.1093/nar/25.17.3389

Babu, M. M., Priya, M. L., Selvan, A. T., Madera, M., Gough, J., Aravind, L., et al. (2006). A database of bacterial lipoproteins (DOLOP) with functional assignments to predicted lipoproteins. *J. Bacteriol.* 188, 2761–2773. doi: 10.1128/JB.188.8.2761-2773.2006

Bertani, G. (1951). Studies on lysogenesis. I. The mode of phage liberation by lysogenic *Escherichia coli*. *J. Bacteriol.* 62, 293–300. doi: 10.1128/jb.62.3.293-300.1951

Bertani, G. (2004). Lysogeny at mid-twentieth century: P1, P2, and other experimental systems. *J. Bacteriol.* 186, 595–600. doi: 10.1128/JB.186.3.595-600.2004

Blackburn, N. T., and Clarke, A. J. (2001). Identification of four families of peptidoglycan lytic transglycosylases. *J. Mol. Evol.* 52, 78–84. doi: 10.1007/s002390010136

Bono, J. L., Elias, A. F., Kupko, J. J. 3rd, Stevenson, B., Tilly, K., and Rosa, P. (2000). Efficient targeted mutagenesis in *Borrelia burgdorferi*. *J. Bacteriol.* 182, 2445–2452. doi: 10.1128/JB.182.9.2445-2452.2000

Carroll, B. L., and Liu, J. (2020). Structural conservation and adaptation of the bacterial flagella motor. *Biomol. Ther.* 10:1492. doi: 10.3390/biom10111492

Charon, N. W., Cockburn, A., Li, C., Liu, J., Miller, K. A., Miller, M. R., et al. (2012). The unique paradigm of spirochete motility and chemotaxis. *Annu. Rev. Microbiol.* 66, 349–370. doi: 10.1146/annurev-micro-092611-150145

Charon, N. W., Goldstein, S. F., Marko, M., Hsieh, C., Gebhardt, L. L., Motaleb, M. A., et al. (2009). The flat ribbon configuration of the periplasmic flagella of *Borrelia burgdorferi* and its relationship to motility and morphology. *J. Bacteriol.* 191, 600–607. doi: 10.1128/JB.01288-08

Chen, S., Beeby, M., Murphy, G. E., Leadbetter, J. R., Hendrixson, D. R., Briegel, A., et al. (2011). Structural diversity of bacterial flagellar motors. *EMBO J.* 30, 2972–2981. doi: 10.1038/emboj.2011.186

Chen, M., Dai, W., Sun, S. Y., Jonasch, D., He, C. Y., Schmid, M. F., et al. (2017). Convolutional neural networks for automated annotation of cellular cryo-electron tomograms. *Nat. Methods* 14, 983–985. doi: 10.1038/nmeth.4405

Cohen, E. J., and Hughes, K. T. (2014). Rod-to-hook transition for extracellular flagellum assembly is catalyzed by the L-ring-dependent rod scaffold removal. *J. Bacteriol.* 196, 2387–2395. doi: 10.1128/JB.01580-14

de la Mora, J., Osorio-Valeriano, M., Gonzalez-Pedrajo, B., Ballado, T., Camarena, L., and Dreyfus, G. (2012). The C terminus of the flagellar muramidase SltF modulates the interaction with FlgJ in *Rhodobacter sphaeroides*. *J. Bacteriol.* 194, 4513–4520. doi: 10.1128/JB.00460-12

Demchick, P., and Koch, A. L. (1996). The permeability of the wall fabric of *Escherichia coli* and *Bacillus subtilis*. *J. Bacteriol.* 178, 768–773. doi: 10.1128/jb.178.3.768-773.1996

Elias, A. F., Bono, J. L., Kupko, J. J. 3rd, Stewart, P. E., Krum, J. G., and Rosa, P. A. (2003). New antibiotic resistance cassettes suitable for genetic studies in *Borrelia burgdorferi*. *J. Mol. Microbiol. Biotechnol.* 6, 29–40. doi: 10.1159/000073406

Garcia-Ramos, M., de la Mora, J., Ballado, T., Camarena, L., and Dreyfus, G. (2018). Biochemical and phylogenetic study of SltF, a flagellar lytic transglycosylase from *Rhodobacter sphaeroides*. *J. Bacteriol.* 200:e00397-18. doi: 10.1128/JB.00397-18

Ge, Y., Old, I. G., Saint Girons, I., and Charon, N. W. (1997). Molecular characterization of a large *Borrelia burgdorferi* motility operon which is initiated by a consensus sigma70 promoter. *J. Bacteriol.* 179, 2289–2299. doi: 10.1128/jb.179.7.2289-2299.1997

Goddard, T. D., Huang, C. C., Meng, E. C., Pettersen, E. F., Couch, G. S., Morris, J. H., et al. (2018). UCSF ChimeraX: Meeting modern challenges in visualization and analysis. *Protein Sci.* 27, 14–25. doi: 10.1002/pro.3235

Gonzalez-Pedrajo, B., de la Mora, J., Ballado, T., Camarena, L., and Dreyfus, G. (2002). Characterization of the flgG operon of *Rhodobacter sphaeroides* WS8 and its role in flagellum biosynthesis. *Biochim. Biophys. Acta* 1579, 55–63. doi: 10.1016/s0167-4781(02)00504-3

Herlihey, F. A., Moynihan, P. J., and Clarke, A. J. (2014). The essential protein for bacterial flagella formation FlgJ functions as a beta-N-acetylglucosaminidase. *J. Biol. Chem.* 289, 31029–31042. doi: 10.1074/jbc.M114.603944

Hirano, T., Minamino, T., and Macnab, R. M. (2001). The role in flagellar rod assembly of the N-terminal domain of Salmonella FlgJ, a flagellum-specific muramidase. *J. Mol. Biol.* 312, 359–369. doi: 10.1006/jmbi.2001.4963

Holtje, J. V., Mirelman, D., Sharon, N., and Schwarz, U. (1975). Novel type of murein transglycosylase in *Escherichia coli*. *J. Bacteriol.* 124, 1067–1076. doi: 10.1128/jb.124.3.1067-1076.1975

Homma, M., and Iino, T. (1985). Locations of hook-associated proteins in flagellar structures of *Salmonella typhimurium*. *J. Bacteriol.* 162, 183–189. doi: 10.1128/jb.162.1.183-189.1985

Jaroszewski, L., Li, Z., Cai, X. H., Weber, C., and Godzik, A. (2011). FFAS server: novel features and applications. *Nucleic Acids Res.* 39, W38–W44. doi: 10.1093/nar/gkr441

Jaroszewski, L., Rychlewski, L., Li, Z., Li, W., and Godzik, A. (2005). FFAS03: a server for profile–profile sequence alignments. *Nucleic Acids Res.* 33, W284–W288. doi: 10.1093/nar/gki418

Jones, C. J., and Macnab, R. M. (1990). Flagellar assembly in *Salmonella typhimurium*: analysis with temperature-sensitive mutants. *J. Bacteriol.* 172, 1327–1339. doi: 10.1128/jb.172.3.1327-1339.1990

Jutras, B. L., Scott, M., Parry, B., Biboy, J., Gray, J., Vollmer, W., et al. (2016). Lyme disease and relapsing fever Borrelia elongate through zones of peptidoglycan synthesis that mark division sites of daughter cells. *Proc. Natl. Acad. Sci. U. S. A.* 113, 9162–9170. doi: 10.1073/pnas.1610805113

Kall, L., Krogh, A., and Sonnhammer, E. L. (2004). A combined transmembrane topology and signal peptide prediction method. *J. Mol. Biol.* 338, 1027–1036. doi: 10.1016/j.jmb.2004.03.016

Kall, L., Krogh, A., and Sonnhammer, E. L. (2005). An HMM posterior decoder for sequence feature prediction that includes homology information. *Bioinformatics* 21(Suppl. 1), i251–i257. doi: 10.1093/bioinformatics/bti1014

Kall, L., Krogh, A., and Sonnhammer, E. L. (2007). Advantages of combined transmembrane topology and signal peptide prediction–the Phobius web server. *Nucleic Acids Res.* 35, W429–W432. doi: 10.1093/nar/gkm256

Kariu, T., Sharma, K., Singh, P., Smith, A. A., Backstedt, B., Buyuktanir, O., et al. (2015). BB0323 and novel virulence determinant BB0238: *Borrelia burgdorferi* proteins that interact with and stabilize each other and are critical for infectivity. *J. Infect. Dis.* 211, 462–471. doi: 10.1093/infdis/jiu460

Koraimann, G. (2003). Lytic transglycosylases in macromolecular transport systems of Gram-negative bacteria. *Cell. Mol. Life Sci.* 60, 2371–2388. doi: 10.1007/s00018-003-3056-1

Kremer, J. R., Mastronarde, D. N., and McIntosh, J. R. (1996). Computer visualization of three-dimensional image data using IMOD. *J. Struct. Biol.* 116, 71–76. doi: 10.1006/jsbi.1996.0013

Li, C., Xu, H., Zhang, K., and Liang, F. T. (2010). Inactivation of a putative flagellar motor switch protein FliG1 prevents *Borrelia burgdorferi* from swimming in highly viscous media and blocks its infectivity. *Mol. Microbiol.* 75, 1563–1576. doi: 10.1111/j.1365-2958.2010.07078.x

Liu, J., Lin, T., Botkin, D. J., McCrum, E., Winkler, H., and Norris, S. J. (2009). Intact flagellar motor of *Borrelia burgdorferi* revealed by cryo-electron tomography: evidence for stator ring curvature and rotor/C-ring assembly flexion. *J. Bacteriol.* 191, 5026–5036. doi: 10.1128/JB.00340-09

Madan Babu, M., and Sankaran, K. (2002). DOLOP–database of bacterial lipoproteins. *Bioinformatics* 18, 641–643. doi: 10.1093/bioinformatics/18.4.641

Moon, K. H., Hobbs, G., and Motaleb, M. A. (2016). *Borrelia burgdorferi* CheD promotes various functions in chemotaxis and the pathogenic life cycle of the spirochete. *Infect. Immun.* 84, 1743–1752. doi: 10.1128/IAI.01347-15

Moon, K. H., Zhao, X., Xu, H., Liu, J., and Motaleb, M. A. (2018). A tetratricopeptide repeat domain protein has profound effects on assembly of periplasmic flagella, morphology and motility of the Lyme disease spirochete *Borrelia burgdorferi*. *Mol. Microbiol.* 110, 634–647. doi: 10.1111/mmi.14121

Motaleb, M. A., Corum, L., Bono, J. L., Elias, A. F., Rosa, P., Samuels, D. S., et al. (2000). *Borrelia burgdorferi* periplasmic flagella have both skeletal and motility functions. *Proc. Natl. Acad. Sci. U. S. A.* 97, 10899–10904. doi: 10.1073/pnas.200221797

Motaleb, M. A., Liu, J., and Wooten, R. M. (2015). Spirochetal motility and chemotaxis in the natural enzootic cycle and development of Lyme disease. *Curr. Opin. Microbiol.* 28, 106–113. doi: 10.1016/j.mib.2015.09.006

Motaleb, M. A., Miller, M. R., Bakker, R. G., Li, C., and Charon, N. W. (2007). Isolation and characterization of chemotaxis mutants of the Lyme disease Spirochete *Borrelia burgdorferi* using allelic exchange mutagenesis, flow cytometry, and cell tracking. *Methods Enzymol.* 422, 421–437. doi: 10.1016/S0076-6879(06)22021-4

Motaleb, M. A., Pitzer, J. E., Sultan, S. Z., and Liu, J. (2011). A novel gene inactivation system reveals altered periplasmic flagellar orientation in a *Borrelia burgdorferi* fliL mutant. *J. Bacteriol.* 193, 3324–3331. doi: 10.1128/JB.00202-11

Nakamura, S., and Minamino, T. (2019). Flagella-driven motility of bacteria. *Biomol. Ther.* 9:279. doi: 10.3390/biom9070279

Nambu, T., Inagaki, Y., and Kutsukake, K. (2006). Plasticity of the domain structure in FlgJ, a bacterial protein involved in flagellar rod formation. *Genes Genet. Syst.* 81, 381–389. doi: 10.1266/ggs.81.381

Nambu, T., Minamino, T., Macnab, R. M., and Kutsukake, K. (1999). Peptidoglycan-hydrolyzing activity of the FlgJ protein, essential for flagellar rod formation in *Salmonella typhimurium*. *J. Bacteriol.* 181, 1555–1561. doi: 10.1128/JB.181.5.1555-1561.1999

Ohnishi, K., Ohto, Y., Aizawa, S. I., Macnab, R. M., and Iino, T. (1994). FlgD is a scaffolding protein needed for flagellar hook assembly in *Salmonella typhimurium*. *J. Bacteriol.* 176, 2272–2281. doi: 10.1128/jb.176.8.2272-2281.1994

Rychlewski, L., Jaroszewski, L., Li, W., and Godzik, A. (2000). Comparison of sequence profiles. Strategies for structural predictions using sequence information. *Protein Sci.* 9, 232–241. doi: 10.1110/ps.9.2.232

Saijo-Hamano, Y., Matsunami, H., Namba, K., and Imada, K. (2019). Architecture of the bacterial flagellar distal rod and hook of *Salmonella*. *Biomol. Ther.* 9:260. doi: 10.3390/biom9070260

Sal, M. S., Li, C., Motalab, M. A., Shibata, S., Aizawa, S., and Charon, N. W. (2008). *Borrelia burgdorferi* uniquely regulates its motility genes and has an intricate flagellar hook-basal body structure. *J. Bacteriol.* 190, 1912–1921. doi: 10.1128/JB.01421-07

Sievers, F., Wilm, A., Dineen, D., Gibson, T. J., Karplus, K., Li, W., et al. (2011). Fast, scalable generation of high-quality protein multiple sequence alignments using Clustal Omega. *Mol. Syst. Biol.* 7:539. doi: 10.1038/msb.2011.75

Sultan, S. Z., Manne, A., Stewart, P. E., Bestor, A., Rosa, P. A., Charon, N. W., et al. (2013). Motility is crucial for the infectious life cycle of *Borrelia burgdorferi*. *Infect. Immun.* 81, 2012–2021. doi: 10.1128/IAI.01228-12

Sultan, S. Z., Pitzer, J. E., Miller, M. R., and Motaleb, M. A. (2010). Analysis of a *Borrelia burgdorferi* phosphodiesterase demonstrates a role for cyclic-di-guanosine monophosphate in motility and virulence. *Mol. Microbiol.* 77, 128–142. doi: 10.1111/j.1365-2958.2010.07191.x

Sultan, S. Z., Sekar, P., Zhao, X., Manne, A., Liu, J., Wooten, R. M., et al. (2015). Motor rotation is essential for the formation of the periplasmic flagellar ribbon, cellular morphology, and *Borrelia burgdorferi* persistence within *Ixodes scapularis* tick and murine hosts. *Infect. Immun.* 83, 1765–1777. doi: 10.1128/IAI.03097-14

Terashima, H., Kawamoto, A., Morimoto, Y. V., Imada, K., and Minamino, T. (2017). Structural differences in the bacterial flagellar motor among bacterial species. *Biophys. Physicobiol.* 14, 191–198. doi: 10.2142/biophysico.14.0_191

Thunnissen, A. M., Dijkstra, A. J., Kalk, K. H., Rozeboom, H. J., Engel, H., Keck, W., et al. (1994). Doughnut-shaped structure of a bacterial muramidase revealed by X-ray crystallography. *Nature* 367, 750–753. doi: 10.1038/367750a0

Tilly, K., Elias, A. F., Errett, J., Fischer, E., Iyer, R., Schwartz, I., et al. (2001). Genetics and regulation of chitobiose utilization in *Borrelia burgdorferi*. *J. Bacteriol.* 183, 5544–5553. doi: 10.1128/JB.183.19.5544-5553.2001

Toker, A. S., and Macnab, R. M. (1997). Distinct regions of bacterial flagellar switch protein FliM interact with FliG, FliN and CheY. *J. Mol. Biol.* 273, 623–634. doi: 10.1006/jmbi.1997.1335

Toledo, A., Huang, Z., Coleman, J. L., London, E., and Benach, J. L. (2018). Lipid rafts can form in the inner and outer membranes of *Borrelia burgdorferi* and have different properties and associated proteins. *Mol. Microbiol.* 108, 63–76. doi: 10.1111/mmi.13914

van Asselt, E. J., Thunnissen, A. M., and Dijkstra, B. W. (1999). High resolution crystal structures of the *Escherichia coli* lytic transglycosylase Slt70 and its complex with a peptidoglycan fragment. *J. Mol. Biol.* 291, 877–898. doi: 10.1006/jmbi.1999.3013

Wolgemuth, C. W., Charon, N. W., Goldstein, S. F., and Goldstein, R. E. (2006). The flagellar cytoskeleton of the spirochetes. *J. Mol. Microbiol. Biotechnol.* 11, 221–227. doi: 10.1159/000094056

Xu, H., He, J., Liu, J., and Motaleb, M. A. (2019). BB0326 is responsible for the formation of periplasmic flagellar collar and assembly of the stator complex in *Borrelia burgdorferi*. *Mol. Microbiol.* 113, 418–429. doi: 10.1111/mmi.14428

Xu, H., Sultan, S., Yerke, A., Moon, K. H., Wooten, R. M., and Motaleb, M. A. (2017). *Borrelia burgdorferi* CheY2 is dispensable for chemotaxis or motility but crucial for the infectious life cycle of the spirochete. *Infect. Immun.* 85:e00264-16. doi: 10.1128/IAI.00264-16

Yang, X. F., Alani, S. M., and Norgard, M. V. (2003). The response regulator Rrp2 is essential for the expression of major membrane lipoproteins in *Borrelia burgdorferi*. *Proc. Natl. Acad. Sci. U. S. A.* 100, 11001–11006. doi: 10.1073/pnas.1834315100

Yonekura, K., Maki, S., Morgan, D. G., DeRosier, D. J., Vonderviszt, F., Imada, K., et al. (2000). The bacterial flagellar cap as the rotary promoter of flagellin self-assembly. *Science* 290, 2148–2152. doi: 10.1126/science.290.5499.2148

Zaloba, P., Bailey-Elkin, B. A., Derksen, M., and Mark, B. L. (2016). Structural and biochemical insights into the peptidoglycan hydrolase domain of FlgJ from *Salmonella typhimurium*. *PLoS One* 11:e0149204. doi: 10.1371/journal.pone.0149204

Zhang, K., Tong, B. A., Liu, J., and Li, C. (2012). A single-domain FlgJ contributes to flagellar hook and filament formation in the Lyme disease spirochete *Borrelia burgdorferi*. *J. Bacteriol.* 194, 866–874. doi: 10.1128/JB.06341-11

Zhao, X., Zhang, K., Boquoi, T., Hu, B., Motaleb, M. A., Miller, K. A., et al. (2013). Cryoelectron tomography reveals the sequential assembly of bacterial flagella in *Borrelia burgdorferi*. *Proc. Natl. Acad. Sci. U. S. A.* 110, 14390–14395. doi: 10.1073/pnas.1308306110

Zheng, S. Q., Palovcak, E., Armache, J. P., Verba, K. A., Cheng, Y., and Agard, D. A. (2017). MotionCor2: anisotropic correction of beam-induced motion for improved cryo-electron microscopy. *Nat. Methods* 14, 331–332. doi: 10.1038/nmeth.4193

Conflict of Interest: The authors declare that the research was conducted in the absence of any commercial or financial relationships that could be construed as a potential conflict of interest.

Publisher's Note: All claims expressed in this article are solely those of the authors and do not necessarily represent those of their affiliated organizations, or those of the publisher, the editors and the reviewers. Any product that may be evaluated in this article, or claim that may be made by its manufacturer, is not guaranteed or endorsed by the publisher.

frontiers in Microbiology

ORIGINAL RESEARCH
published: 26 November 2021
doi: 10.3389/fmicb.2021.765739

Stator Dynamics Depending on Sodium Concentration in Sodium-Driven Bacterial Flagellar Motors

*Tsai-Shun Lin[1], Seiji Kojima[2], Hajime Fukuoka[3], Akihiko Ishijima[3], Michio Homma[2] and Chien-Jung Lo[1]**

[1] Department of Physics and Center for Complex Systems, National Central University, Taoyuan City, Taiwan, [2] Division of Biological Science, Graduate School of Science, Nagoya University, Nagoya, Japan, [3] Graduate School of Frontier Biosciences, Osaka University, Suita, Japan

Bacterial flagellar motor (BFM) is a large membrane-spanning molecular rotary machine for swimming motility. Torque is generated by the interaction between the rotor and multiple stator units powered by ion-motive force (IMF). The number of bound stator units is dynamically changed in response to the external load and the IMF. However, the detailed dynamics of stator unit exchange process remains unclear. Here, we directly measured the speed changes of sodium-driven chimeric BFMs under fast perfusion of different sodium concentration conditions using computer-controlled, high-throughput microfluidic devices. We found the sodium-driven chimeric BFMs maintained constant speed over a wide range of sodium concentrations by adjusting stator units in compensation to the sodium-motive force (SMF) changes. The BFM has the maximum number of stator units and is most stable at 5 mM sodium concentration rather than higher sodium concentration. Upon rapid exchange from high to low sodium concentration, the number of functional stator units shows a rapidly excessive reduction and then resurrection that is different from predictions of simple absorption model. This may imply the existence of a metastable hidden state of the stator unit during the sudden loss of sodium ions.

Keywords: bacterial flagellar motor, sodium-motive force, stator exchange, membrane protein, perfusion

OPEN ACCESS

Edited by:
Gert Bange,
University of Marburg, Germany

Reviewed by:
Kai Thormann,
University of Giessen, Germany
Daniel B. Kearns,
Indiana University Bloomington, United States

****Correspondence:***
Chien-Jung Lo
cjlo@phy.ncu.edu.tw

Specialty section:
This article was submitted to Microbial Physiology and Metabolism, a section of the journal Frontiers in Microbiology

Received: *27 August 2021*
Accepted: *19 October 2021*
Published: *26 November 2021*

Citation:
Lin T-S, Kojima S, Fukuoka H, Ishijima A, Homma M and Lo C-J (2021) Stator Dynamics Depending on Sodium Concentration in Sodium-Driven Bacterial Flagellar Motors. Front. Microbiol. 12:765739. doi: 10.3389/fmicb.2021.765739

INTRODUCTION

The cell membrane is not only the barrier for life but also the working place for many essential cellular functions. Membrane proteins show rich dynamics such as gating (Moreau et al., 2014), diffusing (Oswald et al., 2014; Lin et al., 2018), and exchange (Leake et al., 2006; Tusk et al., 2018; Armitage and Berry, 2020). Earlier investigations focused on the mechanical properties such as the gating mechanism or the diffusivity of membrane proteins. However, very little is known for the membrane protein energetic dynamics. In this report, we use the sodium-driven bacterial flagellar

Abbreviations: BFM, bacterial flagellar motor; IMF, ion-motive force; SMF, sodium-motive force; BFI, back focal-plan interferometry; $[Na^+]_{ex}$, extracellular sodium ion concentration; $[Na^+]_{in}$, internal sodium ion concentration; V_m, membrane potential.

motor (BFM) as an example to study the energetic coupling dynamics of the protein complex with high-throughput and high-resolution optical measurements.

The bacterial flagellum is a large molecular complex spanning across the membranes with extracellular flagellar filaments, universal joint (hook), and motor (rotor and stator) (Nirody et al., 2017; Nakamura and Minamino, 2019), as shown in **Figure 1A**. The rotation of the motor is powered by the transmembrane ion flux through the stator driven by the ion-motive force (IMF). The common driving ions are proton (H^+) and sodium ions (Na^+). About a dozen stator units are bound to the periphery of the motor to interact with the rotor independently (**Figures 1A–C**). A stator unit is composed of 5 MotA(PomA) and 2 MotB(PomB). A MotA(PomA) protein has four transmembrane segments, and the segment between the second and third transmembrane region is responsible for the interaction with the rotor. A MotB(PomB) protein has one transmembrane segment, a plug segment for ion flux control, and a large periplasmic segment with an OmpA-like domain for cell wall binding, as shown in **Figure 1B**. A model has been proposed in which the MotA(PomA) pentamer ring rotates with respect to the axis of MotB(PomB) dimer due to the influx of ions (Deme et al., 2020; Santiveri et al., 2020). The direct physical interaction between specific residues in FliG and PomA/MotA was demonstrated and has provided a mechanism with gear-like motion by the stator–rotor interaction in the flagellar motor (Terashima et al., 2021). The ion movement through the stator is driven by the IMF that comprises electrical and chemical potentials (Nirody et al., 2017).

Subunits of BFMs such as stator units have been found to be dynamic, dating back to the 1980s with so-called "resurrection" experiments (Block and Berg, 1984; Blair and Berg, 1988; Reid et al., 2006). In the stator genes deleted *Escherichia coli* strain, the stator proteins can be expressed from inducible plasmid, and the BFM rotation can be restored in a series of stepwise speed increments. Each speed increment step indicates that the addition of a functional stator unit contributed to the motor rotation. More recently, by using green fluorescent protein (GFP)–fused stator units and fluorescence recovery after photobleaching, the protein exchange of stator units in functional BFMs has been observed (Leake et al., 2006). The stator units can be unbound by reducing IMF, and the stator resurrection can be achieved by restoring the IMF (Tipping et al., 2013a; Sowa et al., 2014). Later it was found that the mechanical load can also affect the number of stator units (Lele et al., 2013; Tipping et al., 2013b; Chawla et al., 2017; Wadhwa et al., 2019). A catch-bond model, describing the bond between stator unit and motor strengthens with applied force (Nord et al., 2017a; Nirody et al., 2019), provides a new insight into the stator–rotor interaction. The number of functional stator unit is therefore not only depending on external load but also IMF and any other factors that would affect the force generation process. In other words, the rotation speed of a BFM depends on the external load, IMF, and the number of bound stator units.

In the stator unit recruitment model, there is a pool of unbound stator units diffusing on the membrane, with the plug of ion channel closed, as shown in **Figure 1**. It has been shown that the plug region of PomB prevents the ion influx by blocking the rotation of the rotor as a spanner to interact with the periplasmic loops of PomA (Homma et al., 2021). Once the stator unit is incorporated into the rotor, the interaction between FliG and stator units promotes stator–peptidoglycan binding, completing the assembly (Terahara et al., 2017; Kojima et al., 2018; Nord and Pedaci, 2020). A simple Hill–Langmuir absorption model has been proposed to describe the dynamic response of stator unit to the change of external load (Nord et al., 2017a; Wadhwa et al., 2019). The model assumes that each stator unit can be either diffusing freely on the membrane or binding to a motor. The unbinding rate k_{off} and the binding rate k_{on} describe the probability of a stator unit switching between the two modes and can be affected by the external load. When the external load changes, the number of bound stator units would adjust to the new state with an exponential transition. However, the detailed role of coupling ions to the stator unit assembly and disassembly dynamics remains unclear.

The chimeric stator, PomA/PotB7^E, was developed in 2003 initially for the research of ion selectivity (Asai et al., 2003). The PotB7^E joining the N terminus of *Vibrio alginolyticus* PomA to the periplasmic C terminus of *E. coli* MotB can function with native PomA from *V. alginolyticus* as the sodium stator in Δ*motAmotB E. coli* cells, shown in **Figures 1A,B**. The sodium-driven stator in *E. coli* provides a useful experimental system to manipulate the sodium gradient of SMF without interfering membrane potential (Lo et al., 2007). The SMF and the torque–speed relationship of chimeric BFM has been reported (Lo et al., 2006, 2007, 2013; Inoue et al., 2008; Nord et al., 2017b). However, very little is known for the critical ion concentration-dependent stator dynamics. Here, we use microfluidic devices to perform computer-controlled fast perfusion and high-throughput experiments to investigate the stator dynamics to the sodium ion concentrations. We found the chimeric BFMs maintain constant speed over a wide range of sodium concentrations by adjusting stator units in compensation to the SMF changes. The number of stator units shows a reduction and then resurrection during a step-down sodium transition. This may imply the existence of a metastable hidden state of the stator unit during the sudden loss of sodium ions.

MATERIALS AND METHODS

Bacterial Strains and Culture Conditions

Bacterial strains and growth medium used in this study are listed in **Table 1**. Briefly, the chimera strain (YS34 with pYS11 and pYS13) with sodium-type stator units in *E. coli* was used (Sowa et al., 2005; Lo et al., 2006, 2007). The wild-type strain with proton-type stator units (SYC12) was modified from *E. coli* strain RP437 by replacing *fliC* on the genome to the sticky filament *fliCst* (Scharf et al., 1998; Ryu et al., 2000; Hata et al., 2020). A dual fluorescent protein fused strain (fluorescent chimera) with chimeric sodium-type stator units in *E. coli* was constructed and derived from JHC36 (Inoue et al., 2008). The stator-unit protein PomA is fused with enhanced GFP (eGFP), and the rotor protein FliN is fused with mCherry.

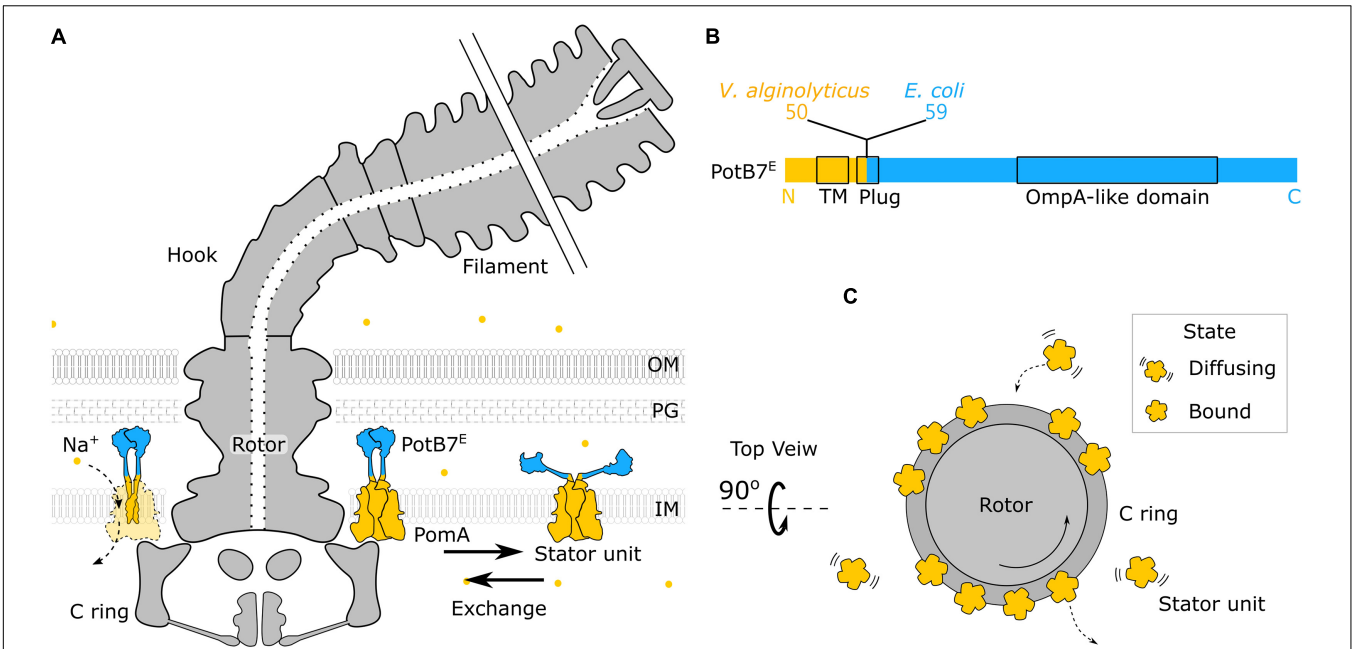

FIGURE 1 | Structure of chimeric bacterial flagellar motor. **(A)** Schematic of the chimeric flagellar motor side view. A stator unit can diffuse on the membrane or bind to the motor. A bounded stator unit can interact with the C ring of the rotor and drive the rotor to rotate. The stator is composed of the PomA (orange) from *Vibrio alginolyticus* and the chimeric PotB7^{E}. The PotB7^{E} joins the N terminus of *V. alginolyticus* PomA to the periplasmic C terminus of *Escherichia coli* MotB. The blue part is from *E. coli*, and the orange part is from *V. alginolyticus*. The chimeric stator units utilize the electrochemical energy of sodium ions (orange dots) to the motor rotation. **(B)** Schematics of the primary structure of a PotB7^{E}. The black boxes represent the identified functional areas. OM, outer membrane; PG, peptidoglycan; IM, inner membrane; TM, transmembrane. **(C)** Top view of the flagellar motor. Stator units dynamically assemble to a motor (Bound) or disassemble from a motor and diffuse on the membrane pool (Diffusing).

TABLE 1 | The list of bacterial strains and medium used in this study.

	Description	References
Bacterial strains		
YS34	*fliC*::Tn10, Δ*pilA,* Δ*motAmotB,* Δ*cheY,* RP4979 derivative	Sowa et al., 2005
Chimera	YS34 + pYS11 + pYS13	Sowa et al., 2005
SYC12 (wild type)	*fliC*::*fliC*st, otherwise wild type, RP437 derivative	Hata et al., 2020
EFS023	*fliC*::*fliC*st, Δ*motAB,* Δ*fliN,* JHC36 derivative	This study
Fluorescent-chimera	EFS023 + pTSK121 + pTSK108	This study
Plasmids		
pYS11	*fliC* sticky filaments, ampicillin resistance, pBR322 derivative	Sowa et al., 2005
pYS13	*pomA*/*potB7*^{E}, IPTG inducible, chloramphenicol resistance, pMMB206 derivative	Sowa et al., 2005
pTSK121	*egfp-pomA*/*potB7*^{E}, arabinose inducible, ampicillin resistance, pBAD24 derivative.	This study
pTSK108	*mCherry-fliN*, salicylate inducible, chloramphenicol resistance, pKG116 derivative.	This study
Growth medium		
LB	1% tryptone (BD Bacto), 0.5% yeast extract (cat. no. Y1625, SIGMA), 0.5% NaCl	
TB	1% tryptone (BD Bacto), 0.5% NaCl	

Cells from frozen stocks were cultured in 2 mL of Luria–Bertani broth (LB) overnight at 37°C. Then, overnight culture was diluted 40× to 2 mL in tryptone broth (TB) for 5 h at 30°C. The required antibiotics and inducers were added to the growth medium to preserve the plasmids and express the proteins. Antibiotics concentrations were 34 μg/mL for chloramphenicol and 50 μg/mL for ampicillin. The inducer concentrations were 25 μM for isopropyl-β-D-thiogalactoside, 0.002% for arabinose, and 313 nM for sodium salicylate.

Beads Assay and Sample Preparation

To truncate flagellar filaments, 1.2 mL of cells in TB was sheared by passing 30 times back and forth through a shearer, a custom-made device with two syringes mounted to two 26-gauge needles connected by a tube. The sheared cells were washed three times

and concentrated to OD 1.0 through centrifugation (5,200*g*, 2 min) with motility buffer (MB, 10 mM potassium phosphate, *X* mM NaCl, *Y* mM KCl, 0.1 mM EDTA, pH 7.0), where *X* depends on the designed sodium ion concentration, and the total ionic strength ($X + Y$) is fixed to 85 mM.

To perform fast perfusion experiments, we used 3-way microfluidic chambers (μ-Slide III 3in1, cat. no. 80311, ibidi). The channel slide was first coated with 60 μL of 0.001 % (wt/vol) poly-L-lysine for 1 min from port B, shown in **Figure 2A**. Then, the coating solution was removed by adding 180 μL MB to each port—1, 2, 3—and the waste was withdrawn from port B. The chamber slide was set up to a microscope, and ports 1 and 3 of the slide were respectively connected to two programmable syringe pumps (Fusion 400, Chemyx) loaded with MB containing specific sodium concentration.

The cells were injected into the slide from port 2 and waited for 30 min for the adhesion. The unattached cells were flushed away by MB from port 2. After that, 0.125 % (wt/vol) of polystyrene beads (0.99-μm diameter, cat. no. 07310, PolySciences) was injected into the slide from port 2 and waited for 30 min for beads attaching to flagella. The unattached beads were flushed away with the flow of MB from port 2. To remove all potential residues, the extra 1 mL MB perfusion from ports 3 and 1 was performed at a flow rate 2,000 μL/min. Finally, a slow washing flow of 20 μL/min was maintained in the channel.

The high-throughput BFM rotation experiments were imaged by a Nikon Ti-U microscope equipped with a 100× objective (N.A. 1.49), a 0.6× relay, and a CMOS camera (UI-3370CP-M-GL, IDS) recording at 450 fps with 2,048 × 350 pixel^2. Simultaneous high-spatial-resolution BFM rotation recording of one BFM can be achieved by back focal-plan interferometry (BFI), shown in **Figure 2A**. The fluorescence experiments were conducted on the same microscope with laser illumination and imaged by an EMCCD camera (Evolve 512, Photometrics). All experiments were conducted at 25°C ± 1°C.

Perfusion Experiment and Data Collection

All perfusion and recording were controlled by the computer for consistency. The high-throughput BFM rotation images were collected from 80 positions in the middle of the channel slide at 450 fps and 1 s long each. During the recording, the channel was kept at a slow constant flow (20 μL/min) of fresh MB.

In sodium switch experiments, three-stage sodium ion concentration sequences were applied to the channel indicated as *X*-*Y*-*X* sequence, where each number represents the extracellular sodium ion concentration ($[Na^+]_{ex}$) in mM. We used the camera program (Streampix 7) and Labview to control perfusion and imaging timing.

The experimental sequence is as follows. First, the cells were maintained at *X* mM $[Na^+]_{ex}$ by the pump connected to port 1 with a constant flow (20 μL/min) for 5 min. The pump was stopped, and the second pump connected to port 3 was activated to perfuse 75 μL with a fast flow rate (2,000 μL/min) for approximately 3 s to switch the $[Na^+]_{ex}$ to *Y* mM. Then, the flow rate was turned down to a slow constant flow (20 μL/min). After 5 min, the pump switching process was repeated, but the order of pumps was inversed to restore the $[Na^+]_{ex}$ to *X* mM for another 5 min.

The image data were collected with dynamic intervals where higher-resolution recording is applied to the fast speed transition regions, **Supplementary Figure 1**. For the first stage, approximately 5-minute period (Δt_1), the steady rotations were recorded 1 s in every 20-second durations (duty cycle 1:20). For the second stage, the recording sequence was continuous 7 s (Δt_{2-1}, duty cycle 1:1), 1 s in every 3 s for a total of 76 s (Δt_{2-2}, duty cycle 1:3), and 1 s in every 20 s (Δt_{2-3}, duty cycle 1:20) for the rest 221 s. Stage 3 is a repeat of stage 2. One BFM rotation was recorded continuously with high spatial and temporal resolution by BFI in the whole experiments at 1-kHz sampling rate (**Figure 2A**).

Data Analysis

To image data, the rotation speeds of BFMs were monitored by the attached 1-μm beads. The stage drift was corrected prior to further processing. The beads' center positions were found by weighting of the intensity signal. For BFI data, the beads' positions were derived by the quadrant photodiode signal as in previous studies (Rowe et al., 2003; Sowa et al., 2005). During the fast flow, the images of attached beads were affected approximately 5 s, including the relaxation of the flow switch. The speed data were excluded in these periods.

The speed was calculated from the power spectrum of combined *x*-*y* position data (Rowe et al., 2003) of 1 s. To ensure the data quality from the bead assay, three criteria were applied to the data analysis. First, the radical fluctuation is small, and the orbit is steady. Second, the rotation radius is within 180 and 220 nm. Third, the rotation speed is stable without any sudden stop unless for low $[Na^+]_{ex}$ conditions.

To calculate the sodium-motive force (SMF), Eqs. 1, 3, and 4 and membrane potential (V_m) from the previous report (Lo et al., 2007) were used. The condition $[Na^+]_{ex} = 0$ leads to an undefined value of Eq. 3. We estimated the maximum sodium residue is 0.08 mM in the sodium-free MB from the ingredients' impurities. Therefore, we use $[Na^+]_{ex} = 0.08$ mM for the SMF estimation in the condition $[Na^+]_{ex} = 0$.

RESULTS

Sodium-Dependent Stator Assembly at Equilibrium

First, we investigated the BFM speed at a different $[Na^+]_{ex}$. The cells are in the desired $[Na^+]_{ex}$ at least for 1 h. Similar to the sodium-driven BFM in *V. alginolyticus* (Sowa et al., 2003), the speed of sodium-driven chimeric BFM in *E. coli* is sodium-dependent with a saturation speed of approximately 80 Hz at 10 mM $[Na^+]_{ex}$ with 1-μm bead load, as shown in **Figure 2B**.

At 1-μm bead high-load condition, the rotation speed is proportional to the number of stator units (Inoue et al., 2008). Here, we assume the speed contribution from each stator unit is equal and independent of the rest of bound stator units. *E. coli*

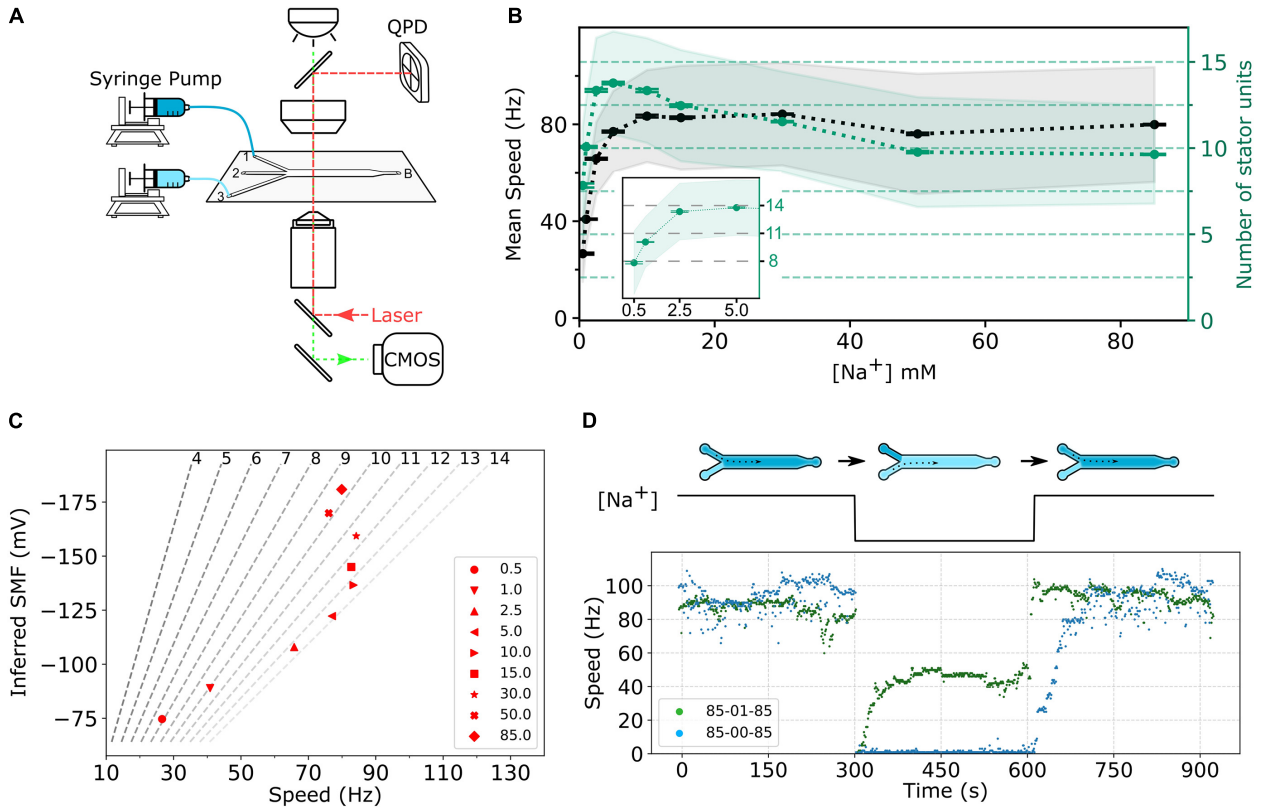

FIGURE 2 | (A) Schematic of the experimental setup. The bacterial cells are immobilized on the surface of a three-way microfluidic chamber. The BFMs' rotations were recorded by a high-speed CMOS camera (green light path), and one BFM rotation can be measured simultaneously by a BFI system (red light path). Two syringe pumps connect to inlet ports 1 and 3, respectively, to supply two different sodium concentrations of MB. Slow constant flow (20 μL/min) is maintained all the time to remove any bacterial waste. **(B)** Sodium ion dependency of BFM speed. The black dots, gray shaded area, and error bar represent average BFM speed, the standard deviation, and the standard error of the mean, respectively, under the load of 1-μm beads as $[Na^+]_{ex}$ varies. The green dots, light-green shaded area, and error bar show the inferred number of stator units, standard deviation, and standard error of the mean, respectively. Inset: Enlarge the number of stator unit data in the low-sodium region. The numbers of measured BFMs are N = 805, 2,463, 1,489, 1,785, 1,149, 1,929, 7,047, 2,562, and 6,833 for $[Na^+]_{ex}$ = 0.5, 1, 2.5, 5.0, 10.0, 15.0, 30.0, 50.0, and 85.0 mM, respectively. **(C)** BFM states diagram. The speed of BFM is dependent on the SMF and the number of stator units. The red dots are the BFM average speed in panel **(B)** and the SMF at that $[Na^+]_{ex}$. The dashed lines are stator unit number contour line from Eq. 2 labeled at the top. **(D)** BFM speed response to the perfusion experiments. The top diagram shows the experimental course with *X*-*Y*-*X* mM $[Na^+]_{ex}$ perfusion. There are three stages in each experiment, and each stage remains approximately 5 min. The numbers in the legend indicate the $[Na^+]_{ex}$ at each stage. The bottom figure shows two represented experimental BFI data sets. For the 85-00-85 mM experiment (blue dots), the BFM speed drops to zero as $[Na^+]_{ex}$ was depleted and resurrected by stepwise speed increase as $[Na^+]_{ex}$ restored to 85 mM. For 85-01-85 mM experiments (green dots), the BFM speed drops to zero and then resurrected to a steady speed as $[Na^+]_{ex}$ changes to 1 mM. The speed returned back to high speed level as $[Na^+]_{ex}$ restored to 85 mM.

has partial homeostasis of internal sodium concentration,

$$[Na^+]_{in} = 7.2\,([Na^+]_{ex})^{0.2}, \quad (1)$$

where $[Na^+]_{in}$ and $[Na^+]_{ex}$ are the intracellular and extracellular sodium ion concentrations, respectively (Lo et al., 2006). Furthermore, the relation between the sodium ion gradient and the single stator unit speed has been reported (Lo et al., 2006),

$$F_s = 6.408 - 2.745\log\frac{[Na^+]_{in}}{[Na^+]_{ex}} \quad (2)$$

where F_s (Hz/stator) is the rotational speed contributed from a single stator unit. Using these relations, the rotational speed contributed by a single stator unit (F_s) can be obtained.

The number of stator units in the steady state is calculated by dividing the average speed by F_s, as shown in **Figure 2B**. The number of stator units is not a monotonic increase with the increase in $[Na^+]_{ex}$. The stator unit number increases rapidly from 0 to 2.5 mM $[Na^+]_{ex}$ and reaches its maximum at approximately 5 mM $[Na^+]_{ex}$ (**Figure 2B**, inset). From 10 to 85 mM $[Na^+]_{ex}$, the number of stator units reduces from 14 to approximately 10. For 85 mM $[Na^+]_{ex}$, the stator unit number is consistent with the previous report (Reid et al., 2006). To further confirm this new finding that the number of bound stator units around the motor does not increase with the increasing $[Na^+]_{ex}$, we measured the average fluorescent intensity of functional BFMs in eGFP-PomA strain, **Supplementary Figure 2**. The results confirmed that there are more stator units in the 1 and 5 mM $[Na^+]_{ex}$ conditions than in 85 mM $[Na^+]_{ex}$. This is different from the general belief that the stator is more stable in the higher $[Na^+]_{ex}$.

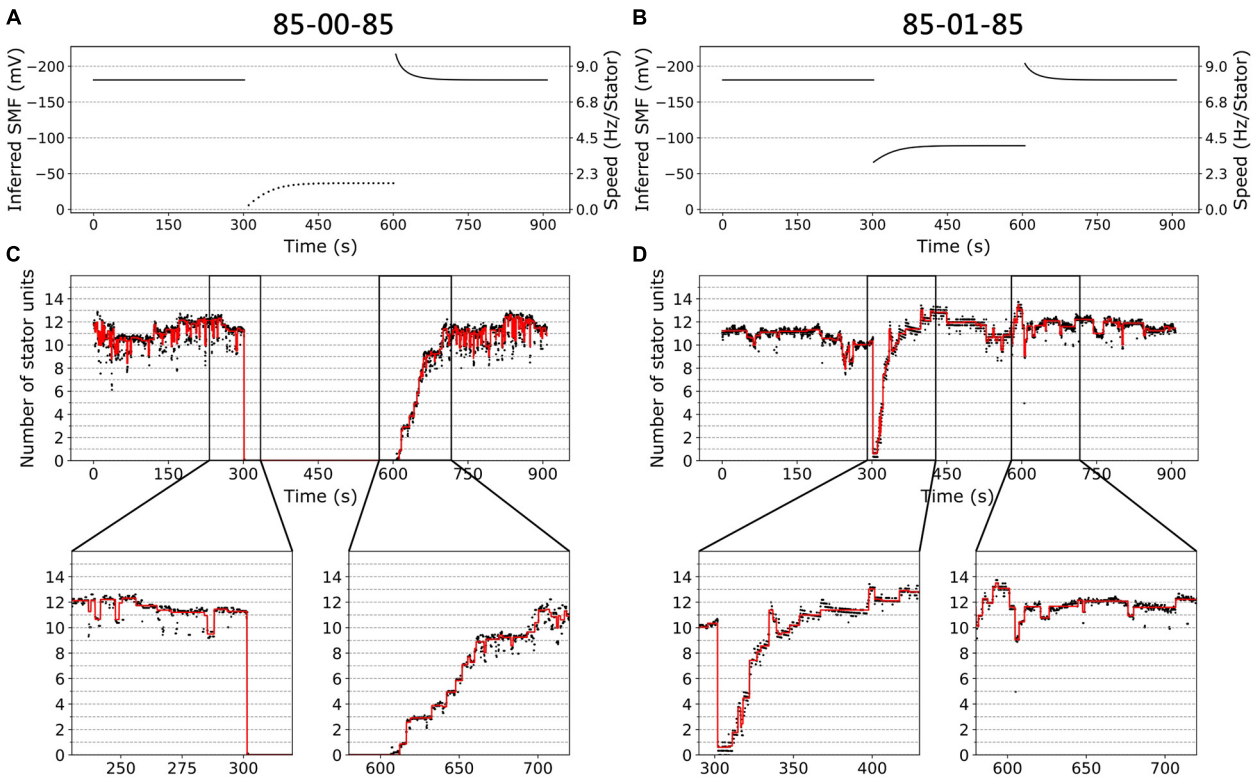

FIGURE 3 | BFM speed and stator dynamics. **(A)** The inferred SMF as a function of time for experiment 85-00-85 mM sequence. The dotted line represents an estimated SMF with the assumption of nonzero $[Na^+]_{ex}$ = 0.08 mM because the sodium gradient term is undefined at zero sodium ion concentration. The right-hand-side *y* axis shows the speed per stator unit. **(B)** The inferred SMF as a function of time for experiment 85-01-85 mM sequence. **(C)** The stator unit number of a representative trace in an experiment with 85-00-85 mM sequence, same data in **Figure 1D**. The insets are the magnification of transition courses (rectangle region). The red line is the stator number filtered by the edge-preserving Chung–Kennedy filter (Chung and Kennedy, 1991) and was stepped by Student *t* test (Leake et al., 2004). **(D)** The stator unit number of a representative trace in experiment 85-01-85 mM sequence, same data in **Figure 1D**.

Stator Number Under Dynamic Sodium-Motive Force

The V_m remains constant in these experimental conditions (Lo et al., 2007). Therefore, the SMF,

$$\mathrm{SMF} = V_m - 2.3\frac{kT}{e}\log\frac{[Na^+]_{ex}}{[Na^+]_{in}} \quad (3)$$

can be calculated, where k is the Boltzmann's constant, T is the absolute temperature, and e is the elementary charge. To illustrate the status of BFM, we plot the BFM state diagram as the function of average speed and SMF with stator-unit number contour lines (**Figure 2C**). It is clear that the BFM remains constant speed over a wide range of $[Na^+]_{ex}$, and the number of stator units is maximized at approximately 5 mM $[Na^+]_{ex}$.

To further investigate the BFM stator units dynamics, we designed fast perfusion experiments for BFM to switch from different states of $[Na^+]_{ex}$. **Figure 2D** shows the typical time course for two experiments with step-down and step-up of $[Na^+]_{ex}$. For the 85-00-85 mM sequence, the BFM speed is initially at approximately 80 Hz in 85 mM $[Na^+]_{ex}$ and stopped immediately as 0 mM $[Na^+]_{ex}$ introduced. The rotational speed recovered in a stepwise fashion within few minutes after the $[Na^+]_{ex}$ is restored to 85 mM (**Figure 2D**, blue dots) as reported (Sowa et al., 2014). For 85-01-85 mM experimental sequence, from the steady state BFM speed and stator unit number data (**Figure 2B**), we expect there is a speed change, but no stator unit number changes. However, the BFM speed shows two-stage speed changes with an overshooting and then recovery to the steady-state speed during the step-down $[Na^+]_{ex}$. When the $[Na^+]_{ex}$ is restored to the initial 85 mM level, the BFMs speed up to the original level quickly.

Because the BFM speed depends on both SMF and the number of stator unit, it is necessary to analyze the SMF contribution during the perfusion. *E. coli* has partial homeostasis of internal sodium concentration and response time for the physiological adjustment to the new steady intracellular sodium concentration (Lo et al., 2006). The dynamic response of intracellular sodium ion concentration can be described as follows:

$$[Na^+]^t_{in} = [Na^+]^i_{in} + \left([Na^+]^f_{in} - [Na^+]^i_{in}\right)\left(1 - e^{-t/\tau}\right) \quad (4)$$

where $[Na^+]^i_{in}$ and $[Na^+]^f_{in}$ are the stationary intracellular sodium concentration before and after perfusion. The response time

constant τ is 29 s as reported (Lo et al., 2006). Given initial and final $[Na^+]_{ex}$, the $[Na^+]^i_{in}$ and $[Na^+]^f_{in}$ can be calculated by homeostasis relation (Eq. 1). Then, we are able to calculate the sodium gradient and SMF as the functions of time from Eqs. 3, 4 and estimate the single stator speed by Eq. 2.

Figures 3A,B show the inferred SMF results for the two conditions of the same traces in **Figure 2D**. The SMF would decrease (more positive) while switching from high to low $[Na^+]_{ex}$. As a result, the speed per stator unit also decreases in the lower $[Na^+]_{ex}$.

We applied the above method to estimate the number of stator units in the whole perfusion experiments (**Figures 3C,D**). For 85-00-85 mM perfusion experiments, the speed recovery trace (0–85 mM) shows stepwise but not equal increment speed recovery (**Figure 2D**, blue dots). This is because the SMF adjusted as well. By our estimation, considering the SMF dynamics, the stepwise changes of stator unit match the discrete stator unit number, which suggests our estimation is reasonable, as shown in **Figure 3C**.

For 85-01-85 mM perfusion experiment, although the steady-state speed changes, however, the stator unit number is close to 11 in both 1 and 85 mM $[Na^+]_{ex}$ conditions (**Figure 3D**). Therefore, we expect there is a direct speed change without number of stator unit changes. Surprisingly, during the 85-01 mM perfusion, the number of stator units reduced to zero and then recovered to the same level as 85 mM (**Figure 3D**). This is very different from the simple Hill–Langmuir absorption model of stator unit dynamics. Further investigation is presented in section "Stator Response to Sodium Concentration Shift."

Sodium-Dependent Stator Kinetics

To quantify the sodium ion dependency of stator units, we systematically investigate the BFM speed and stator unit number dynamics between various $[Na^+]_{ex}$. The experiments were designed as a three-stage perfusion sequence of *X-Y-X* mM $[Na^+]_{ex}$.

First, we investigated the BFMs from different $[Na^+]_{ex}$ to the extreme condition with zero sodium. The BFM stator kinetics shows similar patterns in all conditions. The BFM is driven by sodium ion and stopped at zero $[Na^+]_{ex}$ immediately (**Figures 4A,B**). The BFM speed recovered from zero to its original level once the $[Na^+]_{ex}$ was restored in a few minutes (**Figures 4A,B** and **Supplementary Figure 3**). The stator unit numbers were then recovered as well (**Figure 4C**).

The simplest stator dynamics model has been reported and described by a reversible Hill–Langmuir model (Nord et al., 2017a; Wadhwa et al., 2019). This model assumes that there is a pool of stator units diffusing independently on the membrane. A rotor with N_{max} independent bound stator units was fixed on the membrane. A bound stator unit can unbind with a rate constant k_{off}, and a free stator unit can bind to an empty site with a rate constant k_{on}. To the average stator occupancy, *N(t)* follows:

$$\frac{dN}{dt} = k_{on}(N_{max} - N) - k_{off}N \quad (5)$$

At steady state, that is, *dN/dt = 0,* the steady state stator occupancy is determined by $N_s = N_{max}/(1 + K_D)$ where $K_D = k_{off}/k_{on}$.

When the motor encounters a state transition, the simple model predicts an exponential transition toward the new steady-state occupancy (Nord et al., 2017a; Wadhwa et al., 2019),

$$N(t) = N^f + (N^i - N^f)e^{-Kt} \quad (6)$$

where N^f and N^i are the number of stator units in the initial and final steady states, and

$$k_{on} = \frac{N_s \cdot K}{N_{max}}\ ;\ k_{off} = \frac{(N_{max} - N_s) \cdot K}{N_{max}} \quad (7)$$

The single exponential equation described by a constant rate *K* relates to the stators' on/off rate as $K = k_{on} + k_{off}$.

Based on this model, the stator resurrection process can be fitted by Eq. 6 (**Figure 4C**, line), and rate constant *K*, k_{on}, and k_{off} can be obtained (**Figures 4D,E**). The recovery rate constant *K* increases as the $[Na^+]_{ex}$ increases (**Figure 4D**). In **Figure 4E**, the k_{on} is a constant in the range of $[Na^+]_{ex}$ = 5 to 85 mM, whereas the k_{off} increases in this range. At 5 mM $[Na^+]_{ex}$ conditions, there are more stator units because the k_{off} is at the lowest point. However, in the 2.5–0.5 mM $[Na^+]_{ex}$ range, k_{on} drops rapidly, whereas k_{off} increases a little.

Current understanding of stator unit assembly process comprises the first step of rotor–stator interaction and the second step of stator binding to the cell wall (Kojima et al., 2011; Kojima, 2015). The previous result showed the sodium ion can bind to stator units after its conformational change which leads to the plug open and the structural changes of the cytoplasmic loop (Onoue et al., 2019). That is an assembly-coupled stator activation. It has been reported that the assembly of stator units in the sodium-driven BFMs is sodium-dependent (Fukuoka et al., 2009). Our results support that at least 5 mM $[Na^+]_{ex}$ is required for stator units stabilization and interaction with the rotor.

However, the k_{off} raises as more sodium was introduced. The manner is similar to the load-dependent stator stability that the stator is less stable and k_{off} is higher in the low load conditions. It is the increment of the k_{off} that leads to the drop of stator unit in a higher sodium concentration. It might be interesting to test the stability of stator units in the extremely high sodium concentration within the cell physiology conditions.

Stator Response to Sodium Concentration Shift

The BFM has mechanosensing capability for cells to adapt to the chemical and mechanical changes of environments (Nord et al., 2017a; Wadhwa et al., 2019). However, very little is known for the effect of driving ion concentration on the BFM stator dynamics. In the following section, we reported the investigation of stator adjustment to the nonzero $[Na^+]_{ex}$ change. **Figure 5A** shows the BFM speed under perfusion experiments of 85-01-85 mM $[Na^+]_{ex}$. BFMs rotate stably at 80 Hz in the 85 mM $[Na^+]_{ex}$. There was a dramatic speed drop when 1 mM $[Na^+]_{ex}$ was applied and then resurrected to the 40-Hz steady-state speed.

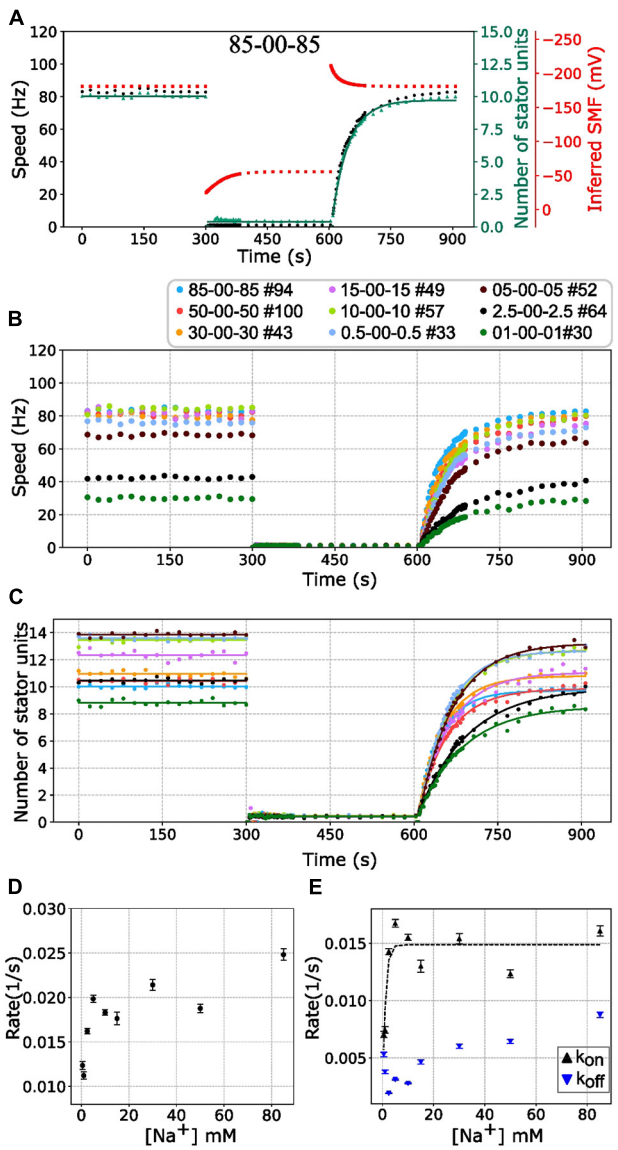

FIGURE 4 | BFM speed and stator number kinetics to zero $[Na^+]_{ex}$. **(A)** Perfusion experiment of 85-00-85 mM sequence. The black dots show the average BFM speed. The red dots represent the inferred SMF. The green dots and line represent the number of stator units and fitting result to the simple Hill–Langmuir absorption model **(B)** BFM speed data collection of perfusion experiments with different $[Na^+]_{ex}$. The legend indicates the perfusion $[Na^+]_{ex}$ sequence and the number of BFM speed data collected. **(C)** The dots and lines show the number of stator units inferred from the speed results in B and the fitting results, respectively. **(D)** The recovery rate constants in the third stages (zero to high $[Na^+]_{ex}$) in C versus $[Na^+]_{ex}$. **(E)** The K_{on} and K_{off} according to the sodium concentration derived from panels **(C,D)**. The black tendency line for the K_{on} is obtained by fitting a simple exponential curve. The error bar in panels **(D,E)** represents the standard deviation of the fitting parameter.

And then, a speed increased when the 85 mM $[Na^+]_{ex}$ was restored to the chamber.

Because the $[Na^+]_{in}$ response time is long (29 s) compared with the perfusion time (3 s), the SMF dropped first and then increased to the steady state when the medium changes to lower $[Na^+]_{ex}$ (**Figure 5A**, red line). There is an inverse response for the perfusion experiment to the higher $[Na^+]_{ex}$ (**Figure 5A**). Therefore, it seems the BFM speed drop is reasonable. However, the number of stator units is also with a sudden change when the medium changes to lower $[Na^+]_{ex}$ (**Figure 5A**, green line). The number of stator units was approximately 10 in the 85 mM $[Na^+]_{ex}$ and drop to 5 right after 1 mM $[Na^+]_{ex}$ was applied. The number of stator units resurrected to 10 in approximately 2 min (**Figure 5A**). The phenomenon was examined in high temporal resolution data of a single motor as well (**Figures 3B,D**). Clearly, there was a fast stator number reduction and stepwise resurrection during the recovery part in the step-down $[Na^+]_{ex}$ (**Figure 3D**, inset).

We further examined BFM speed in different levels of $[Na^+]_{ex}$ changes (**Figure 5B** and **Supplementary Figure 4**) and the number of stator units dynamics (**Figure 5C**). Overall, the speed profiles are similar to the 85-01-85 mM perfusion experiments. Under step-down perfusion, the BFM speeds drop and gradually raise to the steady-state speed.

For 85-30 (mM), 30-05 (mM), and 85-05 (mM) perfusion experiments, the BFM speeds were approximately the same, and the motors recruited more stator units (**Figures 5B,C**). To verify the increase in stator number, we examined the speed data with high time resolution of a single motor (**Supplementary Figure 5**). The stepwise increase in speed is the evidence for recruiting new stator units. For 30-85 (mM), 05-30 (mM), and 05-85 (mM) perfusion experiments, the BFM speed remains approximately the same level, and the number of stator units reduced (**Figures 5B,C**).

For 85-01 (mM) and 30-01 (mM) perfusion experiments, the stator units reduced first and then resurrected. This is different from the reversible Hill–Langmuir model. The two-stage transition may be due to the cell's stator response or physiological response (membrane potential). We examined the perfusion experiment 85-00-85 (mM) in the wild-type *E. coli* proton-driven motor (**Supplementary Figure 6**). When sodium was completely removed, the wild-type motor maintains the same speed. The result suggests that the cell physiology and membrane potential remain the same in the sodium perfusion experiments. It is likely the stator unit has extra mechanism of the sodium response.

To further quantify the initial stator unit jump in the step-down $[Na^+]_{ex}$ perfusion experiment, we compiled the statistic of the number of stator unit changes (**Figure 5D**). For 85-05 (mM) and 30-05 (mM) perfusion, the number of stator units in average shifts approximately 1 and 2, respectively. The positive numbers reflect the increasing affinity for higher stator numbers to maintain the power output. For 85-01 (mM), the stator unit dropped at least 5 of 10 stator units on average, implying that the motor may encounter quick remodeling of stator units.

To characterize the response time scale of the stator unit dynamics, the stator unit resurrection traces are fitting with Eq. 6. In **Figure 5E**, one can find that these k_{on} and k_{off} are very different from stator unit resurrection from 00-01 mM perfusion experiments. The k_{on} for 85-01 mM perfusion is approximately

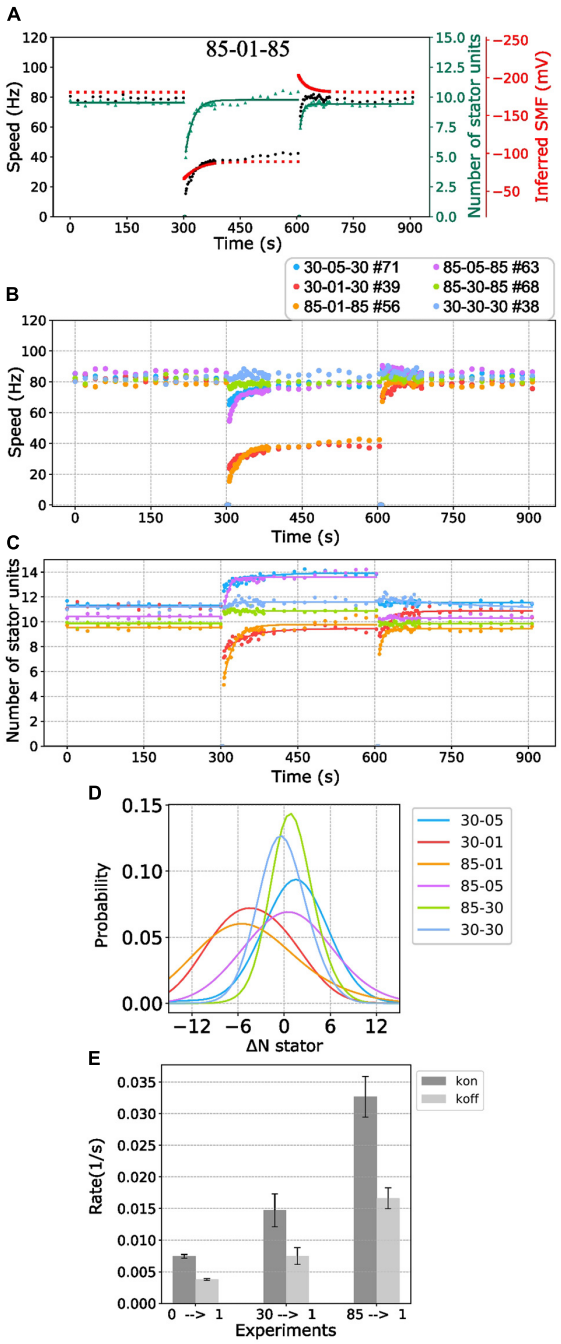

FIGURE 5 | BFM speed and stator number kinetics to nonzero $[Na^+]_{ex}$. **(A)** Perfusion experiment of 85-01-85 mM sequence. The black dots show the average BFM speed. The red dots represent the inferred SMF. The green dots and line represent the number of stator units and its fitting result to the simple Hill–Langmuir absorption model. **(B)** BFM speed data collection of perfusion experiments from high to different nonzero different $[Na^+]_{ex}$. The legend indicates the perfusion $[Na^+]_{ex}$ sequence and the number of BFM speed data collected. **(C)** The dots and lines show the number of stator units inferred from the speed results in B and the fitting results, respectively. **(D)** Kernel density estimate of the number of stator unit differences between step-down sodium perfusion. **(E)** The K_{on}/K_{off} for 0-1, 30-1, and 85-01 mM stator unit resurrection fitting results in C. The error bar is the standard deviation of the fitting parameter.

0.03 (1/s), which is four times faster than 00-01 mM perfusion. These results may imply that the stator recruitment process may be different in these two conditions.

DISCUSSION

In this report, we applied computer-controlled microfluidic devices for fast perfusion to investigate the stator dynamics. The high-throughput and systematic data collection provides a nonbias and ideal data set for analysis.

We found that although the chimeric BFM has constant speed over a wide range of sodium ion concentrations, the stator occupancy does not saturate to its maximal capacity. Previous studies have shown that contribution of a stator unit to the motor speed increases with the rise in sodium concentration, Eq. 2 (Lo et al., 2006). Thus, the plateau region of the speed, in compensation, is the reduction of functional number of stator units on the motor as the SMF increases. This is against the long-held belief that stator unit's stability is proportional to the sodium ion concentration. Wadhwa et al. (2019) have reported the BFM stator stability decreases when the external load decreases and rotational speed increases. Although the molecular mechanism remains unclear, our results show the same conclusion that the BFM stator is less stable in the high-speed conditions. As the output power of a motor is proportional to the rotational speed, the wide-range constant speed suggests a wide range of constant power output, whereas the SMF varies. The wide range of BFM speed may provide biological advantage for bacterial cells to maintain chemotaxis and optimize the energy usage in different external environments.

The stator binding and unbinding rate k_{on} and k_{off} have different sodium dependencies. The stator k_{on} is a constant for the $[Na^+]_{ex}$ higher than 5 mM. This suggests that it required at least 5 mM $[Na^+]_{ex}$ to trigger a stable activation. On the other hand, the unbind rate k_{off} is lowest at 5 mM $[Na^+]_{ex}$ and increases for both increasing and decreasing $[Na^+]_{ex}$. For higher $[Na^+]_{ex}$ end, the BFM drives faster, and the ion flux increases. Similar to the low-load high-speed condition, the stator k_{off} increases (Nord et al., 2017a). A recent stator structure report shows an ion reservoir region in the cytoplasmic region of stator units (Santiveri et al., 2020). Therefore, the ion discharge step might be a rate-limiting step for stator to work at high $[Na^+]_{ex}$ and high-speed region. However, how the rate-limiting step destabilizes the stator binding remains unclear. For low $[Na^+]_{ex}$ end, the number of stator units is reduced due to the low binding affinity. Our finding is consistent with the model that stator stability is mediated by the external load, IMF, and other factors that would affect the force generating process (Armitage and Berry, 2020).

Sodium-driven stators in *V. alginolyticus* showed the $[Na^+]_{ex}$–dependent stator polar localization (Fukuoka et al., 2009). However, there are reports demonstrating that the loss of IMF does not affect the assembly of the stator units in *Salmonella* and *E. coli* (Morimoto et al., 2010; Suzuki et al., 2019). The chimeric stator unit, PotB7^E, is composed of *E. coli* cell wall binding domain that is critical for the stator assembly to the motor, as shown in **Figures 1A,C**. In our experiment of

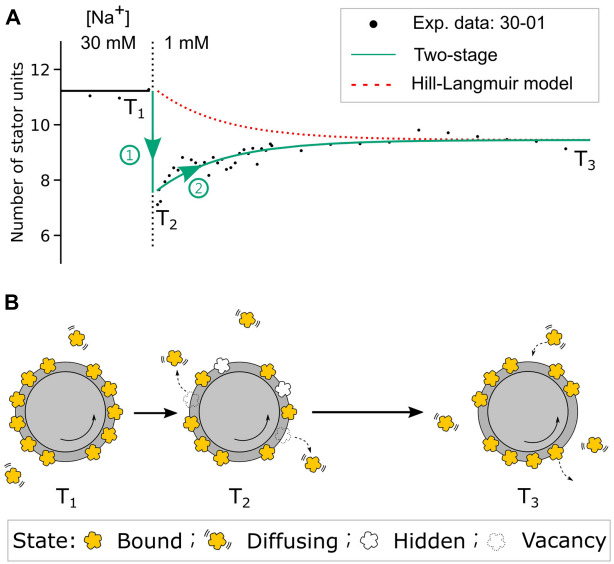

FIGURE 6 | The two-stage stator unit response model. **(A)** The comparison of stator unit numbers dynamics in the step-down 30-01 mM $[Na]_{ex}$ experiment from the two-stage model and the Hill–Langmuir absorption model. Black dots are the experimental data of stator unit numbers. The red dotted line represents the expected stator unit number transition from the Hill–Langmuir absorption model. The green line represents the time course of stator unit number in the two-stage model. T_1 and T_3 are the time points of motors at $[Na]_{ex}$ = 30- and 1-mM steady state, respectively. T_2 is the time point right after the $[Na]_{ex}$ step-down. **(B)** Model diagram of the stator states at three time points. At time point T_1, the number of stator units is dynamically balanced on the motor. Right after the $[Na]_{ex}$ step-down, stage 1 (green circle 1), the numbers of stator units reduced partially by stator units unbound and partially by stator units enter the bound-but-not-functioning hidden state. In the second stage (green circle 2), the stator units resurrect to the steady state until the motor reaches the new steady state at time point T_3. As the new dynamic balance is formed, the average number of bound stator units is less than that at T_1.

85-00 mM perfusion, the BFMs stopped immediately. In the current stator unit recruitment model, the stator units can have only bound and unbound states. One might imagine a possible condition that a stator unit could disengage with the rotor but not lose the cell wall binding, leading to a potential mechanism for the IMF independent stator assembly in *E. coli* (Morimoto et al., 2010). To verify this possibility, we conducted a single-cell fluorescent measurement of the eGFP-fused stator units, **Supplementary Figure 7A**. In a tethered cell setup, the fluorescence intensity indicated that the number of stator units reduced immediately after the 85-00 mM perfusion, **Supplementary Figure 7B**. The fluorescence also recovered after the 85 mM $[Na^+]_{ex}$ was restored. The BFM speed is consistent with stator fluorescence signal, **Supplementary Figure 7B**. We can confirm that the stator units disassembled from the rotor in the 0 mM $[Na^+]_{ex}$ conditions, showing the stator assembly and disassembly were sensitive to SMF in this chimeric motor. The data also support the model that bounded stator units can physically leave the rotor region, and the diffusing stator units can reassemble to the motor.

How the sodium ion affects the stator assembly remains unclear. Recently, Terahara et al. reported that OmpA-like domain folding is sodium-dependent in the sodium-driven MotPS stator unit (Terahara et al., 2017). However, the OmpA-like domain in the chimeric PotB7^E is from proton-driven *E. coli* MotB. We speculate that the ion transition through the stator units is the key for stator assembly in this chimeric motor as previously reported for *V. alginolyticus* (Fukuoka et al., 2009).

From the steady-state BFM speed and stator unit number data (**Figures 2B,C**), we expect no stator change in the 85-01 (mM) perfusion. Surprisingly, the stator unit number initially dropped and then resurrected to stator number in the steady state. The resurrection process is faster than these in 00-01 and 30-01 (mM) perfusion. But we did not find the reverse process as 01-85 mM perfusion experiments. In order to gain a deeper insight into the resurrection after overshooting in step-down sodium perfusion, we conducted fluorescence measurement of eGFP-fused stator units in tethered cell setup. For 30-00 and 30-01 mM perfusion experiments, as expected, tethered cell rotational speed reduced to zero and maintained the same respectively, **Supplementary Figure 7C**. However, the fluorescence intensity of the motor region drops right after the perfusion indicates a stator unit disassembled process, **Supplementary Figure 7D**. The stator unit dropping less in 30-01 mM perfusion suggests there are remaining stator units still bound to the BFM and maintaining the speed. But the resurrection is faster than 00-01 mM perfusion (**Figure 5E**). Based on these data, we proposed a two-stage stator unit response model for $[Na^+]_{ex}$ step-down, as shown in **Figure 6**. Right after the $[Na^+]_{ex}$ step-down, some stator units were disassembled, and some were still in the bind but not in the functional state. Therefore, the number of functional stator units shows a rapidly excessive reduction and then a second-stage resurrection to the steady state. A recent report using kinetic analysis on BFM speed showed multiexponential shapes of dwell-time distribution. It suggested the existence of a hidden state in the stator unit exchange process (Shi et al., 2019). The bound but not functioning state is one of the possible states of a short-life hidden state.

In light of the discussion, we can have three conclusions. First, the chimeric stator is less stable in the higher sodium concentration. Second, the stator assembly and dissemble are sodium dependent. Third, there is a possible stator bound but no functioning state existed. On the basis of our findings and available information, the reversible Hill–Langmuir model is too simple to describe the stator unit dynamics. Correlated microscopy combining BFM speed and fluorescence measurements with computer-controlled microfluidic devices could provide further insight into the stator unit dynamics. It is important to study the protein exchange in response to various factors such as load, temperature, and energetics to obtain a complete understanding of BFM working mechanisms.

DATA AVAILABILITY STATEMENT

The raw data supporting the conclusions of this article will be made available by the authors, without undue reservation.

AUTHOR CONTRIBUTIONS

T-SL and C-JL designed the project. SK, HF, AI, and MH constructed strains and design the experiments. T-SL conducted the experiments, analyzed the data, and wrote the manuscript. C-JL analyzed the data and wrote the manuscript. All authors contributed to the article and approved the submitted version.

FUNDING

This work was financially supported by the Ministry of Science and Technology, Republic of China, under contract No. MOST-107-2112-M-008-025-MY3 and MOST-109-2628-M-008- 001-MY4 to C-JL, and by the MEXT KAKENHI Grant Number JP26115705 to SK.

ACKNOWLEDGMENTS

We acknowledge the gift of *E. coli* strain from Yoshiyuki Sowa. We thank Akiko Abe for constructing the plasmids and Sandy Parkinson for providing the plasmid pKG116. We also thank Ashley Nord for the useful discussion and suggestions. C-JL acknowledge the support from National Center for Theoretical Sciences, Taiwan.

SUPPLEMENTARY MATERIAL

The Supplementary Material for this article can be found online at: https://www.frontiersin.org/articles/10.3389/fmicb.2021.765739/full#supplementary-material

REFERENCES

Armitage, J. P., and Berry, R. M. (2020). Assembly and dynamics of the bacterial flagellum. *Annu. Rev. Microbiol.* 74, 181–200. doi: 10.1146/annurev-micro-090816-093411

Asai, Y., Yakushi, T., Kawagishi, I., and Homma, M. (2003). Ion-coupling determinants of Na^+-driven and H^+-driven flagellar motors. *J. Mol. Biol.* 327, 453–463. doi: 10.1016/S0022-2836(03)00096-2

Blair, D. F., and Berg, H. C. (1988). Restoration of torque in defective flagellar motors. *Science* 242, 1678–1681. doi: 10.1126/science.2849208

Block, S. M., and Berg, H. C. (1984). Successive incorporation of force-generating units in the bacterial rotary motor. *Nature* 309, 470–472. doi: 10.1038/309470a0

Chawla, R., Ford, K. M., and Lele, P. P. (2017). Torque, but not FliL, regulates mechanosensitive flagellar motor-function. *Sci. Rep.* 7:5565. doi: 10.1038/s41598-017-05521-8

Chung, S. H., and Kennedy, R. A. (1991). Forward-backward non-linear filtering technique for extracting small biological signals from noise. *J. Neurosci. Methods.* 40, 71–86. doi: 10.1016/0165-0270(91)90118-J

Deme, J. C., Johnson, S., Vickery, O., Muellbauer, A., Monkhouse, H., Griffiths, T., et al. (2020). Structures of the stator complex that drives rotation of the bacterial flagellum. *Nat. Microbiol.* 5, 1553-1564. doi: 10.1038/s41564-020-0788-8

Fukuoka, H., Wada, T., Kojima, S., Ishijima, A., and Homma, M. (2009). Sodium-dependent dynamic assembly of membrane complexes in sodium-driven flagellar motors. *Mol. Microbiol.* 71, 825–835. doi: 10.1111/j.1365-2958.2008.06569.x

Hata, H., Nishihara, Y., Nishiyama, M., Sowa, Y., Kawagishi, I., and Kitao, A. (2020). High pressure inhibits signaling protein binding to the flagellar motor and bacterial chemotaxis through enhanced hydration. *Sci. Rep.* 10:2351. doi: 10.1038/s41598-020-59172-3

Homma, M., Terashima, H., Koiwa, H., and Kojima, S. (2021). Putative spanner function of the *Vibrio* PomB plug region in the stator rotation model for flagellar motor. *J. Bacteriol.* 203:e0015921. doi: 10.1128/JB.00159-21

Inoue, Y., Lo, C., Fukuoka, H., Takahashi, H., Sowa, Y., Pilizota, T., et al. (2008). Torque – speed relationships of Na^+-driven chimeric flagellar motors in *Escherichia coli*. *J. Mol. Biol.* 376, 1251–1259. doi: 10.1016/j.jmb.2007.12.023

Kojima, S. (2015). Dynamism and regulation of the stator, the energy conversion complex of the bacterial flagellar motor. *Curr. Opin. Microbiol.* 28, 66–71. doi: 10.1016/j.mib.2015.07.015

Kojima, S., Nonoyama, N., Takekawa, N., Fukuoka, H., and Homma, M. (2011). Mutations targeting the C-terminal domain of FliG can disrupt motor assembly in the Na^+-driven flagella of *Vibrio alginolyticus*. *J. Mol. Biol.* 414, 62–74. doi: 10.1016/j.jmb.2011.09.019

Kojima, S., Takao, M., Almira, G., Kawahara, I., Sakuma, M., Homma, M., et al. (2018). The helix rearrangement in the periplasmic domain of the flagellar stator B subunit activates peptidoglycan binding and ion influx. *Structure* 26, 590–598. doi: 10.1016/j.str.2018.02.016

Leake, M. C., Chandler, J. H., Wadhams, G. H., Bai, F., Berry, R. M., and Armitage, J. P. (2006). Stoichiometry and turnover in single, functioning membrane protein complexes. *Nature* 443, 355–358. doi: 10.1038/nature05135

Leake, M. C., Wilson, D., Gautel, M., and Simmons, R. M. (2004). The elasticity of single titin molecules using a two-bead optical tweezers assay. *Biophys. J.* 87, 1112–1135. doi: 10.1529/biophysj.103.033571

Lele, P. P., Hosu, B. G., and Berg, H. C. (2013). Dynamics of mechanosensing in the bacterial flagellar motor. *Proc. Natl. Acad. Sci. U.S.A.* 110, 11839–11844. doi: 10.1073/pnas.1305885110

Lin, T.-S., Zhu, S., Kojima, S., Homma, M., and Lo, C.-J. (2018). FliL association with flagellar stator in the sodium-driven *Vibrio* motor characterized by the fluorescent microscopy. *Sci. Rep.* 8:11172. doi: 10.1038/s41598-018-29447-x

Lo, C.-J., Leake, M. C., and Berry, R. M. (2006). Fluorescence measurement of intracellular sodium concentration in single *Escherichia coli* cells. *Biophys. J.* 90, 357–365. doi: 10.1529/biophysj.105.071332

Lo, C.-J., Leake, M. C., Pilizota, T., and Berry, R. M. (2007). Nonequivalence of membrane voltage and ion-gradient as driving forces for the bacterial flagellar motor at low load. *Biophys. J.* 93, 294–302. doi: 10.1529/biophysj.106.095265

Lo, C.-J., Sowa, Y., Pilizota, T., and Berry, R. M. (2013). Mechanism and kinetics of a sodium-driven bacterial flagellar motor. *Proc. Natl. Acad. Sci. U.S.A.* 110, E2544–E2551. doi: 10.1073/pnas.1301664110

Moreau, A., Gosselin-Badaroudine, P., and Chahine, M. (2014). Biophysics, pathophysiology, and pharmacology of ion channel gating pores. *Front. Pharmacol.* 5:53. doi: 10.3389/fphar.2014.00053

Morimoto, V. Y., Nakamura, S., Kami-ike, N., Namba, K., and Minamino, T. (2010). Charged residues in the cytoplasmic loop of MotA are required for stator assembly into the bacterial flagellar motor. *Mol. Microbiol.* 78, 1117–1129. doi: 10.1111/j.1365-2958.2010.07391.x

Nakamura, S., and Minamino, T. (2019). Flagella-driven motility of bacteria. *Biomolecules* 9:279. doi: 10.3390/biom9070279

Nirody, J. A., Nord, A. L., and Berry, R. M. (2019). Load-dependent adaptation near zero load in the bacterial flagellar motor J. *R. Soc. Interface* 16:20190300. doi: 10.1098/rsif.2019.0300

Nirody, J. A., Sun, Y. R., and Lo, C.-J. (2017). The biophysicist's guide to the bacterial flagellar motor. *Adv. Phys. X.* 2, 324–343. doi: 10.1080/23746149.2017.1289120

Nord, A. L., and Pedaci, F. (2020). Mechanisms and dynamics of the bacterial flagellar motor. *Adv. Exp. Med. Biol.* 1267, 81–100. doi: 10.1007/978-3-030-46886-6_5

Nord, A. L., Gachon, E., Perez-Carrasco, R., Nirody, J. A., Barducci, A., Berry, R. M., et al. (2017a). Catch bond drives stator mechanosensitivity in the bacterial flagellar motor. *Proc. Natl. Acad. Sci. U.S.A.* 114, 12952–12957. doi: 10.1073/pnas.1716002114

Nord, A. L., Sowa, Y., Steel, B. C., Lo, C.-J., and Berry, R. M. (2017b). Speed of the bacterial flagellar motor near zero load depends on the number of stator units. *Proc. Natl. Acad. Sci. U.S.A.* 114, 11603–11608. doi: 10.1073/pnas.1708054114

Onoue, Y., Iwaki, M., Shinobu, A., Nishihara, Y., Iwatsuki, H., Terashima, H., et al. (2019). Essential ion binding residues for Na^+ flow in stator complex of the *Vibrio* flagellar motor. *Sci. Rep.* 9:11216. doi: 10.1038/s41598-019-46038-6

Oswald, F., Bank, E. L. M., Bollen, Y. J. M., and Peterman, E. J. G. (2014). Imaging and quantification of trans-membrane protein diffusion in living bacteria. *Phys.Chem.Chem.Phys.* 16, 12625–12634. doi: 10.1039/c4cp00299g

Reid, S. W., Leake, M. C., Chandler, J. H., Lo, C.-J., Armitage, J. P., and Berry, R. M. (2006). The maximum number of torque-generating units in the flagellar motor of *Escherichia coli* is at least 11. *Proc. Natl. Acad. Sci. U.S.A.* 103, 8066–8071. doi: 10.1073/pnas.0509932103

Rowe, A. D., Leake, M. C., Morgan, H., and Berry, R. M. (2003). Rapid rotation of micron and submicron dielectric particles measured using optical tweezers. *J. Mod. Opt.* 10, 1539–1554. doi: 10.1080/09500340308235228

Ryu, W. S., Berry, R. M., and Berg, H. C. (2000). Torque-generating units of the flagellar motor of *Escherichia coli* have a high duty ratio. *Nature* 403, 444–447. doi: 10.1038/35000233

Santiveri, M., Roa-Eguiara, A., Kühne, C., Wadhwa, N., Hu, H., Berg, H. C., et al. (2020). Structure and function of stator units of the bacterial flagellar motor. *Cell* 183, 244–257. doi: 10.1016/j.cell.2020.08.016

Scharf, B. E., Fahrner, K. A., Turner, L., and Berg, H. C. (1998). Control of direction of flagellar rotation in bacterial chemotaxis. *Proc. Natl. Acad. Sci. U.S.A.* 95, 201–206. doi: 10.1073/pnas.95.1.201

Shi, H., Ma, S., Zhang, R., and Yuan, J. (2019). A hidden state in the turnover of a functioning membrane protein complex. *Sci. Adv.* 5, 2–7. doi: 10.1126/sciadv.aau6885

Sowa, Y., Homma, M., Ishijima, A., and Berry, R. M. (2014). Hybrid-fuel bacterial flagellar motors in *Escherichia coli*. *Proc. Natl. Acad. Sci. U.S.A.* 111, 3436–3441. doi: 10.1073/pnas.1317741111

Sowa, Y., Hotta, H., Homma, M., and Ishijima, A. (2003). Torque-speed relationship of the Na^+-driven flagellar motor of *Vibrio alginolyticus*. *J. Mol. Biol.* 327, 1043–1051. doi: 10.1016/S0022-2836(03)00176-1

Sowa, Y., Rowe, A. D., Leake, M. C., Yakushi, T., Homma, M., Ishijima, A., et al. (2005). Direct observation of steps in rotation of the bacterial flagellar motor. *Nature* 437, 916–919. doi: 10.1038/nature04003

Suzuki, Y., Morimoto, Y. V., Oono, K., Hayashi, F., Oosawa, K., Kudo, S., et al. (2019). Effect of the MotA(M206I) mutation on torque generation and stator assembly in the *Salmonella* H^+-driven flagellar motor. *J. Bacteriol.* 201:e00727–18. doi: 10.1128/JB.00727-18

Terahara, N., Kodera, N., Uchihashi, T., Ando, T., Namba, K., and Minamino, T. (2017). Na^+-induced structural transition of MotPS for stator assembly of the *Bacillus* flagellar motor. *Sci. Adv.* 3, 1–10. doi: 10.1126/sciadv.aao4119

Terashima, H., Kojima, S., and Homma, M. (2021). Site-directed crosslinking identifies the stator-rotor interaction surfaces in a hybrid bacterial flagellar motor. *J. Bacteriol.* 203:e00016–e21. doi: 10.1128/JB.00016-21

Tipping, M. J., Delalez, N. J., Lim, R., Berry, R. M., and Armitage, J. P. (2013b). Load-dependent assembly of the bacterial flagellar motor. *mBio* 4, 1–6. doi: 10.1128/mBio.00551-13

Tipping, M. J., Steel, B. C., Delalez, N. J., Berry, R. M., and Armitage, J. P. (2013a). Quantification of flagellar motor stator dynamics through in vivo proton-motive force control. *Mol. Microbiol.* 87, 338–347. doi: 10.1111/mmi.12098

Tusk, S. E., Delalez, N. J., and Berry, R. M. (2018). Subunit exchange in protein complexes. *J. Mol. Biol.* 22, 4557–4579. doi: 10.1016/j.jmb.2018.06.039

Wadhwa, N., Phillips, R., and Berg, H. C. (2019). Torque-dependent remodeling of the bacterial flagellar motor. *Proc. Natl. Acad. Sci. U.S.A.* 116, 11764–11769. doi: 10.1073/pnas.1904577116

Conflict of Interest: The authors declare that the research was conducted in the absence of any commercial or financial relationships that could be construed as a potential conflict of interest.

Publisher's Note: All claims expressed in this article are solely those of the authors and do not necessarily represent those of their affiliated organizations, or those of the publisher, the editors and the reviewers. Any product that may be evaluated in this article, or claim that may be made by its manufacturer, is not guaranteed or endorsed by the publisher.

Advantages of publishing in Frontiers

OPEN ACCESS
Articles are free to read for greatest visibility and readership

FAST PUBLICATION
Around 90 days from submission to decision

HIGH QUALITY PEER-REVIEW
Rigorous, collaborative, and constructive peer-review

TRANSPARENT PEER-REVIEW
Editors and reviewers acknowledged by name on published articles

Frontiers
Avenue du Tribunal-Fédéral 34
1005 Lausanne | Switzerland

Visit us: www.frontiersin.org
Contact us: frontiersin.org/about/contact

REPRODUCIBILITY OF RESEARCH
Support open data and methods to enhance research reproducibility

DIGITAL PUBLISHING
Articles designed for optimal readership across devices

FOLLOW US
@frontiersin

IMPACT METRICS
Advanced article metrics track visibility across digital media

EXTENSIVE PROMOTION
Marketing and promotion of impactful research

LOOP RESEARCH NETWORK
Our network increases your article's readership